

Studies Related to Polymerization and Colloid Formation of Actinides Under Off-normal Conditions

By

N. PRIYADARSHINI

Enrollment No: CHEM02200904001

Indira Gandhi Centre for Atomic Research, Kalpakkam

*A Thesis Submitted to the
Board of Studies in Chemical Sciences
In partial fulfillment of requirements
for the Degree of*

DOCTOR OF PHILOSOPHY

of

HOMI BHABHA NATIONAL INSTITUTE



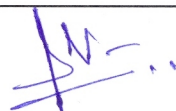
November, 2014

Homi Bhabha National Institute

Recommendations of the Viva voce Committee

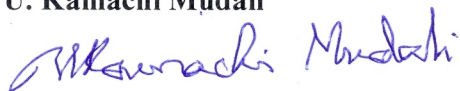
As members of Viva Voce Committee, we certify that we have read the dissertation prepared by **Miss N. Priyadarshini** entitled “**Studies related to polymerization and colloid formation of actinides under off-normal conditions**” and recommend that it may be accepted as fulfilling the dissertation requirement for the award of Degree of Doctor of Philosophy.

Chairman - **Dr. T. G. Srinivasan**



Date: 27.8.15

Guide / Convener – **Dr. U. Kamachi Mudali**



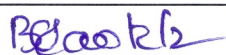
Date: 27/8/15

Examiner – **Dr. Basavaraja Madivala Gurappa**



Date: 27/08/2015

Member 1 - **Dr. B. V. R. Tata**



Date: 27/08/2015

Member 2 - **Dr. A. Bharathi**



Date: 27/08/2015

Technology Advisor – **Shri. Shekhar Kumar**



Date: 27/08/15

Final approval and acceptance of this dissertation is contingent upon the candidate's submission of the final copies of dissertation to HBNI.

I hereby certify that I have read this thesis prepared under my direction and recommend that it may be accepted as fulfilling the dissertation requirement.

Date: 27/8/15

Place: IGCAR,
Kalpakkam



Dr. U. Kamachi Mudali
Guide

STATEMENT BY AUTHOR

This dissertation has been submitted in partial fulfillment of requirements for an advanced degree at Homi Bhabha National Institute (HBNI) and is deposited in the library to be made available to borrowers under rules of the HBNI.

Brief quotations from this dissertation are allowable without special permission, provided that accurate acknowledgement of source is made. Requests for permission for extended quotation from or reproduction of this manuscript in whole or in part may be granted by the Competent Authority of HBNI when in his or her judgment the proposed use of the material is in the interest of scholarship. In all other instances, however, permission must be obtained from the author.



(N. Priyadarshini)

DECLARATION

I, hereby declare that the investigation presented in the thesis entitled “**Studies related to polymerization and colloid formation of actinides under off-normal conditions**” submitted to **Homi Bhabha National Institute (HBNI)**, Mumbai, India for the award of **Doctor of Philosophy in Chemical Sciences** has been carried out by me under the guidance of **Dr. U. Kamachi Mudali**. The work is original and has not been submitted earlier as a whole or in part for a degree / diploma at this or any other Institution / University.



(**N. Priyadarshini**)

LIST OF PUBLICATIONS

INTERNATIONAL JOURNAL PUBLICATIONS

1. "Light scattering studies to determine molecular weight of freshly prepared Zr(IV) hydrous polymer", **N. Priyadarshini**, M. Sampath, Shekhar Kumar, U. Kamachi Mudali, R. Natarajan, *Journal of Radioanalytical and Nuclear Chemistry*, **2013**, 295, 1093-1096.
2. "Particle size variation and prediction of molecular weight of Bi(III) hydrolyzed polymer using light scattering technique", **N. Priyadarshini**, M. Sampath, Shekhar Kumar, U. Kamachi Mudali, *ISRN Inorganic Chemistry*, **2013**, 2013, 1-5.
3. "A combined spectroscopic and light scattering study of hydrolysis of uranium(VI) leading to colloid formation in aqueous solutions", **N. Priyadarshini**, M. Sampath, Shekhar Kumar, U. Kamachi Mudali, R. Natarajan. *Journal of Radioanalytical and Nuclear Chemistry*, **2013**, 298, 1923-1931.
4. "Probing uranium(IV) hydrolyzed colloids and polymers by light scattering", **N. Priyadarshini**, M. Sampath, Shekhar Kumar, U. Kamachi Mudali, R. Natarajan, *Journal of Nuclear Chemistry*, **2014**, 2014, 1-10.
5. "Light scattering studies on formation and determination of molecular weight of Th(IV) aquatic colloids", **N. Priyadarshini**, M. Sampath, Shekhar Kumar, U. Kamachi Mudali, *Journal of Radioanalytical and Nuclear Chemistry*, **2015**. doi:10.1007/s10967-015-4274-3.

NATIONAL/INTERNATIONAL CONFERENCES

1. **N. Priyadarshini**, M. Sampath, Shekhar Kumar, U. Kamachi Mudali, Determination of micro-level Zr(IV) in aqueous solution. Chemistry Research Scholars Meet (CRSM – 2011), Indira Gandhi Centre for Atomic Research (IGCAR), Kalpakkam, 14th – 15th July 2011.
2. **N. Priyadarshini**, M. Sampath, Shekhar Kumar, U. Kamachi Mudali, Light scattering as analytical tool to study hydrolysis of Aluminium in aqueous systems, Theme meeting on recent advances in analytical chemistry (TRAC-2012), Madras University, Chennai, 30th & 31st August, 2012.
3. **N. Priyadarshini**, M. Sampath, Shekhar Kumar, U. Kamachi Mudali, Hydrolysis of Bi(III) -Light scattering studies, Eleventh biennial DAE-BRNS symposium on Nuclear and Radiochemistry, NUCAR-2013, Govt. Model Science College, R. D. University, Jabalpur, Madhya Pradesh, 19th – 23rd February, 2013, pp. 185-186.
4. **N. Priyadarshini**, M. Sampath, Shekhar Kumar, U. Kamachi Mudali, Light scattering studies for estimation of hydration number of Sr(II) and Al(III) ions in dilute solutions of nitric acid. Fifth symposium on Nuclear Analytical Chemistry (NAC-V), Bhabha Atomic Research Centre (BARC), Mumbai, 20th -24th January, 2014, pp. 238-239.
5. **N. Priyadarshini**, M. Sampath, Shekhar Kumar, U. Kamachi Mudali, Hydrolysis of Uranium(IV) – Light scattering studies. DAE – BRNS Biennial symposium on Emerging Trends in Separation Science and Technology (SESTEC-2014), Bhabha Atomic Research Centre (BARC), Mumbai, 25th - 28th February, 2014, pp. 259.

6. **N. Priyadarshini**, M. Sampath, Shekhar Kumar, U. Kamachi Mudali, Studies on size variation of U(IV) colloids formed in aqueous nitric acid solutions. Chemical Engineering in Nuclear Technology (CHEMENT-2014), Indira Gandhi Centre for Atomic Research, Kalpakkam, 6th and 7th March 2014.

OTHER PUBLICATIONS

1. Shekhar Kumar, Rajendra Singh Shekhawat, Abhishek Singh, M. Balamurugan, **N. Priyadarshini**, M. Sampath and U. Kamachi Mudali, Characterization of submicron size entrainment in the aqueous product stream of a 40 mm diameter centrifugal extractor for 30% TBP/HNO₃ biphasic system, *Int. J. Nuclear Energy Science and Technology*, 8 (2014) 49-60.

AWARDS

BEST POSTER AWARDS

1. **N. Priyadarshini**, M. Sampath, Shekhar Kumar and U. Kamachi Mudali, Light scattering as analytical tool to study hydrolysis of Aluminium in aqueous systems. Theme meeting on recent advances in analytical chemistry (TRAC-2012), University of Madras, Chennai, India, 30th & 31st August, 2012.
2. **N. Priyadarshini**, M. Sampath, Shekhar Kumar and U. Kamachi Mudali, Light scattering studies for estimation of hydration number of Sr(II) and Al(III) ions in dilute solutions of nitric acid. Fifth symposium on Nuclear Analytical Chemistry (NAC V), Bhabha Atomic Research Centre, Mumbai, India, 20th – 24th January 2014.



(**N. Priyadarshini**)



***Dedicated To
My Beloved
"Father & Sister"***



ACKNOWLEDGEMENTS

At this moment of accomplishment, first and foremost I wish to express my sincere respect and gratitude to my guide and supervisor **Prof. Dr. U. Kamachi Mudali**, Associate Director, Corrosion Science and Technology Division (CSTD) and Head, Reprocessing Research and Development Division (RR&DD), Indira Gandhi Centre for Atomic Research (IGCAR), for his constant encouragement and support. This work would not have been possible without his help. His unflinching courage and activeness always inspires me and I am very much grateful to him for his valuable advice, suggestions and discussions throughout my course of study.

I am also extremely indebted to my technology advisor **Shri. Shekhar Kumar** for providing necessary infrastructure and resources to accomplish my research work. I am very much thankful to him for his valuable guidance, advice, extensive discussions and his timely help through out my research work.

My heartfelt thanks to **Director, IGCAR** for providing me the opportunity to continue the research work at IGCAR.

I thank **Dr. R. Natarajan**, Director RpG for providing the facilities to carry out the research activities.

I express my sincere gratitude to my doctoral committee chairman **Dr. T. G. Srinivasan**, and members **Dr. B. V. R. Tata**, **Dr. A. Bharathi** for their fruitful discussions, valuable suggestions, constant support and encouragement.

I am thankful to **Dr. M. Sai Baba** for his kind advice, support and encouragement.

I expand my warm thanks to **Mr. M. Sampath** for his kind help and extended support. My sincere thanks to **Dr. C. Mallika** and **Shri. N. K. Pandey** for their encouragement.

My special thanks to **Mr. S. Sundaramurthy** for his kind support and **Dr. R. Srinivasan** for his encouraging words.

I take this opportunity to sincerely acknowledge all my colleagues of PDES, RR&DD, **Mr. S. Balasubramanion**, **Mr. D. Sivakumar**, **Mr. M. Balamurugan**,

Mr. Pranay Kumar Sinha, Mr. Bijendra Kumar, Mr. Jeyendra Jalatar, Mr. Bharathi, Mr. Ravikanth, Mr. Iyyappa for their kind support.

I would also like to express my sincere thanks to **Mr. Rahul Trikha, Dr. S. Ganesh, Mr. A. Chinnusamy, Mrs. S. Subha, Mr. P. Velavendan, Ms. Remya Murali, Ms. Elizabeth, Mr. U. Veeramani, Mr. T. Selvan, Mr. C. V. Joyakin**, for their help, care and friendliness which have made my research life more smooth and enjoyable at RR&DD.

Ms. Devi, and **Mr. Naguran** of RR&DD office deserves special mention here for their non-technical assistance.

I would like to express my deepest appreciation and thanks to my seniors **Dr. P. Ilaiyaraja, Dr. Debasmita Dash, Dr. Pravati Swain, Dr. Joy Nambam** and **Dr. Saravana Kumar**.

I would like to thank my friend **Mr. Arun Chandran** who gave a good support from the beginning to the end of my research work.

I owe my great pleasure and thanks to my friends **Shuaib, Srinivasan, Rama, Kesavan, Jerry, Ravikirana, Haripriya, Sashwat, Benedict Rakesh, Prema, Shravanti, Karthickeyan, Yadhagiri, Bonu, Devidas** and all my research scholar friends.

My heartfelt thanks to my dear friends **Anbu, Leona** and **Mahendran** for making my life more amiable and charming during my stay at JRF Enclave, Kalpakkam.

It's my fortune to gratefully acknowledge my dearest **Father Mr. K. Natarajan**, my sister **Ms. N. Samyuktha**, **Grandmother, Uncle & Aunt, Mr. Mani & Mrs. Vasanthi** for their generous care, moral support and staying beside me during the happy and hard moments to push me and motivate me. I owe them my eternal gratitude.

Finally, I thank the Almighty for providing me good health, courage, enormous blessings and enabling me to complete the thesis.



N. Priyadarshini

CONTENTS

Sl. No.	Title	Page No.
I.	Synopsis.....	i
II.	List of figures.....	xii
III.	List of tables.....	xix
IV.	Abbreviations.....	xxi

CHAPTER 1

Introduction

		1
1.1.	Nuclear energy and nuclear power program in India.....	1
1.2.	Need for nuclear fuel reprocessing.....	3
1.3.	Problems in spent fuel reprocessing and waste disposal due to hydrolysis of Actinides.....	6
1.4.	Hydrolysis of metal ions.....	7
1.5.	Hydrolysis of actinides.....	9
1.6.	Plutonium.....	10
1.6.1.	Problems in Pu aqueous chemistry.....	11
1.6.2.	Pu(IV) polymerization.....	12
1.6.3.	Parameters influencing the formation of Pu(IV) polymers/colloids.....	14
1.6.4.	Probing the formation and structure of Pu(IV) polymer.....	17
1.6.5.	Size and morphology of Pu(IV) colloid.....	21
1.6.6.	Hydrolysis and solubility of Pu(IV).....	23
1.6.7.	Molecular weight of Pu(IV) polymer.....	25
1.7.	Pu(VI) hydrolysis.....	25

1.8. Ways to remove polymers.....	26
1.8.1. Extraction of Pu(IV) polymer/colloid.....	26
1.8.2. Depolymerization.....	27
1.8.2.1 Proposed method for depolymerizing Pu(IV) polymer.....	28
1.9. Analogues taken to study hydrolytic behavior of Pu(IV).....	30
1.9.1. Zirconium.....	30
1.9.2. Thorium.....	31
1.9.3. Uranium.....	32
1.10. Colloids.....	32
1.10.1. Sources.....	33
1.10.2. Forces responsible for colloid stability.....	34
1.10.3. Migration behavior of actinide colloids in environment.....	35
1.10.4. Characterization of colloids.....	36
1.11. Motivation.....	39
1.12. Objectives.....	40
1.13. Overview.....	40

CHAPTER 2

Experimental Section

2.1. Chemicals and reagents.....	42
2.2. Experimental techniques.....	43
2.2.1. Light scattering technique-Theory.....	43
2.2.1.1. Dynamic light scattering.....	46
2.2.1.2. Static light scattering.....	52
2.2.2. UV-Visible spectrophotometry.....	55

2.2.3. Attenuated Total Reflectance-FTIR.....	58
2.2.4. Refractometer.....	61
2.2.5. pH measurements.....	63
2.2.6. X-ray diffraction.....	64

CHAPTER 3

Hydrolysis of Sr(II), Al(III) and Bi(III) Ions in Aqueous Nitric acid Solutions 65

3.1. Introduction.....	65
3.1.1. Aluminium(III) hydrolysis.....	66
3.1.2. Strontium(II) hydrolysis.....	67
3.1.3. Hydrolysis of Bismuth (III).....	67
3.2. Experimental.....	68
3.3. Results and Discussion.....	69
3.3.1. Diameter of hydrated Al ³⁺ ion.....	69
3.3.2. Molecular weight of hydrated Al ³⁺ ion.....	70
3.3.3. Diameter of hydrated Sr ²⁺ ion.....	73
3.3.4. Molecular weight of hydrated Sr ²⁺ ion.....	74
3.3.5. Variation of particle size with concentration of Bi(III).....	77
3.3.6. Molecular weight of Bi(III) hydrous polymer.....	78
3.4. Conclusions.....	81

CHAPTER 4

Hydrolysis and Polymerization of Zirconium(IV) in Aqueous Nitric Acid Solutions 83

4.1. Introduction.....	83
-------------------------------	-----------

4.2. Experimental work.....	86
4.2.1. Preparation of standard solution for determination of Zr(IV).....	86
4.2.2. Preparation of colloidal Zr(IV).....	86
4.3. Results and discussions.....	87
4.3.1. Procedure for determination of micro-level Zr(IV) in aqueous solutions.....	87
4.3.2. Light scattering studies on hydrolysis of Zr(IV).....	90
4.3.2.1. Formation of Zr(IV) colloids.....	90
4.3.2.2. Effect of pH on size of Zr(IV) colloidal polymer..	92
4.3.2.3. Size of Zr(IV) colloidal polymer aged at different time intervals.....	94
4.3.2.4. Molecular weight of Zr(IV) hydrous polymer.....	96
4.3.2.4.1. Freshly prepared polymer.....	96
4.3.2.4.2. Aged polymer.....	98
4.4. Conclusion.....	101

CHAPTER 5

<u>Hydrolysis of Uranium(IV & VI)</u>	103
5.1. Introduction.....	103
5.2. Uranium(IV) hydrolysis.....	104
5.2.1. Experimental section.....	105
5.2.1.1. Preparation of aqueous U(IV) solutions by electrolytic reduction of U(VI).....	105
5.2.1.2. Synthesis of U(IV) colloids.....	107
5.2.2. Results and discussion.....	107
5.2.2.1. Particle size.....	107

5.2.2.2. Molecular weight of U(IV) hydrolyzed polymer	118
5.3. Hydrolysis of uranium(VI).....	121
5.3.1. Experimental work.....	123
5.3.1.1. Aqueous U(VI) solutions.....	123
5.3.2. Results and discussion.....	123
5.3.2.1. UV-Visible spectrophotometric studies on hydrolysis of U(VI).....	123
5.3.2.2. ATR-FTIR spectra.....	125
5.3.2.3. Particle size of hydrolyzed U(VI) colloids formed in neutral solution.....	129
5.3.2.4. Molecular weight of U(VI) hydrolyzed colloid....	138
5.4. Conclusions.....	141

CHAPTER 6

Hydrolysis and Polymerization of Thorium(IV) in Aqueous Nitric Acid solutions

6.1. Introduction.....	143
6.2. Experimental	145
6.2.1. Synthesis of Th(IV) colloids.....	145
6.3. Results and discussion.....	145
6.3.1. 10 mM – 20 mM Th(IV) solutions.....	146
6.3.1.1. Size variation of Th(IV) colloids.....	146
6.3.1.2. Molecular weight of Th(IV) colloids formed at two different pH domains.....	150
6.3.2. 0.05 M – 0.4 M Th(IV) solutions.....	154
6.3.2.1. Size variation of Th(IV) colloids.....	154
6.3.2.2. Molecular weight.....	157

6.4. Conclusions.....	161
------------------------------	------------

CHAPTER 7

<u>Summary and Scope for Future Work</u>	163
7.1. Summary.....	163
7.1.1. Hydrolysis of Sr(II), Al(III) and Bi(III).....	164
7.1.2. Hydrolysis and polymerization of Zr(IV).....	164
7.1.3. Hydrolysis of U(IV) and U(VI).....	165
7.1.4. Hydrolysis and polymerization of Th(IV).....	166
7.4. Future Perspectives.....	167
V. List of References.....	169



SYNOPSIS

The use of nuclear energy for production of electricity leads to generation of a substantial amount of high level radioactive waste. The spent fuel from nuclear reactor contains radioactive actinides and fission products. Thus, it is a renewable resource that can be reprocessed into new nuclear fuel and valuable isotopes. Plutonium and other actinide elements present in the spent fuel dominate in radio-toxicity. It takes millions of years for reducing radio-toxicity. Most of the fission products have half life of less than 10 years [1]. Hence in order to recover useful actinides from the spent fuel, to reduce generation of substantial amount of high level radioactive waste, and to reduce the hazard due to radiotoxicity, the spent fuel needs to be reprocessed. PUREX (Plutonium – Uranium Reduction Extraction) is one of the most widely used and well established methods of separation of fission products and minor actinides from spent nuclear fuel. It is basically liquid-liquid extraction, which involves separating components of a solution by exploiting an unequal distribution of the components between two immiscible liquid phases. One phase will be aqueous solution containing the components to be separated and the other phase will be an organic solvent having a high affinity for some specific component in solution. In PUREX process, the aqueous phase is nitric acid solution and the organic phase is 30% tri-butyl phosphate in *n*-paraffin hydrocarbon or *n*-dodecane as diluents [2]. There are many challenges associated with the management of nuclear waste. One of the major challenges encountered during aqueous reprocessing, and waste disposal in geological repositories, is the hydrolysis and polymerization leading to colloid formation of actinides. Actinides are hard Lewis acids, and exhibit a strong tendency towards hydrolysis and subsequent polymerization or ‘eigen-colloid’ formation

mainly due to the electrostatic interaction energy between the actinide ion and the OH⁻ ligand [3]. Among the actinide elements, Pu has high ionic potential and hence shows inordinate tendency to undergo hydrolysis and forms polynuclear species/colloids of larger aggregates with 10 to 10¹⁰ units whose molecular weight varies from 4000 Da to 10¹⁰ Da [4]. This can be clearly understood from the general order of hydrolysis chemistry of tetravalent actinides, Pu⁴⁺ > Np⁴⁺ > U⁴⁺ > Pa⁴⁺ > Th⁴⁺ [5].

During aqueous reprocessing, the hydrolysis reactions occur due to accidental dilution of fuel or leaking cooling coils or steam lines and sometimes by overheating of solutions by evaporation operations leading to the formation of polymers and colloids [6]. These polymeric colloidal species are different from those of their mononuclear precursors. They are resistant to extraction by ion exchange, leads to emulsification and interfacial crud formation during solvent extraction [7]. It exhibits a marked resistance toward depolymerization which increases with ageing at extended period of times at room temperature and at high temperatures. They also undergo surface complexation and pose greatest risk to the environment by enhancing the colloid mediated radionuclide transport because it was believed that colloids may enhance the migration of radioactive elements in aquifer systems [8]. With respect to repository failure, and release of plutonium to the ground water, it is important to understand the hydrolytic behaviour of plutonium due to its high radiotoxicity, long half-life and very complex aqueous chemistry. It also requires knowledge of the possible plutonium compounds and their state of aggregation as a prerequisite to predict plutonium transport in the ground water, for safety assessment of nuclear repositories and to avoid its formation during process operations. But there are many

complications associated with the study of aqueous chemistry of Pu. Some of the problems associated with it are,

- i. ***Disproportionation reaction:*** Equilibrium of two or more oxidation state may occur in solution due to same redox potentials.
- ii. ***Reproportionation reaction:*** Two plutonium ions of different oxidation state may get simultaneously oxidised and reduced to form two ions of the same oxidation state.
- iii. ***Pu isotopes are radioactive:*** One milligram of Pu emits about 10^6 alpha particles per second, and the radioactive decay is constantly adding energy to the Pu solution. This leads to radiolytic decomposition of water producing redox reagents such as short lived radicals $\cdot\text{H}$, $\cdot\text{OH}$, and $\cdot\text{O}$. These radicals recombine to form H_2 , O_2 and H_2O_2 . Thus radiolysis tends to reduce Pu(VI) and Pu(V) to Pu(IV) and Pu(III) states.

All the reactions take place simultaneously and it becomes very difficult to study one particular reaction without the interference of the other. Hence as a common practice in radiochemistry, preliminary experiments were performed with stable or less radioactive analogs prior to the investigation of the element of interest mainly to validate new experimental methods, to minimize radioactive dose and to save rare material. In the case of tetravalent plutonium, two most frequently used homologues are the stable element zirconium and the very long lived actinide isotope ^{232}Th . Both elements form exclusively tetravalent ions in solution and offer the possibility to study complexation processes and perform solubility experiments without interference of the complex redox chemistry which is typical for plutonium. Another element

which can be considered is uranium. It is the heaviest naturally occurring element and is mainly used as fuel in nuclear reactors by increasing the relative concentration of ^{235}U (only fissile isotope of uranium). U(IV) also shows high tendency for hydrolysis, polymerization and colloid formation. Finally, in order to avoid polymers during process operation, to understand the role of colloids in waste disposal and for precise geochemical modeling to know the relative stability of the compounds, it is necessary to understand the source and mechanism of formation of colloids.

Colloids can be characterized by different techniques. Since aquatic colloids are delicately balanced systems and are very sensitive to handling, characterization of these colloids requires a non-invasive technique which can serve the purpose without disturbing the whole system. Hence light scattering technique (based on interaction of system with visible light) is considered as a better option as it is one of the most standard size characterization techniques which allow in-situ measurements without sample preparation. It is very sensitive, non invasive and non destructive colloid characterization technique which allows detection of colloids whose size ranges from 2 nm – 2 μm . Also during process operation, the molecular weight of polymers plays significant role. In addition to characterizing the size variation of colloids, the molecular weight of the polymers can also be determined using static light scattering technique [9].

The main objective of the thesis is to investigate the hydrolytic behaviour of Zr(IV), U(IV), U(VI) and Th(IV) by light scattering technique and to correlate their behaviour with Pu(IV). In the present work, preliminary studies were performed on metal ions such as Sr^{2+} , Al^{3+} and Bi^{3+} . Light scattering studies were carried out for polymeric solutions of Zr(IV), U(IV), U(VI) and Th(IV) and the results were

correlated to the data of Pu(IV) reported in literature. Spectroscopic techniques were used to detect the initial formation of colloids, and molecular weight of the colloidal polymers was determined using static light scattering technique. The thesis consists of seven chapters and the summary of each chapter is as follows:

Chapter 1

This chapter gives a detailed introduction on the importance of nuclear energy and the development of nuclear power program in India. Spent nuclear fuel reprocessing and its needs are also discussed in this chapter. PUREX process is the well established aqueous reprocessing method which is used widely in the nuclear industry. The general procedure involved in the process is given in detail. The major challenges faced during aqueous reprocessing due to hydrolysis of tetravalent metal ions are discussed. In addition to that, the basic introduction to metal ion hydrolysis and the difficulties in studying the behavior of a metal ion in aqueous systems are elaborated. Plutonium is considered as one of the key component of spent fuel and it has a very complicated aqueous chemistry. Important literature data available on hydrolysis of Pu(IV) are briefed. A summary of the reported data available on the mechanism of formation of colloids, studies performed to probe its structure, size and morphology, solubility of colloids and different methods to remove or avoid its formation are briefly described. Reasons for choosing zirconium, thorium and uranium as surrogate to study Pu hydrolytic behaviour is also discussed. As tetravalent metal ions are highly prone to the formation of colloids and polymer in aqueous systems, a general introduction on colloids, the parameters necessary for the stability of colloidal system and the various techniques used for characterizing the colloids are also discussed. The occurrences, chemical properties of Zr, U and Th which are taken as analogues for the

present study are elaborated. A short note on motivation, objective of the present study and overview of the thesis concludes this chapter.

Chapter 2

Chapter 2 provides a detailed description on the chemicals and the experimental techniques used for the present work. The hydrolysis reaction is monitored using spectroscopic techniques such as Ultraviolet-visible and Attenuated Total Reflectance – Fourier Transform Infrared spectroscopy (ATR- FTIR). Formation of colloids or polymeric species can be identified by the change in spectrum. Theory and its experimental details are included in this chapter. Light scattering technique is used for the present study to characterize colloids formed in the system. Mean size of the colloids were determined by using this technique. Theory of light scattering (dynamic and static) and the details of the experimental set up used are also discussed. Since colloids were synthesized at various pH conditions, details of pH measurements are also discussed in detail. Debye plot is generated to determine the second virial coefficient and weight average molecular weight of the polymers. In order to generate the plot, parameter such as differential refractive index and the density has to be given as input. A brief account on the working principle of refractometer and its experimental details are also included in this chapter. X-ray diffraction is used to investigate the precipitates that are formed at different pH conditions.

Chapter 3

Chapter 3 covers the light scattering studies related to hydrolysis reactions of multivalent metal ions such as Sr^{2+} , Al^{3+} and Bi^{3+} in aqueous nitric acid solutions. Different concentrations of the metal ions were prepared in aqueous nitric acid solutions. For Sr^{2+} and Al^{3+} only initial hydrolysis was investigated. The change in

refractive index of the solution with change in concentration of solute was measured using refractometer. The differential refractive index was obtained from its slope and used for generating Debye plot. The weight average molecular weight of the hydrated Sr^{2+} and Al^{3+} was determined from the intercept of the plot. In case of Bi^{3+} , polymerization and colloid formation at different pH conditions is also investigated. The variation in size at different pH conditions was monitored. The weight average molecular weight and the second virial coefficient which measures solute-solvent interaction parameter were determined and the results are discussed.

Chapter 4

Chapter 4 discusses the results obtained from the hydrolysis of tetravalent zirconium. A spectrophotometric method was developed in order to determine the micro-level concentration of Zr(IV) in aqueous solution. Zr(IV) colloids were synthesized in nitric acid medium at high acidity. Size of the colloids was determined using dynamic light scattering technique. pH was varied and the change in the size of the colloids were also reported. The polymers were aged at different time intervals. Size and molecular weight of freshly prepared and aged polymers were determined and the results were discussed in detail in this chapter.

Chapter 5

Chapter 5 mainly deals with the hydrolysis reactions leading to polymerization and colloid formation of tetravalent and hexavalent uranium. U(VI) hydrolysis was monitored by UV-visible and FTIR spectroscopy. The colloids formed at different acidities were studied using dynamic light scattering. The solid phase formed at near neutral condition was dried and analysed by x-ray diffraction. Size variation at different pH conditions was investigated and the molecular weight of the colloid was

determined. The results obtained from these studies were discussed in first part of the chapter. The second part of the chapter constitutes the results obtained from the studies performed on U(IV) which was generated using electrolytic reduction of U(VI). The method adopted for U(IV) generation was given in detail. Stability of U(IV) at the condition of investigation was ensured by monitoring the UV-visible spectrum. U(IV) colloids were synthesized by varying the acidities. The course of the reaction was monitored by UV-visible and ATR-FTIR spectroscopy. Size of the colloids formed at varying conditions was measured. The second virial coefficient and weight average molecular weight of freshly prepared as well as colloids aged for different time intervals were determined and the results were discussed in detail in this chapter.

Chapter 6

Chapter 6 describes the results obtained from the hydrolysis and polymerization reactions of tetravalent thorium. Th(IV) polymers were prepared by varying pH of the solution. Sizes of the colloids formed at different pH are measured. The molecular weight of the freshly formed polymer as well as polymers aged at different time intervals are determined using Debye plot. Second virial coefficient was also determined and the results are discussed in detail.

Chapter 7

This chapter constitutes the summary of the results discussed in the thesis. Use of light scattering technique as one of the method for immediate detection of polymers formed during process operation is clearly demonstrated. The investigations on aqueous species forming in solutions of tetravalent ions which are compiled in the present work are sub divided into four categories, i.e., the experiments performed on

Al^{3+} , Sr^{2+} and Bi^{3+} and those performed on Zr^{4+} , $\text{U}^{(4+, 6+)}$ and Th^{4+} . The highlights of the results obtained are as follows:

- Light scattering technique was used to determine the diameter of the hydrated ion of Sr(II) and Al(III) ions in aqueous nitric acid medium. At high acidity with OH/Al ratio of 0, the number of solvating molecules was observed to be 5 and for strontium, 9 water molecules were in the primary hydration sphere possibly existing in the form of $\text{Sr}(\text{H}_2\text{O})_9^{2+}$.
- Particle size of hydrolyzed Bi^{3+} increases as the concentration of Bi increases. The weight average molecular weight of hydrolyzed species shows that Bi^{3+} undergoes hydrolysis and forms hydrous polymers with 5-6 units.
- The investigations on Zr(IV) showed unambiguously that colloids are formed at very low pH. The molecular weight of the colloid shows that around ~10 zirconium atoms are present in the freshly prepared Zr(IV) polymer and it increases to ~30 in the case of aged polymer. Hydrolysis of Zr(IV) followed a similar behaviour to Pu(IV).
- The onset of colloid formation starts at pH = 3.46 in 2.5 mM U(IV) solutions. It is now proposed that in case of U(IV), colloids are formed in different domains of pH and U(IV) concentrations and that these colloids may differ in their structure. In the more acidic range, the size of the colloids formed is very small and thus considered to be crystalline in nature. However, at higher pH amorphous colloids form spontaneously from the over saturated solution. The colloids of U(IV) formed in low pH domain are oxo bridged and those formed at high pH are hydroxo bridged species. Ageing of colloids for 3 days lead to increase of molecular weight from ~1,800 to 13,000 Da. About 40-50 atoms of U are considered to be present in the aged

polymer. Positive value of second virial coefficient shows that solute-solvent interaction is high leading to stable suspension.

➤ Light scattering measurements were performed on colloidal U(VI) solutions formed at pH range of 7-8. The average particle diameter was determined as 32-36 nm. Well defined colloidal species are formed with no considerable change in particle size with increasing U(VI) concentration. The weight average molecular weight of colloidal species was predicted as ~763 Da by Debye plot. The behaviour of U(VI) is contradictory to U(IV) and Zr(IV). Even at neutral pH conditions there was no indication of polymerization and only oligomers with 2 – 3 uranyl units are considered to be present.

➤ Th(IV) forms colloids in solutions of pH = 1-3 with $[\text{Th(IV)}]_{\text{tot}} = 0.2$ to 10 mM and 0.05 to 0.4 M. Colloids are formed at two different pH domains and Th(IV) concentration. Th(IV) forms polymers of high molecular weight similar to that of Pu(IV).

➤ In contrast to the continuous transformation from mononuclear to polynuclear species the onset of colloid formation for Zr(IV), U(IV) and Th(IV) seems to behave differently. But similarity is the formation of polymers of considerable size up to billions of atomic mass unit. The light scattering measurements for Zr(IV), U(IV) and Th(IV) gives direct evidence that their hydrolysis behaviour is similar to Pu(IV) and hence it will help in future investigations on its chemical behaviour and for basic insights in polymer and colloid chemistry of tetravalent Pu. Light scattering technique provides faster and non-invasive measurement which is considered to be more advantageous compared to other methods for immediate detection of colloids.

References

1. A. Geist, K. Gompper, M. Weigl, T. Fanghanel, Nachrichten-FZK 97 (2004).
2. G. Choppin, J. Rydberg, J. O. Liljenzin (2001) Radiochemistry and nuclear chemistry. Third Edition, ISBN:978-0-7506-7463-8.
3. V. Neck, J. I. Kim, B.S. Seidel, C. M. Marquardt, K. Dardenne, M. P. Jensen, W. Hauser, Radiochim. Acta. 89 (2001) 439-446.
4. G. L. Johnson, L. M. Toth, Plutonium(IV) and Thorium(IV) hydrous polymer chemistry. Technical Report ORNL/TM-6365 (1978).
5. C. Walther, From hydrolysis to the formation of colloids-Polymerization of tetravalent Actinide ions. PhD Thesis, Universitat Mainz (2008).
6. R. E. Biggers, D. A. Costanzo, Preliminary report. ORNL TM-585 (1963).
7. J. M. Cleveland (1970) The chemistry of plutonium, Gordon and Breach, New York, ISBN:0677023103.
8. R. Kretzschmar, K. Barmettler, D. Grolimund, Y-d. Yand, M. Borkovec, H. Sticher, Water Resour. Res. 33 (1997) 1129-1137.
9. C. Walther, M. A. Denecke, Chem. Rev. 113 (2013) 995-1015.

List of Figures

Sl. No.	Title	Page No.
Fig. 1.1.	Schematics of a typical thermal reactor fuel cycle	4
Fig. 1.2.	Hydrolysis of metal ions.....	9
Fig. 1.3.	The redox potential differences for the plutonium aquo ions in 1M perchloric acid, as well as the potential difference between the plutonium aquo ions and pure Pu.....	11
Fig. 1.4.	Plutonium oxidation state distribution depending on $-\log[H^+]$	13
Fig. 1.5.	Picture showing emerald green color Pu(IV) colloidal polymeric solution and its corresponding structure.....	13
Fig. 1.6.	Schematics showing the conversion of hydroxyl bridged polymer to oxo bridged polymer.....	14
Fig. 1.7.	(a) Characteristic colors of each oxidation state of Pu and Pu colloids.....	16
	(b) Absorption spectra of different oxidation state of Pu and Pu colloids.....	16
Fig. 1.8.	Schematics showing mechanism of hydrolysis and polymerization of $Pu^{4+}_{(aq)}$ leading to formation of nm size colloids.....	18
Fig. 1.9.	Structure of $[Pu_{38}O_{56}]^{40+}$ core in the crystal structure of $Li_{14}(H_2O)_{20}[Pu_{38}O_{56}Cl_{54}(H_2O)_8]$ and $Li_2[Pu_{38}O_{56}Cl_{42}(H_2O)] \cdot 15H_2O$	19
Fig. 1.10.	Schematic representation of a model for observed Pu(IV) polymer.	20
Fig. 1.11.	IR spectra of PuO_2 and Pu(IV) polymer precipitated and dried in air.....	22
Fig. 1.12.	Solubility of amorphous $Pu(OH)_4$ comparing available literature data.....	25
Fig. 1.13.	Partitioning of colloidal Pu from the bottom aqueous phase to top organic TCA/n-octanol organic phase.....	27
Fig. 1.14.	Effect of uranyl nitrate on Pu(IV) polymerization rate ($[Pu(IV)] = 0.05$ M, $[HNO_3] = 0.11$ M, at 50° C).....	29

Fig. 1.15.	Leaching or dissolution of radioactive waste leading to formation of intrinsic and pseudo colloids in solution.....	34
Fig. 2.1.	Scattering geometry showing laser beam, wave vectors (\vec{k}), scattering vector (\vec{q}) and scattering angle (θ).....	44
Fig. 2.2.	A schematic representation of the light scattering experiment.....	45
Fig. 2.3.	Schematics showing constructive and destructive interference of waves.....	47
Fig. 2.4.	(a) Intensity of scattered light from suspensions containing small and large particles.....	47
	(b) The time-averaged autocorrelation function of the scattered intensity as a function of time.....	47
Fig. 2.5.	Schematics showing different distribution curves (Number, volume and intensity distribution).....	49
Fig. 2.6.	Schematics of the light scattering system showing the development of controlled reference at the probe tip and fluid interface.....	50
Fig. 2.7.	Microtrac particle size analyzer with measurement range of 0.8nm to 6.4 μ m used for the present study.....	51
Fig. 2.8.	Calibration curve for measuring particle size distribution.....	52
Fig. 2.9.	A typical Debye plot.....	54
Fig. 2.10.	Schematics of a conventional UV-Vis spectrophotometer.....	57
Fig. 2.11.	Schematics of a simple FTIR spectrometer.....	60
Fig. 2.12.	Schematics of a multiple reflection ATR system.....	61
Fig. 2.13.	Schematics of an automatic refractometer.....	62
Fig. 2.14.	Schematic representation of a combination electrode.....	63
Fig. 3.1.	Intensity size distribution curve of Al ³⁺ hydrated ion.....	70
Fig. 3.2.	A plausible structure of Al ³⁺ hydrated ion.....	71
Fig. 3.3.	The dn/dC curves obtained for different concentration of Al ³⁺ solution.....	71

Fig. 3.4.	Debye plot for various concentrations of Al ³⁺ solution.....	72
Fig. 3.5.	Intensity size distribution curve of Sr ²⁺ hydrated ion.....	73
Fig. 3.6.	Sr ²⁺ ion surrounded by 9 water molecules in the primary hydration sphere.....	74
Fig. 3.7.	The dn/dC curves obtained for different concentration of Sr ²⁺ solution.....	75
Fig. 3.8.	Debye plot for various concentrations of Sr ²⁺ solution.....	75
Fig. 3.9.	Coordination number distribution of first and second hydration shell of Sr(II) in aqueous solution obtained by QM/MM MD simulations.....	76
Fig. 3.10.	A comparison plot for intensity averaged particle diameter (d ₅₀) variation with different concentration of polymeric Bi solutions prepared in aqueous nitric acid medium.....	78
Fig. 3.11.	The dn/dC curves obtained for different concentration of Bi(III) solution	79
Fig. 3.12.	Debye plot for various concentrations of Bi ³⁺	80
Fig. 4.1.	Calculated distribution of mononuclear hydroxide complexes (HCl/NaCl solutions of I=0.5 M) in the absence of polynuclear species, at very low metal ion concentration.....	84
Fig. 4.2.	Representation of two octamer configurations A) Sheet octamer B) Stacked octamer.....	85
Fig. 4.3.	(a) UV-visible absorption spectra of Zr(IV)	89
	(b) Plot showing a linear relationship between zirconium concentration and removal of phosphate ions from the solutions....	89
Fig. 4.4.	General equilibrium reaction for hydrolysis of Zr(IV).....	90
Fig. 4.5.	Intensity distribution curve of Zr(IV) polymer formed in aqueous nitric acid solution ([Zr(IV)] = 0.1 M).....	91
Fig. 4.6.	Increasing colloidal size with increasing pH for 1 M Zr(IV) solution.....	92
Fig. 4.7.	Intensity size distribution of Zr(IV) colloid (a) Aged for 3 days (b) Aged for 7 days (c) Schematics of growth process of Zr polymeric species forming rod like particles.....	95

Fig. 4.8.	Refractive index increment of different concentration of Zr(IV) solution.....	96
Fig. 4.9.	Debye plot for freshly prepared Zr(IV) hydrous polymer.....	98
Fig. 4.10.	Refractive index increment of different concentration of polymeric Zr(IV) solution aged for 7 days.....	99
Fig. 4.11.	Debye plot for 7 days aged Zr(IV) hydrous polymer.....	99
Fig. 5.1.	The redox potential differences for the uranium ions and pure U....	103
Fig. 5.2.	Schematic diagram of electrolytic setup used for U(IV) generation.	106
Fig. 5.3.	UV-Vis spectra of U(IV) solution in the course of its dilution.....	108
Fig. 5.4.	Size distribution curve of 0.4 mM U(IV) solution at pH 4.5.....	109
Fig. 5.5.	Picture showing 6.5 mM U(IV) solution and the colloidal U(IV) solution formed at pH 3.1.....	110
Fig. 5.6.	Intensity averaged particle diameter (d_{50}) of U(IV) hydrolyzed colloid formed in 3.78 mM solution diluted to different pH.....	110
Fig. 5.7.	Intensity averaged particle diameter (d_{50}) of U(IV) hydrolyzed colloid formed in 5.2 mM solution diluted to different pH.....	111
Fig. 5.8.	Intensity averaged particle diameter (d_{50}) of U(IV) hydrolyzed colloid formed in 6.5 mM solution diluted to different pH.....	111
Fig. 5.9.	Intensity averaged particle diameter (d_{50}) of U(IV) hydrolyzed colloid formed in 7.8 mM solution diluted to different pH.....	112
Fig. 5.10.	(a) FT-IR ATR spectra of [U(IV)] = 19 mM diluted to pH 1 (b) [U(VI)] = 2.52 mM diluted to pH 3.46.....	113
Fig. 5.11.	Variation of particle size with time at the point of precipitation for 7.8 mM U(IV) solution at pH 3.65.....	114
Fig. 5.12.	(a) Intensity averaged particle diameter (d_{50}) of U(IV) hydrolyzed colloid formed in 9.2 mM solution diluted to different pH..... (b) Variation of particle size with time at the point of precipitation for 9.2 mM U(IV) solution at pH 3.3.....	115 115
Fig. 5.13.	(a) Intensity averaged particle diameter (d_{50}) of U(IV) hydrolyzed colloid formed in 13 mM solution diluted to different pH.....	116

	(b) Variation of particle size with time at the point of precipitation for 13 mM U(IV) solution at pH 2.61.....	116
Fig. 5.14.	(a) Intensity averaged particle diameter (d_{50}) of U(IV) hydrolyzed colloid formed in 19 mM solution diluted to different pH (b) Variation of particle size with time at the point of precipitation for 19 mM U(IV) solution at pH 2.42.....	117
Fig. 5.15.	The dn/dC curves obtained for different concentration of U(IV) colloidal solution.....	119
Fig. 5.16.	Debye plot for of U(IV) polymeric solution aged at different time intervals.....	120
Fig. 5.17.	UV-Visible electronic absorption spectra of U(VI) aqueous solutions in 1M nitric acid. $[\text{UO}_2^{2+}] = 4\text{mM}$ and pH values are given on the figure.....	124
Fig. 5.18.	(a) FT-IR ATR spectra of U(VI) solutions, $[\text{UO}_2^{2+}] = 12\text{ mM}$ diluted to pH=1.....	125
	(b) FT-IR ATR spectra of U(VI) solutions, $[\text{UO}_2^{2+}] = 12\text{ mM}$ diluted to pH= 6.8.....	126
	(c) FTIR-ATR spectra of 12 mM U(VI) solutions diluted to pH=7.4.....	127
Fig. 5.19.	Speciation diagram of U(VI) ions as a function of pH in aqueous solution at atmospheric condition.....	129
Fig. 5.20.	(a) Picture showing the yellow deposits formed during centrifugation and the dried yellow powder.....	130
	(b) XRD pattern recorded for the solid phase ($[\text{UO}_2^{2+}] = 12\text{ mM}$ at pH 7.4).....	131
Fig. 5.21.	Intensity averaged particle diameter (d_{50}) of uranyl hydrolyzed colloid formed in 4mM UO_2^{2+} solution diluted to pH 8.2 (a) Before centrifugation (b) After centrifugation.....	132
Fig. 5.22.	Intensity averaged particle diameter (d_{50}) of uranyl hydrolyzed colloid formed in 8mM UO_2^{2+} solution diluted to pH 7.7. (a) Before centrifugation (b) After centrifugation.....	133
Fig. 5.23.	Intensity averaged particle diameter (d_{50}) of uranyl hydrolyzed colloid formed in 12mM UO_2^{2+} solution diluted to pH 7.4 (a) Before centrifugation (b) After centrifugation.....	134

Fig. 5.24.	Intensity averaged particle diameter (d_{50}) of uranyl hydrolyzed colloid formed in 16mM UO_2^{2+} solution diluted to pH 7.1 (a) Before centrifugation (b) After centrifugation.....	135
Fig. 5.25.	Intensity averaged particle diameter (d_{50}) of uranyl hydrolyzed colloid formed in 20mM UO_2^{2+} solution diluted to pH 6.98 (a) Before centrifugation (b) After centrifugation.....	136
Fig. 5.26.	Intensity averaged particle diameter (d_{50}) of uranyl hydrolyzed colloid formed in 24mM UO_2^{2+} solution diluted to pH 6.6 (a) Before centrifugation (b) After centrifugation.....	137
Fig. 5.27.	The dn/dC curves obtained for different concentration of U(VI) solution.....	139
Fig. 5.28.	Debye plot for various concentrations of colloidal U(VI) solutions	140
Fig. 5.29.	Supernatant solution aged for 1 day [UO_2^{2+}] = 12 mM, pH =7.4....	141
Fig. 6.1.	Speciation diagram of Th(IV) ions as a function of pH in aqueous solution at atmospheric condition.....	143
Fig. 6.2.	Particle size distribution of Th(IV) colloids formed at pH ~ 1.9	147
Fig. 6.3.	Particle size distribution of Th(IV) colloids aged for 3-5 days.....	148
Fig. 6.4.	Particle size of Th(IV) colloids formed at pH > 3.4.....	149
Fig. 6.5.	Refractive index increment for colloids formed at pH ~1.9 and pH ~3.4.....	151
Fig. 6.6.	Debye plot for initially formed colloids at pH 1.9 and 3.4.....	151
Fig. 6.7.	Debye plot for Th(IV) colloids aged for different time intervals at pH ~ 3.4.....	153
Fig. 6.8.	Particle size of Th(IV) colloids formed at pH ~ 0.8.....	154
Fig. 6.9.	Particle size after ageing for 3 days.....	155
Fig. 6.10.	Picture showing precipitation in 0.2 and 0.3 M Th(IV) colloidal solutions after 3 days of ageing.....	156
Fig. 6.11.	Particle size of Th(IV) colloids formed at pH ~ 2.....	157
Fig. 6.12.	Refractive index increment for colloids formed at pH ~0.8 and pH ~2.0.....	158
Fig. 6.13.	Debye plot for freshly formed colloids at pH~0.8 and pH~2.0.....	159

Fig. 6.14. Debye plot for Th(IV) colloids aged at different time intervals at pH~2..... 160

List of Tables

Sl. No.	Title	Page No
Table 1.1.	Half times for depolymerization of Pu(IV) polymer.....	27
Table 1.2.	Different methods for determination of colloid size and the corresponding nature of the technique, where S = single particle, P = Populations are determined, S(P) = Single particle on an average over many measurements.....	38
Table 2.1.	Properties of ZnSe ATR crystal.....	61
Table 3.1.	Comparison of experimentally determined diameter of hydrated Al ³⁺ ion data with literature reported value.....	69
Table 3.2.	Peak summary for size distribution curve of Al ³⁺ hydrated ion.....	70
Table 3.3.	Calculated parameters from the Debye plot for hydrated Al ³⁺ ion.....	72
Table 3.4.	Peak summary for size distribution curve of Sr ²⁺ hydrated ion.....	73
Table 3.5.	Calculated parameters from the Debye plot for hydrated Sr ²⁺ ion	76
Table 3.6.	Peak summary for size distribution curve different concentration of polymeric Bi solutions.....	77
Table 3.7.	Calculated parameters from the Debye plot for Bi(III) hydrous polymer.....	80
Table 4.1.	Peak summary for Intensity distribution curve of Zr(IV) hydrous polymer.....	91
Table 4.2.	Calculated parameters from the Debye plot for freshly prepared Zr(IV) hydrous polymer.....	98
Table 4.3.	Calculated parameters from the Debye plot for 7 days aged Zr(IV) hydrous polymer.....	100
Table 5.1.	Concentration of U(IV) and pH at the onset of colloid formation, intensity average size (d ₅₀), pH at maximum colloid formation....	118
Table 5.2.	Calculated parameters from the Debye plot for U(IV) polymeric solution aged at different time intervals.....	121

Table 5.3.	Characteristic infrared spectra peak of hydrolyzed U(VI) solution.....	128
Table 5.4.	Peak summary of intensity distribution curves of U(VI) hydrolyzed colloids before and after centrifugation.....	138
Table 5.5.	Calculated parameters from the Debye plot for U(VI) hydrolyzed oligomers.....	141
Table. 6.1.	Calculated parameters from the Debye plot for freshly formed Th(IV) colloids in 10-20 mM Th(IV) solutions.....	152
Table. 6.2.	Parameters from the Debye plot for Th(IV) colloids aged at different time intervals [[Th(IV)] = 10-20 mM, pH~3.4].....	153
Table 6.3.	Calculated parameters from the Debye plot for freshly formed Th(IV) colloids in 0.05-0.4 M Th(IV) solutions.....	159
Table 6.4.	Calculated parameters from the Debye plot for colloids aged at different time intervals [[Th(IV)] = 0.05-0.4 M, pH~2].....	160

Abbreviations

MWe	: Mega Watt electric
MOX	: Mixed Oxide
FBRs	: Fast Breeder Reactors
PUREX	: Plutonium Uranium Reductive Extraction
TBP	: Tributyl Phosphate
An	: Actinide
SANS	: Small Angle Neutron Scattering
SAXS	: Small Angle X-ray Scattering
XAFS	: X-ray Absorption Fine Structure
EXAFS	: Extended X-ray Absorption Fine Structure
LIBD	: Laser Induced Breakdown Detection
TEM	: Transmission electron microscope
XRD	: X-ray Diffraction
K_{sp}	: Solubility product
ATR	: Attenuated Total Reflection
TOC	: Total Organic Carbon
DLS	: Dynamic Light Scattering
FFT	: Fast Fourier Transform
PCS	: Photon Correlation Spectroscopy
SLS	: Static Light Scattering
LED	: Light Emitting Diode
A₂	: Second virial coefficient
M_w	: Weight average molecular weight

NDIS	:	Neutron Diffraction with Isotopic Substitution
QMMD	:	Quantum Mechanical Molecular Dynamics Simulation
AXD	:	Anomalous X-ray Diffraction
LAXS	:	Low Angle X-ray Scattering
γ	:	Activity coefficient
a_w	:	Water activity
β	:	Hydrolysis constant
ESI-MS	:	Electrospray Ionization Mass Spectrometry

Chapter 1



CHAPTER 1

Introduction

1.1. Nuclear energy and nuclear power program in India

Nuclear energy is emerging as a promising solution for satisfying emerging energy crisis in India. It has lot of advantages over other means of producing electricity, constituting the potential platform for long term energy security. It is clean, safe, reliable and sustainable with intense source of energy. For instance, 10,000 MWe nuclear power capacity needs only about 300-350 tons of natural uranium per annum against 35-50 million tons of coal fired thermal power station. In addition to that it is environment friendly, ie. every unit of nuclear power generated saves 1 kg of CO₂ emissions when compared to predominant coal technology which results in the emission of about 1 kg/kWh [1]. The unique feature that makes nuclear energy so special among all other options is that the fuel gets rejuvenated while being used.

All the nuclear reactors operating worldwide are based on nuclear fission reaction. The various activities associated with the production of electricity from nuclear reactions are collectively referred as the nuclear fuel cycle. The nuclear fuel cycle is comprised of many steps starting from the extraction of ore and terminates with nuclear waste disposal. It is divided into two classes, “*open or once through fuel cycle*”, where the spent fuel discharged from the reactor is stored as waste. The

second is called “*closed fuel cycle*”, where the spent fuel discharged from the reactor is reprocessed, and the products are partitioned into uranium (U) and plutonium (Pu) suitable for fabrication of oxide or mixed oxide (MOX) for recycle back into reactor [2].

At present, nuclear energy contributes only 3% of the total electricity generation in India [3-4]. To satisfy the growing demand due to enormous population growth and for the betterment of life, the Department of Atomic Energy of India has been pursuing the three stage nuclear power program to produce more energy (from present day 2,770 MWe to 63,000 MWe by 2,032) [5]. The main aim of this program is to utilize the mined uranium resources to the maximum extent. It is based on closed fuel cycle concept, involving reprocessing of spent fuel from every reactor and reused in the next stage reactor, leading to more economical nuclear power generation and less environmental risk [6].

Uranium is the main constituent of nuclear fuel. Naturally occurring uranium has three isotopes. Uranium-238 (with natural abundance of 99.2739 - 99.2752%), uranium-235 (0.7198-0.7202%) and uranium-234 (0.0050 - 0.0059%). Among them, only ^{235}U is fissionable, while ^{238}U is a fertile material [7-8]. For energy production, it needs to be converted to fissile ^{239}Pu . Conversion can be done in nuclear reactor where uranium is used as fuel.

- ***First stage***

The first stage comprises of Pressurized Heavy Water Reactor (PHWR) which employs natural uranium as fuel. ^{235}U present in small fraction results in production of excess neutrons. These excess neutrons get absorbed in major isotope ^{238}U leading to

the production of ^{239}Pu . The spent fuel is reprocessed to separate uranium and plutonium and other fission products.

- ***Second stage***

The second stage constitutes Fast Breeder Reactors (FBRs). It uses mixed carbides/oxide of ^{238}U and ^{239}Pu obtained from first stage. In FBRs, ^{239}Pu undergoes fission producing energy, and also produces ^{239}Pu by transmutation of ^{238}U . Thus they produce more plutonium than they consume and thus the name “Breeder”.

- ***Third stage***

The third stage of the program envisages the utilization of thorium as fuel. It is mainly because, the waste produced by irradiation of thorium does not contain long-lived radioactive minor actinides compared to uranium or plutonium fuel. ^{232}Th is not fissile and hence it has to be converted to ^{233}U . This is achieved by introducing ^{232}Th as blanket material in the second stage, once sufficient nuclear capacity is built through plutonium based FBRs [9].

1.2. Need for nuclear fuel reprocessing

The spent fuel from nuclear reactor contains actinides and fission products. Thus it is a renewable resource that can be reprocessed into new nuclear fuel and valuable isotopes. Plutonium and other actinide elements present in the spent fuel dominate in radiotoxicity. It takes hundreds and thousands of years for reducing radio-toxicity. Most of the fission products have half life of less than 10 years [10]. Hence in order to recover useful actinides from the spent fuel, to reduce generation of substantial amount of high level radioactive waste and to reduce the hazard due to radiotoxicity, the spent fuel needs to be reprocessed. It also facilitates to increase the

available energy from fissile and fertile atoms. The fuel cycle is mainly divided into a front end and a back end part where the nuclear power station is the dividing line. The front end comprises uranium exploration, mining and refining, isotope enrichment and fuel element fabrication. The back end involves reprocessing and radioactive waste handling [11]. Figure 1.1 is a schematic representation of typical nuclear fuel cycle pursued in India.

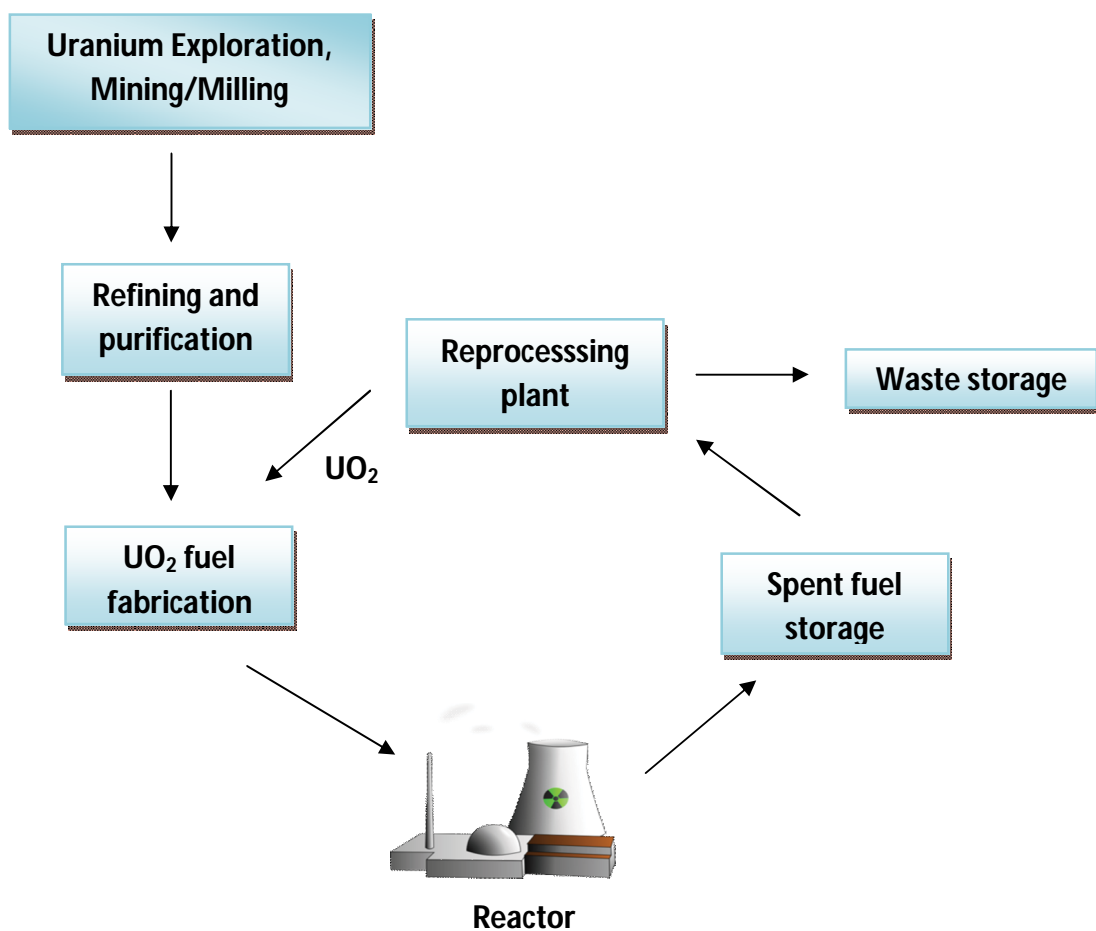


Fig. 1.1. Schematics of a typical thermal reactor fuel cycle

Initial step in reprocessing of used nuclear fuel involves dissolution of spent fuel in acidic (conc. nitric acid) aqueous solution. The resulting solution is chemically processed to separate uranium and/or plutonium. In addition to that minor actinides,

and other fission products present are also separated during different cycles of this process. Most widely used method for separation is PUREX (Plutonium – Uranium Reduction Extraction) process. It is basically liquid-liquid extraction, which involves separating components of a solution by exploiting an unequal distribution of the components between two immiscible liquid phases. One phase will be aqueous solution containing the components to be separated and the other phase will be an organic solvent having a high affinity for some specific component in solution. In PUREX process, the aqueous phase is nitric acid solution and the organic phase is 30% tri-butyl phosphate in *n*-paraffin hydrocarbon or *n*-dodecane as diluent. The processing step involves decladding and exposing the fuel material within its cladding to a nitric acid solution in order to allow dissolution. The resulting solution contains nitrates of uranium, plutonium, minor actinides and fission products. During dissolution process, the elements such as iodine, krypton and xenon are volatilized and the off gas is treated to remove those isotopes which have radiological significance. The dissolved species are subjected to chemical conditioning of the fuel amenable for solvent extraction. It is then fed forward to the solvent extraction process where U(VI) and Pu(IV) are separated as a result of different affinities with the aqueous and organic phases. Co-extraction of fission products from the organic phase was done by scrubbing it with different concentrations of nitric acid. Manipulation of Pu valence state was done in order to make it less extractable into the organic phase. Uranium and plutonium are separated from each other and then purified and converted into solid products through thermal denitration in case of uranium and oxalate precipitation and calcination in case of plutonium. Finally, solution containing fission products and minor actinides are evaporated in order to

reduce its storage volume before being converted to its final form by calcination and vitrification. Spent solvent is treated for reuse [12-13].

1.3. Problems in spent fuel reprocessing and waste disposal due to hydrolysis of actinides

One of the major challenges posed during aqueous reprocessing and waste disposal in geological repositories is the hydrolysis and polymerization of tetravalent actinides. In case of aqueous reprocessing, the hydrolysis reactions occur due to accidental dilution of fuel or leaking cooling coils or steam lines and sometimes by overheating of solutions during evaporation operations leading to the formation of polymers and colloids [14]. These hydrolysis products influence processes such as adsorption onto mineral surfaces, the tendency of metal cations to form colloidal suspensions, the solubility of hydroxide/oxide phases and the extent to which the metal can be complexed in solution or extracted from solution by various complexing agents. Pu polymers have high tendency to adsorb on steel and glass surfaces which are difficult to remove [15]. The polymers formed as a result of hydrolysis are resistant to extraction by ion exchange and leads to emulsification and interfacial crud formation during solvent extraction. It exhibits a marked resistance towards depolymerization which increases with ageing at extended period of times at room temperature and at high temperatures [16].

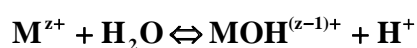
Secondly, during disposal of radioactive waste in deep geological repositories, the colloids formed due to hydrolysis of metal ions pose greater risk to the environment by enhancing the colloid mediated radionuclide transport. It is believed that colloids may enhance the migration of radioactive elements in aquifer systems [17]. Hence in order to avoid polymer formation during reprocessing

operation, to understand the role of colloids in waste disposal and for precise geochemical modeling to know the relative stability of the compounds, it is necessary to understand the source and mechanism of formation of colloids. The subsequent section discusses the possible mechanism for polymerization and colloid formation of actinides.

1.4. Hydrolysis of metal ions

Before discussing hydrolysis of actinides, it is essential to understand the basic chemical reaction of metal ions when it comes in contact with water. Consider in general, when a metallic element enters into an aqueous solution, its chemical behavior is determined by the nature of the ionic or molecular species that it forms. In the absence of strong complexing ligands and depending on the acidity of the solution the simple cation of the element often reacts with water it-self (hydrolyzes) to form complexes with the hydroxide ion. This is due to the fact that in aqueous medium, the metal cations M^{Z+} are solvated by dipolar water molecules giving rise to aquo ions $[M(OH_2)_n]^{Z+}$. Charge transfer occurs through the M-OH₂ σ bond. Electron density is transferred from molecular orbital of coordinated water molecule to empty orbitals of metal cation. This results in the weakening of O-H bond and finally deprotonation takes place leading towards the formation of bonds with oxygen and OH⁻ ligand [18]. In addition to that, hydroxide ions are always present in water at concentrations varying from >1 to $<10^{-14}$ m as a result of small self dissociation constant of water. The resulting complexes may be cations, neutral molecules or anions, and may be mononuclear or polynuclear which means they may contain one metal atom or several [19]. The ability of hydrated metal ions to hydrolyze depends on the charge and size of metal ions, in other words it depends on the ionic potential (charge to size ratio) of

the metal. Small and highly charged metal ions are very prone to hydrolysis. In case of differently charged metal ions, the hydrolysis constant increases in the order $M^{4+} > M^{6+} > M^{5+} > M^{3+}$ mainly due to decrease in ionic radius and increase in Lewis acidity of the metal ion [20]. The initial step in the hydrolysis of a cation is usually the formation of the mono-nuclear species $MOH^{(z-1)+}$ and in general it is represented as



Complete reaction is represented by including water of solvation



In the above reaction a proton is lost by a solvating water molecule and on further hydrolysis,



and so on. But in reality complete hydrolysis does not happen, instead other chemical reactions or aggregation of two or more hydrolyzed species takes place and in general it is represented in figure 1.2.

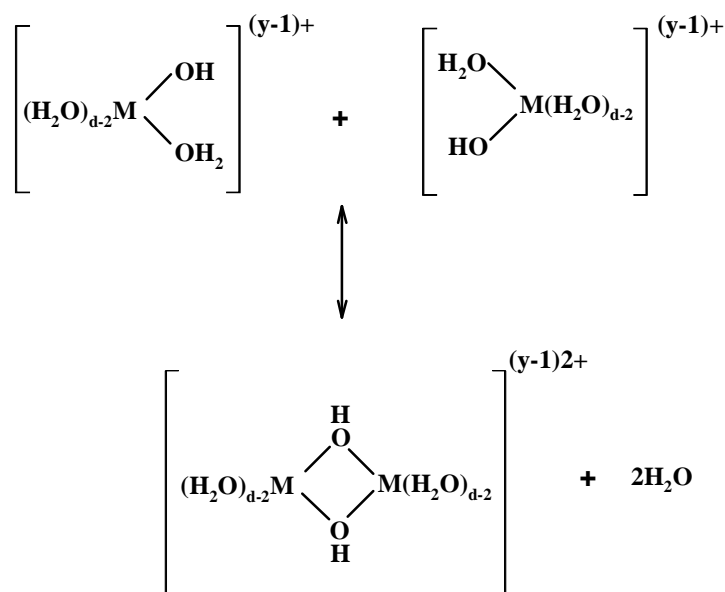


Fig. 1.2. Hydrolysis of metal ions

When this reaction further continues, there is a possibility of formation of high molecular weight polynuclear chains. The determination of the identity and stability of dissolved hydrolysis products have proven to be a difficult and challenging task primarily for the following reasons.

- Formation of a greater variety of species during the hydrolysis process.
- Many hydrolysis products are present in the solution simultaneously in appreciable amounts.
- The range of pH over which the formation of soluble hydrolysis products can be studied is often limited by the precipitation of the hydroxide or the oxide of the metal cation [21].

1.5. Hydrolysis of Actinides

Hydrolysis reactions are important primary complexation reactions of actinide elements in aqueous solution. It is mainly correlated with the electrostatic

interaction energy between the actinide ion and the OH⁻ ligand [22-24]. Being hard Lewis acids, tetravalent actinide ions exhibit extensive hydrolysis chemistry following the general order $\text{Pu}^{4+} > \text{Np}^{4+} > \text{U}^{4+} > \text{Pa}^{4+} > \text{Th}^{4+}$. The effective charge of the actinide ions decreases in the order of $\text{An}^{4+} > \text{AnO}_2^{2+} > \text{An}^{3+} > \text{AnO}^{2+}$. Due to high electric charge, tetravalent actinides can hydrolyze even under very acidic conditions (pH < 3 depending on actinide) [25]. In the near neutral pH, $\text{An}(\text{OH})_{(\text{aq})}$ species dominates in the absence of other complexing ligands. Actinide ions in the trivalent and tetravalent states in acidic solutions are in the form of the simple hydrated ions An^{3+} and An^{4+} . Whereas An^{5+} and An^{6+} exist as trans-dioxo cations. This is due to large positive charges which make them readily strip oxygen atoms from water molecules. They are extremely stable and have a symmetry and nearly linear structure $[\text{O}=\text{An}=\text{O}]^{n+}$ where $n = 1, 2$. This structure decreases the effective charge on the central actinide ion making it less prone for hydrolysis as compared to tetravalent actinides [26].

1.6. Plutonium

Among the actinides, plutonium is the most chemically diverse and fascinating element in the periodic table. Plutonium is generated by transmutation of uranium in nuclear reactors in large scale. Plutonium has 18 isotopes. The most common among these are ^{238}Pu ($t_{1/2} = 86$ years) and ^{239}Pu ($t_{1/2} = 24,110$ years). Due to high toxicity and long half life, Pu has to be considered as the most important actinides for the safety assessment of radioactive waste disposal [27]. The ground state electronic configuration of atomic Pu is $[\text{Rn}]5f^67s^2$. Plutonium ions in solution exists in +3, +4, +5 and +6 oxidation states as Pu^{3+} , Pu^{4+} , PuO_2^+ , PuO_2^{2+} [28]. The chemistry of Pu is in great contrast to the light elements of periodic table. In particular

it is very difficult to control. Some of the complexities of Pu chemistry in aqueous medium are listed as follows.

1.6.1. Problems in Pu aqueous Chemistry

Three reaction pathways have to be considered while investigating plutonium in aqueous systems. Hydrolysis, polymerization and colloid formation, and redox reactions of different oxidation states of plutonium. It is difficult to study one particular reaction without the interference of the other. Since all the reaction takes place simultaneously due to similar redox potentials of the couples, Pu (III)/Pu (IV) ($E^0 = -1.031\text{V}$), Pu (IV)/Pu (V) ($E^0 = -0.936\text{V}$), an equilibrium of two or more oxidation state may occur in solution. Differences in redox potentials for different oxidation states of Pu are given in figure 1.3.

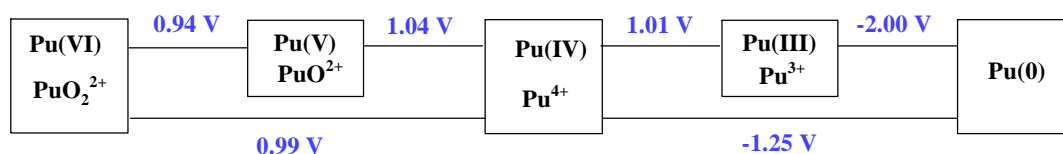
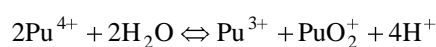
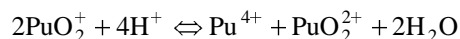


Fig. 1.3. The redox potential differences for the plutonium aquo ions in 1M perchloric acid, as well as the potential difference between the plutonium aquo ions and pure Pu.

In other words, Pu acts both as oxidizing and reducing agent at the same time. This is called disproportionation reaction. The disproportionation reaction mainly happens at elevated temperature. The equations governing the redox reactions for Pu ions under acidic conditions are,





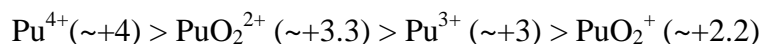
Disproportionation is the predominant reaction for low concentrations of Pu(IV) and pH 3, but polymerization dominates at pH greater than about 3.5.

➤ Conversely, under some conditions, two plutonium ions of different oxidation states can react by means of a reproporationation reaction. The two ions are simultaneously oxidized and reduced to form two ions of the same oxidation state.

➤ Another important complexity is that all plutonium isotopes are radioactive. One milligram of Pu emits about 10^6 alpha particles per second, and the radioactive decay is constantly adding energy to the Pu solution. This leads to radiolytic decomposition of water producing redox reagents such as short lived radicals $\cdot\text{H}$, $\cdot\text{OH}$, and $\cdot\text{O}$. These radicals recombine to form H_2 , O_2 and H_2O_2 . Thus radiolysis tends to reduce Pu(VI) and Pu(V) to Pu(IV) and Pu(III) states [29].

1.6.2. Plutonium (IV) polymerization

The tendency towards hydrolysis, polymerization and further to colloid formation is strongest for tetravalent plutonium as compared to other oxidation states due to its high effective charge. The effective charges for different oxidation state of plutonium are



Pu(IV) is stable only at highly acidic conditions and considerable amount of Pu(III), Pu(V), Pu(VI) are formed at $\text{pH} > 0$ as shown in figure 1.4.

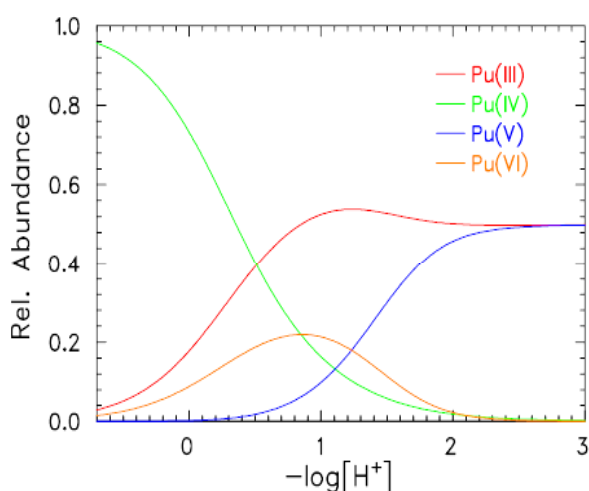


Fig. 1.4. Plutonium oxidation state distribution depending on $-\log[H^+]$ [30]

Only at $\text{pH} < 0.5$ $\text{Pu}^{4+}_{(\text{aq})}$ is the dominant species whereas with increasing pH the hydrolysis reaction leads to the quantitative formation of mononuclear complexes $\text{Pu}(\text{OH})_n^{4-n}$ where, $n = 1-4$. Rapid polymer formation takes place even in 1×10^{-3} and 1×10^{-4} M $\text{Pu}(\text{IV})$ solutions and close to solubility [31]. The polymeric plutonium refers to a hydrolytic form which is characterized by its bright emerald green color (Figure 1.5).

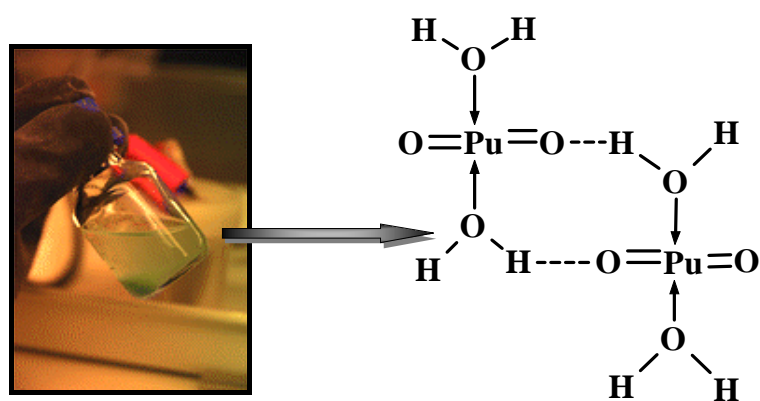


Fig. 1.5. Picture showing emerald green color $\text{Pu}(\text{IV})$ colloidal polymeric solution and its corresponding structure

The only means by which polymer formation can be avoided is to detect colloids that are formed initially in the solution. This is because the freshly formed polymer can be depolymerized whereas aged ones are difficult due to conversion of amorphous to crystalline form which involves the modification of hydroxyl bridges to oxo bridges (Figure 1.6) [32].

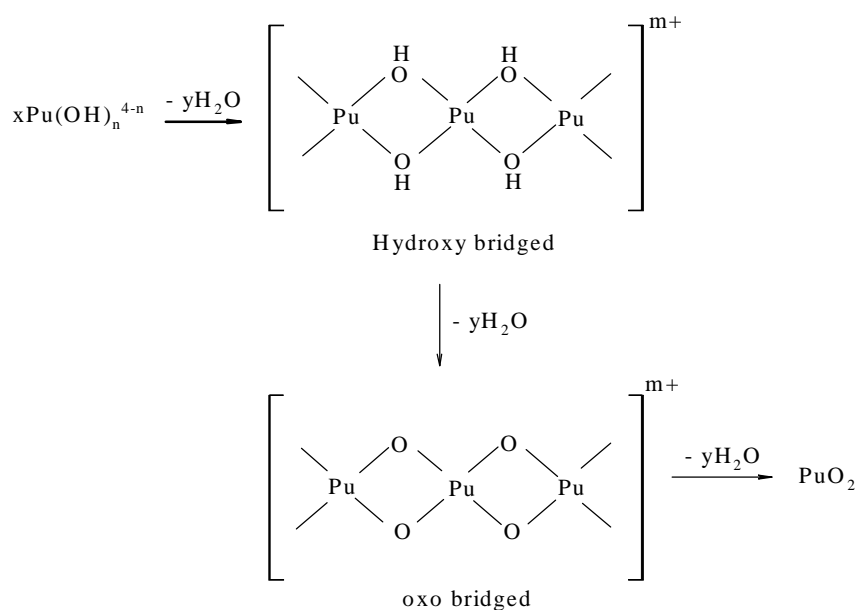


Fig. 1.6. Schematics showing the conversion of hydroxyl bridged polymer to oxo bridged polymer [32]

1.6.3. Parameters influencing the formation of Pu polymers/colloids

The formation and properties of polymers and colloidal hydroxides are directly dependent on *pH of the solution*. At alkaline pH, some hydroxide can form anionic complexes and possibly polymers. With increase in pH the degree of polymerization and formation of colloidal aggregates also increases [33]. *Ionic strength* of the electrolyte affects the solubility. Increase in ionic strength increases the coagulation. *Concentration of metal ion* has direct effect on polymerization and

colloid formation [21]. With decrease in Pu(IV) concentration, the pH of colloid formation increases [34]. The rate of polymerization is a function of *temperature*.

Polymerization can occur even at room temperature in solution less acidic than 0.3 M H⁺ and in 1.26 M H⁺ at boiling temperatures. The amount of polymer formed at 75°C is ~ 3.5 times greater than the amount at 25°C when the initial acidity is 0.075 M [35].

The free energy of plutonium polymer is estimated as about -341.9 kcalmol⁻¹ whose solubility product of Pu(OH)₄ corresponding to this number is 2.5×10⁻⁵⁶ [36]. This shows that the polymerization phenomenon is a very rapid and irreversible process. Order of polymerization of Pu(IV) reaction is estimated to be 3 [37]. Under conditions of low acidity and elevated temperature, the polymeric species require drastic treatment for conversion to the ionic state. The presence of low concentrations of Pu in natural waters and in disposal streams is of much interest to those concerned with radiation safety. These solutions are usually nearly neutral and any plutonium is probably in the polymeric state. Hence knowledge of the polymer is highly required in order to avoid its formation. Formation of Pu colloids can be detected by spectroscopic studies as each oxidation state of Pu and polynuclear Pu has its own characteristic color (figure 1.7a).

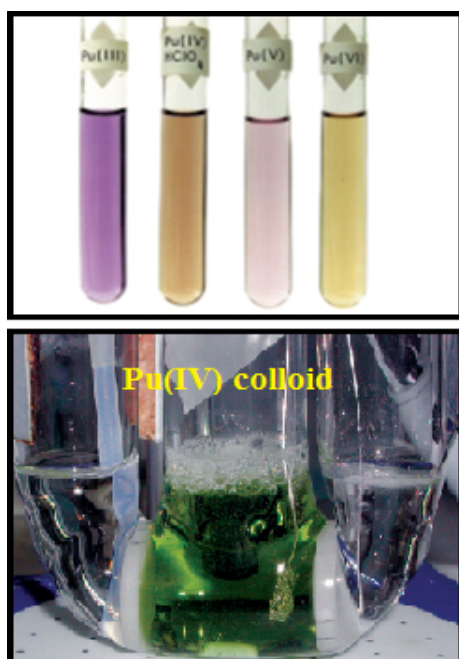


Fig. 1.7.a. Characteristic colors of each oxidation state of Pu and Pu colloids[29]

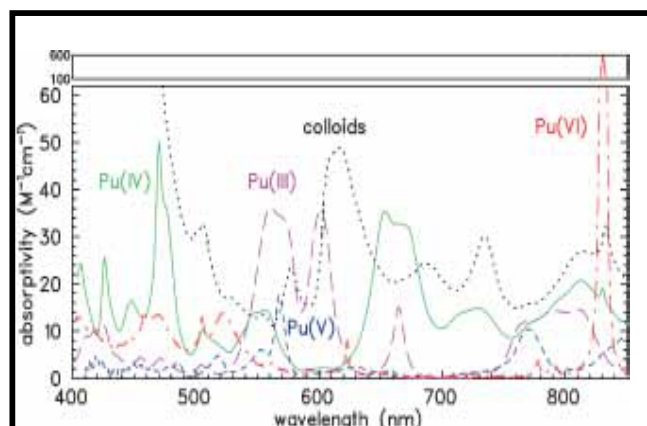


Fig. 1.7.b. Absorption spectra of different oxidation state of Pu and Pu colloids[38]

The absorption spectrum of polymeric Pu(IV) state is different from those of other Pu species (figure 1.7b). At pH 0-2, there is a steady decrease in the characteristic absorption band at 470 nm which is characteristic of ionic Pu(IV). They also show relatively broad, low intensity bands and rather intense with increasing absorption below 460 nm [38]. Polymerization of Pu(IV) leads to alterations in redox equilibria and additional easily identifiable spectral feature around 620 nm appears for the presence of small Pu(IV) colloids. Absorption spectra of aged polymers do not show any difference with that of fresh polymers except the pronounced 620 nm peak [16].

1.6.4. Probing the formation and structure of Pu(IV) polymer

Though first step in the formation of polynuclear species is the condensation of mononuclear species, there are no reports on the solution structure of Pu(IV) mononuclear hydroxides. As an evidence for the presence of dimer, an X – ray diffraction study has reported a solid state structure of $\text{Pu}_2(\text{OH})_2(\text{SO}_4)_3 \cdot 4\text{H}_2\text{O}$ with dimeric $[\text{Pu}_2(\text{OH})_2]^{6+}$ units linked by bridging sulfate ligands [39]. Electrospray mass spectrometry studies on dimers, trimers and tetramers revealed the presence of mixed oxidation states of Pu i.e Pu(III) and Pu(V) [40]. This gives an insight for the coexistence of monomeric and pentavalent Pu species with colloids and also their interference in redox reactions [41-43]. A hexanuclear $[\text{Pu}_6(\text{OH})_4\text{O}_4]^{12+}$ core with glycine ligands containing both oxo and hydroxo bridges were also reported [44]. The same linkage was also found in case of lanthanides [45]. Many studies were performed to probe the structure of polynuclear Pu(IV) species or colloids. The formation of the polynuclear species is assumed to involve hydroxide or oxygen bridging of plutonium ions but some reviews consider such species to be thermodynamically unstable [46-47]. As an alternative, they favor colloid formation from mononuclear hydroxide complexes. Thus Pu(IV) colloids are more stable in contrast to other tetravalent species such as Th(IV), U(IV) etc. The most widely accepted mechanism of formation of Pu colloid involves the condensation of $[\text{Pu}(\text{OH})_n]^{(4-n)+}$ through an olation reaction to yield hydroxo-bridged species. On further condensation, the hydroxo bridged oligomers produce mixed Pu oxide hydroxides [48]. X-ray absorption fine structure (XAFS) and Laser induced breakdown detection (LIBD) measurements proposed that the formation of Pu(IV) colloids follows by stacking 8 fold coordinated Pu units. It involves the formation of a

trinuclear species through hydrolysis and condensation of a monomeric $\text{Pu}(\text{OH})_2(\text{H}_2\text{O})_6^{2+}$ unit with a binuclear species to form single edge sharing, leading to the formation of neutrally charged species as product or a double edge sharing species with common corner. The dimers and trimers agglomerate and eventually form nm sized colloids (figure 1.8).

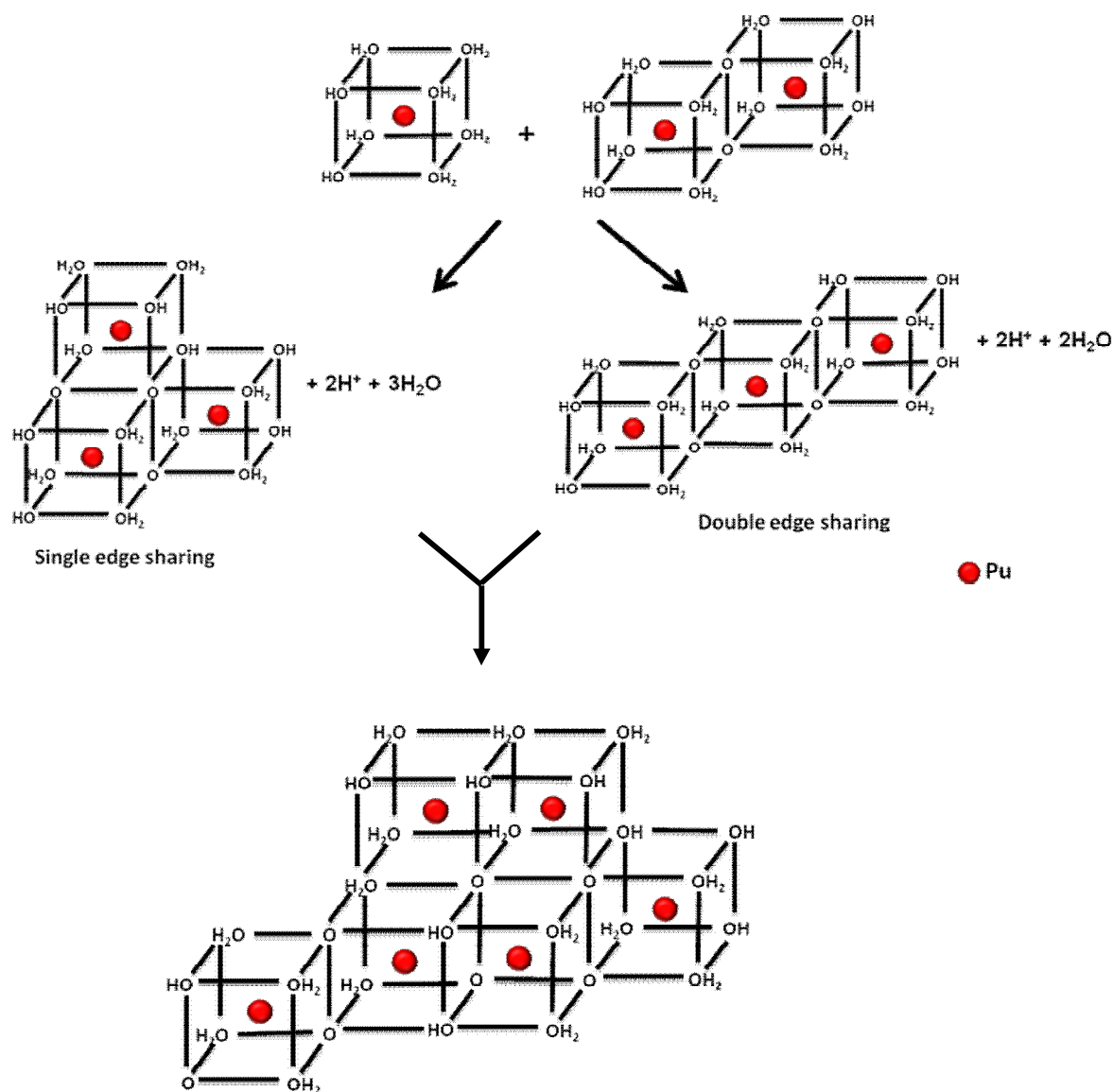


Fig. 1.8. Schematics showing mechanism of hydrolysis and polymerization of $\text{Pu}^{4+}_{(\text{aq})}$ leading to formation of nm size colloids [71]

The predominant species contain highly asymmetric oxygen coordination which indicates the presence of different Pu-O bond lengths from different coordinated oxygen atoms (-O, -OH, -OH₂). Pu_xO_y(OH)_{4x-2y}(H₂O)_z (0 ≤ y ≤ 2x) has been proposed as colloid structure formed by stacking of mononuclear or polynuclear building blocks on top of each other. During this process, the cubic subunits are preserved and form a distorted fluorite like Pu lattice [49]. Single crystals of 38 Pu nanoclusters [Li₁₄(H₂O)₂₀[Pu₃₈O₅₆Cl₅₄(H₂O)₈] and Li₂[Pu₃₈O₅₆Cl₄₂(H₂O)]·15H₂O were isolated for structural characterization using single crystal X-ray diffraction. Both structures consist of the [Pu₃₈O₅₆]⁴⁰⁺ core shown in figure 1.9, wherein 38 8-coordinate Pu(IV) cations are bridged exclusively via oxo linkages.

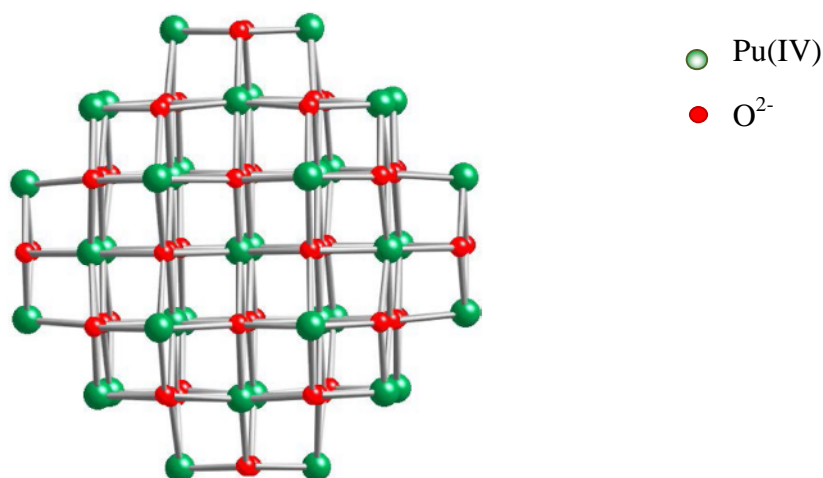


Fig. 1.9. Structure of [Pu₃₈O₅₆]⁴⁰⁺ core in the crystal structure of Li₁₄(H₂O)₂₀[Pu₃₈O₅₆Cl₅₄(H₂O)₈] and Li₂[Pu₃₈O₅₆Cl₄₂(H₂O)]·15H₂O [50]

The data clearly shows that intracuster packing and structural topology of clusters of composition [Pu₃₈O₅₆Cl₅₄(H₂O)₈]⁴⁰⁺ is identical with PuO₂ and the surface is occupied by chloride ion and water molecules [50-51]. However the solid state structure of the crystal does not contain Pu-OH moieties which contradict the structure proposed by

Rothe *et al* [49]. Small angle neutron scattering experiments were carried out on colloidal Pu(IV) suspensions in aqueous phase and polymer extracted into C_6D_6 solutions by alkyl esters of phosphoric acid. The results revealed the presence of long, thin rod like polymer in both the phases. However the diameter of ellipsoids of extractant-Pu(IV) polymer complexes in C_6D_6 are larger than that of aqueous polymer. This increase in diameter is due to the attachment of extractant molecules around the rod shaped Pu polymer. The length of aqueous Pu(IV) polymer is larger than the polymer extracted in C_6D_6 [52]. Figure 1.10 shows the schematics of Pu polymer in both aqueous and organic phase and their corresponding structure revealed by X-ray diffraction.

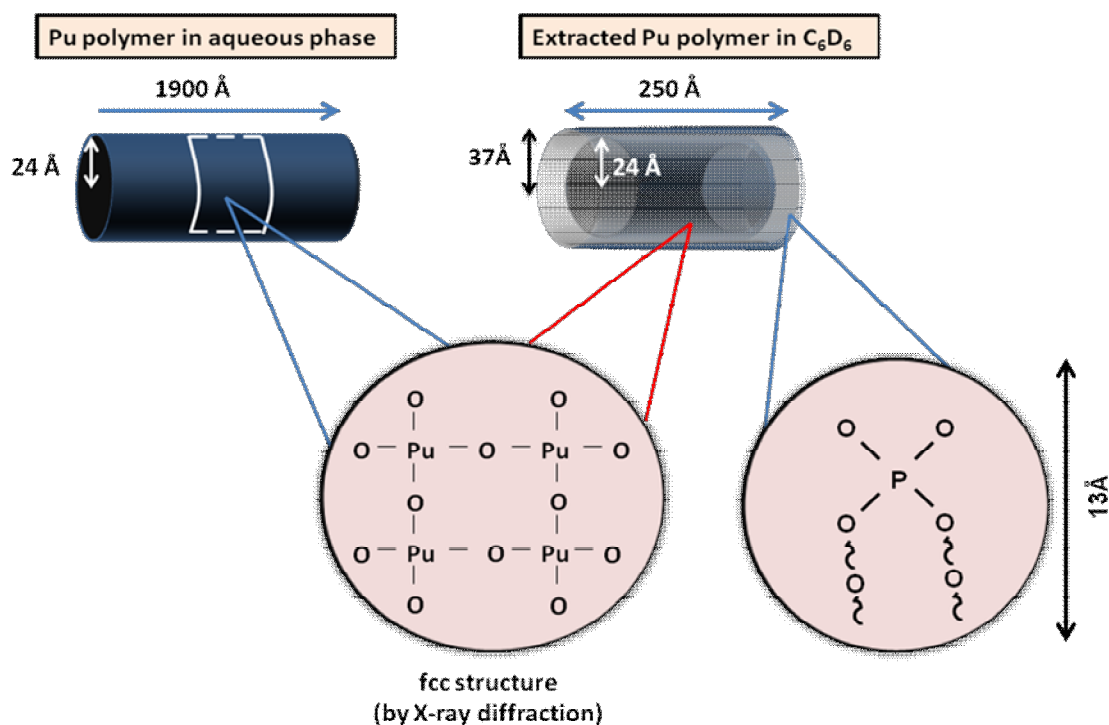


Fig. 1.10. Schematic representation of a model for observed Pu(IV) polymer [52]

A comparative study was also made between freshly prepared and five year old Pu(IV) colloids using Pu L_3 -edge EXAFS. The aged colloidal particles contains only

3-4 Pu atoms with a structure very similar to solid Pu(IV) oxide but with shorter Pu-O and Pu-Pu distances which was caused due to partial oxidation of Pu(IV) to Pu(V)/Pu(VI) [53].

1.6.5. Size and morphology of Pu(IV) colloid

Polymeric plutonium was observed in two forms: amorphous and crystalline primary particles and secondary particles which appeared to be aggregates of the primary particles. The X-ray diffraction patterns of precipitated Pu show a faint PuO₂ structure, suggesting that the hydroxide is in reality hydrated PuO₂ rather than Pu(IV) hydroxide. The precipitate becomes more crystalline when aged at elevated temperatures [54]. Similarly the precipitates aged in a basic or neutral medium display a crystalline pattern that corresponds to the cubic PuO₂ structure and was confirmed by electron diffraction pattern. Colloidal particles formed in highly acidic media differ from those formed at higher pH [55]. Thus colloid morphology varies strongly depending on the method of preparation, conditions of formation and on the age of the solutions. For instance, fast neutralization of Pu(IV) solutions with a base or water usually forms less ordered structures [56]. Scanning Electron Microscopy (SEM) and Transmission Electron Microscopic (TEM) images shows amorphous morphology for these polymers [57].

The IR spectrum of Pu(IV) polymer showed major bands at 360 and 3400 cm⁻¹. They are assigned to Pu-O vibration similar to crystalline PuO₂ and to OH stretching vibration of a water group which is either hydrated or occluded in the polymer structure. The comparison of the IR spectrum of PuO₂ and the Pu(IV) polymer precipitated and dried in air are shown below (figure 1.11).

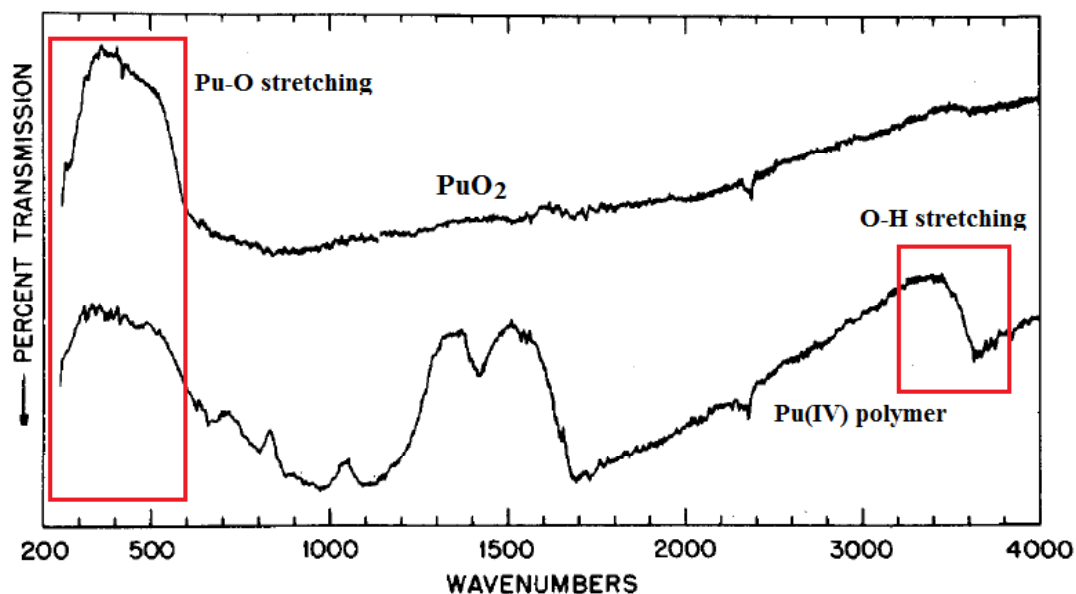


Fig. 1.11. IR spectra of PuO₂ and Pu(IV) polymer precipitated and dried in air [38]

The close resemblance of the polymer bands in the 250-600 cm⁻¹ region suggests a similar lattice structure in the two compounds. Unlike PuO₂, water and possibly hydroxyl groups are present in the polymer [58]. The size of Pu(IV) colloids ranges from a few nanometers to almost micrometers, depending on the conditions of generation [59-60].

Electron micrograph shows that the primary particles are extremely small of the order of 5 to 20 Å whereas the amorphous primary particles are in the order of 10 Å [61]. TEM analyses of dried solutions show evidence of small PuO₂ like clusters with a diameter of about 2 nm [58]. LIBD experiments gave mean particle size of 5 nm to 12 nm [25]. It is observed that, the particle size may increase to the point of precipitation. In acidic solutions (pH 0.4-1) the weighted mean colloid size increases from 12 to 25 nm with increasing degree of oversaturation with respect to amorphous Pu(IV) hydroxide. They are said to be composed of small crystalline particle covered

by an amorphous layer [62]. The SAXS and X-ray diffraction affirmed the presence of $< 40 \text{ \AA}$ PuO_2 clusters [52]. Dynamic light scattering (DLS) and field flow fractionation (FFF) indicates that the hydrodynamic radii of colloids vary on the order of $20 - 200 \text{ \AA}$ and also, the colloid density is slightly lower than the density of PuO_2 [63].

As a matter of fact, the size of Pu colloids should increase with ageing time. But in contrary, a recent report suggested that there was reduction in size of 5 year aged colloid due to partial oxidation of Pu(IV) resulting in shorter Pu-O and Pu-Pu bond distance [53].

1.6.6. Hydrolysis and solubility of Pu(IV)

The hydrolysis reactions of Pu^{4+} ions are generally written as



The hydrolysis constants K_{xn}' in a given medium and K_{xn}^0 (at infinite dilution) are given by

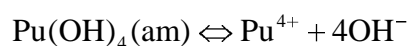
$$K_{\text{xn}}' = \frac{[\text{Pu}_x(\text{OH})_n^{4x-n}][\text{H}^+]^n}{[\text{Pu}^{4+}]^x} = \frac{K_{\text{xn}}^0 (\gamma_{\text{Pu}^{4+}})^x (a_w)^n}{(\gamma_{\text{Pu}_x(\text{OH})_n^{4x-n}})(\gamma_{\text{H}})^n}$$

And the corresponding formation constants β_{xy}' and β_{xy}^0

$$\beta_{\text{xn}}' = \frac{[\text{Pu}_x(\text{OH})_n^{4x-n}]}{[\text{Pu}^{4+}]^x [\text{OH}^-]^n} = \frac{\beta_{\text{xn}}^0 (\gamma_{\text{Pu}^{4+}})^x (\gamma_{\text{OH}^-})^n}{(\gamma_{\text{Pu}_x(\text{OH})_n^{4x-n}})(\gamma_{\text{H}})^n}$$

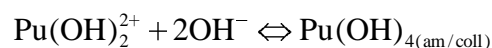
γ is the activity coefficient and a_w is the activity of water. The value of $\log \beta_{11}^0$, was found as 14.6 from experiments at trace levels of Pu where the formation of polynuclear species is less likely [64]. Another most important property of tetravalent

actinide ions in aqueous medium is the solubility. It is important mainly for mobility of Pu colloids in aquifer systems. Since Pu(IV) hydroxide phases or colloids span wide range of structural features and surface properties, such as amorphous/crystallinities, size distributions [65] and stabilities and it therefore exhibits wide range of solubilities [66-67] and thus the reported solubility product show considerable discrepancies [68-70]. In general the solubility products of the amorphous An(IV) hydroxide decrease in the series, Th(IV) > U(IV) > Np(IV) > Pu(IV) due to decrease in An-O distance in the lattice [66,47]. The same trend is observed for crystalline An(IV) dioxides. The solubility products K_{sp}' and K_{sp}° (at infinite dilution) of amorphous Pu(IV) oxide or hydroxide, Pu(OH)₄(am) is given by the following equilibrium,



$$K_{sp}' = [\text{Pu}^{4+}][\text{OH}^-]^4 \text{ and } K_{sp}^{\circ} = K_{sp}'(\gamma_{\text{Pu}})(\gamma_{\text{OH}})^4$$

$\log K_{sp}^{\circ}$ for crystalline PuO₂ is -64.0 and for amorphous hydrated hydroxide -58.3 [47]. Thus crystalline PuO₂ is far less soluble than its amorphous hydroxide. The slope of the solubility curve obtained from LIBD studies (figure 1.12) provides further evidence that the dihydroxo-complex (Pu(OH)₂²⁺) is the prominent species in the range 1.0 < pHc < 1.6. The slope = -2 for the solubility curve, infers that colloid formation proceeds from Pu(OH)₂²⁺ *via* consumption of 2OH⁻ per Pu(IV) ion suggesting the reaction [71].



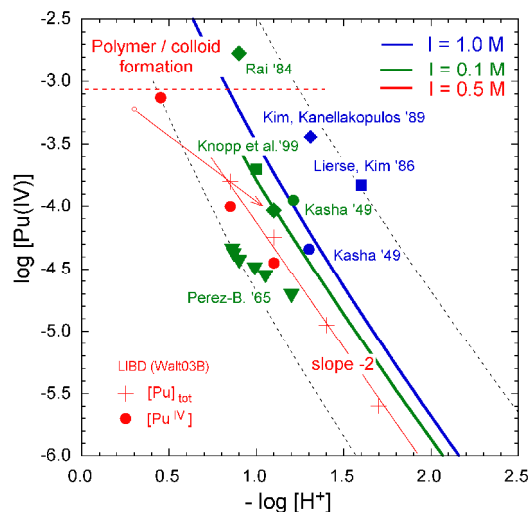


Fig. 1.12. Solubility of amorphous $\text{Pu}(\text{OH})_4$ comparing available literature data [71]

1.6.7. Molecular weight of Pu(IV) polymer

The free diffusion experiments indicate the minimum molecular weight of polymeric Pu(IV) to be 4×10^3 Da [72-73]. Track counting in a nuclear emulsion gave an average molecular weight of 10^{10} for large particles. Other values of 4×10^5 Da by diffusion studies and 2×10^7 Da by high speed centrifugation have also been reported [74]. The molecular weight of the colloid increase with ageing time and it depends on condition of formation [75].

1.7. Pu(VI) hydrolysis

Pu(VI) hydrolysis did not gain much importance as compared to Pu(IV) hydrolysis due to relatively lower hydrolysis rates (in minutes). But the alpha decay of ^{239}Pu in aqueous solution results in the radiolytic formation of peroxide and radicals, which reduce Pu(VI) over composition and concentration, pH, nature and concentration of additional species present to Pu(IV) which eventually forms colloids at low acidities [41].

1.8. Ways to remove polymers

Two ways can be adopted to remove the polymers formed in the system. They can be either extracted or depolymerized.

1.8.1. Extraction of Pu(IV) polymer/colloid

Attempts were made to extract Pu polymers or colloids using neutral extractant TOPO (trioctylphosphine oxide), CMPO (octylphenyl-N,N-diisobutylcarbamoylmethylphosphine oxide) and the bifunctional extractants DHDECMP (dihexyl-N,N-diethylcarbamoylmethyl phosphonate). But in most of the cases there is crud formation. They also co-extract metals of other oxidation state [76]. Back-extraction of the polymer was done either in a silica sol or requires large concentrations of salts to reverse the extraction [77]. A novel approach was made by dissolving the $[\text{Pu}_{38}\text{O}_{56}\text{Cl}_{54}(\text{H}_2\text{O})_8]^{14-}$ nanocluster in aqueous solution of LiCl producing green solution of colloidal Pu which was confirmed by the optical spectra. Addition of 6M HCl changes green coloured solution to red with change in the spectrum. The rapid change involves ion- or ligand exchange reaction between water and Cl⁻. But the core moiety, $\text{Pu}_{38}\text{O}_{56}$ remains unperturbed. Trichloroacetic acid (TCA) in *n*-octanol was chosen as extractant due to its immiscibility with water. The well defined surface of Pu colloids can be altered and manipulated which can involve in ion and ligand exchange reactions resulting in selective extraction of only Pu colloid leaving other Pu species in aqueous phase [51]. Figure 1.13 shows the extracted colloid in TCA/*n*-octanol organic phase.

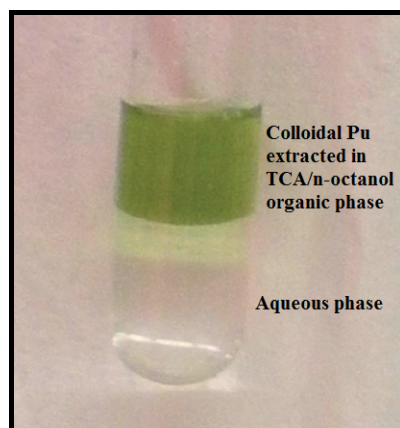


Fig. 1.13. Partitioning of colloidal Pu from the bottom aqueous phase to top organic TCA/n-octanol organic phase [73]

1.8.2. Depolymerization

Depolymerization of Pu polymer is a slow process. Freshly formed polymer can be depolymerised, whereas aged or polymers heated to higher temperatures are difficult to depolymerize and it needs drastic conditions. In other words, it leads to very low depolymerization rates due to conversion of amorphous to crystalline primary particles which involves more extensive cross linking [78-79]. Table 1.1 clearly shows the halftimes for depolymerization of Pu(IV) polymer formed at different temperatures and acidities [28].

Table 1.1. Half times for depolymerization of Pu(IV) polymer [28]

Formation Temperature (°C)	[HNO ₃]			
	2M	4M	6M	10M
25	20 days	400 min	100 min	30 min
80	1 year	-	15 days	-

Some of the reported methods applied for depolymerizing the polymer if formed accidentally are listed below.

1.8.2.1. Proposed methods for depolymerizing Pu(IV) polymer

- Pu(IV) polymers can be depolymerized in the presence of reductants and oxidants such as hydroquinone, H_2O_2 , hydroxylamine, U(IV) and KMnO_4 , $\text{H}_2\text{O}_2 + \text{Fe}(\text{NO}_3)_3$, $\text{Na}_2\text{S}_2\text{O}_8 + \text{catalysts}$, Co(III) in 0.533M HNO_3 . This is because Pu(III) and Pu(VI) formed due to reduction and oxidation are not prone to polymerization [80-81].
- Passing direct current through an aqueous nitric acid solution which contains Pu(IV) polymer converts the polymer to Pu^{3+} and PuO_2^{2+} and Pu^{3+} and PuO_2^{2+} ions in turn are converted to Pu^{4+} ions in the solution, followed by the step in which Pu^{4+} ions are extracted from the solution. This can be done by contacting the acid solution with a solution containing about 30% tri-n-butyl phosphate and 70% hydrocarbon diluent (such as dodecane). It can also be done with ion exchange resin [82].
- To avoid the complications of colloid formation, Pu has often been injected as the citrate complex, prepared by adding $\text{Pu}(\text{NO}_3)_4$ in concentrated nitric acid to a 0.3-2.0% solution of tri-sodium citrate followed by adjustment with base to pH 4-7. The rate of depolymerisation is directly proportional to citrate concentration, time and acidity [83].
- Depolymerization is accelerated by introducing, fluoride, sulfate and other ions into the system which can form strong complexes with Pu^{4+} [84].

- The process of depolymerization is accelerated on exposure to UV radiation [85-86].
- *Uranyl nitrate effect*

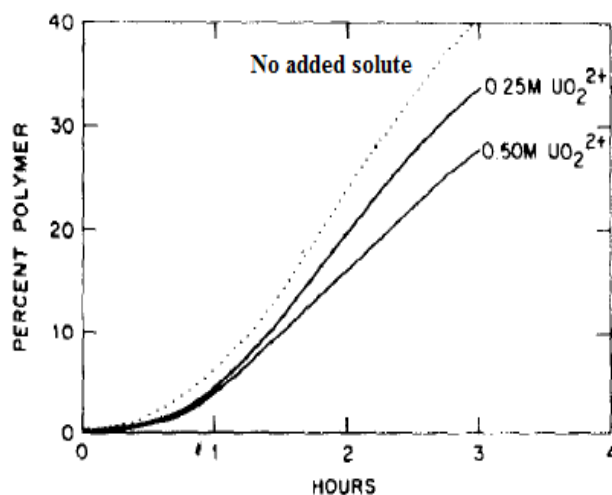


Fig. 1.14. Effect of uranyl nitrate on Pu(IV) polymerization rate ([Pu(IV)] = 0.05 M, [HNO₃] = 0.11 M, at 50° C) [87]

Solutions of Pu will commonly be used in the presence of large amounts of U. Therefore the effect of uranyl ion on the polymer chemistry is of considerable interest. Much uncertainty exists about the effect of UO₂(NO₃)₂ on the formation rate of Pu(IV) polymer because this solute provides nitrate ions which could either complex with Pu(IV) and stabilize it with respect to hydrolysis and polymerization or through complexation with Pu(IV), shift the disproportionation equilibrium to the left, thereby decreasing the real acid concentration of the solution and causing a corresponding increase in the rate of hydrolysis and polymerization. UO₂²⁺ functions as a chain terminator through the formation of hydroxyl bridges to terminal uranyl groups [87].

Also, Pu(IV) polymer formed in the presence of uranium are shorter than those which are formed in the absence of uranium. This shows that presence of U in a polymerizing Pu(IV) solution reduces the rate of polymer formation about 30% without appreciably entering the polymer [52]. Figure 1.14 clearly depicts the effect of uranyl nitrate on Pu(IV) polymerization rate.

- Costanzo & Biggers [88] prepared polymer in 5N HNO₃ and aged for several months. It is observed that for aged polymers the depolymerization half time is 320 hrs and it is only 20 hrs for freshly prepared polymer.
- There are also published data on the chemical and physical methods of depolymerization of plutonium [89]. For example, at 90°C in 6M HNO₃ this process occurs easily. Decomposition of S₂O₈ yields H₂SO₄ favoring Pu(IV) depolymerization. Thus polymer can be dissolved using Na₂S₂O₈.

1.9. Analogues taken to study hydrolytic behavior of Pu(IV)

It is a common practice in radiochemistry to perform preliminary experiments with stable or less radioactive analogues prior to the investigation of the element of interest mainly to validate new experimental methods, to minimize radioactive dose and to save rare material. In case of plutonium, elements such as zirconium, thorium and uranium are often chosen as analogues. The reasons for choosing the above said elements are as follows.

1.9.1. Zirconium

The name Zirconium is derived from the word “zargon” meaning gold-like. It is mainly obtained from the ores zircon (ZrSiO₄) and baddleyite (ZrO₂) by Kroll process [90]. The corrosion resistant (resistance towards attack by acids, bases

and even sea water) property of metallic zirconium led to extensive use of it in chemical industries. Zirconium is of great importance in nuclear industry where it is widely used as cladding for nuclear fuel (UO_2) rods in water cooled reactors. Zircalloys are favored over stainless steel owing to lower neutron cross section and thermal conductivity [91]. Zirconium hydride is used as moderators in nuclear reactors. Zirconia is an important ceramic product which finds application in fields like ceramic engineering, piezoelctronics, ion exchange and catalysis. Zirconium is a highly stable element and has strong tendency towards hydrolysis. It occurs as tetravalent ion in solution. The onset of hydrolysis of zirconium occurs in strongly acidic solution ($\text{pH} < 0$) and is dominated by the formation of polynuclear species [92]. Due to similar ionic radii compared to that of Pu(IV), Zr(IV) serves as a homologue for Pu(IV).

1.9.2. Thorium

Thorium is an attractive nuclear material, mainly due to its abundance, the opportunity to reduce the need for enrichment in the fuel cycle, the high conversion ratios (to ^{233}U) achievable in a thermal neutron spectrum, and also due to other neutron and thermal physical properties. ^{232}Th is the major isotope found in nature. It has the longest half-life among all actinides ($T_{1/2} = 1.4 \times 10^{10}$ y) [93]. None of the thorium isotopes are fissile. Small amounts of millimolar solutions remain far below the permitted limit that can be handled in inactive laboratories which opens up wide range for many experimental validations. In aqueous solution, thorium exists only in the tetravalent state. Thorium has an ionic radius of 1.09 Å in nine coordination making it the largest stable tetravalent metal ion and in spite of its high valence, it is least susceptible to hydrolyze [94]. The hydrolytic behavior of the ion is known to be

extremely complex because of the presence of extensive polymerization reactions, which occurs in a narrow pH range which is similar to Pu(IV). Hence it is believed to be a better analogue for Pu(IV).

1.9.3. Uranium

Uranium is the heaviest naturally occurring element and is found at an average concentration of 0.0003% (3 mg/kg) in the earth's crust. It is mainly used as fuel in nuclear reactors by increasing the relative concentration of ^{235}U (only fissile isotope of uranium). Uranium exists in different oxidation state. In nature it mainly occurs in oxidized form U(VI), which is the stable state. The chemistry of uranium in aqueous solution is governed by the dioxo cation UO_2^{2+} . U(IV) aqueous chemistry are of particular interest only under reducing conditions. Reducing condition prevails in both the inside of nuclear waste repositories and under deep uranium mines [95]. U(IV) also shows high tendency for hydrolysis, polymerization and colloid formation which are the reasons why it has been chosen as analogue for Pu(IV).

1.10. Colloids

Understanding the polymer-colloid chemistry of actinides needs a general introduction on colloids, their properties and the parameters necessary for their stability. The term "*colloid*" was coined by Thomas Graham in 1860 to represent substances which do not diffuse through a semi-permeable membrane. It normally refers to two phase systems in which finely divided particles of one phase, the dispersed phase are distributed in a second phase, the dispersion medium. The IUPAC definition for the term colloidal refers to "state of sub-division in which molecules or polymolecular particles dispersed in a medium have at least a dimension roughly

between 1 nm and 1000 nm in size” [96-97]. Colloidal systems are subject to large variety of interparticle forces which determine the macroscopic properties of the colloidal suspension.

1.10.1. Sources

All natural waters contain sub-micrometer size colloids formed as a result of weathering of rocks and minerals (e.g., clays, silica, aluminum oxide minerals) as well as hydroxide or hydrated oxides of metals (e.g., iron), soils and plants. Various natural organic colloids (humic or fulvic substances) are also present. The amount and nature of these colloids depend on the surrounding geologic structure. They are present in large numbers ranging from 10^6 particles per ml in granitic waters to 10^{12} particles per ml in near surface waters [98]. Sources of actinide particles in the environment other than the above said means originate from nuclear explosions, minor occurrences such as nuclear powered satellites, nuclear power plant accidents and particle contaminants released from military activities such as nuclear submarines, ammunition etc., and mainly from activities related to nuclear power production (e.g., mining and fuel fabrication). With a time scale of >1000 years water might corrode the containers and can cause leaching of glass leading to release of radionuclides into the environment [99]. Two kinds of colloids are formed in natural waters. Intrinsic colloids are formed by condensation and aggregation of hydrolyzed actinide hydroxide molecules or ions as discussed earlier and pseudo colloids are formed by adsorption of actinide ions on aquatic colloids (Figure 1.15) [100].

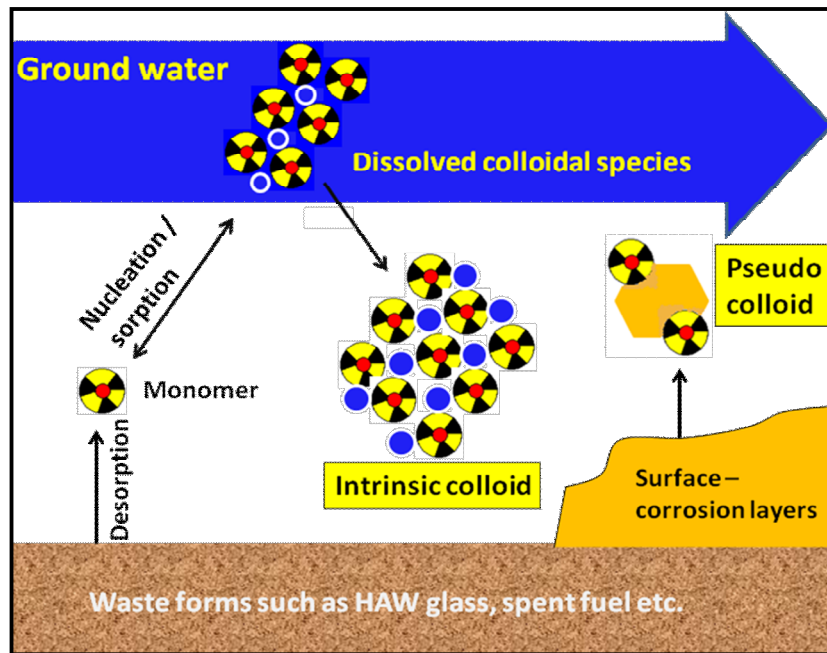


Fig. 1.15. Leaching or dissolution of radioactive waste leading to formation of intrinsic and pseudo colloids in solution [30].

1.10.2. Forces responsible for colloid stability

Three fundamental forces operate on fine particles in solution are, a *gravitational force*, tending to settle or raise particles depending on their density relative to the solvent. A *viscous drag force*, which arises as a resistance to motion, since the fluid has to be forced apart as the particle moves through it. The '*natural*' *kinetic energy* of particles and molecules, which causes Brownian motion.

In colloidal dispersion, the kinetic random motion dominates the behavior of small particles which will not allow settling and the dispersion will be completely stable. If a colloidal particle is brought to a short distance to another particle, they are attracted to each other by the Van der Waals force. If attractive forces (such as van der Waals forces) prevail over the repulsive ones (such as the electrostatic ones) particles

aggregate as clusters. Electrostatic stabilization and steric stabilization are the two main mechanisms for stabilization against aggregation.

- Electrostatic stabilization of colloids

In liquid dispersion media, ionic groups can adsorb to the surface of a colloidal particle forming charged layer. To maintain electroneutrality, an equal number of counter-ions with the opposite charge will surround the colloidal particles and give rise to overall charge-neutral double layers. In charge stabilization, it is the mutual repulsion of these double layers surrounding particles that provides stability.

- Polymeric stabilization of colloids

Polymeric stabilization of Colloids involves polymeric molecules added to the dispersion medium in order to prevent the aggregation of the colloidal particles. The polymeric molecules create a repulsive force counterbalancing the attractive van der Waals force acting on a particle approaching another particle. There are two types of polymeric stabilization:

- *Steric stabilization* of colloids is achieved by polymer molecules attached to the particle surface and forming a coating, which creates a repulsive force and separates the particle from another particle.
- *Depletion stabilization* of colloids involves unanchored (free) polymeric molecules creating repulsive forces between the approaching particles [101].

1.10.3. Migration behavior of actinide colloids in environment

The particulate matter has a high surface to mass ratio. The surface area of a 1 cm diameter sphere ($4\pi r^2$) is 3.14 cm², whereas the surface area of the same

amount of material but in the form of 0.1 mm diameter spheres (i.e. the size of the particles in latex paint) is 3,14,000 cm². The enormous difference in surface area is one of the reasons why the properties of the surface become very important for colloidal solutions [102]. The migration of radioactive species away from a geological disposal facility (GDF) is mainly due to their potential for sorbed radionuclides. Since actinide colloids formed in natural waters are very small ~ 50 nm, the large surface to volume ratio of colloids in conjunction with often considerable surface charge makes them chemically reactive species. In addition to that they have large surface to volume ratio which enhances their mobility. It is well known that aquatic colloids migrate faster in the aquifer under certain conditions. The mobility enhancement due to colloid mediated transport is most pronounced for substances of low solubility (particularly the tri and tetravalent actinides) which are expected to form precipitates in or close to the repository. Plutonium, once thought immobile in the subsurface, can be transported with the colloidal fraction of groundwater. Under most soil conditions, even Pu(V), reduces to more insoluble Pu(IV) on the surface of minerals and sediments and can attach to naturally occurring colloids or it can hydrolyze to become its own colloids. They are transported by the groundwater flow. Intrinsic Pu nanocolloids are 2-5 nm in diameter and hence have high mobility [103-104]. Characteristics of actinide colloids need further research mainly to avoid the ill effects of such particles on human health and impact on environment.

1.10.4. Characterization of colloids

Particle size distribution is one of the very important parameter of a colloidal suspension. It can be determined by different techniques available and each of them is characterized by their nature of measurement. Invasive nature of a

technique refers to disturbing the system as a whole and destructiveness of a technique refers to damaging the system and making it unavailable for further investigation. Table 1.2 lists the different techniques applied most frequently for deriving size distribution of colloidal dispersion. Among the different techniques listed in the table, photon correlation spectroscopy (PCS) or in general light scattering technique (based on interaction of system with visible light) is one of the most standard size characterization techniques which allow in-situ measurements without sample preparation. DLS measures the hydrodynamic radius of the colloidal particle. By definition, the DLS measured radius is the radius of a hypothetical hard sphere that diffuses with the same speed as the particle under examination. This is always not true with regard to visualization, since hypothetical hard spheres are non-existent. In practice, macromolecules in solution are non-spherical, dynamic and solvated. As such, the radius calculated from the diffusional properties of the particle is indicative of the apparent size of the dynamic hydrated/solvated particle. Hence the terminology, 'hydrodynamic' radius. It is very sensitive, non invasive and non destructive colloid characterization technique which allows detection of colloids whose size ranges from 2 nm – 2 μ m. However the sensitivity of detection strongly depends on the particle size. Since aquatic colloids are very sensitive to handling and delicately balanced systems, non-invasive nature of this technique allows the possibility of characterizing aquatic colloids without disturbing the whole system. Molecular weight of colloidal polymers can also be determined which adds another advantage to this technique.

Table 1.2. Different methods for determination of colloid size and the corresponding nature of the technique, where S = single particle, P = Populations are determined, S(P) = Single particle on an average over many measurements [52].

Method	Size (nm)	Concentration	Statistics	In- situ	Preparation	Invasive/ Destructive	Ref.
Centrifugation	50-10 ⁵	ppb	P	(x)	Med.	x/(-)	105
Filtration	>1	ppb	P	(x)	Med.	x/(-)	106
Sedimentation	>10	ppm	P	-	Med.	x/x	107
Field flow fractionation, FFF	>2	DM	P	-	Low	x/-	108
Transmission electron microscopy, TEM	0.5-100	ppm	S	-	High	x/x	109
Scanning electron microscopy, SEM	>10	ppm	S	-	High	x/x	110
Atomic force microscopy, AFM	1-1000	ppm	S	(x)	Med.	x/(-)	111
Static light scattering, SLS	>100	ppm	S(P)	x	None	-/-	112
Single particle counter, SPC	>30	ppq	S(P)	x	None	-/-	113
Photon correlation spectroscopy, PCS	2-2000	ppm	S(P)	x	None	-/-	114
Laser induced breakdown detection, LIBD	>5	ppt	S(P)	x	None	-/x	103

1.11. Motivation

Hydrolysis and subsequent polymerization of the tetravalent plutonium in process work may result in a variable loss of plutonium in the aqueous waste because polymeric plutonium is neither extracted by usual solvents, nor sorbed on ion-exchange resins. Pu(IV) polymer is inert to ion exchange techniques and most organic extraction systems. The polymeric form of Pu(IV) is easily adsorbed on to surfaces with which it comes into contact. The presence of colloid also causes foaming in concentration by evaporation and emulsification in solvent extraction operations. This polymerization phenomenon is a very rapid, irreversible process under conditions of low acidity and elevated temperature, and the polymeric species require drastic treatment for conversion to the ionic state. The presence of low concentrations of Pu in natural waters and in disposal streams is of much interest to those concerned with reactor and radiation safety. These solutions are usually nearly neutral and any plutonium is probably in the polymeric state. Therefore, the removal of such plutonium will require the knowledge of colloid polymer with respect to their behavior in aqueous solution. To study plutonium polymers and colloids, some of the safety requirements have to be met. Hence the inactive analogues such as zirconium, thorium and uranium can be used for investigation and the results can be used for understanding the hydrolytic behaviour of plutonium. Colloidal polymers can be characterized by many methods depending on the size and concentration range. PCS is being used in the present study to characterize the colloids formed in aqueous systems due to the applications as mentioned earlier. Characterizing the colloidal polymers of actinides formed at different concentration and acidities by using light scattering technique forms the primary motive of the present study.

1.12. Objectives

The main objectives of the present work are the following:

- To obtain insight into the hydrolytic reactions of metal ions such as Sr(II), Bi(III), Al(III), Zr(IV), U(IV), Th(IV) and U(VI) by Dynamic Light Scattering (DLS) technique.
- To understand the mechanism of colloid formation and to find the molecular weight of freshly prepared colloids as well as colloids aged at different time intervals by static light scattering technique.
- To find the interaction parameters existing between the polymer and solvent using the second virial coefficient.

1.13. Overview

The thesis consists of seven chapters. **Chapter 1** gives a brief introduction about the nuclear power program, review of reported literature data on the aqueous chemistry of actinides with special emphasis on polymerization and colloid formation of plutonium and their consequences on reprocessing and storage of nuclear waste under deep geological repositories, colloids and their stability, motivation and objectives of the present study. **Chapter 2** describes the details of sample preparation, the experimental tools used to probe the size, molecular weight and stability of colloids. The hydrolysis of Sr(II) and Al(III) at high acid medium was studied by light scattering technique and the hydration number was predicted. Bi(III) hydrolysis was studied at various acidities and the size and molecular weight of the colloids formed were also determined. The results from these studies are summarized in **chapter 3**. Hydrolytic behavior of tetravalent zirconium which was taken as analogue for Pu(IV) was studied.

Spectrophotometric method was developed to determine zirconium in ppm range under acidic condition. The polymer formed was characterized by DLS. Molecular weight for freshly formed as well as aged at different time was reported. The comprehensive compilation of results from these studies forms **chapter 4**. **Chapter 5** focuses on the hydrolysis reactions of both tetravalent and hexavalent uranium. The colloids formed were detected by spectroscopic technique and it was then characterized by DLS. The polymers were aged at different time intervals and molecular weight was predicted. **Chapter 6** mainly focuses on hydrolysis reactions of Th(IV). Similar experiments were carried out and the results were discussed in detail in this chapter. **Chapter 7** summarizes the results obtained, conclusions drawn and the scope for future work.

Chapter 2



CHAPTER 2

Experimental Section

This chapter describes about various experimental techniques used for the present study. This comprises of basic principles involved in the techniques such as UV-Vis spectrophotometry, Attenuated Total Reflection - Fast Fourier Transform spectrometry (ATR-FTIR), Refractometer, X-ray diffraction and light scattering technique (both dynamic and static light scattering) that have been used for the investigation.

2.1. Chemicals and reagents

All the chemicals used in this study were of analytical grade and used without further purification. The chemicals were obtained from the following suppliers.

M/s Acros Organics: Aluminium nitrate nonahydrate ($\text{Al}(\text{NO}_3)_3 \cdot 9\text{H}_2\text{O}$) with minimum assay of >99.0%.

M/s Wilson lab: Zirconium nitrate $\text{Zr}(\text{NO}_3)_4$ with minimum assay of >99.0%.

M/s Loba Chemie, Mumbai, India: Zirconyl nitrate monohydrate ($\text{ZrO}(\text{NO}_3)_2 \cdot \text{H}_2\text{O}$).

M/s Glaxo Laboratories: Bismuth nitrate pentahydrate ($\text{Bi}(\text{NO}_3)_3 \cdot 5\text{H}_2\text{O}$) in crystalline form (minimum assay of 98.0%).

M/s Alfa Aesar: Anhydrous strontium nitrate ($\text{Sr}(\text{NO}_3)_2$) with a minimum assay of 99.0%.

M/s British Drug Houses Ltd. (M/S BDH): Uranyl nitrate hexahydrate ($(\text{UO}_2)(\text{NO}_3)_2 \cdot 6\text{H}_2\text{O}$)

M/s S. D. Fine Chemicals Ltd.: Sodium dihydrogen phosphate dihydrate ($\text{NaH}_2\text{PO}_4 \cdot 2\text{H}_2\text{O}$) with minimum assay of 97%, Thorium nitrate pentahydrate ($\text{Th}(\text{NO}_3)_4 \cdot 5\text{H}_2\text{O}$) with minimum assay of 99.0%.

M/s Merck, Mumbai: Ammonium molybdate ($(\text{NH}_4)_6\text{Mo}_7\text{O}_{24} \cdot 4\text{H}_2\text{O}$) with minimum assay of 99.0%, Sodium hydroxide pellets in pure form with minimum assay of 97%.

M/S Fisher: Nitric acid solutions were prepared from concentrated HNO_3 (assay of 69-71% w/w). The concentration of the solutions was estimated by titrimetry by using standard NaOH solution using phenolphthalein as indicator.

ASTM Grade-1 water obtained as per ASTM D-1193 with a resistivity of 18.2 $\text{M}\Omega \cdot \text{cm}$ at 298.15 K and TOC < 15 ppb from a MILLIPORE Simplicity system was used in the experiments for reagent/solution preparation and water as standard.

All the salts used for the study were weighed in a precision Shimadzu AUW220D balance (220 g, 0.01 mg resolution).

2.2. Experimental Techniques

2.2.1. Light scattering technique -Theory

When light (electromagnetic radiation) is directed towards a solution, the photons are either absorbed, transmitted (they do not interact with solution) or reemitted as light of lower frequency (fluorescence, phosphorescence) or scattered.

Scattering occurs due to non-homogeneties in the medium through which they pass. In case of light scattering, this is the interaction of the electric light vector with electrons.

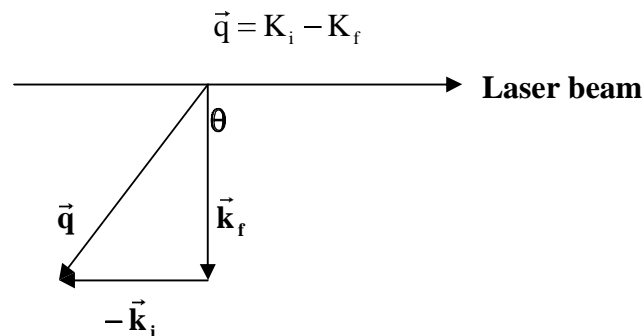


Fig. 2.1. Scattering geometry showing laser beam, wave vectors (\vec{k}), scattering vector (\vec{q}) and scattering angle (θ) [115]

The momentum transfer vector or the scattering vector, \vec{q} is defined as the vector difference between the scattered (k_f) and the incident (k_i) wave vectors. From the geometry of scattering arrangement (figure 2.1), the magnitude of the scattering vector is given as,

$$|q| = \frac{4\pi n}{\lambda_i} \sin\left(\frac{\theta}{2}\right)$$

where n is the refractive index of the medium and θ is the scattering angle. q has the dimension of an inverse length. Typical values of q^{-1} for visible light and the commonly used scattering angles are in the range of roughly 10 to 100 nm. In order to obtain useful information from a scattering experiment the length scales of the heterogeneities in the investigated samples must be comparable to the value of q^{-1} . Therefore light scattering is an adequate technique for studying the colloidal systems.

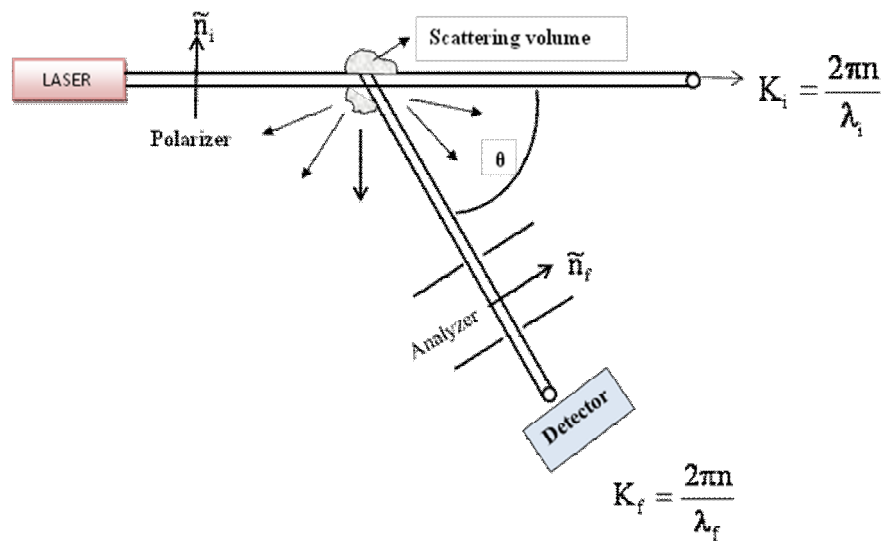


Fig. 2.2. A schematic representation of the light scattering experiment [116]

In a light scattering experiment, light from a laser passes through a polarizer to define the polarization of the incident beam and then impinges on the scattering medium. The scattering light then passes through an analyzer which selects a given polarization and finally enters a detector. The position of the detector defines the scattering angle θ . The intersection of the incident beam and the beam intercepted by the detector defines a scattering region of volume V (Figure 2.2). Light scattering in general are classified into,

- Elastic scattering - Where the frequency of the scattered light to be detected is same as incident light (Rayleigh scattering) ($K_i = K_f$).
- Quasi elastic light scattering – The frequency of the scattered light to be detected is slightly different from that of the incident light, typically in the range of few Hz to few hundred Hz ($K_i \sim K_f$).
- Inelastic scattering - The scattered frequency differs by an amount much larger than few hundred Hz from that of the incident light due to involvement of

other forms of energy such as vibrational, rotational energy of scatterers in Raman scattering, phonon-phonon interaction in Brillouin scattering ($K_i \neq K_f$).

2.2.1.1. Dynamic light scattering

Dynamic light scattering (DLS) is based on quasi-elastic light scattering. When a light incident on a particle, it gets scattered in all directions. If the particle is stationary the scattered, light is of the same frequency as the incident light. Consider in case of colloidal systems where particles are in Brownian motion (random collisions of particles suspended in dispersion with thermally excited molecules of the fluid), i.e., if the particles are moving at some velocity relative to the light source, the scattered light is shifted in frequency by an amount proportional to the particle velocity. An ensemble of particles with a certain velocity distribution will thus have a unique distribution of frequency shifts. For submicron particles diffusing in an aqueous medium these Doppler shifts are typically about 1 kHz for incident light from a typical laser such as helium-neon having a frequency of about 10^{15} Hz. The DLS also known as Photon Correlation spectroscopy or Quasi-elastic light scattering is a popular method used to determine size of particles based on the scattering of light by particles in Brownian motion and the measurement of the very tiny Doppler shifts in the scattered laser light due to the presence of this motion. The colloidal particles undergoing Brownian motion when projected on to a screen a speckle pattern (bright and dark patches) is observed due to constructive and destructive interference of the particles. In Constructive interference, the path length difference is multiples of wavelength of incident light ($\lambda, 2\lambda, 3\lambda\dots$). Total intensity will be twice that from single particle (figure 2.3).

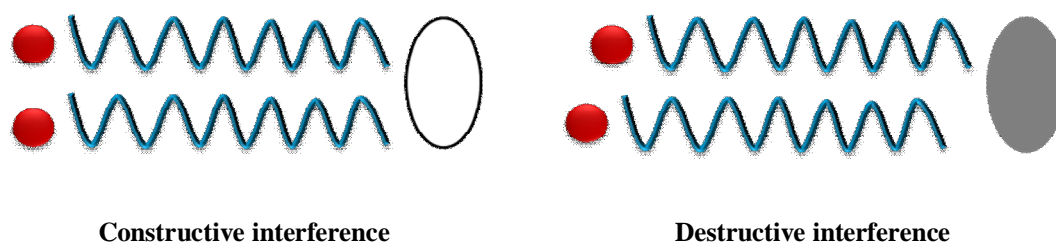


Fig. 2.3. Schematics showing constructive and destructive interference of waves

Where as in destructive interference the path length difference is equal to $\lambda/2$, $3\lambda/2$...The resultant intensity is zero. The intensity of scattered light depends on the size and shape of particles. According to Rayleigh approximation, large particles scatter more light than small particles, $I \propto d^6$, d is the diameter of a particle. Large particles move slowly and hence speckle pattern will also fluctuate slowly. But small particles as they are moving quickly, intensity of speckle pattern also fluctuate quickly (Figure 2.4 a & b).

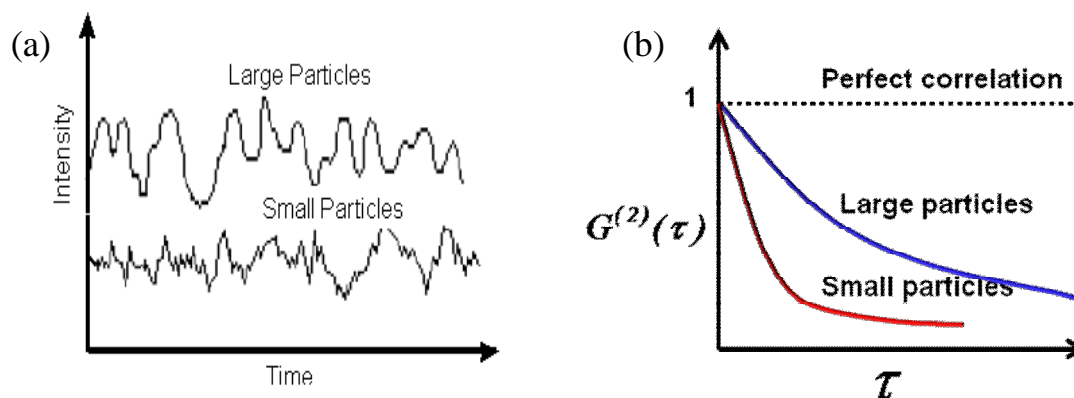


Fig. 2.4. (a) Intensity of scattered light from suspensions containing small and large particles. (b) The time-averaged autocorrelation function of the scattered intensity as a function of time [116]

It also depends on wavelength of incident light and angle of observation. Hence the intensity seen by the detector will be a randomly fluctuating signal with time. And this carries the information about the diffusion coefficient of the particle. DLS

measures the time dependent fluctuations in the intensity of the scattered light. Analysis of this intensity fluctuation allows the determination of the translation diffusion coefficient of the particles. The intensities are measured at short time intervals τ (micro to milliseconds) for long period of time t (milliseconds to seconds). For large particles, the signal will be changing slowly and the correlation will persist for a long time due to slow movement of particles. Where as for small particles, the correlation will disappear quickly due to rapid motion of particles. In order to quantify the time dependence, the autocorrelation function $G(\tau)$ is calculated from the product of two photon counts at time t and $t + \tau$ such that $G(\tau) = \langle I(t)I(t + \tau) \rangle$. The normalized intensity autocorrelation function $g(\tau)$ is given by

$$g^{\text{int}}(\tau) = \frac{\langle I(t)I(t + \tau) \rangle}{\langle I(t)I(t) \rangle}$$

Where $I(t)$ is the scattered intensity at time t and $I(t + \tau)$ is the scattered intensity at small interval τ . The intensity autocorrelation function is related to the electric field autocorrelation function $g^{\text{field}}(\tau)$ by the Siegert relationship

$$g^{\text{field}} = 1 + C |g^{\text{int}}(\tau)|^2$$

where τ is the delay time and C is the Siegert constant (experimental parameter of the measuring device). For dilute dispersion of macromolecules, $g^{\text{int}}(\tau)$ becomes

$$g^{\text{int}}(\tau) = e^{-\Gamma\tau}$$

where Γ is the diffusion of particles under investigation. The relation between the diffusion coefficient (D) and the parameter Γ can be related by

$$D = \frac{\Gamma}{q^2}$$

where q is the scattering vector. From the diffusion coefficient, the hydrodynamic particle radius R_h can be derived via the Stokes–Einstein relation.

$$R_h = \frac{K_B T}{6\pi\eta D}$$

where k_B is Boltzmann's constant, T is the temperature, η is viscosity of the solvent.

Finally, the information obtained from correlation function is used to calculate the size distribution. A typical size distribution curve appears as shown in figure 2.5.

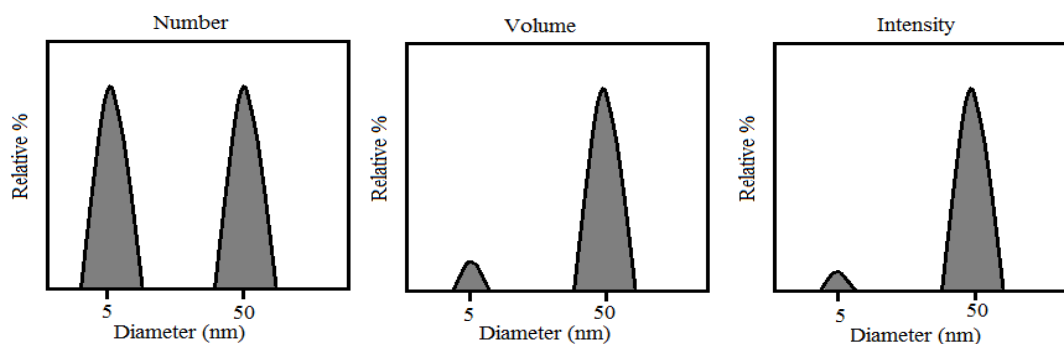


Fig. 2.5. Schematics showing different distribution curves (Number, volume and intensity distribution)

In the present work, the size distribution of colloidal solutions is determined by using Microtrac (Nanotracs ULTRA) particle size analyzer. The schematics of working principle and picture of the instrument used for the present study are shown in figure 2.6 and 2.7.

The measurement range of the instrument is 0.8 nm to 6.54 μm . The light source was a 780 nm, 3mW diode laser. It can operate at temperature range of 10° C to 82° C. An external fiber optic probe measuring 1.5 m in length was dipped inside a beaker containing the sample solution. Sample volume can be varied from 3 ml to 10 ml for standard-volume cell and 0.1 ml to 2 ml for small – volume cell.

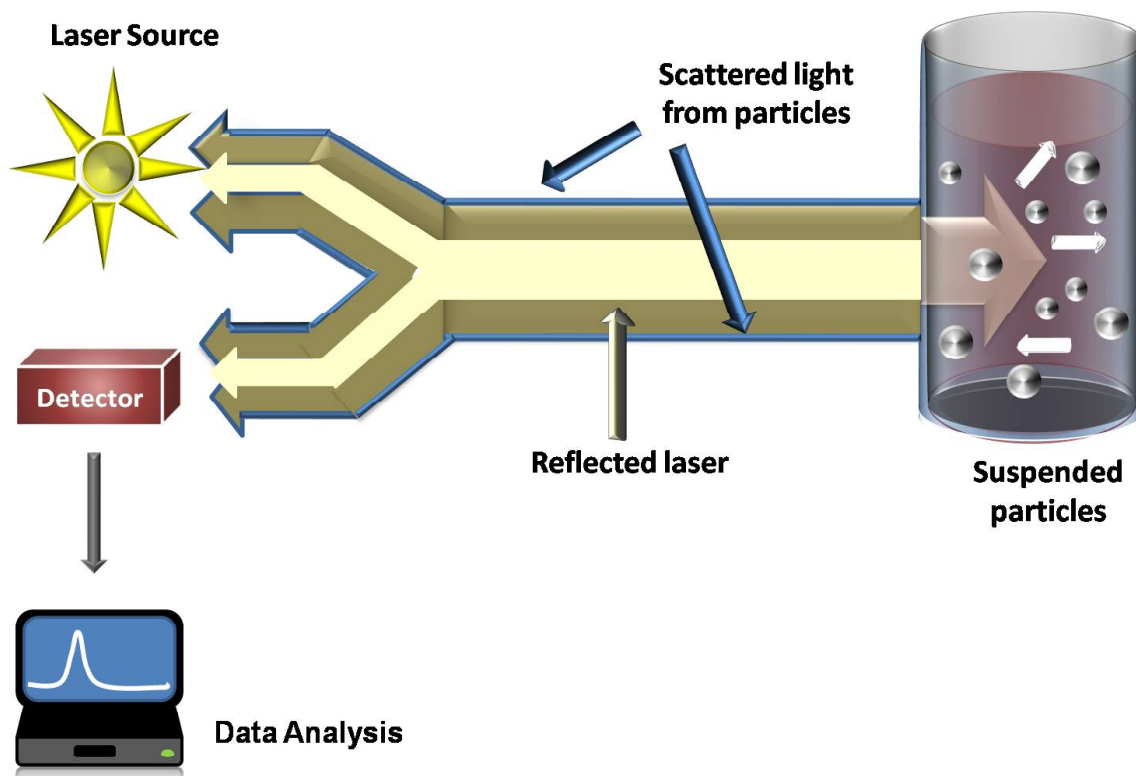


Fig. 2.6. Schematics of the light scattering system showing the development of controlled reference at the probe tip and fluid interface

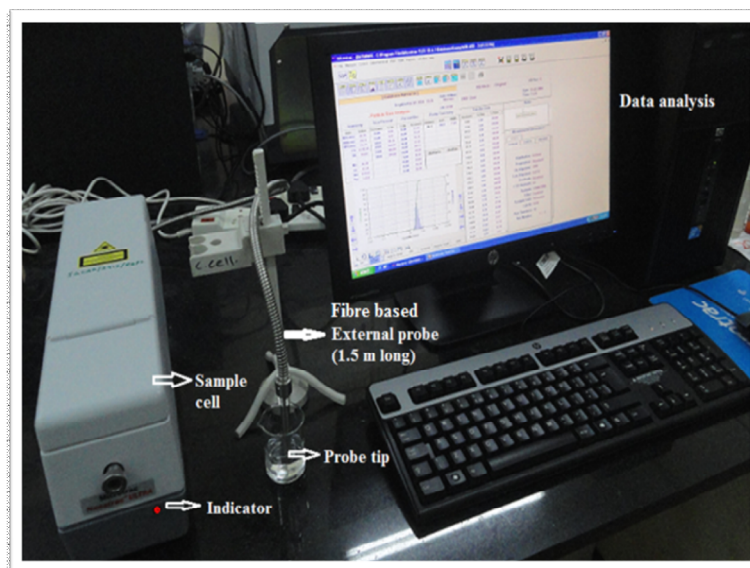


Fig. 2.7. Microtrac particle size analyzer with measurement range of 0.8 nm to 6.4 μm used for the present study

The interface between the sample and the probe is the sapphire window. Initially it reflects the original laser back through the beam splitter to a photo detector. This signal which has the same frequency as the original laser acts as a reference signal, offering heterodyne detection (Heterodyne detection involves combining Doppler (frequency) shifted light scattered from moving particles with a reference beam of light from the same source, not Doppler shifted, reflected from a stationary surface). The laser then passes through the sapphire window and is scattered by the particles under Brownian motion. According to the Doppler effect, the laser is frequency shifted relative to the velocity of the particle. Light is scattered in all directions including 180° backwards. This scattered, frequency shifted light is transmitted through the sapphire window to the optical splitter in the probe to the photodetector. These signals of various frequencies combine with the reflected signal of un-shifted frequency (Controlled Reference) to generate a wide spectrum of heterodyne

difference frequencies. The power spectrum of the interference signal is calculated with dedicated high speed FFT (Fast Fourier Transform) digital signal processor hardware. The power spectrum is then inverted to give the particle size distribution. The scattered light was measured at an angle of 180° . The performance of the instrument was checked with the reference material (100 nm polystyrene microsphere suspended in water) prior to particle size measurements. 50 scans were taken for each sample. The uncertainty in the measurement was found to be ± 1 nm. The calibration graph is shown in figure 2.8.

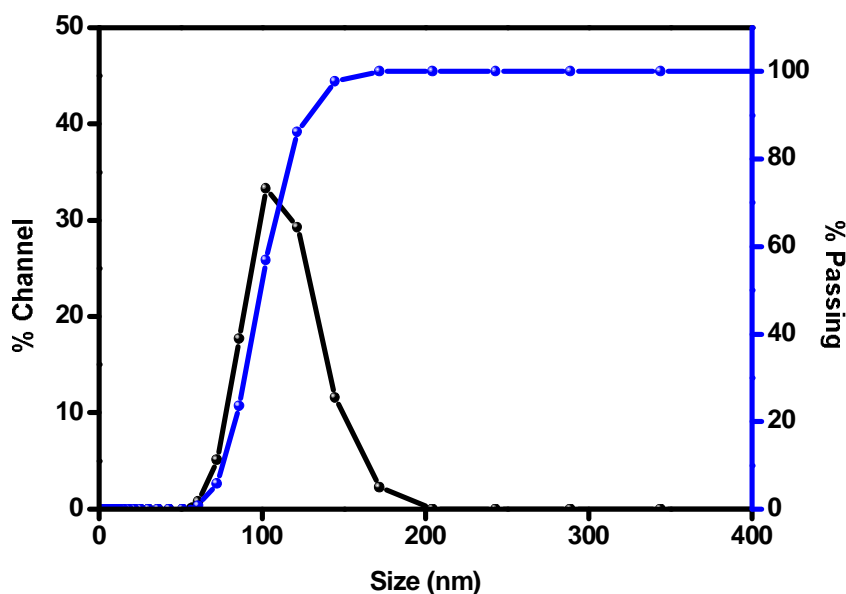


Fig. 2.8. Calibration curve for measuring particle size distribution

% Channel: The measuring range of the instrument is divided into fixed “channel” or “particle” sizes. The channel size increase according to the fourth root of 2, i.e the progression follows $(2)^{1/4}$. The instrument calculates the particle size channels as a

progression where each larger size is determined by multiplying the previous larger size by $(2)^{1/4}$.

% Passing: The cumulative data values are on the same line as the particle size data and are read as % passing (or percent smaller than).

2.2.1.2. Static light scattering

Static light scattering measures the time averaged intensity of scattered light. The intensity of the scattered light depends on the polarizability and the polarizability in turn depends on molecular weight. This property of light scattering makes it a valuable tool for measuring molecular weight. Static light scattering contrasts other measured properties such as colligative property, osmotic pressure which depends on the number of particles and therefore gives number average molecular weight. Whereas SLS gives weight average molecular weight. Since polymeric solutions exhibits non ideality, it also allows to determine a virial coefficient. The weight average molecular weight of a polymer is determined by measuring the sample at different concentration and applying the Rayleigh equation 2.1,

$$\frac{KC}{R_{\theta}} = \left(\frac{1}{M_w} + 2A_2C \right) \quad (2.1)$$

Where the optical constant $K = [2\pi n(dn/dC)]^2 / N_A \lambda_o^4$, R_{θ} is the excess Rayleigh ratio, M_w is the weight average molecular weight of the solute, C is the concentration (in g/ml), A_2 is the second virial coefficient, λ_o is the wavelength of light used, N_A is

Avogadro's number and dn/dC is the refractive index increment due to the solute under a given set of solution conditions [116-117].

Debye Plot

Figure 2.9 shows a typical Debye plot which is used to arrive at molecular weight and second virial coefficient.

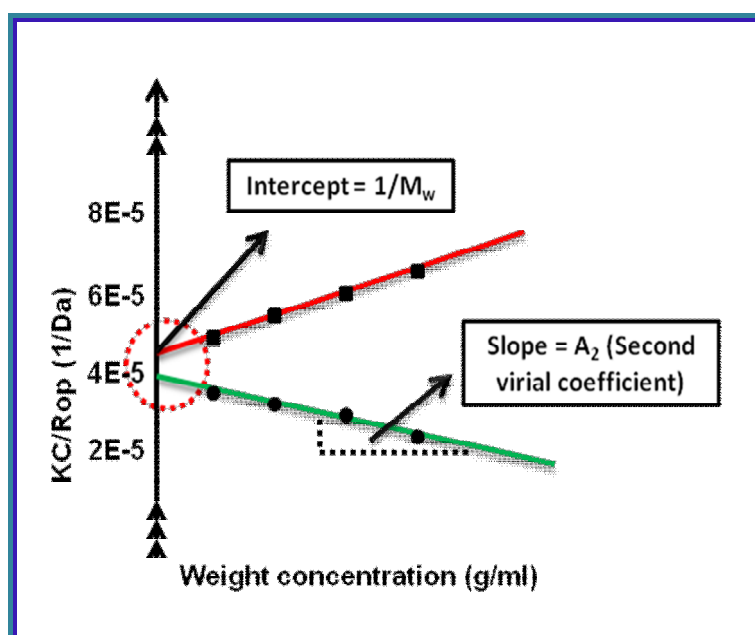


Fig. 2.9. A typical Debye plot

The intensity of scattered light that a particle produces is proportional to the product of the weight-average molecular weight and the concentration of the particle. Microtrac measures the intensity of the scattered light (K/CR_θ) of various concentrations (C) of sample at one angle. Molecular weight is measured by doing several individual measurements through samples of various concentrations. The graphical representation of this is called a Debye plot and allows for the determination

of weight average molecular weight and 2nd virial coefficient. The weight average molecular weight (M_w) is determined from the intercept point on the x axis. i.e. $KC/R_\theta = 1/M_w$ in Daltons. The weight average molecular weight is defined as

$$M_w = \frac{\sum_i n_i M_i^2}{\sum_i n_i M_i}$$

Where n_i is the number of particles of weight M_i .

The 2nd virial coefficient (A_2) is determined from the gradient of the Debye plot. The second virial coefficient is a parameter which measures the interaction strength between the molecule and the solvent. Positive value ($A_2 > 0$) infers that the solute likes the solvent more than the solute itself leading to stability of the system. Whereas negative value of second virial coefficient ($A_2 < 0$) leads to aggregation in the system i.e. solute likes itself more than the solvent. And, $A_2 = 0$ is said to be theta solution if the solute-solvent interaction is equal to solvent-solvent interaction.

Statistical thermodynamics allows us to derive an expression that shows the relationship between the second virial coefficient and the intermolecular potential that represents the interaction between two particles. This expression is

$$B(T) = -2\pi N_A \int_0^\infty \left(e^{-\frac{U(r)}{KT}} - 1 \right) r^2 dr$$

Where, $U(r)$ represents the intermolecular potential energy, K is Boltzmann constant, N_A is Avagadro number.

2.2.2. UV-Visible spectrophotometry

The absorption of electromagnetic radiation in the ultraviolet and visible regions causes the promotion of the outer orbital electrons to higher energy levels in case of atoms and electronic transitions in case of molecules. The ultraviolet (UV) region is scanned from 190 to 400 nm and the visible region is from 400 to 800 nm. The wavelength of the absorption maxima (λ_{\max}) is a highly specific property of molecular structure. UV-Visible spectrophotometry can be used to obtain qualitative as well as quantitative information of samples. Qualitative analysis involves mainly the identification of the presence of conjugated π -electron in a system or to identify the presence of a particular group. Quantitative analysis involves the determination of concentration of an absorbing analyte which is linearly related to absorbance 'A' as given by Beer Lambert's law,

$$A = \epsilon cl$$

where, A is the absorbance with no units, ϵ is the molar absorbance or absorption coefficient (in $\text{dm}^3\text{mol}^{-1}\text{cm}^{-1}$) which gives intensity of absorption band, c is the concentration in mol dm^{-3} and l is the path length of light in the sample (in cm). Figure 2.10 shows the schematics of a conventional UV-Visible spectrophotometer.

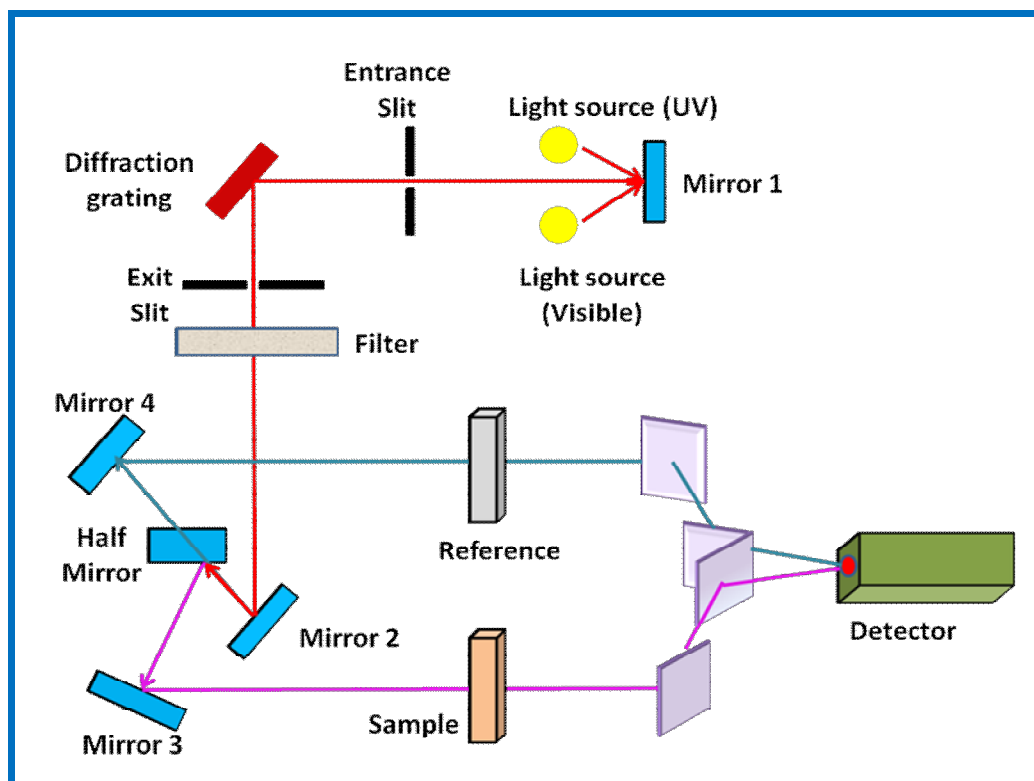


Fig. 2.10. Schematics of a conventional UV-Vis spectrophotometer [118]

A typical UV-Vis spectrophotometer comprises of light source (deuterium or hydrogen lamp for ultraviolet region and tungsten filament lamp for visible region), a dispersion device (gratings or prisms) that selects a particular wavelength from the broadband radiation of the source, concave mirrors or lenses to focus light through the instrument, sample cell (Quartz cuvettes), photo-detector to measure the intensity of radiation.

Radiation from the source is allowed to pass into the monochromator (comprises an entrance slit, a dispersion device and an exit slit) through a mirror system. A narrow beam of radiation coming out of the monochromator through the exit slit passes through the filter which removes unwanted higher order of diffraction. It is then passed into a splitter which divides the beam into two halves. One passes

through the sample cell and the other through the reference. The intensity of the incident beam (which passes through the reference) is defined as I_0 and the intensity of the scattered beam (which passes through the sample) is defined as I . Both the beams are then allowed to fall on a detector where they are compared and converted into electrical signals. The signals are amplified and then transmitted into the recorder where the absorbance ($A = I_0/I$) or transmittance ($T = I/I_0$) is recorded [118].

UV-visible electronic absorption spectra of all the samples are recorded with a Shimadzu UV-visible-NIR 3600 spectrophotometer. The instrument is equipped with photomultiplier tube for the ultraviolet and visible regions. It uses a high-performance double monochromator which makes it possible to attain an ultra-low stray-light level (0.00005% max. at 340 nm) with a high resolution. The maximum spectral resolution is 0.1 nm. Absorption spectra are recorded between 300 and 600 nm with an accuracy of 0.1 nm. Cuvette of 1 cm path length is used for all measurements.

2.2.3. Attenuated Total Reflectance – Fourier Transform Infrared Spectrometry

When IR radiation is passed on a sample, it enables the excitation of vibrational or vibrational-rotational transitions of molecules involving transitions from/to rotational and/or vibrational levels in the same electronic state. The spectra are unique for particular molecule. In other words, the spectra are frequently characteristics of various functional groups within the molecule. They are said to fall in the finger print region ($\sim 1200\text{-}400\text{ cm}^{-1}$). It is unique to each molecule. FT-IR are preferred over other dispersive IR instruments mainly because of the advantages

which includes, throughput, high resolving power, wavelength reproducibility, greater signal to noise ratio, greater speed and greater sensitivity.

Fourier transform spectrometers are capable of simultaneous analysis of full spectral range using interferometry. Michelson interferometer is used for this purpose which is coupled to computer that can calculate the spectrum from the interferogram. Irradiation from the source is fed into the beam splitter. It allows the generation of two beams, one of which falls on a fixed mirror and the other on a mobile mirror which moves very short distance away from the beam splitter. The two beams reflect off their respective mirrors and are recombined when they meet back at the beam splitter. When the moving mirror is in such a position that the path travelled by both the beams are the same length, the light composition of exiting beam is identical with that of the beam that enters. Since the position of the moving mirror keep on changing, composition of the light beams vary due to loss of phase between the two beams. The transmitted signal which varies with time is recorded as interferogram. The interferogram contains thousands of data points and each data point carries information about every infrared frequency which comes from the source. But the interferogram cannot be interpreted directly and hence the mathematical technique called Fourier Transformation is applied to extract information of each individual frequency. Usual procedure to obtain FTIR spectrum is to get a reference interferogram by scanning the reference many times and storing the data in the memory of the instrument. A sample is then inserted into the radiation path and the process is repeated. This is where specific frequencies of energy characteristic of the sample are absorbed. Finally the beam reaches the detector where the measured signal is digitized and fourier transformation takes place in the computer. Finally the

ratio of sample and reference spectral data is then compared to give the transmittance at various frequencies. The schematics of simple FTIR spectrometer is shown in figure 2.11.

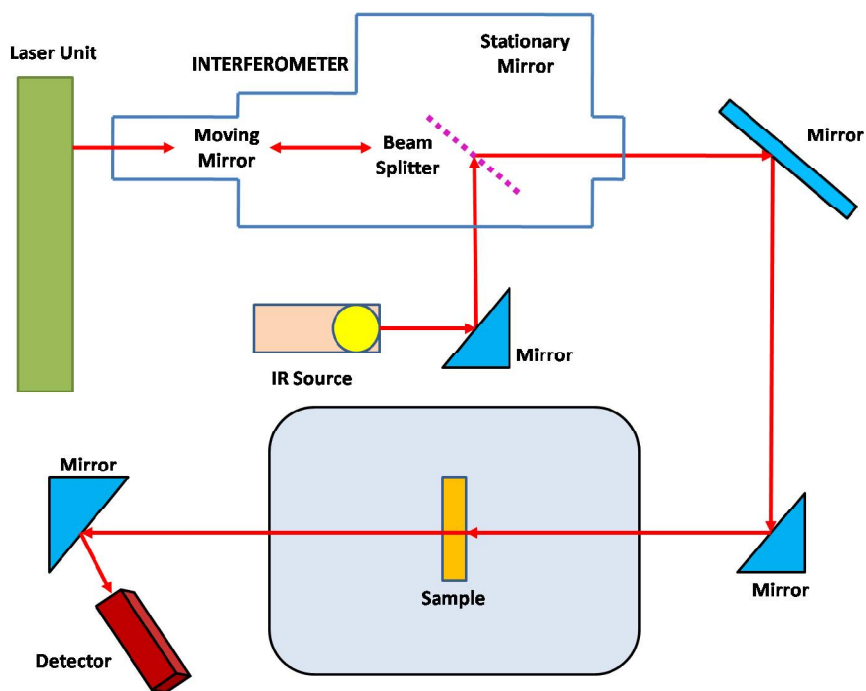


Fig. 2.11. Schematics of a simple FTIR spectrometer [119]

For the present study, FTIR equipped with ATR crystal was used. ATR-FTIR is a widely used FTIR sampling tool allowing both qualitative and quantitative analysis of samples with no sample preparation and great speed in sample analysis. An infrared beam is directed onto an optically dense crystal with high refractive index at a certain angle. There is greater penetration depth of IR beam into the sample and it is a function of wavelength (λ), refractive index of the crystal (n) and angle of incident radiation (θ). Due to internal reflection, an evanescent wave is developed that extends beyond the surface of the crystal. In the regions of infrared spectrum, where the sample absorbs energy, the evanescent wave will be attenuated or altered. The

attenuated energy from each evanescent wave is passed back to the IR beam which then exits the opposite end of the crystal and is passed to the detector. Figure 2.12 shows horizontally arranged multiple reflection ATR system.

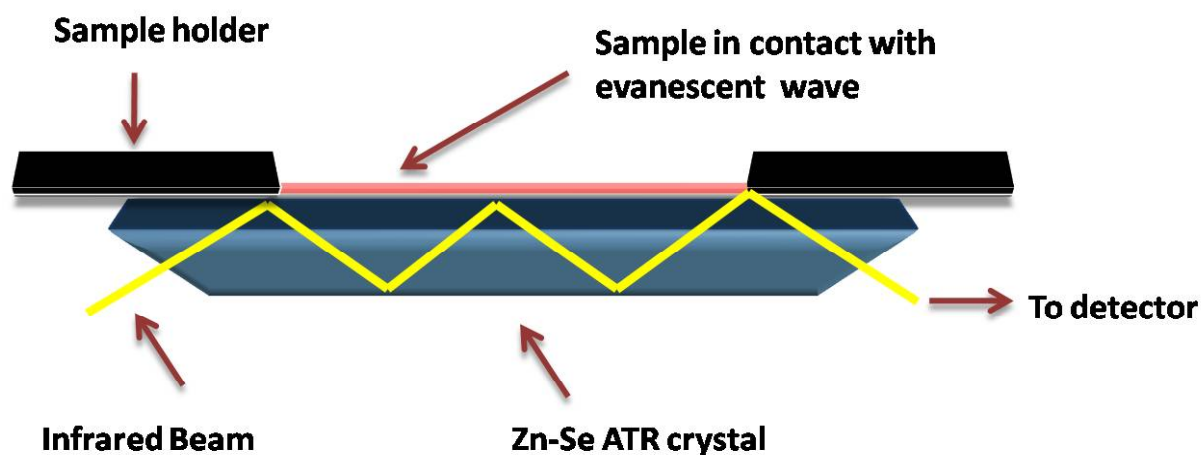


Fig. 2.12. Schematics of a multiple reflection ATR system
 URL: <http://coatings.mst.edu/v6i1/v6i3/> [Accessed 17 May 2015]

The ATR-FTIR spectra of the samples were recorded using a Fourier transform IR ABB MB3000 spectrometer equipped with DTGS (deuterated triglycine sulphate) detector and an ATR attachment. It employs solid state laser as source for IR radiation. The interferometer was equipped with a non hygroscopic-ZnSe beam splitter. Zinc selenide is a low cost material and is ideal for analyzing liquids and non-abrasive paste. The properties of Zn-Se used as ATR crystal is given in table 2.1.

Table 2.1. Properties of ZnSe ATR crystal [119]

Window material	Useful range (cm^{-1})	RI	Properties
Zn-Se	20000 - 500	2.4	Insoluble in water, organic solvents, dilute acids and bases

All the spectra were measured at a spectral resolution of 4 cm^{-1} and 100 scans were taken per sample. The frequency accuracy was $< 0.06\text{ cm}^{-1}$. Solutions were placed on the horizontal ATR crystal. Horizon MB software was used to analyze the spectra [119-120].

2.2.4. Refractometer

When composition of a substance changes so does its refractive index. Thus Refractive index is one of the physical properties that can be used for the characterization and identification of a material. It is defined as the ratio of the speed of light in air to the speed of a light in the medium.

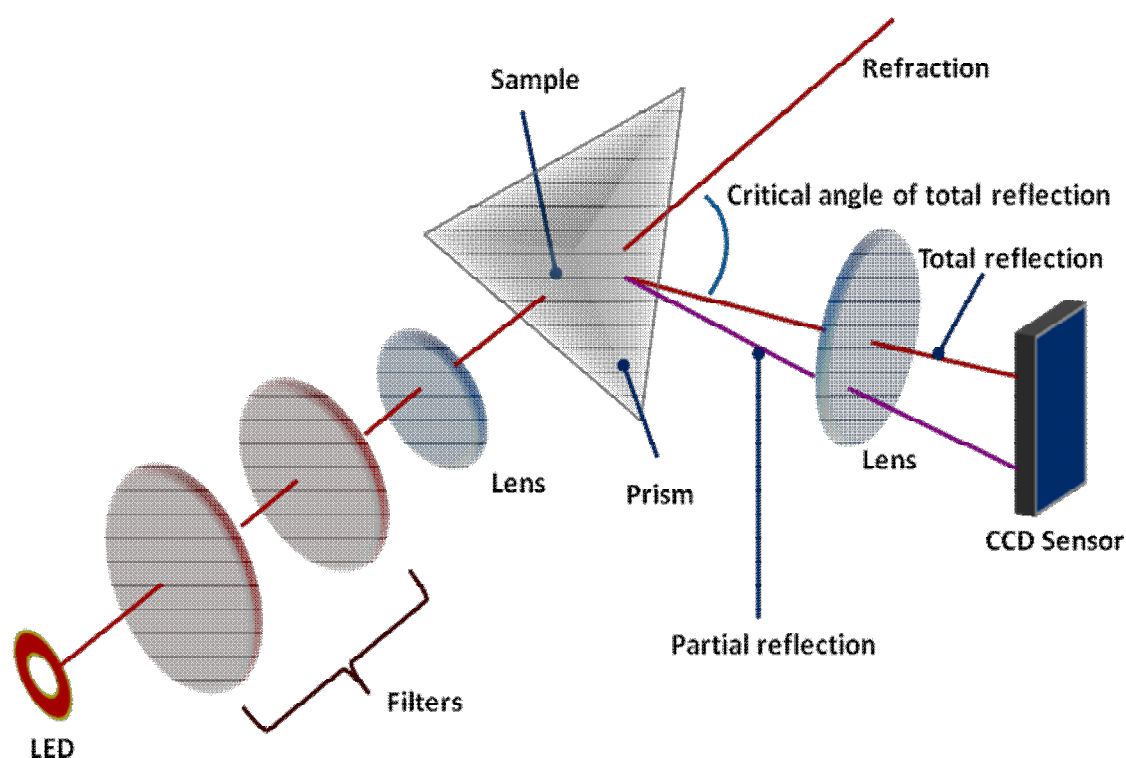


Fig. 2.13. Schematics of an automatic refractometer

Anton Paar GmbH, URL: www.anton-paar.com [Accessed 17 May 2015]

The instrument used in the present study for the accurate measurement of refractive index was Anton-Paar ABBEMAT RXA 156. Range of the instrument is 1.32 to 1.56 nD with standard deviation of 2×10^{-5} nD. The general procedure for measuring refractive index is to keep the sample in contact with the measuring prism. It is then irradiated by an LED source. The critical angle of the total reflection at 589.3 nm sodium D wavelength is measured with a high resolution sensor array. The refractive index (nD) is calculated from the value of critical angle. The sample and the measuring prism are thermostated precisely via Peltier technology to get highly accurate results. Figure 2.13 shows the schematics of an automatic refractometer.

2.2.5. pH measurements

A pH measuring circuit consists of a measuring electrode (glass electrode), a reference electrode (usually calomel electrode) and a temperature sensor immersed in the solution (Figure 2.14).

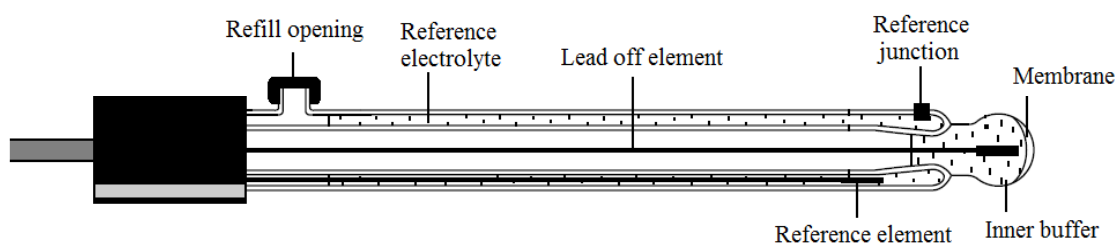


Fig. 2.14. Schematic representation of a combination electrode

The glass electrode is made of a special glass of low melting point and high electrical conductivity blown in the form of a bulb attached to the bottom of a glass tube. It is filled with a solution of 0.1 M HCl which furnishes constant hydrogen

ion concentration. A platinum wire is inserted to make electrical contact. The reference electrode has a defined stable potential independent of the measured solution and it contains a reference element immersed in a defined electrolyte. This electrolyte must be in contact with measured solution through a porous ceramic junction. When the pH sensitive glass electrode comes in contact with the measuring solution, a gel layer develops on the glass membrane and also inside of the membrane which is in contact with the defined inner buffer solution. The H^+ ions either diffuse out or into the gel layer depending on the pH value of the measured solution. Charge is developed on outer side of the gel layer. The potential at inner surface of the membrane is constant. The total membrane potential is a result of the difference between the inner and outer charge. Since the potential of the reference electrode is known, that of the glass electrode can be calculated and the pH of the experimental solution is evaluated. The changes in the pH of the solutions were monitored using Thermo scientific Orion 3-star bench-top pH meter. The glass electrode used for the measurement was calibrated with buffer solutions of pH 4.01 and 7.00. The accuracy of pH measurements was ± 0.01 units.

2.2.6. X-ray diffraction

X-ray diffraction (XRD) analysis was carried out using INEX-XRG-3000 diffractometer with a curved position sensitive detector using Cu $K\alpha 1$ ($\lambda = 0.15406$ nm) radiation with grazing angle (ω) as 5° .

Chapter 3



CHAPTER 3

Hydrolysis of Sr(II), Al(III) and Bi(III) ions in Aqueous Nitric Acid Solutions

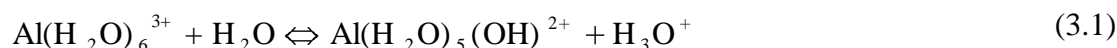
3.1. Introduction

Formation of solution involves interaction of solute with solvent. Water is the most commonly used liquid solvent. Water molecules that are the nearest neighbors of metal cation form the primary hydration sphere in an aqueous system. An existence of so-called secondary hydration sphere (sometimes called a second hydration shell) is a typical phenomenon in case of aqueous solutions of electrolytes. The primary hydration sphere can have 4 to 12 solvent molecules surrounding the cations, depending on ion size and electronic nature. However, the majority of metal ions, particularly those of d-block elements, have a primary hydration number of six. For monovalent metal ions (Na^+ , Li^+) a structured first hydration shell can be identified. The alkaline earth metal ions which includes Mg^{2+} , Ca^{2+} , Sr^{2+} , Ba^{2+} , they all show characteristic hydration behavior when dissolved in water. The structures of these ions in aqueous solution has already been studied by using neutron diffraction with isotopic substitution (NDIS) [121], extended x-ray absorption fine structure (EXAFS) [122], total x-ray diffraction [123], molecular dynamics simulation studies (MD) [124] and anomalous x-ray diffraction studies (AXD) [125]. But for highly charged metal ions it becomes difficult to obtain information regarding the structure because estimating energy difference between their various isomers is more difficult

and challenging. It need to include higher order coordination spheres in the calculation and also other solvent interaction. The present chapter deals with hydrolysis of Al(III), Sr(II) and Bi(III).

3.1.1. Aluminium(III) hydrolysis

Aluminum is the third most abundant element in Earth's crust after oxygen and silicon. Aluminium exists in normal environment as Al^{3+} cation. It is a hard Lewis acid with greater charge density. It can accommodate around 6 ligands in the inner coordination sphere [126]. Hydrolysis and hydration of the Al(III) ion in aqueous solution play a fundamental role in the reactivity and mobility of the Al(III) hydrolysis species that are important in materials chemistry, geochemistry, environmental science and medicine [127]. In aqueous systems, at $\text{pH} < 3$ it exists as octahedral $\text{Al}(\text{H}_2\text{O})_6^{3+}$. The initial hydrolysis of Al can be understood from the following equation 3.1.



Most of the studies show that the hydrolytic species are predominantly mononuclear. The species present were $[\text{Al}(\text{OH})]^{2+}$, $[\text{Al}(\text{OH})]^+$, $[\text{Al}(\text{OH})_3]$, $[\text{Al}(\text{OH})_4]^-$ [78]. But it has been proved that Al-hydrolysis is not simply mononuclear but those monomers polymerize by bridging to form dimers $[\text{Al}_2(\text{OH})_2(\text{H}_2\text{O})_4]^{4+}$, trimers $[\text{Al}_3(\text{OH})_4(\text{H}_2\text{O})_9]^{5+}$, tridecamers $[\text{Al}_{13}\text{O}_4(\text{OH})_{24}(\text{H}_2\text{O})_{12}]^{7+}$ and at elevated temperatures the recently characterized $[\text{Al}_{30}\text{O}_8(\text{OH})_{56}(\text{H}_2\text{O})_{26}]^{18+}$ species are also formed [128]. Sometimes polynuclear species also exists at $\text{pH} > 7$. The first hydrolysis product $\text{Al}(\text{OH})^{2+}$, is hexacoordinate [129]. But by Car–Parrinello simulations and ab initio methods it has also been found that the pentacoordinate structure was stable

[130-131]. Meanwhile, by using density functional theory (DFT), a five-coordinate geometry for $\text{Al}(\text{OH})_3(\text{H}_2\text{O})_3$ was more stable than the hexacoordinate structure for $\text{Al}(\text{OH})_3(\text{H}_2\text{O})_3$ [132-133].

3.1.2. Strontium(II) hydrolysis

Strontium is an alkaline earth metal, located in the fifth period of the periodic table. ^{90}Sr is a major radioactive fission product and has received increased interest due to its long life time (half life ~ 29 years), contributing a large part of heat load and radiation in high level liquid wastes during the reprocessing of spent nuclear fuel [134]. It shows characteristic hydration properties when dissolved in water. Hydrated $^{90}\text{Sr}(\text{II})$ has been investigated by various methods such as X-ray diffraction (XRD) [123], X-ray absorption fine structure (XAFS) [135] and extended X-ray absorption fine structure (EXAFS) [136] which show that it has an associated coordination number ranging from 7-10. But recent studies by Quantum mechanical molecular dynamic simulation shows that Sr has coordination number of 9 with highest probability [137]. In addition to that anomalous X-ray diffraction (AXD) studies predicted a coordination number of 9.0 for hydrated Sr(II) [125]. Neutron diffraction with isotope substitution (NDIS) has overestimated that 15 water molecules are present within the first shell of Sr(II) [138].

3.1.3. Hydrolysis of Bismuth(III)

Aqueous chemistry of Bi is primarily dominated by trivalent complexes (Bi^{3+}) [139]. Bi(III) readily hydrolyzes in aqueous solutions ($\text{p}K_a = 1.51$) and has high affinity to oxygen. In addition to that bismuth is a strong Lewis acid and begins to undergo hydrolysis even at low pH values ($\text{pH} \sim 1$) [140-141]. Bi^{3+} aqua ion

$[\text{Bi}(\text{H}_2\text{O})_n]^{3+}$ has been characterized by using many techniques which includes extended X-ray absorption fine structure (EXAFS), low angle X-ray scattering (LAXS) spectroscopy and concluded that 8 water molecules are coordinated to Bi^{3+} . But dynamic simulation studies shows that the number of coordinated water molecules is 9 (i.e. $[\text{Bi}(\text{H}_2\text{O})_9]^{3+}$) and it is analogous to structures found among lanthanides [142]. Numerous studies on hydrolysis of Bi show that the predominant species at higher H^+ concentration is Bi^{3+} . It has been widely agreed that the hydrolyzed species of Bi are polymeric existing as dimers $\text{Bi}_2\text{O}_2^{2+}$, pentamers $\text{Bi}_5\text{O}_5^{5+}$ and the most important among them is the hexameric species $\text{Bi}_6\text{O}_6^{6+}$ at moderate Bi concentrations ($\geq 10^{-2}$ m) in acidic solutions with pH ~ 2-5. Further hydrolysis over pH range of 4-6 leads to the formation of Bi_9 polynuclear complexes [19]. Sedimentation equilibrium measurements indicates that there were 5 or 6 bismuth atoms in the predominant complex present in solutions with approximately 2 hydroxide ions bound per bismuth atom [143]. Since Bi-Pb eutectic composition are heavy liquid coolant for nuclear reactors and several recent reactor prototypes use steam generation modules in direct contact with liquid metal coolant, Bi speciation under hydrothermal condition is very important to optimize the separation of Bi from concentrates such as Cu, Pb and Mo [144-145].

The ambiguities in the nature of hydrolysis of Al(III), Sr(II) and Bi(III) has been clearly clarified by the present investigation.

3.2. Experimental

- $\text{Al}(\text{NO}_3)_3 \cdot 9\text{H}_2\text{O}$ is dissolved in 1M nitric acid to a concentration of 0.1 to 0.3 M of Al.

- Anhydrous $\text{Sr}(\text{NO}_3)_2$ is dissolved in 1 M nitric acid to a concentration of 0.025 to 0.125 M of Sr.
- Four different solutions of Bismuth were prepared by dissolving nitrate, $\text{Bi}(\text{NO}_3)_3 \cdot 5\text{H}_2\text{O}$ in 1 M nitric acid to a concentration of 0.0064, 0.0121, 0.0246, 0.0367 gm^{-1} . The resulting solutions were diluted by gradually adding 0.1 M NaOH until slight turbidity occurs. The pH of the solution was maintained as 1 ± 0.1 .
- Preparation of solutions and light scattering measurements are done at room temperature.

3.3. Results and discussions

3.3.1. Diameter of hydrated Al^{3+} ion

Light scattering measurement was performed without the addition of base to the solution. At high acidity, that is with $\text{OH}/\text{Al} = 0$, the ionic diameter of hydrated Al^{3+} ion was estimated as 0.95 nm which can be validated with the earlier reported values predicted by various methods like diffusion studies [146], individual ion activity method [147]. The comparison of the reported value with the experimental data is given in table 3.1. The intensity size distribution curve is shown in figure 3.1.

Table 3.1. Comparison of experimentally determined diameter of hydrated Al^{3+} ion data with literature reported value

Method	Diameter of hydrated Al^{3+} ion (in nm)
Individual ion activity	0.90
Diffusion studies	0.96
Dynamic light scattering	0.95

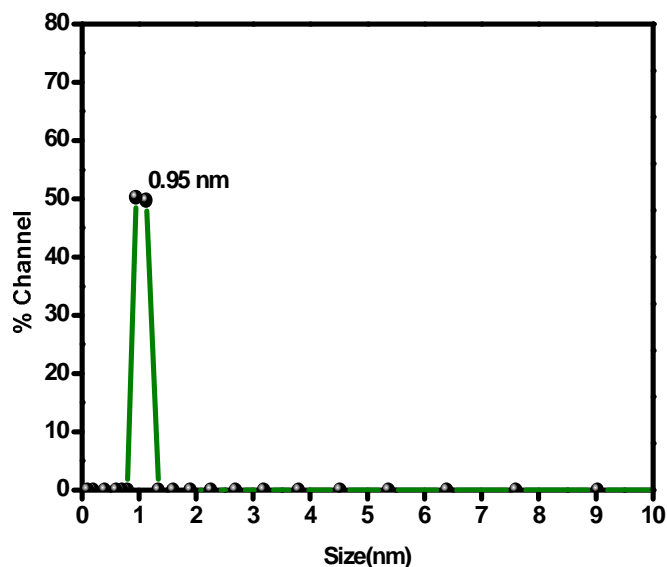


Fig. 3.1. Intensity size distribution curve of Al³⁺ hydrated ion

The diameter of the hydrated ion includes only the primary hydration sphere. Peak summary is given in table 3.2. It provides the statistics of the calculated size distribution such as diameter (50% of each mode reported), volume% (volume % of each mode reported) and width (a measure of the broadness of each mode reported).

Table 3.2. Peak summary for size distribution curve of Al³⁺ hydrated ion

Diameter(nm)	Volume%	Width
0.95	100.0	0.20

3.3.2. Molecular weight of hydrated Al³⁺ ion

The molecular weight of the hydrated ion was determined as ~113 Da from the Debye plot. It shows that there is a possibility of Al³⁺ ion penta-coordinated by water molecules. The plausible structure of the hydrated ion is shown in figure 3.2.

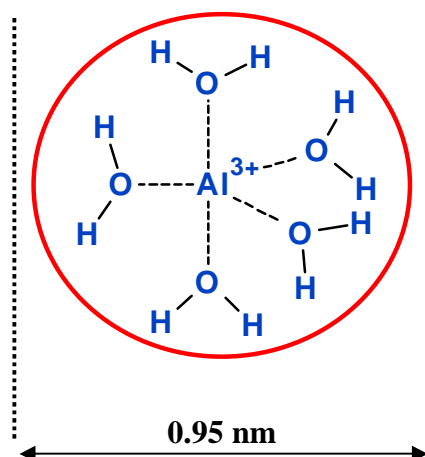


Fig. 3.2. A plausible structure of Al^{3+} hydrated ion

For generating the Debye plot, the refractive index increment has to be given as input. In order to obtain dn/dC value, refractive index was measured for different concentrations of Al^{3+} solutions. dn/dC was calculated from the slope of the plot. The refractive index of the solution increases as the concentration of the solute increases and gives a positive slope whose value is determined to be 0.0931 mlg^{-1} . The change in refractive index of the solution with change in concentration is shown in figure 3.3.

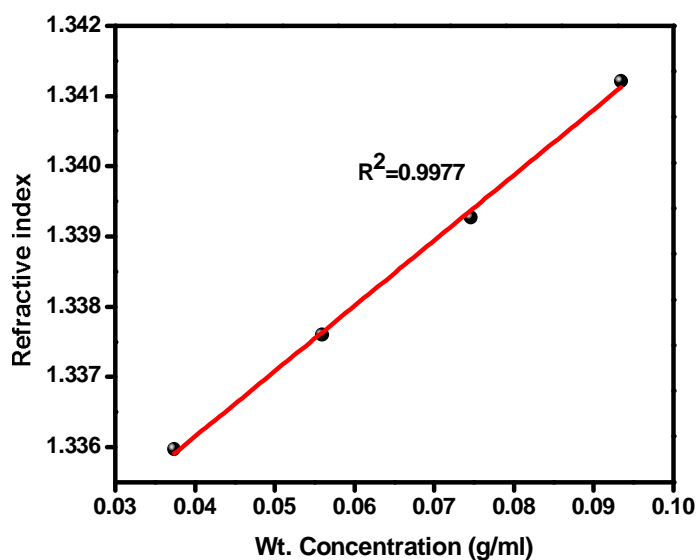


Fig. 3.3. The dn/dC curves obtained for different concentration of Al^{3+} solution

Particle refractive is another parameter used for obtaining the Debye plot. A value of 1.54 was given as input. The Debye plot obtained for different concentration of Al^{3+} solution is shown in figure 3.4. The slope of the plot gives the value of second virial coefficient. The significance of second virial coefficient is discussed earlier in section 2.2.1.2. In the present case, Debye plot (figure 3.4) gave negative slope suggesting that there is aggregation. The values for weight average molecular weight of hydrated Al^{3+} ion and the second virial coefficient are given in table 3.3.

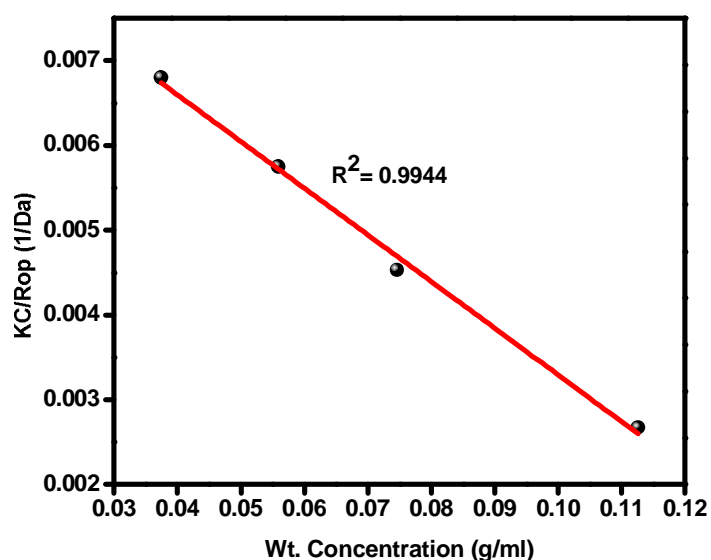


Fig. 3.4. Debye plot for various concentrations of Al^{3+} solution

Table 3.3. Calculated parameters from the Debye plot for hydrated Al^{3+} ion.

Substance	Measured at $\lambda = 780 \text{ nm}$	
	M_w (Da)	Second virial coefficient, A_2 (ml/g Da)
Al^{3+} (hydrated)	113	-5.48E-02

3.3.3. Diameter of hydrated Sr^{2+} ion

The diameter of hydrated ion of Sr(II) was determined as 0.5 nm by diffusion studies [134]. It was difficult to predict the size of hydrated Sr^{2+} ion by the present method due to limitation in the detection range of the instrument (0.8 nm to 6.54 μm). Figure 3.5 shows the intensity size distribution of hydrated Sr^{2+} ion where the intensity distribution is at the minimum detection limit of the instrument (0.8 nm). The corresponding details of the peak are given in table 3.4.

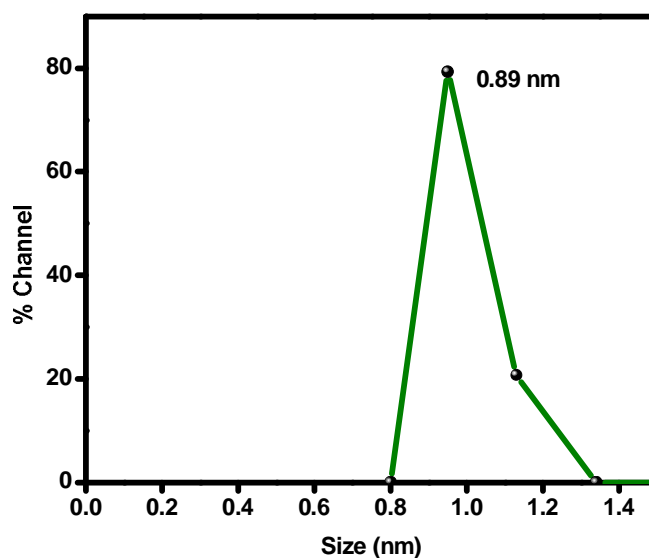


Fig. 3.5. Intensity size distribution curve of Sr^{2+} hydrated ion

Table 3.4. Peak summary for size distribution curve of Sr^{2+} hydrated ion

Diameter(nm)	Volume%	Width
0.89	100.0	0.14

3.3.4. Molecular weight of hydrated Sr^{2+} ion

The molecular weight of the hydrated Sr^{2+} was determined as ~ 253 Da. This shows that Sr^{2+} is probably solvated by 9 water molecules in the primary hydration sphere. The plausible structure of the hydrated ion is shown in figure 3.6.

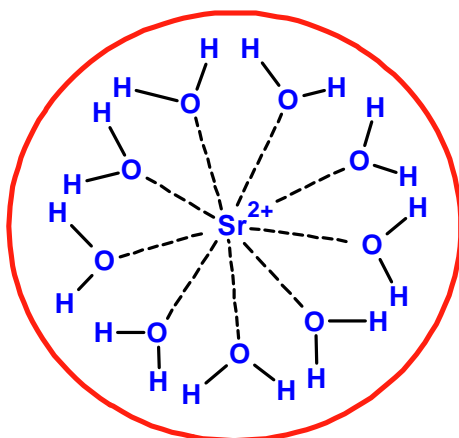


Fig. 3.6. Sr^{2+} ion surrounded by 9 water molecules in the primary hydration sphere

The differential refractive index increment (dn/dc) was determined as 0.1087 mlg^{-1} from the slope of the plot shown in figure 3.7.

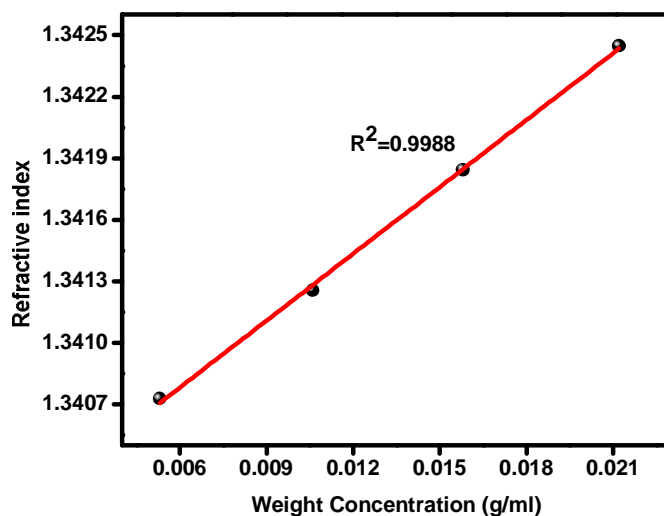


Fig. 3.7. The dn/dC curves obtained for different concentration of Sr^{2+} solution

The particle refractive index was assumed as 1.58 [148] for generating the Debye plot (figure 3.8). The slope of the plot gave a negative value which shows the probability of aggregation in the system. The calculated parameters from the plot are summarized in table 3.5.

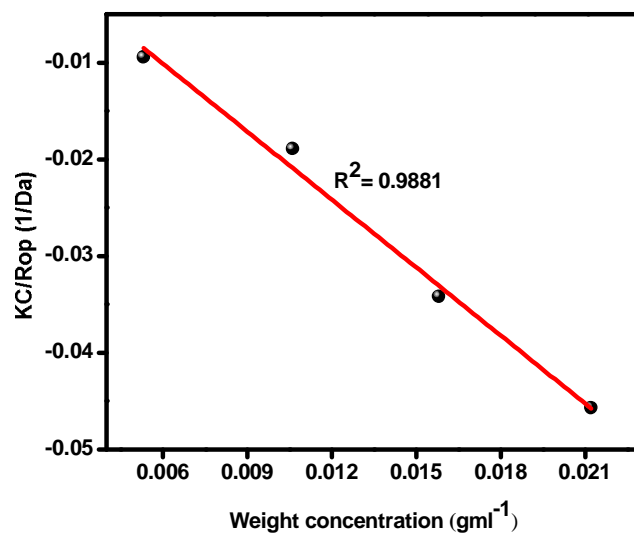
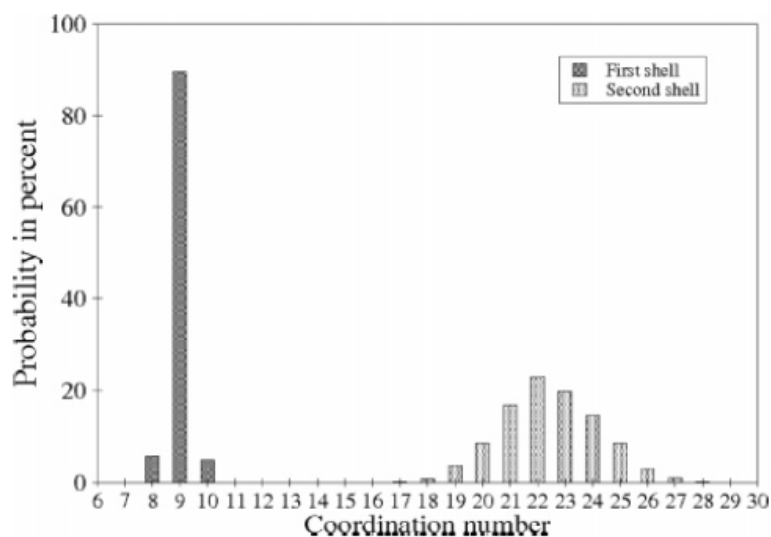


Fig. 3.8. Debye plot for various concentrations of Sr^{2+} solution

Table 3.5. Calculated parameters from the Debye plot for hydrated Sr^{2+} ion

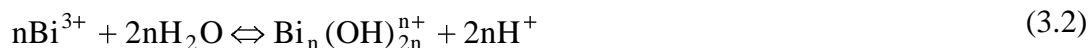
Substance	Measured at $\lambda = 780 \text{ nm}$	
Sr^{2+} (hydrated)	M_w (Da)	Second virial coefficient, A_2 (ml/g Da)
	253	-2.35

The present investigation is in good agreement with the QM/MM MD simulation studies which postulated that nine-fold coordination dominates within the first shell occurring with 89.5%. Whereas configurations with coordination numbers 8 and 10 are present as well, but with very low probabilities (5.7% for 8 coordination and 4.9% for 10 coordination) [137]. Figure 3.9 shows the coordination number distribution plot generated by QM/MM MD simulation studies.

**Fig. 3.9. Coordination number distribution of first and second hydration shell of Sr(II) in aqueous solution obtained by QM/MM MD simulations [137]**

3.3.5. Variation of particle size with concentration of Bi(III)

The general equilibrium for hydrolysis reaction of Bi^{3+} is given in equation 3.2 as follows:



With increase in pH, Bi hydrolyses to form polynuclear species. Dynamic light scattering measurements were performed at $\text{pH } 1 \pm 0.1$. The size of the particle formed at the point of precipitation increases with increase in concentration of solute and it is due to aggregation of particles at higher concentration. Figure 3.10 shows the comparison plot for varying particle size as the concentration of the solution varies. The d_{50} for 0.0064 gml^{-1} of Bi is 121.3 nm and it increases to 192.2 nm for 0.0367 gml^{-1} of Bi. The polymeric species are formed as a result of the condensation reaction between the monomeric species. The peak summary is given in table 3.6.

Table 3.6. Peak summary for size distribution curve different concentration of polymeric Bi solutions

Concentration (g/ml)	Particle Diameter (nm)	Volume %	Width
0.0064	121.3	97.7	54.7
0.0121	153.4	100.0	51.8
0.0246	160.4	100.0	81.8
0.0367	192.2	100.0	29.53

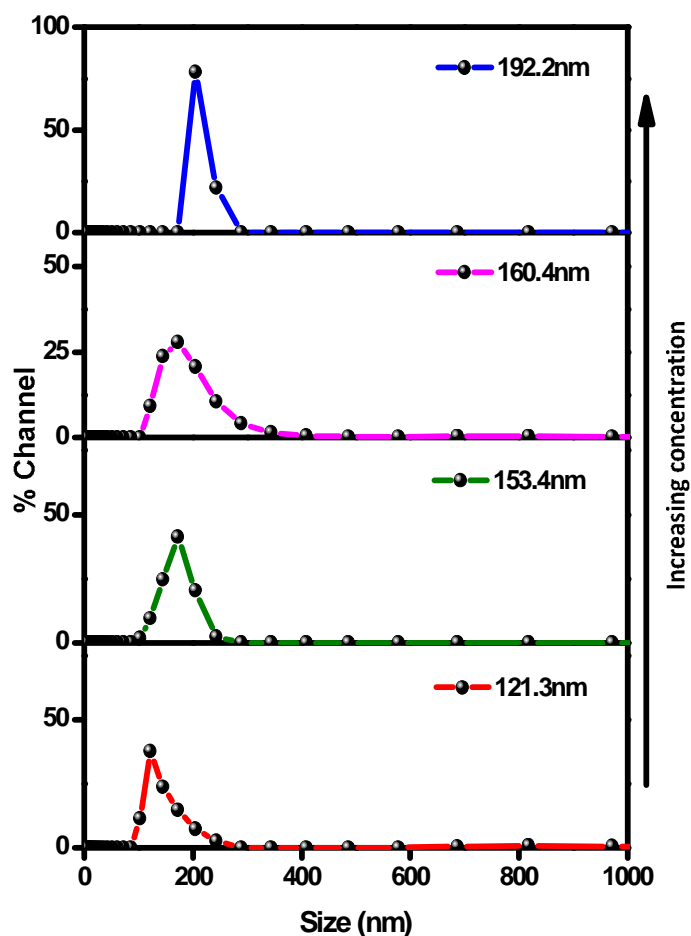


Fig. 3.10. A comparison plot for intensity averaged particle diameter (d_{50}) variation with different concentration of polymeric Bi solutions prepared in aqueous nitric acid medium.

3.3.6. Molecular weight of Bi(III) hydrous polymer

Figure 3.11 shows the refractive index increment of different concentration of Bi(III) solution. dn/dc was determined from the slope and used for obtaining the Debye plot.

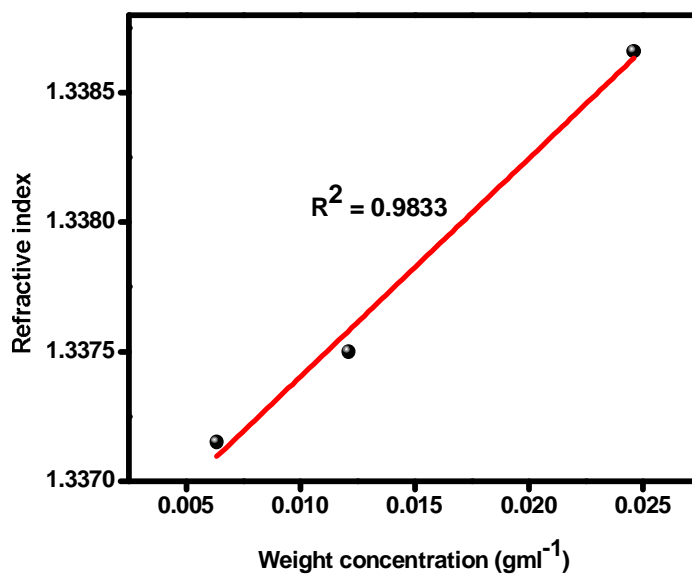


Fig. 3.11. The dn/dC curves obtained for different concentration of Bi(III) solution

As the concentration increases the refractive index of the solution also increases giving a positive slope, $dn/dC = 0.1304 \text{ ml g}^{-1}$. Refractive index of the particle was assumed as 1.9 which corresponds to bismuth hydroxide. The Debye plot is shown in figure 3.12 and the parameters obtained from the plot are given in table 3.7.

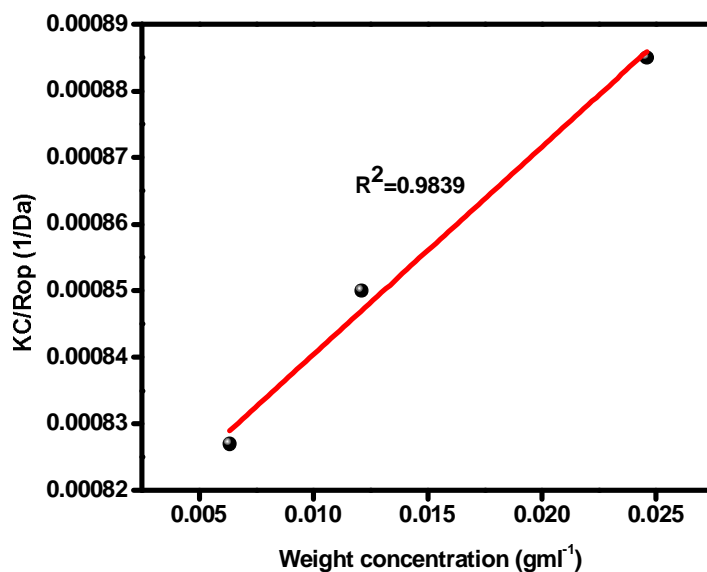


Fig. 3.12. Debye plot for various concentrations of Bi³⁺

Table 3.7. Calculated parameters from the Debye plot for Bi(III) hydrous polymer

Substance	Measured at $\lambda = 780$ nm	
	M_w (Da)	Second virial coefficient, A_2 (ml/g Da)
Bi(III) hydrous polymer	1,236	6.24E-03

The molecular weight of the polymer was determined as ~1,236 Da from the intercept of the plot. Second virial coefficient was determined as 6.24E-03 ml/g Da. The molecular weight from the Debye plot shows that Bi undergoes hydrolysis at low pH and forms polymers with more than 5 monomer units. Earlier it was reported that compounds with composition of $[\text{Bi}_6\text{O}_4(\text{OH})_4](\text{OH})(\text{NO}_3)_5 \cdot 0.5\text{H}_2\text{O}$ has been isolated above pH=1.6 [149].

The second virial coefficient (A_2) has a positive value which indicates that the overall net interactive force is repulsive between the solute species and hence stable in the aqueous nitric acid medium. Thermodynamically, the positive value of second virial coefficient shows a positive ΔG for polymer chain interpenetration which leads to steric stabilization [150]. The resulting stabilization could be the result of positive ΔH or negative ΔS , where positive enthalpy reflect the release of bound solvent and negative entropy reflect the loss of configurational freedom as the polymer chains interpenetrate. At this condition the dispersion is sterically stabilized. Thus nitric acid is found to be good solvent medium.

3.4. Conclusions

- Light scattering technique has provided a new approach to understand the nature of ion solvent interaction and its possibility to arrive at hydration number of metal cation under investigation.
- The diameter of the hydrated ion can be measured using dynamic light scattering method. Debye plot has been used to estimate the molecular weight of hydrated ion. The second virial coefficient has also been determined which gives the nature of solute solvent interaction. This simple method applies only to salts whose particle refractive index is different from that of the fluid refractive index.
- Th case of Al(III) hydrolysis, the initial hydrolysis at high acidity with OH/Al of 0, the number of solvating molecules was observed to be 5. Similarly for Sr(II) 9 water molecules are surrounding the Sr(II) ion in the primary hydration sphere possibly existing in the form of $\text{Sr}(\text{H}_2\text{O})_9^{2+}$.

- The second virial coefficient was negative in both the cases which show there is aggregation in the system.
- Though many techniques such as X-ray diffraction, centrifugation, electrophoretic and tyndallometric studies were employed to determine the speciation of Bi in aqueous medium, the present investigation attempts to determine the particle size and molecular weight of the hydrolysed species of Bi.
- The particle size increases with increase in concentration of the solute, due to increase in aggregation. This shows that polymerization of Bi strongly depends on concentration.
- The second virial coefficient has also been determined and the positive value shows that there is repulsion between the molecules making the polymeric solution stable.
- The weight average molecular weight of polymers of Bi(III) formed in aqueous nitric acid medium has confirmed that the hydrolysed species has 5-6 atoms of Bismuth.

Chapter 4



CHAPTER 4

Hydrolysis and Polymerization of Zirconium(IV) in Aqueous Nitric Acid Solutions

4.1. Introduction

Hydrolysis and polymerization of zirconium in aqueous solutions have found renewed interest mainly for its application in sol gel processes, ceramic engineering and also due to the fact that zirconium has high yield among the uranium fission products of fast neutron spectrum and it is considered as a high priority element for the assessment of radioactive nuclear waste repositories [21]. Zr(IV) is mainly taken as an analogue for Pu(IV) to understand its hydrolytic behavior. This is due to its similar tendency towards hydrolysis [151]. The first hydrolysis constant for $M(OH)^{3+}$ are $\beta_{1,1}^0=14.3$ [152] and $\beta_{1,1}^0=14.0$ [153] for Zr(IV) and Pu(IV) also matches.

Zr^{4+} is stable only at very acidic condition and the onset of hydrolysis starts even at $pH < 0$ similar to Pu(IV) [92]. Mononuclear species dominates only at low concentration of Zr ($< 10^{-5}$ M) [154]. For increasing pH, degree of polymerization increases leading to the formation of polynuclear species such as tetramers, pentamers, octamers. They are found to exist in concentrated solutions of zirconium salts ($[Zr] > 10^{-5}$ M) even at high acidities [155]. Close to the solubility limit large

polymers are also formed which is yet another parallel to Pu(IV) [92]. Figure 4.1 compares the species distribution in dilute solutions when polynuclear complexes are not present in the system.

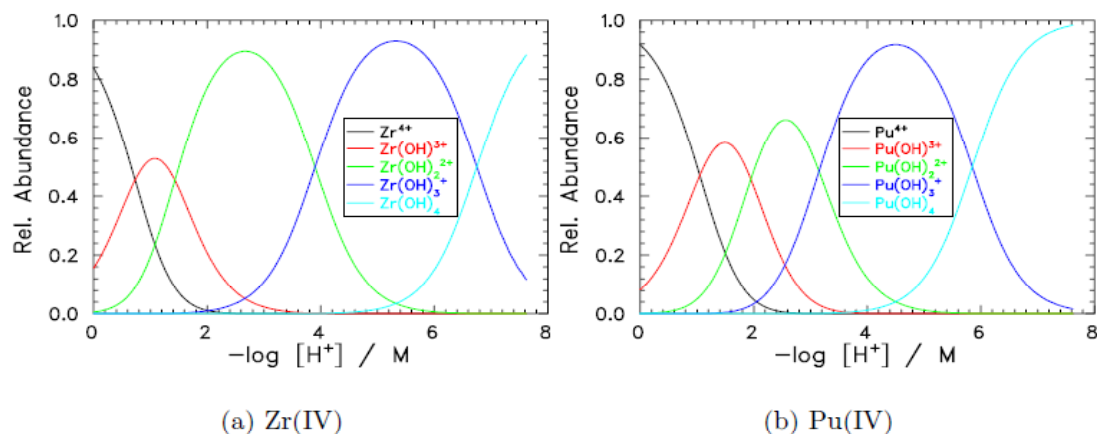


Fig. 4.1. Calculated distribution of mononuclear hydroxide complexes (HCl/NaCl solutions of $I=0.5 M$) in the absence of polynuclear species, at very low metal ion concentration [30]

Polymerization of zirconium can be identified by slow conductivity changes in the solution and freezing point depression [156-157], potentiometry, titration with base or by using desktop ESI-MS [158]. Earlier works reported the existence of trimeric [$Zr_3(OH)_4^{8+}$ or $Zr_3(OH)_5^{7+}$] and tetrameric [$Zr_4(OH)_8^{8+}$] solution species. X-ray scattering studies have shown that [$Zr_4(OH)_8(H_2O)_{16}$] $^{8+}$ species is the major form present in solutions and tetramers are stable even at high concentration ($[Zr] = 2M$) [159-162]. Various studies were performed to elucidate the structure of these polymeric species. Some of the important results are as follows.

Computational study on tetrameric species indicates a planar form comprising eight-coordinated Zr^{4+} ions with an antiprism/irregular dodecahedron ligand arrangement in an aqueous environment [163]. Studies also reported that these tetrameric units aggregate as two dimensional sheets [164]. SAXS measurements

performed on zirconium acidic aqueous solutions also identified tetrameric species and in addition they have also demonstrated that octameric species also exists in equilibrium with tetrameric species. These octamers are formed by stacking two tetramers on top of each other [165]. Nanoelectrospray mass spectrometry combined with XAFS investigation also confirmed the same results [154]. The two plausible configurations for the octameric species are shown in figure 4.2.

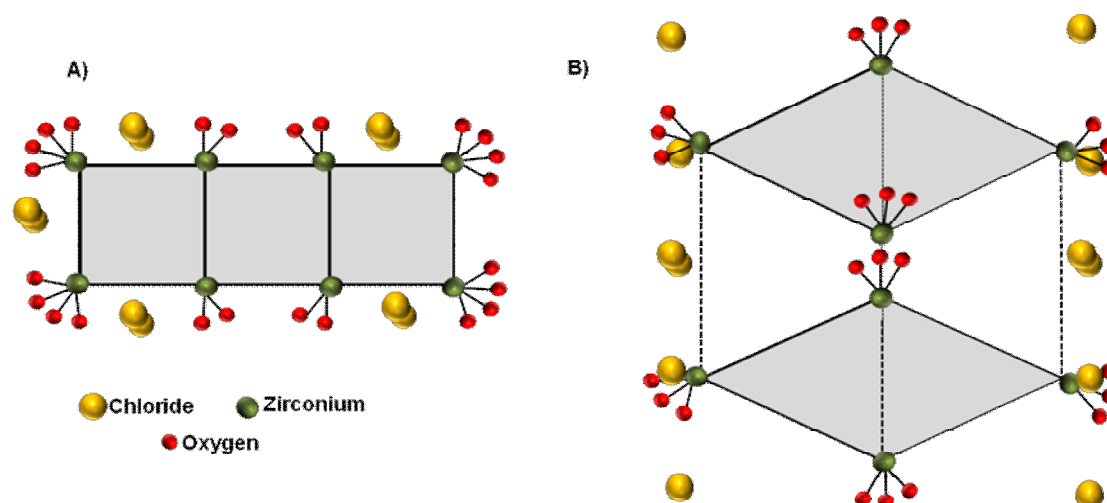


Fig. 4.2. Representation of two octamer configurations A) Sheet octamer B) Stacked octamer [160]

These layers further aggregate and form a three dimensional fluorite structure by a condensation process that result in loss of water from the structure [166]. Another mechanism also supported the two dimensional sheet like structure [167]. SAXS measurements made on $ZrOCl_2$ solutions heated to elevated temperatures showed that the shape of clusters at earlier stages of growth is close to rod rather than sheet [168]. EXAFS on samples of oligomeric and polymeric species postulates that the structure of these solution species is not a simple ZrO_2 ; it has neither the monoclinic, cubic, orthorhombic, nor tetragonal ZrO_2 structure. Its structure cannot be derived from

simple stacking of tetrameric $[\text{Zr}_4(\text{OH})_8(\text{H}_2\text{O})_{16}]_{8+}$ units as discussed earlier. The species are built up of primarily ZrO_8 building blocks. The ZrO_8 building blocks can take on different geometries and related polyhedra being cube, square antiprism, dodecahedron and hendecahedron [169].

But there are very limited information available related to polymers and colloids formed due to hydrolysis of zirconium. Thus the present chapter deals with the conditions of colloids formed, ageing effect and determining the molecular weight of freshly prepared and polymers aged at different time intervals.

4.2. Experimental work

4.2.1. Preparation of standard solution for determination of Zr(IV)

- Four solutions of 0.025, 0.05, 0.075 and 0.1 mg of zirconium per ml were prepared in 1 N nitric acid. The solutions were prepared by dissolving required amount of zirconium nitrate in 1 N nitric acid to avoid hydrolysis.
- Standard phosphate solution was prepared by dissolving 0.05 g of sodium dihydrogen phosphate in distilled water and diluting it to 100 ml.
- A 10% solution of ammonium molybdate was prepared by dissolving 5 g of ammonium molybdate in distilled water, filtered and diluted to 50 ml.
- 10 N sodium hydroxide solution and 2.8 N nitric acid was prepared freshly by dissolving desired amount and diluted to 50 ml with distilled water.

4.2.2. Preparation of colloidal Zr(IV) solutions

- Formation of polynuclear species and colloids must be investigated in an environment extremely clean with respect to crystallization germs/impurities

which could cause premature precipitation and formation of colloids. Thus prior to the investigation, the sample cells were thoroughly cleaned and in order to ensure that the solutions are colloid free, the following procedure was followed,

- The sample cell was thoroughly cleaned with conc. HNO₃.
 - The stock solution was always prepared in 1M HNO₃ to avoid any initial hydrolysis which can lead to colloid formation.
 - The solutions are then centrifuged at a speed of 20,000 rpm.
 - Finally scattering measurements were performed to ensure there is no signal corresponding to the presence of colloid.
- Zirconium solutions of various concentrations (0.0125 to 0.05 gml⁻¹) were prepared from zirconyl nitrate monohydrate in 1 M nitric acid in order to avoid initial hydrolysis. 0.1 M sodium hydroxide and 0.1 M nitric acid was added to adjust pH and light scattering measurements were performed to determine the onset of colloid formation. All the measurements were performed at 27±1°C.

4.3. Results and discussions

4.3.1. Procedure for determination of micro-level Zr(IV) in aqueous solutions

Solutions of zirconium salts can contain Zr⁴⁺, ZrO²⁺ and several polymerized ions if the concentration of metal is higher and also depending on the acidity of the solution. The Zr⁴⁺ ion reacts with many reagents much faster and this fact is used for determining microquantities of the metal ion. Several organic reagents were used as complexing agents such as xylenol orange [170], Arsenazo I and III

[171], pyrocatechol violet [172] for trace determination of Zr and have certain limitations with sensitivities and they will be stable only at particular pH. The gravimetric determination of zirconium as zirconium phosphate is another most widely used method for determining zirconium but it is applicable only for macro amounts of Zr. Hence a method to determine micro-level zirconium in aqueous solution at high acidities is required in order to avoid the interference of its hydrolyzed species.

In the present method, zirconium is precipitated as zirconium phosphate by the addition of standard phosphate solution and the remaining concentration of phosphate in the supernatant solution is determined by converting it into molybdiphosphoric acid which has a characteristic yellow colour. The concentration of zirconium in the present investigation ranges about 25-100 ppm. A 20 ml of the prepared zirconium solution is transferred to 50 ml beaker and 5 ml of concentrated nitric acid is added to it. To that, 10 ml of standard phosphate solution is added and the solution is allowed to stand for about 4 hours. The treatment of acidic solution of zirconium ions with excess of phosphate solution results in the precipitation of zirconium as zirconium phosphate. The resultant solution is centrifuged for 15 min. About 25 ml of the supernatant solution is transferred into 50 ml beaker and neutralized with 10 N sodium hydroxide solution. 5 ml of concentrated nitric acid is added to it and then diluted to the mark with distilled water. 5 ml of the molybdate solution is added to the above solution. Yellow colour develops. Ammonium molybdate solution is used as blank. For different concentration of zirconium solutions the maximum absorbance is measured at $\lambda_{\text{max}} = 369$ nm. As the concentration of zirconium in the solution increases the phosphate ions in the solution

decreases because large amount of zirconium will be precipitated as zirconium phosphate. Hence the intensity of the colour which is the characteristic of molybdiphosphoric acid will decrease. This results in the decrease of absorbance at higher concentration of zirconium. Figure 4.3 a & b shows the absorption spectra and calibration graph of zirconium(IV). It shows that the molybdiphosphoric acid system confirms the Beer's law. That is a definite relationship exists between the concentration of zirconium and the removal of phosphate ions from the solution. For the determination of microamounts of zirconium, the proposed method is simple and sensitive. Therefore this procedure assumes significant importance in view of scarcity of good methods available for determining zirconium.

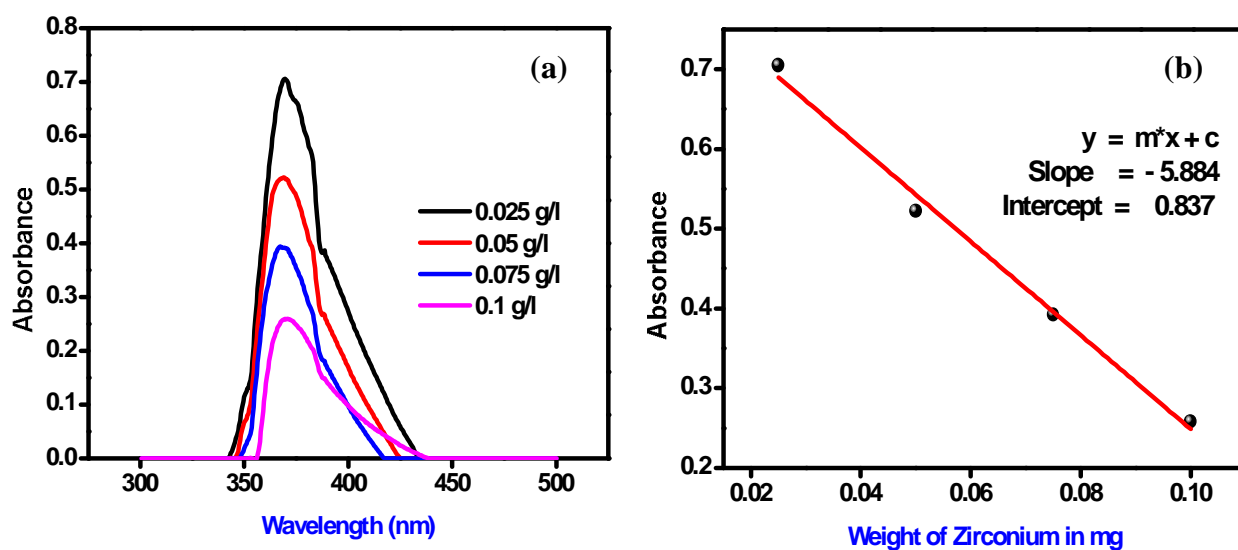


Fig. 4.3.(a). UV-visible absorption spectra of Zr(IV) **(b).** Plot showing a linear relationship between zirconium concentration and removal of phosphate ions from the solutions

4.3.2. Light scattering studies on hydrolysis of zirconium(IV)

4.3.2.1. Formation of Zr(IV) colloids

Light scattering measurements were performed for different concentrations between $[\text{Zr(IV)}]_{\text{tot}} = 0.1 - 0.5 \text{ M}$. The hydrolysis of Zr species is a continuous process which leads to charge compensation through the sequential substitution of water molecules by hydroxide ligands close to the solubility of $\text{Zr(OH)}_4(\text{am})$ leading to polymers of colloidal dimensions. The general equilibrium reaction for hydrolysis of Zr(IV) is shown in figure 4.4.

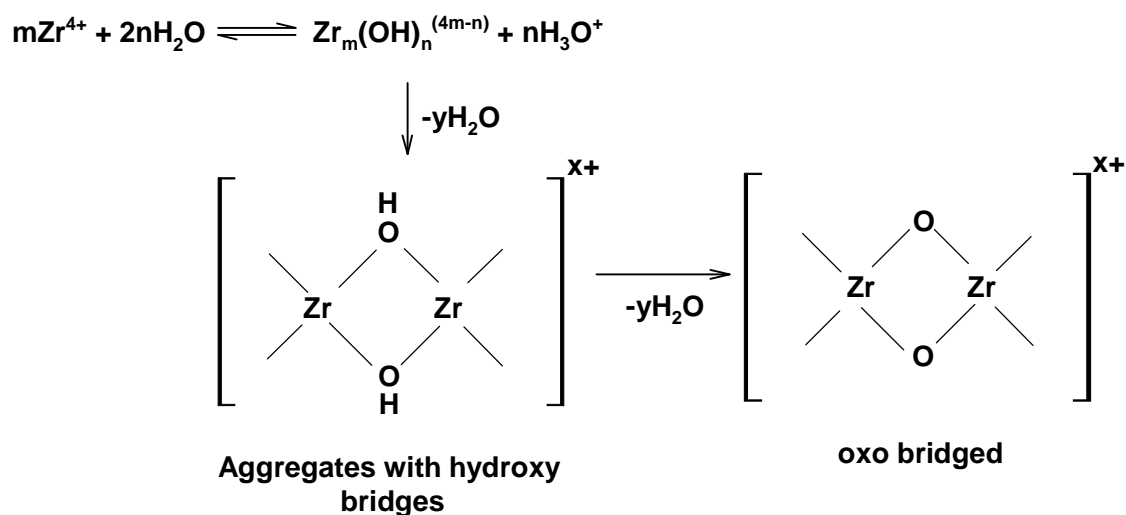


Fig. 4.4. General equilibrium reaction for hydrolysis of Zr(IV)

The formation of colloids after exceeding the solubility limit was observed by DLS as described in section 2.2.6. The onset of colloid formation starts at $\text{pH} = 0.3$ for initial concentration of 0.1 M Zr and the pH of onset of colloid formation still decreases with increase in the concentration of zirconium. The intensity data of DLS is taken as the average size of the particle and it is found to be 255 nm (figure 4.5) formed in 0.1 M Zr(IV) solution of $\text{pH} \sim 2.0$ at 27°C . The size of the particle is not constant and it

increases with increase in Zr concentration. The polydispersity index of the polymer is 0.1. For decreasing Zr concentration (i.e. $[Zr] < 0.1$ mM) it was difficult to observe colloid formation because DLS technique is restricted to suspensions of large colloids. At $[Zr]_{tot} = 0.1$ mM diluted to $pH > 3.0$ small number of colloids of $>1\mu m$ was observed. The summary of the peak is given in table 4.1.

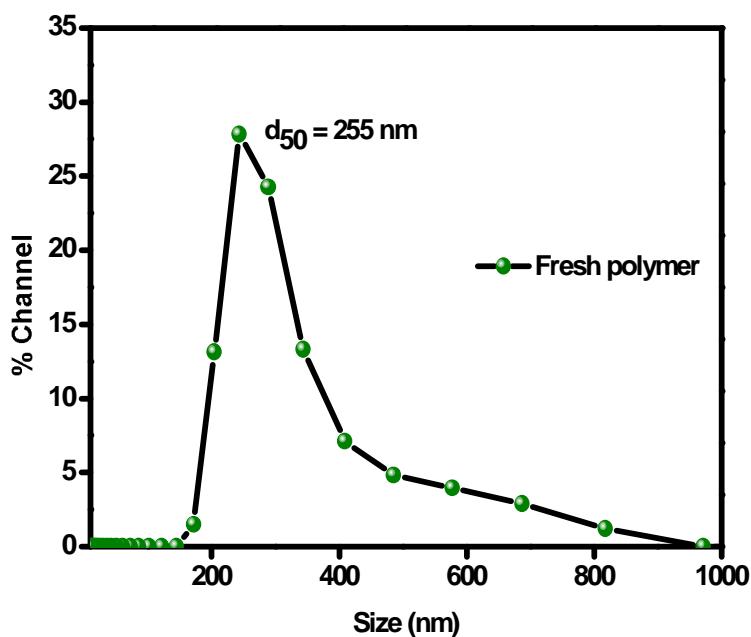


Fig. 4.5. Intensity distribution curve of Zr(IV) polymer formed in aqueous nitric acid solution ($[Zr(IV)] = 0.1$ M)

Table 4.1. Peak summary for Intensity distribution curve of Zr(IV) hydrous polymer

Particle Diameter (nm)	Volume %	Width
255.0	100	168.10

The polymeric species are considered to be linked through hydroxyl bridges. There are many reports available in order to support this assumption. For instance, the

structure of the tetrameric unit is believed to be a ring of four zirconium atom each linked to its neighbor through a pair of hydroxyl bridges. These tetrameric species are composed of two dimeric units ($\text{Zr}(\text{OH})_2\text{Zr}$) bridged by hydroxyl groups [173]. A hard sphere model was proposed for polynuclear hydrolysis species of Zr(IV). It was considered to follow the same trend as tetravalent actinides, i.e. polymers are bridged by hydroxide ions and not by oxygen bridges.

4.3.2.2. Effect of pH on size of Zr(IV) colloidal polymer

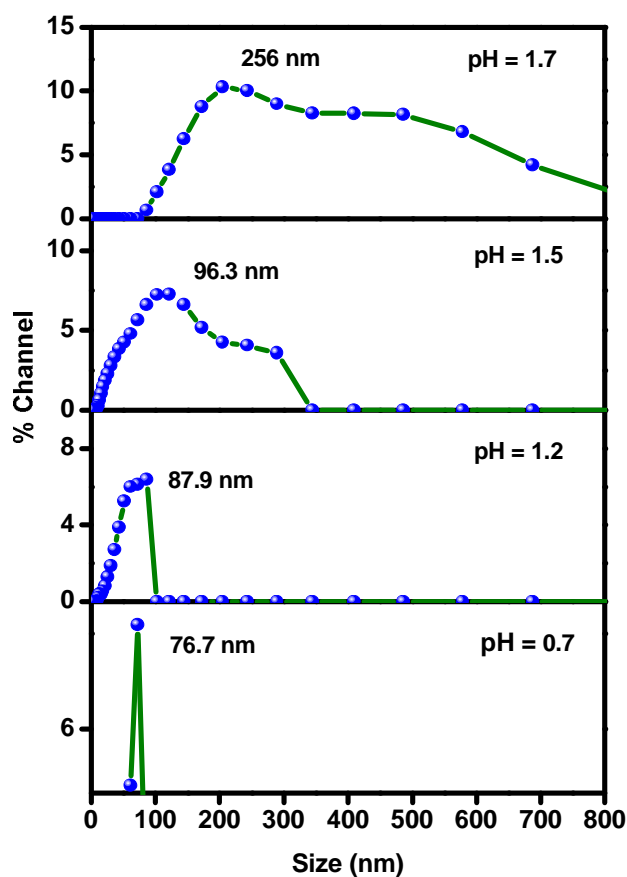


Fig. 4.6. Increasing colloidal size with increasing pH for 1 M Zr(IV) solution

Figure 4.6 shows the effect of pH on size of the polymer formed at constant concentration of zirconium. The initial concentration taken for investigating the pH

dependent size variation is 1 M Zr(IV) solution. In the present case, the size of the colloids formed initially is ~ 25 nm at pH<0.1. The size of the initially formed colloids are very small when compared to colloids formed in 0.1 M Zr(IV) solution. This may be due to the microcrystalline nature of colloids. This can also be understood from the scattering solubility data due to existence of different phases. It exists as microcrystalline phase of very small size at low pH and less ordered amorphous phase of larger particles at high pH [92, 174]. This is similar to Pu(IV), whose amorphous Pu(IV) hydroxide colloid formed has weighted mean colloid size of 12 – 25 nm which is much bigger than the 2 nm crystalline PuO₂ colloids.

When pH of the solution is increased, the size of the colloids also increases. With increase in the pH of the solution, the reaction for the deprotonation step required in the condensation process increases. Thus, creation of a larger number of OH sites on the polymer increases the probability of contact in other direction leading to the increase in growth rate of the polymer. Polymerization of Zr(IV) hydrolyzed species proceeds more slowly at low pH than at high pH due to limited number of OH groups available and hence it is considered that colloids formed at lower pH has more ordered structure [167]. In figure 4.6, beyond pH~1.5, the size of the colloid immediately increases and reaches 256 nm at pH 1.7. This shows that there is rapid aggregation at higher pH. A further increase in pH i.e. pH > 1.7 results in lower number of colloids and colloids smaller than 200 nm were not detected at all due to size screening effect i.e., decrease in signal proportional to d^6 . In other words large particles if present in even small quantities will be accounted during data analysis.

4.3.2.3. Size of Zr(IV) colloidal polymer aged at different time intervals

0.1 M Zr(IV) solution diluted to pH = 0.3 was aged for around 7 days. Further growth of colloids was observed with ageing. The colloid growth was accompanied by a slight increase in acidity due to release of H⁺ into the solution which can be understood from the following equation 4.1.



Colloids of two different sizes were obtained at ~215 nm and another at ~402 nm for solutions aged for 3 days (figure 4.7(a)). The particle size corresponding to 215 nm may be due to the primary particle that was formed initially in the system. On ageing the solution, the primary particles form large aggregates. Peak corresponding to 402 nm may be due to larger aggregates formed. This on further ageing for 7 days gave a similar size distribution pattern. But there is a slight shift in the 402 nm peak (figure 4.7(b)). This is due to more aggregation with increase in time. Figure 4.7(c) depicts the overall growth process. Zirconium oxychloride solutions prepared at different pH were heated at elevated temperature for various aging periods to gain understanding of growth mechanism and structure of zirconium hydrous polymers. SAXS (Small angle X-ray scattering) measurements were made on these solutions. The scattering data indicated that a rod shaped primary particle is formed at pH 1.2 and on increase in pH, the primary particles become more branched. On aging more than 1250 min at 95°C, these primary particles form large aggregates. These aggregates restructure while growing in size and eventually transform into dense particles [164].

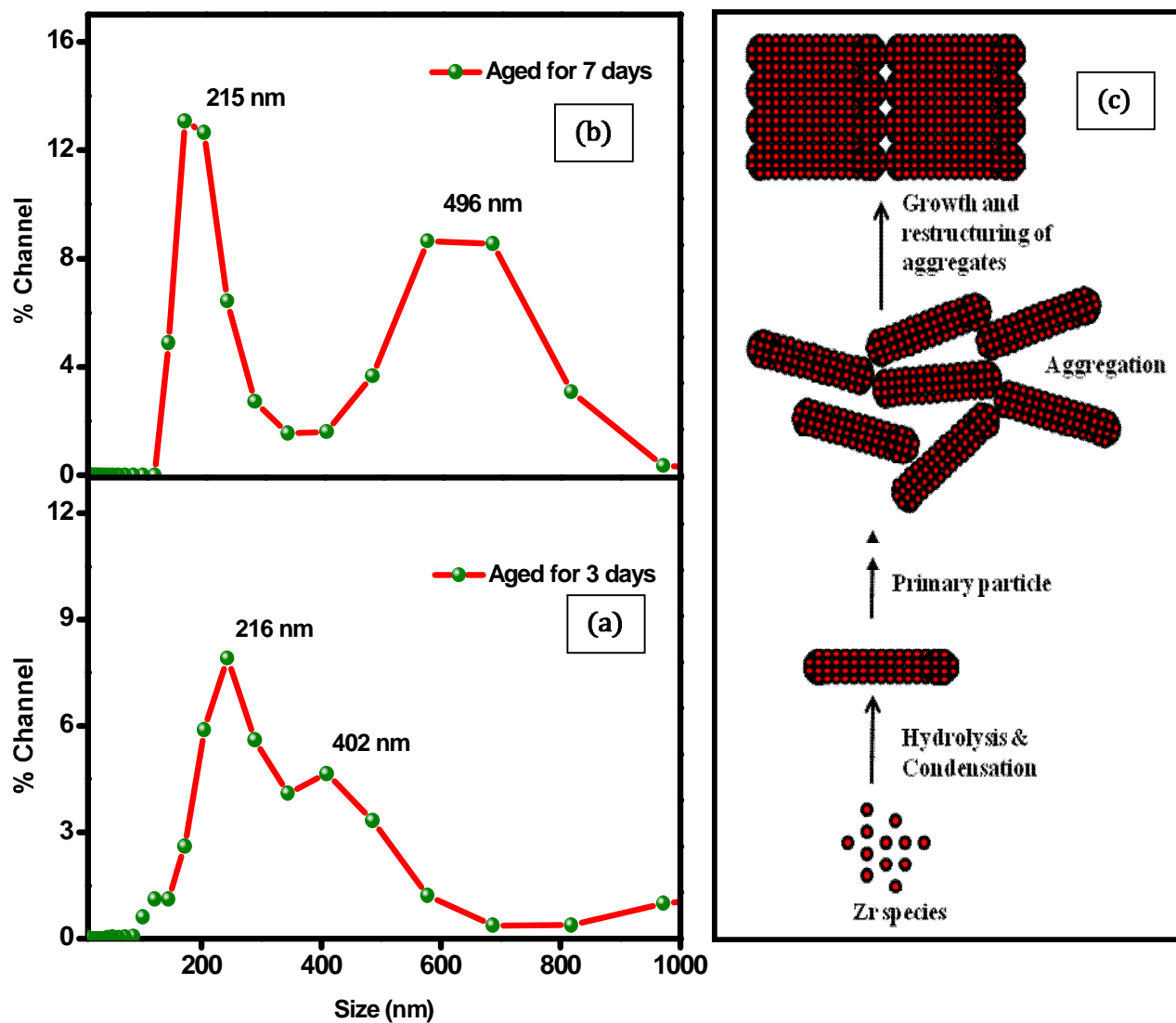


Fig. 4.7. Intensity size distribution of Zr(IV) colloid
(a) Aged for 3 days
(b) Aged for 7 days
(c) Schematics of growth process of Zr polymeric species forming rod like particles [164]

4.3.2.4. Molecular weight of Zr(IV) hydrous polymer

4.3.2.4.1. Freshly prepared polymer

Figure 4.8 shows the refractive index increment for different concentrations of Zr. As the concentration of the solute increases the refractive index of the solution also increases giving a positive slope with $dn/dc = 0.1278 \text{ mlg}^{-1}$. This value has been used as an input for generating the Debye plot. A value of 3.25 gcc^{-1} was used for particle density which corresponds to hydrous ZrO_2 .

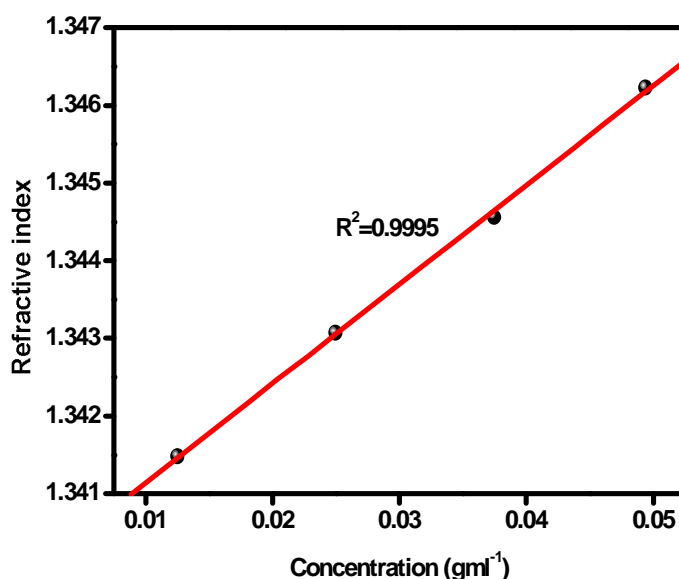


Fig. 4.8. Refractive index increment of different concentration of Zr(IV) solution

Shape of the particle is an important parameter to determine molecular weight of polymers. As mentioned in earlier investigations, Zr polymer at its earlier stages of growth is rod shape. Hence molecular weight measurements were done considering the shape of the system as irregular. Following are the steps followed to obtain Debye plot.

- Preparation of different concentrations of Zr(IV) polymer solutions.
- Concentration of the solution and differential refractive index values were given as input in the software.
- For each individual concentration, the KC/R_{θ} was obtained.
- Finally a plot of KC/R_{θ} Vs C (g/ml) was generated.
- The Molecular weight (M_w) is determined from the intercept point on the Y axis. i.e. $KC/R_{\theta} = 1/M_w$ in Daltons.
- The 2nd Virial Coefficient (A_2) is determined from the gradient of the Debye plot.

The weight average molecular weight of the freshly prepared polymer was determined as 1,610 Da from the intercept of the Debye plot shown in figure 4.9. The calculated parameters from the Debye plot are shown in table 4.2. The negative value of second virial coefficient (A_2) indicates that the intermolecular interaction i.e. solute-solute interaction dominates over solute-solvent interaction. Thus there is aggregation in the system. Degree of polymerization is calculated from the ratio of weight average molecular weight and molecular mass of monomer.

$$\text{Degree of polymerization} = \sum w_i M_i / m$$

In the present case, $\sum w_i M_i = 1,610$, $m = 125$. It shows that around 10 atoms of Zr are present in the freshly prepared polymeric unit which is similar to Pu(IV) polymer whose molecular weight is 4,000 Da if freshly prepared containing around 10 Pu atoms in the polymer unit [73].

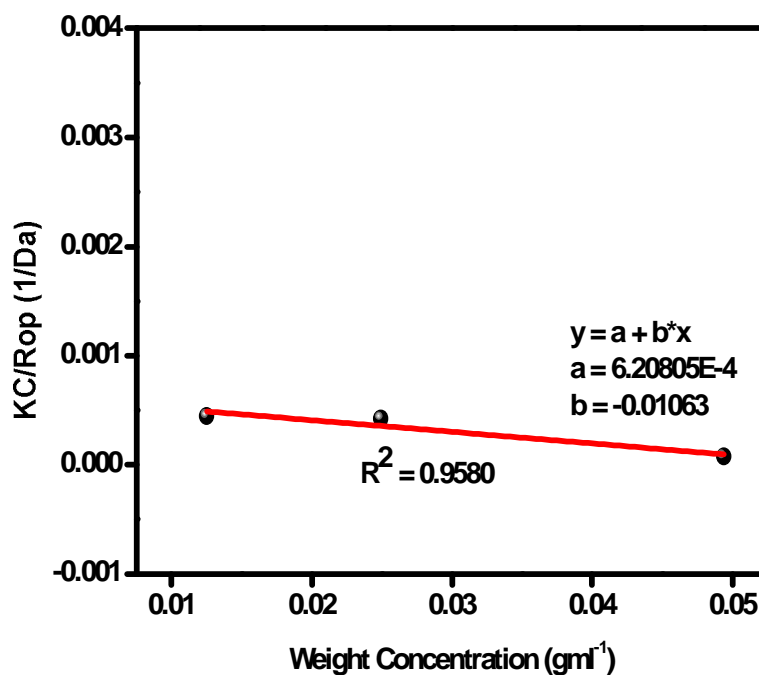


Fig. 4.9. Debye plot for freshly prepared Zr(IV) hydrous polymer

Table 4.2. Calculated parameters from the Debye plot for freshly prepared Zr(IV) hydrous polymer

Substance	Measured at $\lambda = 780$ nm	
	M_w (Da)	Second virial coefficient A_2 (ml/g Da)
Zr(IV) hydrous polymer (freshly prepared)	1,610	-0.0106

4.3.2.4.2. Aged polymer

The colloidal solution was kept to age for 7 days and growth of colloids was observed. Figure 4.10 shows the refractive index increment for different concentrations of Zr. As the concentration of the solute increases the refractive index of the solution also increases giving a positive slope with $dn/dc = 0.1278$ mlg⁻¹.

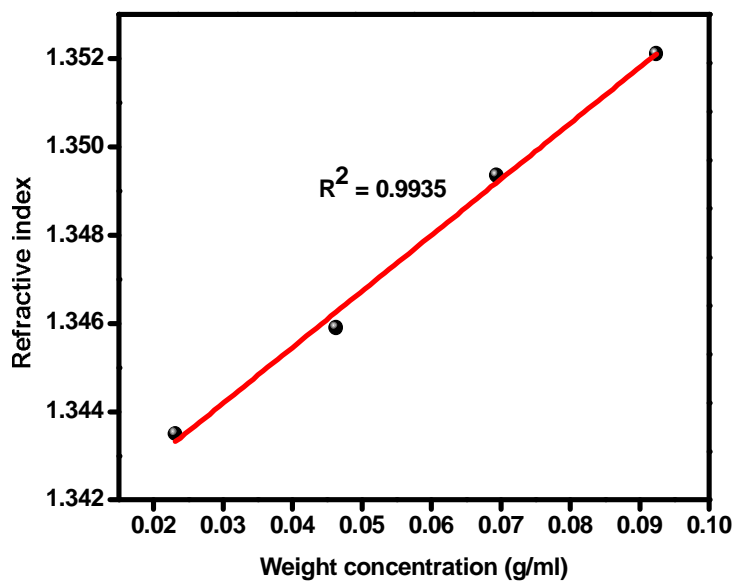


Fig. 4.10. Refractive index increment of different concentration of polymeric Zr(IV) solution aged for 7 days

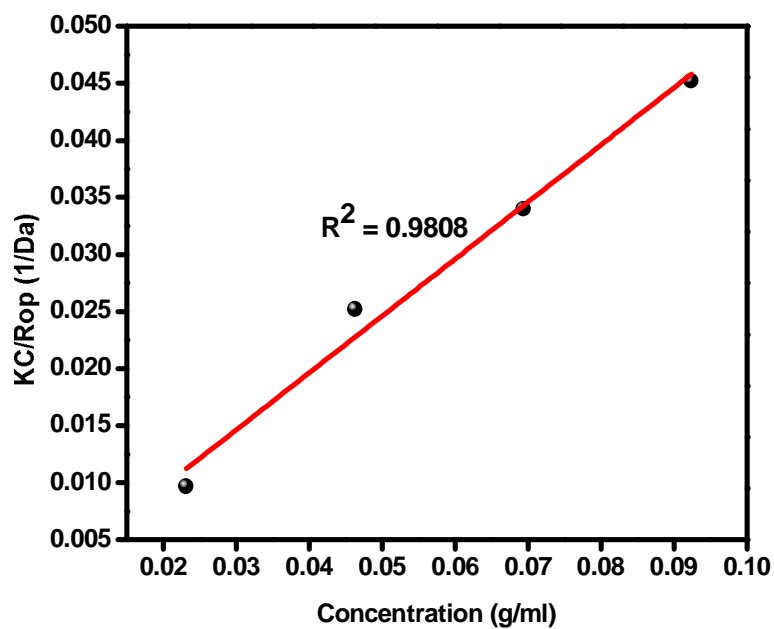


Fig. 4.11. Debye plot for 7 days aged Zr(IV) hydrous polymer

Table 4.3. Calculated parameters from the Debye plot for 7 days aged Zr(IV) hydrous polymer

Substance	Measured at $\lambda = 780 \text{ nm}$	
	M_w (Da)	Second virial coefficient, A_2 (ml/g Da)
Zr(IV) hydrous polymer (aged for 7 days)	3,000	0.499

The weight average molecular weight of the polymer aged for seven days was determined as 3,000 Da from the intercept of the Debye plot shown in figure 4.11. The positive value Second virial coefficient (A_2) is positive which indicates that the intermolecular interaction i.e. solute-solvent interaction dominates over solute-solute interaction. Thus after few days, the colloids are stable and there was no settling or precipitation. It shows that Zr form larger aggregates after the solubility limit is exceeded and these colloids do not dissolve for longer time. The growth of the colloid continues until equilibrium is reached [169]. Recent studies have also suggested that ageing of freshly prepared amorphous zirconium hydroxide polymers leads to phase transformation towards a more crystalline phase [169]. The calculated parameters from the Debye plot are summarized in table 4.3. Weight average molecular weight of the polymer shows that ~ 30 atoms of Zr are present in the polymeric unit aged for 7 days which is similar to Pu(IV) polymer whose molecular weight is 10^{10} Da for aged polymer with 100 - 1000 Pu atoms in the polymer unit [73].

4.4. Conclusions

- The gravimetric determination of zirconium as zirconium phosphate is one of the most widely used macro-methods for determining zirconium. The present method was to develop a spectrophotometric method applicable to the micro determination of zirconium.
- At a given Zr(IV) concentration, and with increasing pH, the degree of polymerization increases.
- The size of initially formed colloids at lower concentration is much higher than that of the colloids formed at higher concentration due to existence of different phases.
- Close to the solubility limit, continuous growth of the polymers was found which leads to the formation of large polynuclear species and colloids of ~ 1,600 Da.
- On further ageing for 7 days, the weight average molecular weight of the polymers increases to ~3,000 Da. This shows that the ageing of the polymer is accompanied by addition of more monomeric unit to the polymer.
- Second virial coefficient indicates that there was aggregation during the initial formation of polymer and the colloids become stable in the solution with increase in time.
- The molecular weight of Zr(IV) polymers formed in acidic solution has not been reported in the literature. The present study provides an insight to

determine molecular weight of colloidal polymers and also the nature of interaction of the solute with the solvent.

- Molecular weight determination of polymers by light scattering is simple and sensitive than other proposed techniques.
- It is also clear that the aqueous chemistry of Zr(IV) is similar to Pu(IV) and serves as an excellent homologue.

Chapter 5



CHAPTER 5

Hydrolysis of Uranium(IV & VI)

5.1. Introduction

Due to high electric charge, tetravalent actinides have an inordinate tendency to undergo hydrolysis leading to formation of polynuclear species of colloidal dimensions even under very acidic conditions. Such processes are observed for tetravalent ions such as Th(IV), Pu(IV), U(IV), Np(IV), Pa(IV) and to a lesser extent for the hexavalent actinyl ions U(VI) and Pu(VI) [20, 175]. In nuclear reactors, uranium is handled in large quantities when compared to other actinide elements. The behavior of uranium in radioactive waste repositories and the migration of U in the environment depends on its oxidation state and its speciation is determined by pH, presence of complexing anions and total salt background. Uranium exists in different oxidation states (from +3 to +6). The known redox states of uranium are U(II), U(III), U(IV), U(V) and U(VI) and their corresponding reduction potentials are given in figure 5.1.

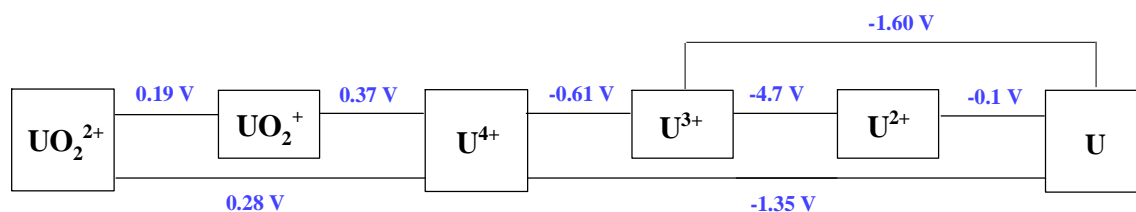


Fig. 5.1. The redox potential differences for the uranium ions and pure U [20]

Uranium(III) can exist only under anaerobic and strongly reducing conditions. U(IV) is also considered as toxic waste under strongly reducing conditions that is often accepted to be present in deep geological repositories [176]. U(V) is unstable and disproportionates. U(VI) is the most common species in the environment. Under natural aquatic systems, uranium exists as U(IV) and U(VI).

5.2. Uranium(IV) hydrolysis

U(IV) aqueous chemistry is of particular interest under reducing conditions which prevails in both inside of nuclear waste repositories and under deep uranium mines [177]. Due to hydrolysis, U(IV) occurs in the form of $[\text{U}(\text{OH})_x]^{(4-x)+}$ [178]. The hydrolysis reactions of U(IV) resulting in the formation of polynuclear hydrolysis complexes is given in equation 5.1.



U(IV) is readily oxidized to U(VI) when reducing conditions are not maintained carefully. The solubility of U(IV) is lesser than U(VI) by many orders of magnitude. The solubility product of crystalline $\text{UO}_2(\text{cr})$ formed at $\text{pH} \sim 1$ and amorphous hydrous oxide $\text{UO}_2 \cdot x\text{H}_2\text{O}(\text{am})$ formed at $\text{pH} \sim 3$ was determined as $\log K_{\text{sp}}^{\circ} = -59.6 \pm 1$ and $\log K_{\text{sp}}^{\circ} = -54.1 \pm 1$ by combined coulometric titration and LIBID experiments. Compounds containing U(IV) are insoluble in mildly acidic and alkaline medium. Under certain conditions, U(IV) forms stable colloids which lead to its mobilization. Attempts were made to produce colloids of U(IV) by electrochemical reduction of U(VI) and EXAFS investigation performed on those colloids showed correspondence with amorphous $\text{UO}_2 \cdot n\text{H}_2\text{O}$. U(IV) hydrolysis is not solely of interest due to its existence only at highly acidic conditions [177]. But if the required

conditions are met, the results will be significant in order to compare with Pu which cannot be handled directly.

5.2.1. Experimental Section

5.2.1.1. Preparation of aqueous U(IV) solutions by electrolytic reduction of U(VI)

U(IV) is commonly prepared by a variety of chemical methods which use reducing agent such as aluminum dust, sodium formaldehyde sulfoxalate, formic acid catalysed by platinum dispersed on alumina, catalytic reduction by hydrogen over platinised alumina catalyst, photochemical methods or by electrochemical methods. The chemical reductants contaminate the fuel with impurities like sulphur, which affect the sintering characteristics of the oxide. Being only an electron transfer process, the electrochemical methods does not introduce any foreign ion in the U(IV) solution and hence it is found to be more suitable than chemical methods. In the present work, feed uranyl solution was prepared by dissolving U_3O_8 powder by using 1-1.5 M HNO_3 . Feed solution is subjected to electrolysis by appropriate dilution to maintain an initial acidity of the solution as 3 M. Because the rate of production of nitrous acid during electrolytic reduction of U(VI) in nitric acid solutions is directly related to nitric acid concentration, it is necessary to minimize possible reoxidation of U(IV) to U(VI). Hence it is best to operate at low nitric acid concentration as possible.

A cylindrical titanium vessel of 250 ml capacity was used for electrolytic generation of U(IV). The vessel itself was used as cathode and a platinum wire placed in the connecting limb was used as anode. The current density applied was 15-20 mA/cm^2 . 0.5 – 1M HNO_3 is used as analyte and 100 – 150 g per litre of uranyl as catholyte. U(VI) solution was electrolyzed for an hour. 0.5 M hydrazine is added in

order to avoid oxidation of U(IV) to U(VI). UV-visible absorption spectra of the initial and final solutions were recorded to make sure that U(VI) was reduced to U(IV) during electrolysis. Concentrations of hydrazine and nitric acid were adjusted in such a way that the final free acidity of the solution was 0.1 M and concentration of hydrazine was always around 0.05 M. The reactions taking place at the cathode, anode and overall reactions are given in equations 5.2 – 5.5 [179]. The set up used for U(IV) generation is shown in figure 5.2.

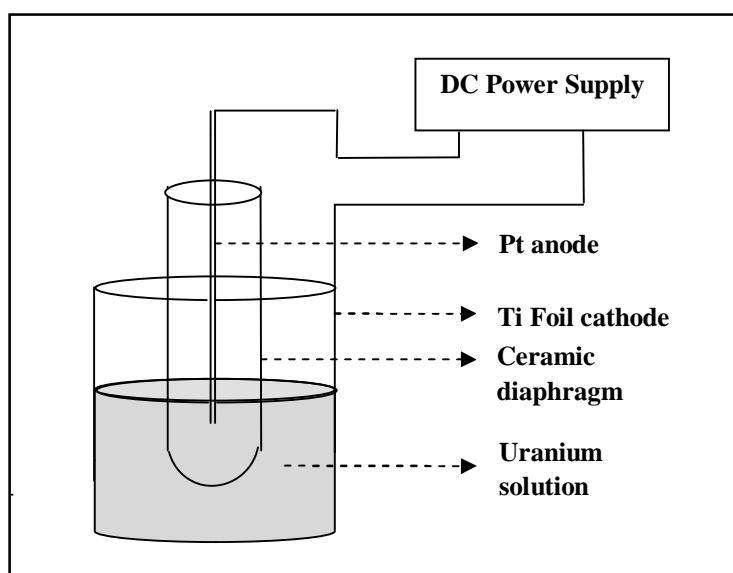
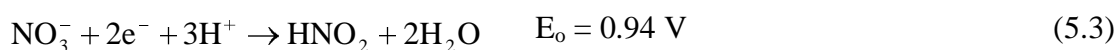
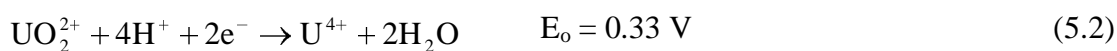
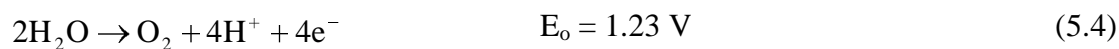


Fig. 5.2. Schematic diagram of electrolytic setup used for U(IV) generation [179]

At cathode:



At anode:



The overall electrolysis reaction is



5.2.1.2. Synthesis of U(IV) colloids

U(IV) solution of different concentration of 0.4 mM to 19 mM was prepared by diluting the solution with millipore water. Water used for making the solutions was ASTM grade I water with a resistivity of $18.2 \text{ M}\Omega \cdot \text{cm}^{-1}$ at 298.15 K and TOC < 15 ppb, obtained from a Millipore simplicity system. pH of the solution was adjusted by gradually adding 0.1 M NaOH.

5.2.2. Results and discussion

5.2.2.1. Particle size

Figure 5.3 shows the UV-Vis spectra taken for the stock solution and diluted solution with a total uranium concentration of 0.4 mM.

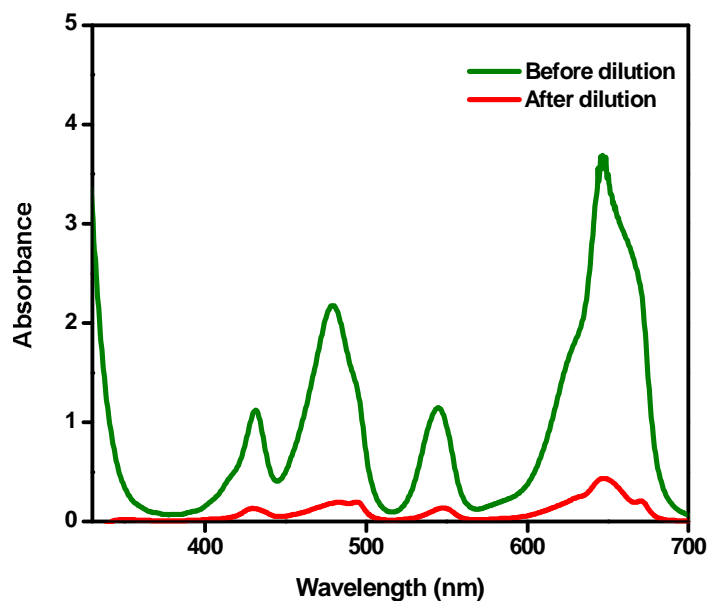


Fig. 5.3. UV-Vis spectra of U(IV) solution in the course of its dilution

Before proceeding with the experiments, it was ensured that there was no oxidation after dilution and U(IV) species are stable at the present condition by taking a blank run in UV-visible spectrophotometer as it can be used to detect higher concentration of U(IV) of the order of 5×10^{-5} M. There was no considerable change in the spectrum of diluted U(IV) solution and hence it was confirmed that the maximum species present are U(IV). A series of U(IV) solutions were measured by light scattering with concentrations of 0.4 mM - 19 mM. For each series, the pH was varied, starting at pH 1 and increasing to pH 4 by gradually adding 0.1 M NaOH. The particle refractive index was assumed as 1.95 corresponding to uranium oxide in order to obtain the size distribution [180].

i. 0.4 – 2.5 mM U(IV) solutions

In case of 0.4 – 2.5 mM U(IV) solutions, the pH of the solution is increased and light scattering measurements are made every 0.2 units until pH 3. It is observed that there is no signal corresponding to colloids in the starting solutions which shows that these solutions are colloid free. Beyond pH~4 there are only particles greater than 1000 nm which is considered to be the amorphous precipitates that have been formed in the solution (figure 5.4).

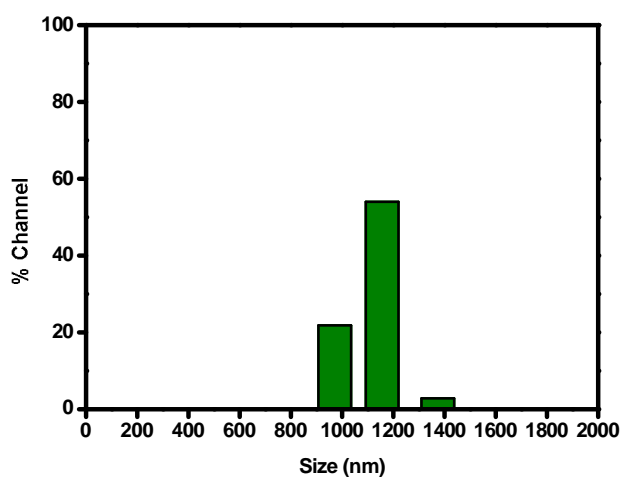


Fig. 5.4. Size distribution curve of 0.4 mM U(IV) solution at pH 4.5

ii. 3 – 7 mM U(IV) solutions

The solution darkens when pH is increased, consistent with the presence of colloidal U(IV) (figure 5.5) [154]. The intensity distribution curves for colloidal 3.78 mM U(IV) solution at different pH are shown in figure 5.6.



Fig. 5.5. Picture showing 6.5 mM U(IV) solution and the colloidal U(IV) solution formed at pH 3.1

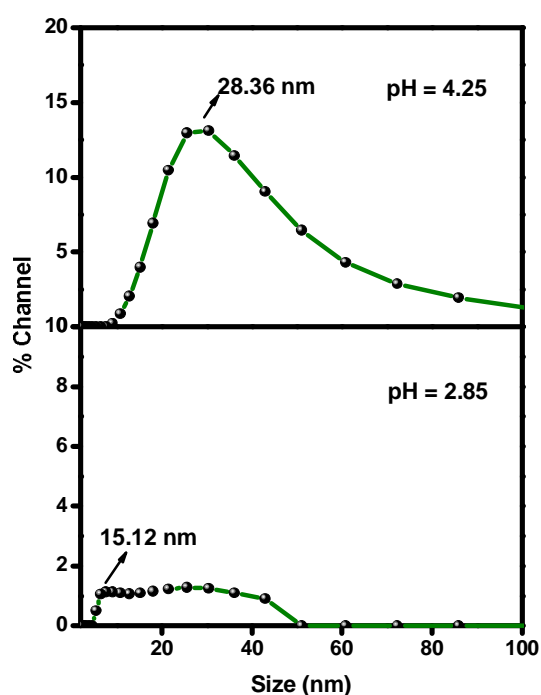


Fig. 5.6. Intensity averaged particle diameter (d_{50}) of U(IV) hydrolyzed colloid formed in 3.78 mM solution diluted to different pH

The initial colloid formation starts at pH 2.85 and the size of the colloids initially formed is found to be 15.12 nm. When pH is increased to 4.25 the size of the particle also increases to 28.36 nm and the colloid content is even higher which could be observed from the volume of the distribution curve. Laser induced breakdown detection measurements shows that precipitation from higher concentrated solutions with respect to uranium leads to small particles of $dP \sim 10$ nm at pH around 1.

Solutions with low uranium content gave larger particles of roughly 100 nm at pH around 3 [177]. A combined LIBD and UV-Visible studies carried out on Pu(IV) hydrolysis products proved that the colloid formation is preceded by formation of small polynuclear species <5 nm and colloids larger than 5 nm are formed with increasing pH [49]. Same behavior is observed in the present case. The volume of peak for initially formed colloid is small in all cases irrespective of concentration. Similar behavior is observed for 4–7 mM U(IV) solutions.

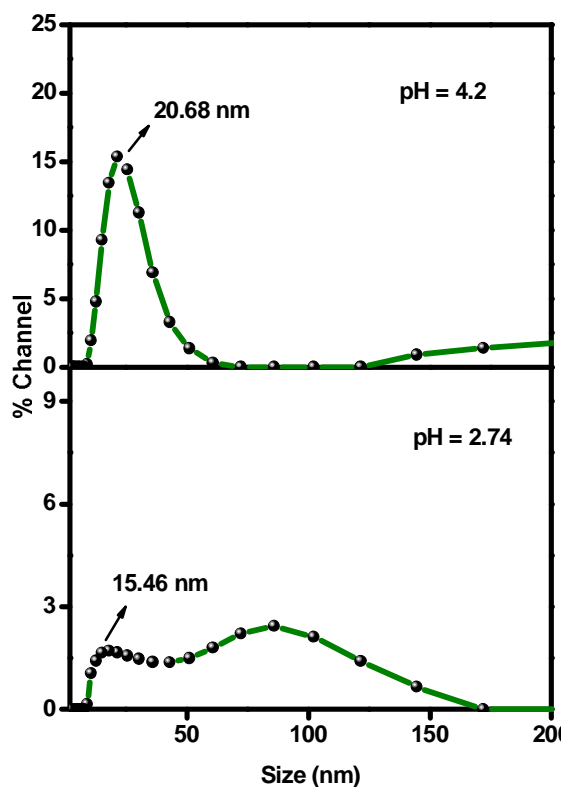


Fig. 5.7. Intensity averaged particle diameter (d_{50}) of U(IV) hydrolyzed colloid formed in 5.2 mM solution diluted to different pH

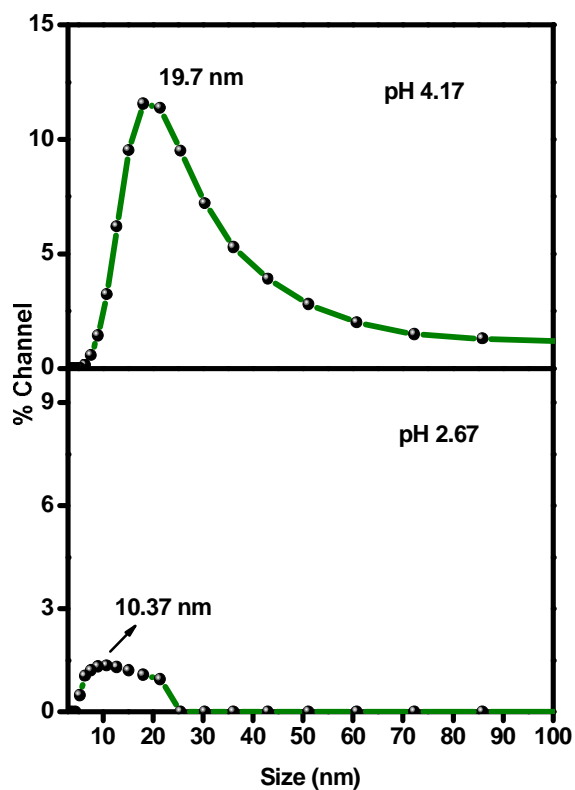


Fig. 5.8. Intensity averaged particle diameter (d_{50}) of U(IV) hydrolyzed colloid formed in 6.5 mM solution diluted to different pH

Figure 5.7 and 5.8 shows the intensity size distribution for 5.2 - 6.5 mM U(IV) solutions with varying pH. The colloids formed at these concentrations were found to be stable for longer time and there was no much variation in particle size with increasing pH.

iii. 7.8 – 19 mM U(IV) solutions

When the concentration of the solution is increased to 7.8 mM there is further decrease in size of initially formed colloids. This is mainly due to increase in crystallinity of colloids formed at higher concentration [177]. Figure 5.9 shows the size variation of 7.8 mM U(IV) solutions at different pH.

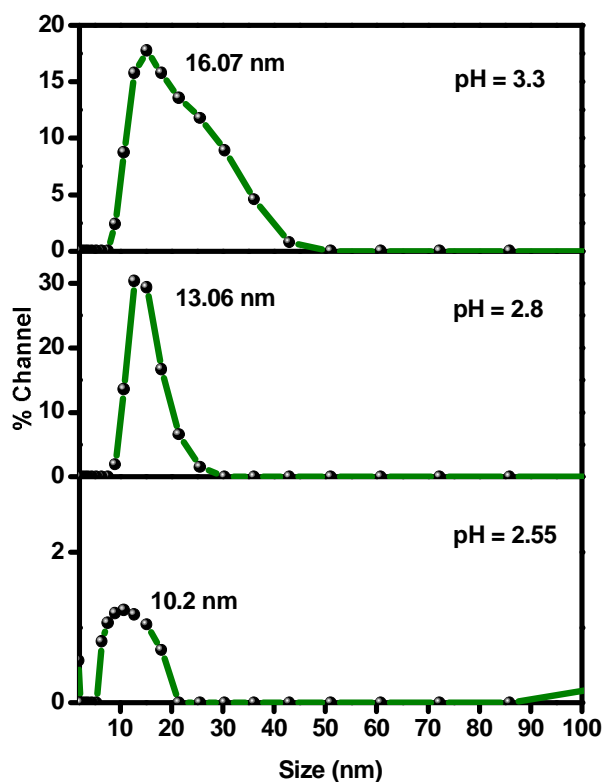


Fig. 5.9. Intensity averaged particle diameter (d_{50}) of U(IV) hydrolyzed colloid formed in 7.8 mM solution diluted to different pH

FTIR spectra recorded for 19 mM U(IV) solutions shows a band at 931 cm^{-1} due to U-O stretching which is not seen in 0.4 mM U(IV) solution. Figure 5.10a and 5.10b shows the FTIR spectra for 19 mM diluted to pH 1.8 and 2.52 mM diluted to pH 3.46. It may be due to the presence of UO moiety that makes the colloids more crystalline [181].

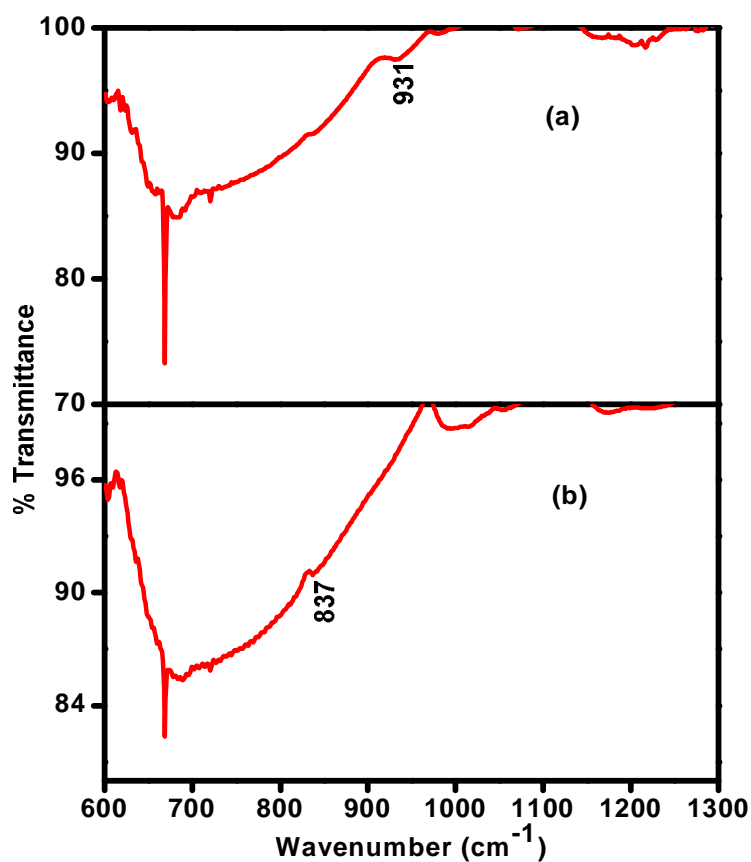


Fig. 5.10. (a). FT-IR ATR spectra of $[\text{U(IV)}] = 19\text{ mM}$ diluted to pH 1
(b). $[\text{U(IV)}] = 2.52\text{ mM}$ diluted to pH 3.46

When pH of the solution is increased to 3.65, the colloidal suspension starts precipitating and the size variation at the point of precipitation at different time intervals clearly shows that the colloidal species aggregates to particles of bigger size. It has also been reported that the size of Pu(IV) colloids formed ranges from a few

nanometers to almost micrometers depending on the conditions of generation. SANS measurements on Pu polymer shows that the size ranges from 10 Å to 1000 Å [52]. The above results show the similarity in hydrolytic behavior of U(IV) with Pu(IV). Figure 5.11 shows the variation of particle size with time at the point of precipitation.

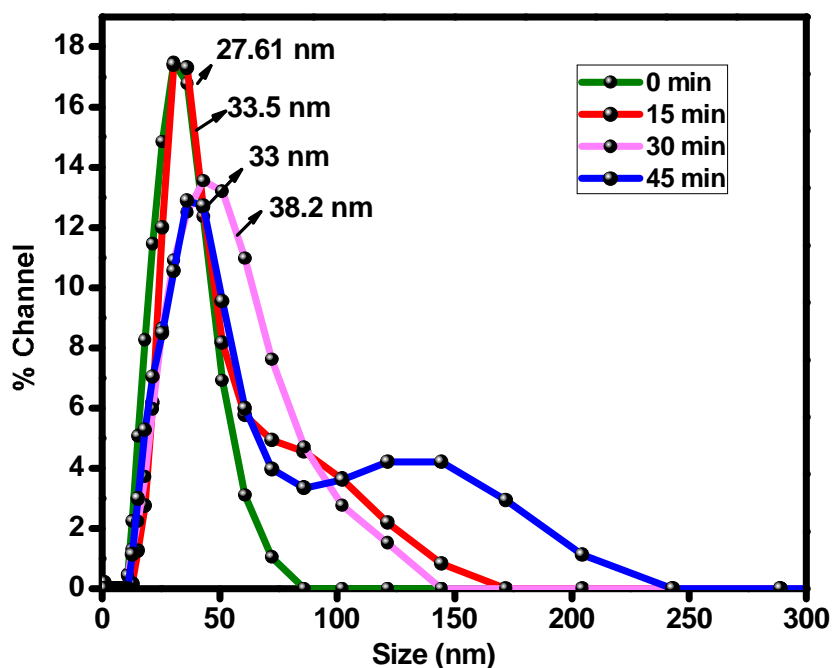


Fig. 5.11. Variation of particle size with time at the point of precipitation for 7.8 mM U(IV) solution at pH 3.65

Similar trend is observed when concentration of U(IV) is increased. But in case of higher concentration, there is a drastic change in particle size within short interval of time. This is due to the fact that with increase in concentration, the degree of polymerization increases. Figure 5.12a, 5.13a, 5.14a shows the size variation of 9.2 – 19 mM U(IV) solutions at different pH. Figure 5.12b, 5.13b, 5.14b shows the variation of particle size with time at the point of precipitation for 9.2 – 19 mM

U(IV) solution at a particular pH. As concentration increases, the corresponding pH at the point of precipitation decreases.

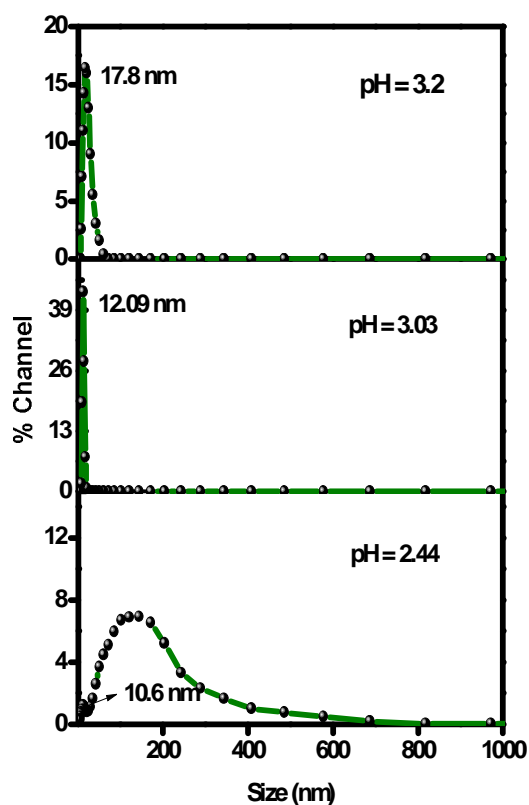


Fig. 5.12a. Intensity averaged particle diameter (d_{50}) of U(IV) hydrolyzed colloid formed in 9.2 mM solution diluted to different pH

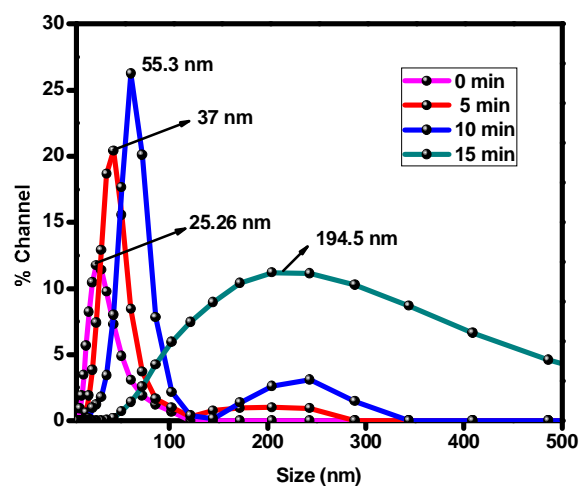


Fig. 5.12b. Variation of particle size with time at the point of precipitation for 9.2 mM U(IV) solution at pH 3.3

pH at the onset of colloid formation for different concentration of U(IV) and pH at which maximum colloids are formed are given in table 5.1.

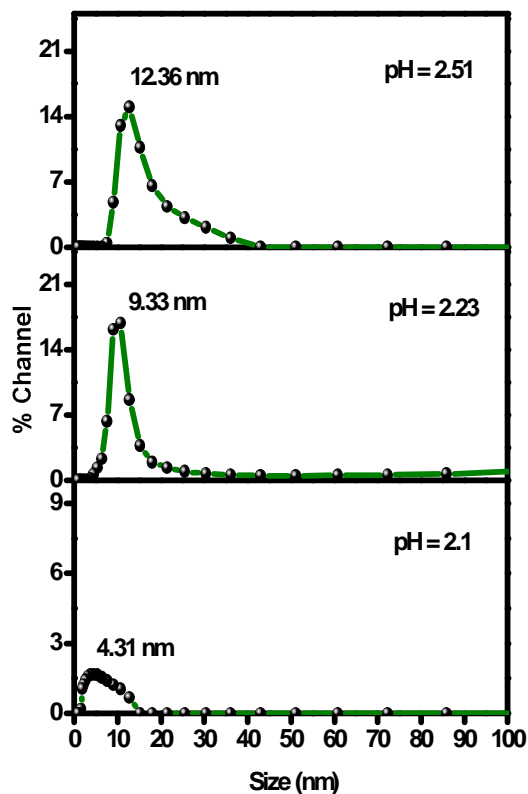


Fig. 5.13a. Intensity averaged particle diameter (d_{50}) of U(IV) hydrolyzed colloid formed in 13 mM solution diluted to different pH

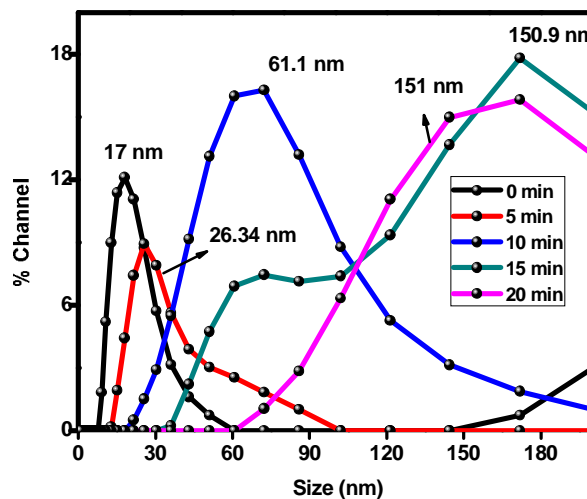


Fig. 5.13b. Variation of particle size with time at the point of precipitation for 13 mM U(IV) solution at pH 2.61

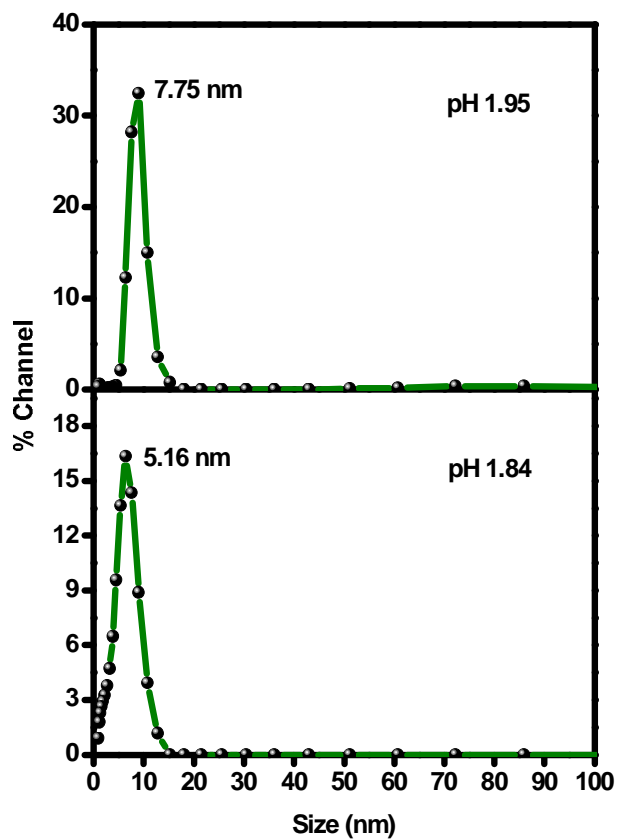


Fig. 5.14a. Intensity averaged particle diameter (d_{50}) of U(IV) hydrolyzed colloid formed in 19 mM solution diluted to different pH

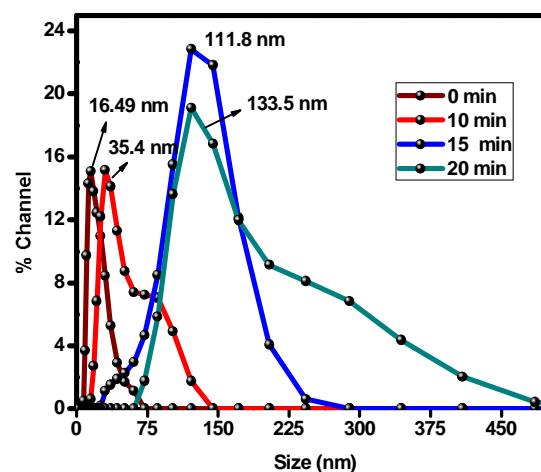


Fig. 5.14b. Variation of particle size with time at the point of precipitation for 19 mM U(IV) solution at pH 2.42

The colloidal polymers of U(IV) formed at higher pH are amorphous due to the conversion of coordinated water molecules into hydroxo bridges.

Table 5.1. Concentration of U(IV) and pH at the onset of colloid formation, intensity average size (d_{50}), pH at maximum colloid formation

[U(IV)] in mM	pH at initial colloid formation	d_{50} in nm	pH at maximum colloid formation
0.4202	Colloids not observed	-	-
1.2605	Colloids not observed	-	-
2.5210	3.46	20.59	-
3.7815	2.85	15.12	4.25
5.2100	2.74	15.46	4.20
6.5126	2.67	10.37	4.17
7.8151	2.52	10.02	3.30
9.1176	2.44	10.60	3.03
13.0	2.10	4.31	2.51
19.0	1.84	5.16	1.95

5.2.2.2. Molecular weight of U(IV) hydrolyzed polymer

The change in refractive index with concentration has been plotted. The differential refractive index has a positive slope. The refractive index of the solution increases with increase in the concentration of the solute. The dn/dC value is determined as 0.0927 g ml^{-1} . This value is used for generating the Debye plot. Figure 5.15 shows the refractive index variation with concentration of U(IV).

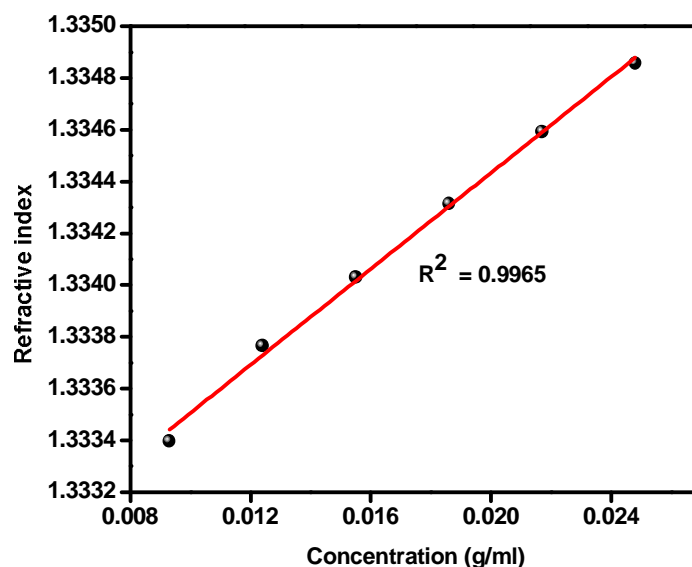


Fig. 5.15. The dn/dc curves obtained for different concentration of U(IV) colloidal solution

The extent of polymerization in case of Pu is found to vary from 10 to 10^8 molecular units as mentioned earlier. The molecular weight of the freshly formed Pu polymer has been reported as 4.2×10^5 Da by diffusion studies and 2×10^7 by ultracentrifugation [74]. The variation is possibly due to the method of preparation. But in general it was widely accepted that the molecular weight of freshly formed Pu(IV) colloidal polymer is 4,000 Da and it reaches a maximum of 10^{10} Da when aged [72-73]. The molecular weight of polymers formed can be measured by Debye plot if the particle size is much smaller than the wavelength of the incident light. Since the particle size of U(IV) colloids formed are very small, the molecular weight of the polymer is determined from the Debye plot. All the particles are assumed to be spherical. The molecular weight of U(IV) polymer when measured immediately after preparation has a value of 1,800 Da. When aged for around 1 day it increases to 4,000 Da. At the end of third day it reached a maximum of 13,000 Da. This is in good agreement with the behavior

of Pu(IV) polymer whose molecular weight increases with ageing. The size of the polymeric colloid was ~ 10 nm when freshly prepared and at the end of the third day it was 44 nm. This is due to addition of many monomeric units to the polymer. From the calculated molecular weight it has been predicted that ~ 15 atoms of U are present in the polymeric unit at the initial stage and increases to ~ 50 atoms with increase in time. As all the experiments were done at open atmosphere, ageing beyond three days was difficult as U(IV) gets oxidized to U(VI).

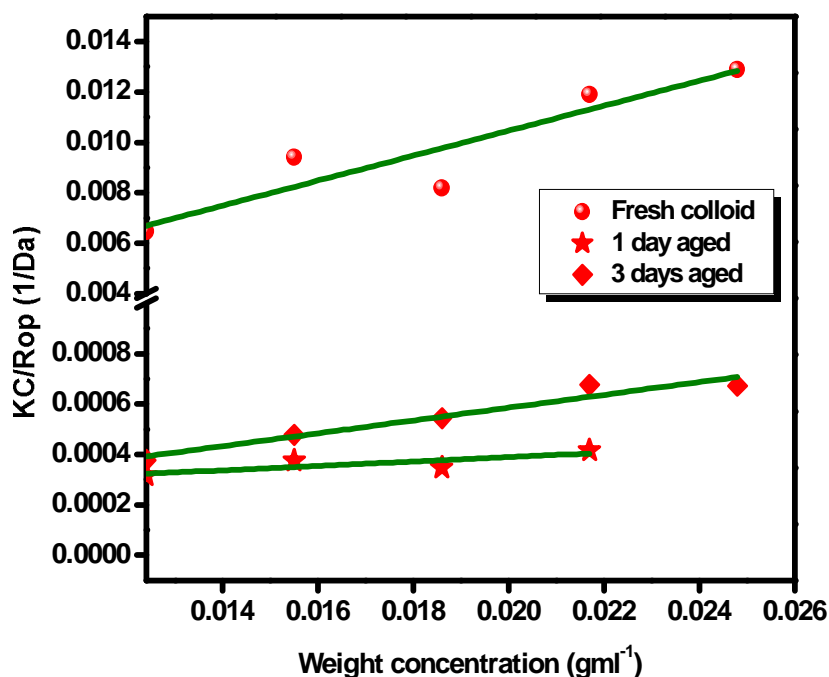


Fig. 5.16. Debye plot for U(IV) polymeric solution aged at different time intervals

The nature of solute-solvent interaction existing in the solution can be determined by evaluating the second virial coefficient. The slope of the Debye plot gave a positive value. It shows that the colloidal U(IV) suspension is stable due to higher solute-solvent interaction. The molecular weight (M_w) and A_2 values are

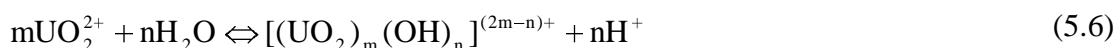
tabulated in table 5.2 at different ageing time. Figure 5.16 shows the Debye plot for U(IV) colloidal polymers aged at different time intervals.

Table 5.2. Calculated parameters from the Debye plot for U(IV) polymeric solution aged at different time intervals

Substance	Measured at $\lambda = 780 \text{ nm}$		
	Ageing time (days)	M_w (Da)	Second virial coefficient, A_2 (ml/g Da)
U(IV) hydrolyzed polymer	Fresh colloid	1,820	4.96×10^{-1}
	1	4,630	8.68×10^{-3}
	3	13,000	2.54×10^{-2}

5.3. Hydrolysis of uranium(VI)

Tetravalent uranium shows a high tendency for hydrolysis, polymerization and colloid formation as understood from previous studies. But under aerobic conditions, hexavalent uranium is more relevant. U(VI) is thermodynamically most stable form with relatively high solubility [182-183]. Being a hard lewis acid, it shows strong interactions with hard donor-ligands resulting in a tendency to undergo hydrolysis, formation of soluble complexes with carbonates, phosphates and the most important is its ability to form colloids which will increase the migration behavior in natural systems [184]. Hence it becomes mandatory to study the speciation and related reaction products of uranium in aqueous systems, under well defined conditions such as pH, ionic strength, concentration, presence of other ligands etc. The hydrolysis equilibrium reaction of uranyl ion in general can be written as given in equation 5.6.



The solution chemistry of U(VI) is dominated by the linear dioxo cation UO_2^{2+} [185]. In aerated aqueous solutions at $\text{pH} \leq 2.5$, the uranyl ion is very stable. The hydrolysis of uranyl ion starts at pH values greater than 3 [186] and also if the concentration of uranyl exceeds 10^{-3} M [187]. UO_2OH^+ is the only mononuclear hydrolysis product present at appreciable concentration upto pH~7 in 10^{-5} M or more concentrated U(VI) solutions [188]. The well established dinuclear species $(\text{UO}_2)_2(\text{OH})_2^{2+}$ is present over the pH range 3-6 and accounts for at most 40% of the total U(VI) in 10^{-2} M solutions. $(\text{UO}_2)_3(\text{OH})_5^+$, $(\text{UO}_2)_4(\text{OH})_7^+$ and $(\text{UO}_2)_3(\text{OH})_7^-$ are the dominant polynuclear species from pH 5 to 9 in solutions of 10^{-2} to 10^{-5} M U(VI), accounting for up to 100% of the total uranium in solution. Potentiometric measurement [189], time-resolved fluorescence spectroscopy [190], Raman spectroscopy [87, 191-192], attenuated total reflection infrared [193-194] and electrospray mass spectrometry [186] studies reveals that in acidic solutions of pH levels ($2 \leq \text{pH} \leq 5$) UO_2^{2+} , $(\text{UO}_2)_2(\text{OH})_2^{2+}$ and $(\text{UO}_2)_3(\text{OH})_5^+$ are the predominant species. Complexes $(\text{UO}_2)_3(\text{OH})_7^-$, $(\text{UO}_2)_3(\text{OH})_8^{2-}$, $(\text{UO}_2)_3(\text{OH})_{10}^{4-}$, $(\text{UO}_2)_3(\text{OH})_{11}^{5-}$ and $(\text{UO}_2)_3(\text{OH})_4^{2-}$ have also been suggested by various methods [185, 195-197]. There is consensus that several polynuclear species coexist in alkaline solution. A number of structures that contain chains or extended structures of hydroxo- and oxo- bridged UO_2^{2+} have been reported. U(VI) hydrolysis products form a structurally diverse class of materials. U(VI) natural mineral structures and synthetic inorganic U(VI) materials including those with chains, extended sheets, and/or three-dimensional architectures built from hydroxo/oxo-bridged U(VI) metal centers formed as a result of hydrolysis and condensation of

U(VI) in aqueous solution has also been reported [198]. Most of the methods are indirect and restricted to micromolar and acidic pH range. However, despite these extensive investigations the aqueous chemistry of U(VI) at near neutral pH and alkaline condition is rather limited because of the poor solubility of the solid meta-schoepite phases.

5.3.1. Experimental work

5.3.1.1. Aqueous U(VI) solutions

Uranyl nitrate solution of different concentration of 4 mM to 24 mM was prepared from $(\text{UO}_2)(\text{NO}_3)_2 \cdot 6\text{H}_2\text{O}$. All the solutions were prepared in 1 M nitric acid at room temperature (~ 300 K). The resulting solutions were diluted by gradually adding 0.1 M NaOH. The pH was adjusted with 0.1 M nitric acid.

5.3.2. Results and discussion

5.3.2.1. UV-Visible spectrophotometric studies on hydrolysis of U(VI)

In UV-visible absorption spectroscopy, the absorption intensity and band shift depends mainly on the U(VI) hydrolysis species formed in the solution. As the colour of the solution deepens with increasing pH the absorption spectroscopy becomes a promising tool to study the changes involved. Figure 5.17 shows UV-visible absorption spectra for the pH range from 0.99 to 5.1 recorded for solution with uranyl concentration of 4 mM. Background correction was done by subtracting spectra of respective blank solutions (1 M HNO_3) under the same conditions as those of the U(VI) samples. The spectrum with lowest absorption band and good band definition with $\lambda_{\text{max}} = 414.5$ nm, was recorded for UO_2^{2+} in an acidic pH range of 0.99 (Figure 5.17a).

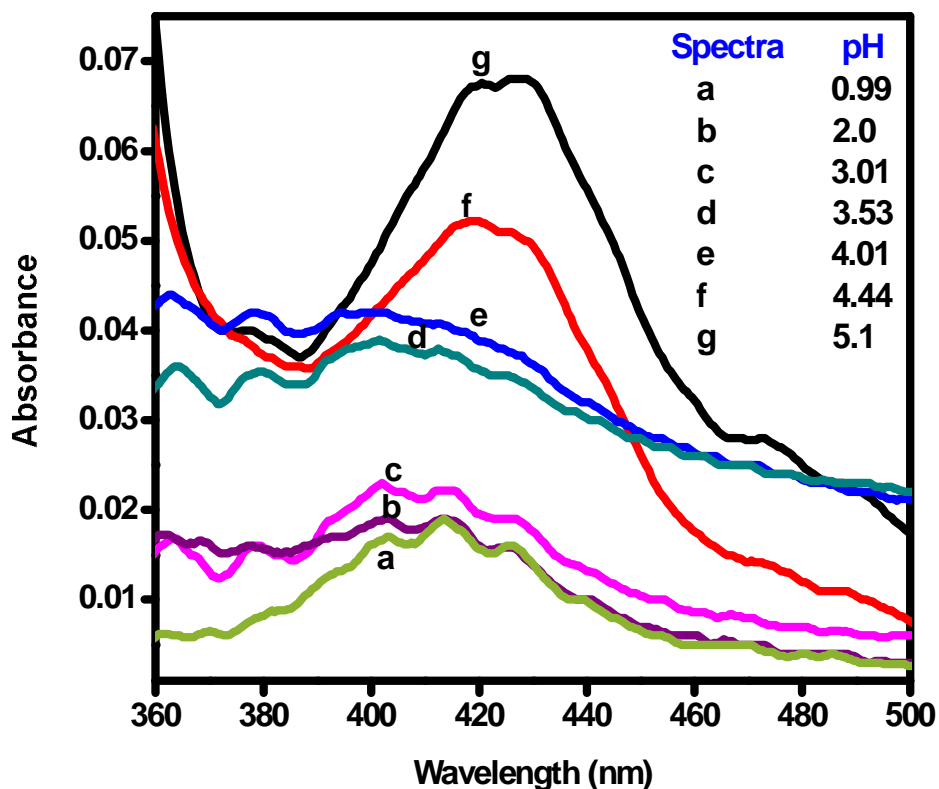


Fig. 5.17. UV-Visible electronic absorption spectra of U(VI) aqueous solutions in 1M nitric acid. $[\text{UO}_2^{2+}] = 4\text{mM}$ and pH values are given on the figure.

With the increase of pH from 0.99 to 3 there is increase in the absorption intensity. But there is no shift in the absorption band (Figure 5.17b,c). When pH is raised further, $\text{pH} > 3$ there was broadening with poor band definition (Figure 5.17d,e). This shows that uranyl hydrolysis starts around $\text{pH} \sim 3$ [186]. At $\text{pH} = 4.4$ a sharp band at $\lambda_{\text{max}} = 419 \text{ nm}$ was obtained (Figure 5.17f). There is red shift in the absorption maximum with decrease in acidity. This sharp band is due to the presence of $(\text{UO}_2)_2(\text{OH})_2^{2+}$. The uranyl hydrolysed species that is the oligomers are well defined in UV-Visible spectra. With increase in pH the intensity of absorption increases due to the formation of large number of hydrolysed species in the solution. At pH 5.1

there exist another well defined band at $\lambda_{\max} = 428$ nm (Figure 5.17g). This corresponds to the oligomer $(\text{UO}_2)_3(\text{OH})_5^+$. Upto pH 8.1 there was no change in λ_{\max} . But there was increase in the absorbance of the solution. Beyond pH 8.1 spectrum was deformed due to Rayleigh scattering and considerable information was difficult to obtain. The sharp peak around 401 nm corresponds to $(\text{UO}_2)(\text{CO}_3)$. λ_{\max} values matches with the reported values [199].

5.3.2.2. ATR-FTIR Spectra

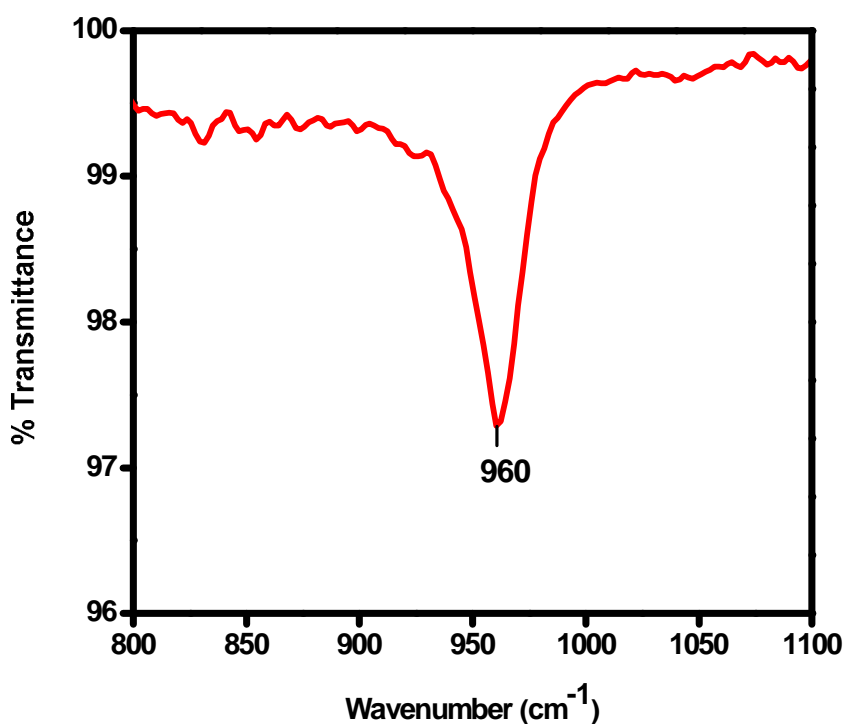


Fig. 5.18a. FT-IR ATR spectra of U(VI) solutions, $[\text{UO}_2^{2+}] = 12$ mM diluted to pH=1

Vibration spectroscopy also provides important information related to uranyl complexation as well as the speciation in solution. Complexation of uranyl with inorganic ligands weakens the O=U=O bonds which shifts the characteristic symmetric and antisymmetric stretching frequency of uranyl to lower wavenumber

[188]. In addition to that it can also be used to predict the colloids formed in the solution. Hydrolysis of U(VI) can be identified by the significant change in the absorption band corresponding to antisymmetric stretching mode (ν_3) of the UO_2^{2+} ion. FTIR studies on hydrolysis of uranyl ion over wide range of pH have already been reported in detail [193, 200]. Figures 5.18a – 5.18c, show the ATR-FTIR spectra of solutions recorded for uranyl concentration of 12 mM at pH 1, 6.8 and 7.4.

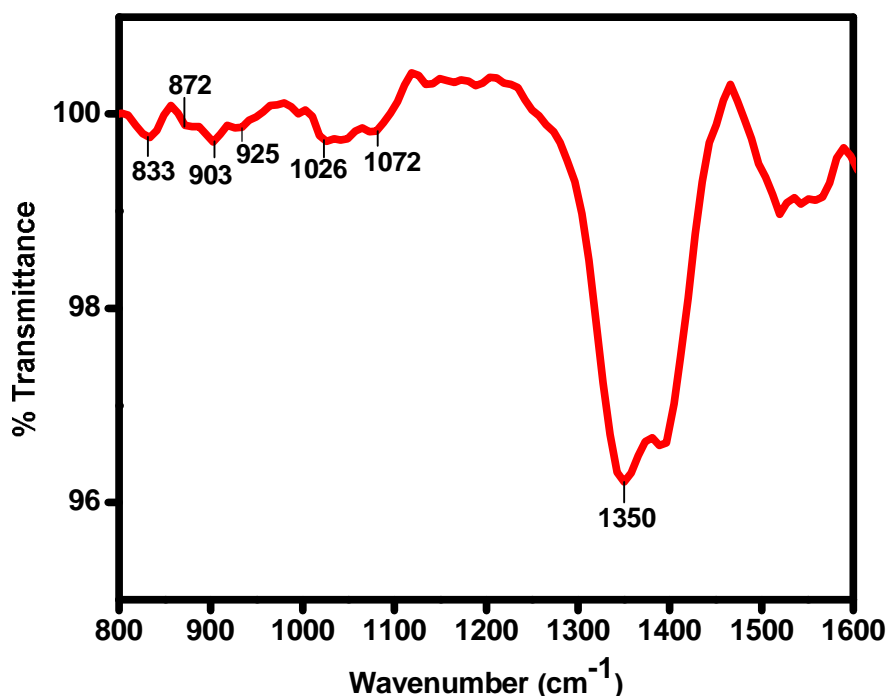


Fig. 5.18b. FT-IR ATR spectra of U(VI) solutions, $[\text{UO}_2^{2+}] = 12 \text{ mM}$ diluted to pH=6.8.

In acidic pH range there was a band at 960 cm^{-1} which was due to UO_2^{2+} antisymmetric stretching vibration mode (figure 5.18a). This shows that at very low pH, UO_2^{2+} ion is the predominant species in the solution. The uranyl stretching frequency depends on the nature of coordination environment. This has been

confirmed by the shift in the stretching frequency to lower values upon hydrolysis. At pH 6.8 three peaks were obtained at 872, 903 and 925 cm^{-1} . This is due to the formation of polymeric species at higher pH. The bands are broad and poorly resolved. At pH 7 with uranyl concentration of 10 mM there was a prominent peak around 938 cm^{-1} . The formation of colloidal species can be confirmed with the appearance of the band at this wavenumber [201].

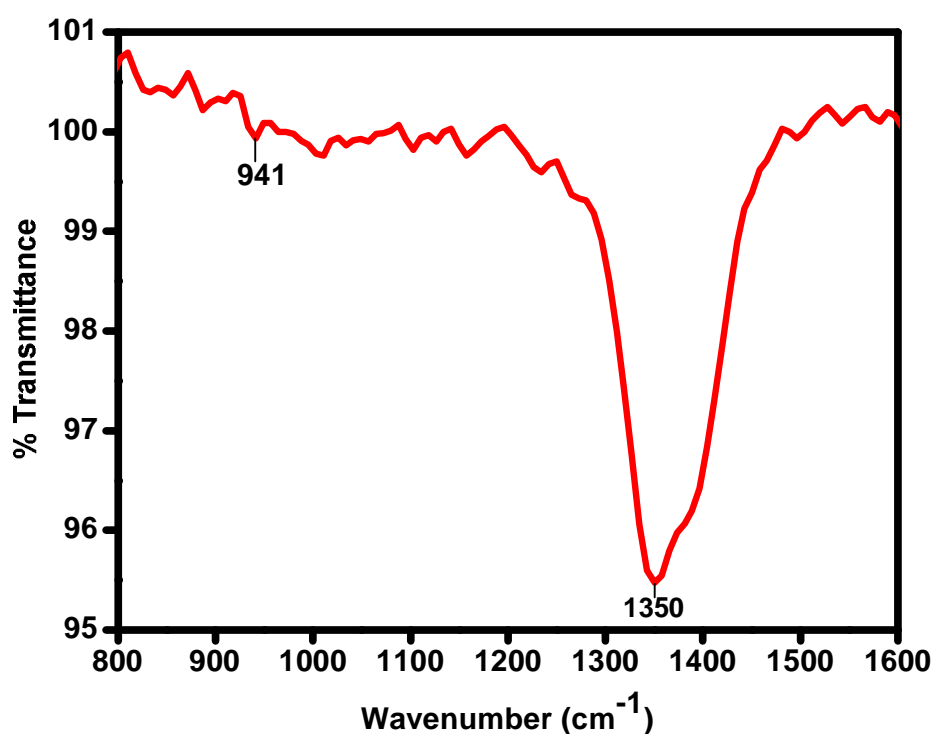


Fig. 5.18c. FTIR-ATR spectra of 12 mM U(VI) solutions diluted to pH=7.4

In the present case it has been found that at pH 7.4 with U(VI) concentration of 12 mM there was a band at 941 cm^{-1} showing the presence of colloidal species of U(VI). This peak was not observed in the spectra recorded at pH 6.8. The details of the peaks are given in Table 5.3.

Table 5.3. Characteristic infrared spectra peak of hydrolyzed U(VI) solution

Peak position (cm ⁻¹)	Assignment
833	NO ₃ ⁻ out of plane
872	UO ₂ antisymmetric stretching of (UO ₂) ₃ (OH) ₁₁ ⁵⁻ [193]
925	UO ₂ antisymmetric stretching of (UO ₂) ₃ (OH) ₅ ⁺ [193]
903	O=U=O stretching weakened due to hydrolysis
1026	Symmetric stretching of N-O bonds
1350	Asymmetric and symmetric stretching of CO ₃ ²⁻ in UO ₂ (CO ₃) ₃ [202]

(a) Ref [193]

(b) Ref [202]

A band at 833 cm⁻¹ observed was due to nitrate ions. As all the experiments were carried out at aerated conditions, there was a strong band around 1350 cm⁻¹ mainly due to dissolved uranyl carbonate species in the solution. This can be clearly understood from the distribution of U(VI) species in aqueous solutions at atmospheric conditions. Near pH 7, uranyl ion forms stable complexes with carbonate and it dominates the solution upto pH 10 (figure 5.19).

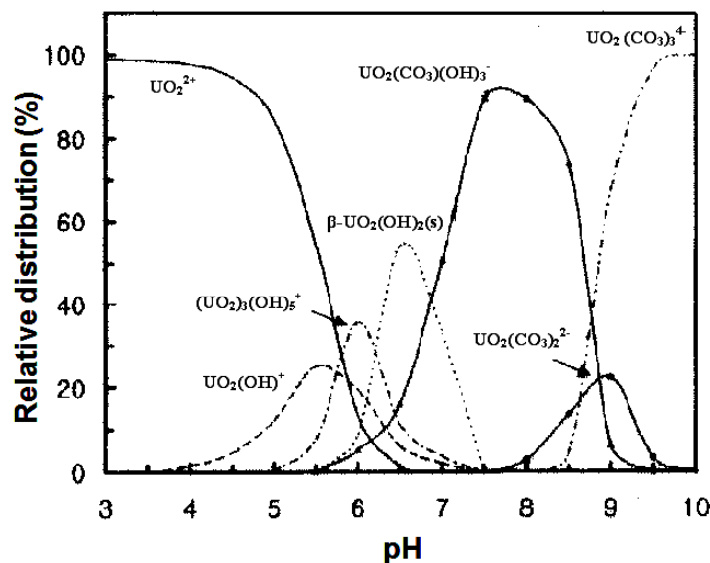


Fig. 5.19. Speciation diagram of U(VI) ions as a function of pH in aqueous solution at atmospheric condition [203]

5.3.2.3. Particle size of hydrolyzed U(VI) colloids formed in neutral solution

Hydrolyzed species aggregate and reach colloidal dimensions and exists as suspended sols in the aqueous medium. Particle size is an important property to define a colloidal system. It influences the behavior of colloids during diffusion, aggregation etc. DLS studies were performed on different concentrations of uranyl solution diluted to neutral pH. The particle refractive index was taken as 1.95 [180] in order to obtain size distribution. All the particles were assumed spherical and the size distribution was recorded on the solution prepared without any treatment. For 4 mM U(VI) solution, the colloid formation was observed around pH 8.2. The distribution curve showed three prominent peaks and it was difficult to identify the peak corresponding to the colloids formed in the solution. Hence the solutions were centrifuged for 15 minutes with 2000 rpm and allowed to settle. There was a yellow deposit at the bottom of the centrifuge tube. It was then filtered and dried. X-ray diffraction studies performed on the yellow deposits showed that it was meta-schoepite phase with a

composition of $\text{UO}_3 \cdot 2\text{H}_2\text{O}$ [204]. The yellow deposits formed during centrifugation and the XRD pattern of the dried powder are shown in figure 5.20a and 5.20b.

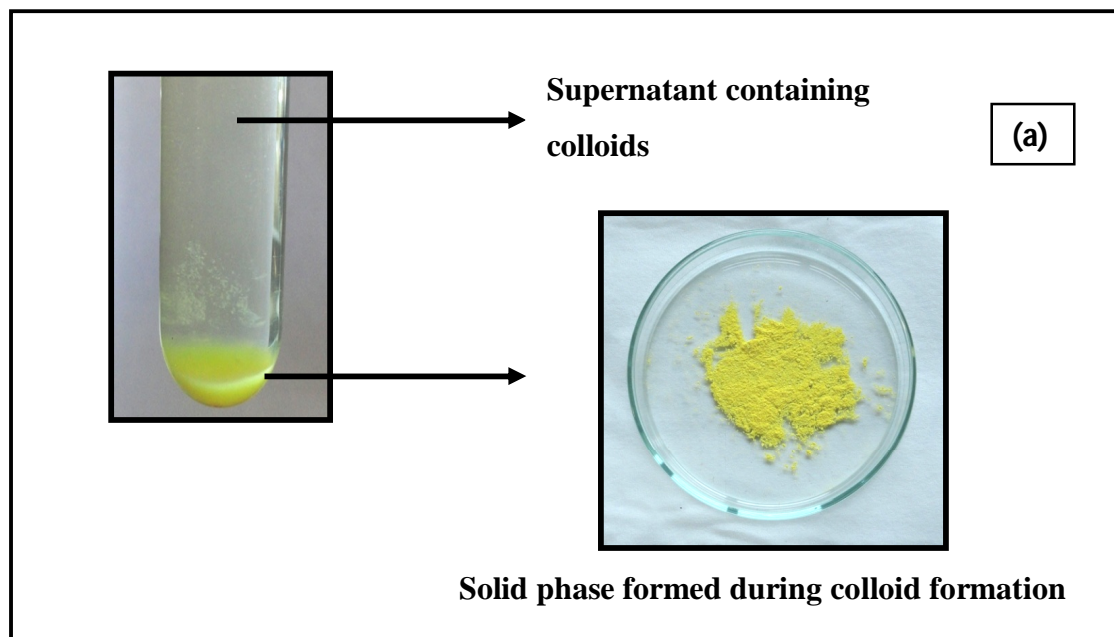


Fig. 5.20a. Picture showing the yellow deposits formed during centrifugation and the dried yellow powder

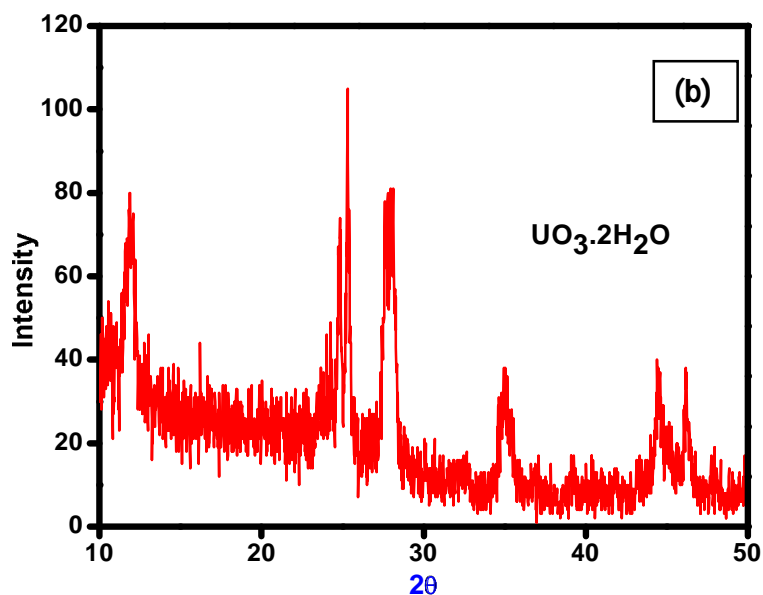


Fig. 5.20b. XRD pattern recorded for the solid phase ($[\text{UO}_2^{2+}] = 12 \text{ mM}$ at pH 7.4)

The supernatant solution was taken out for further analysis. It was found that the volume of the peak which was already present at 32-36 nm range has considerably increased after centrifugation. This is because the solid phases formed were deposited due to gravitation and only the colloids are suspended in the supernatant. The particles in the region greater than 200 nm were shifted right and their peak volume has reduced. The peaks greater than 200 nm might be due to the formation of solid phases of uranyl at higher concentration and at basic pH range. However, it was difficult to remove the solid phase completely. Similar studies were performed by increasing the concentration of UO_2^{2+} greater than 12 mM, and it has been found that the peak corresponding to colloids were very small whereas those corresponding to solid phases were larger and it may be due to immediate precipitation at higher concentration. But a peak around 32-36 nm was observed on all the concentration range of U(VI). Hence it has been confirmed that the colloids has size of ~32 – 36 nm.

With increasing concentration of uranyl ions the pH for colloid formation decreases considerably. Figure 5.21 – 5.26 shows the size distribution of colloidal U(VI) solutions formed at different concentration of UO_2^{2+} and at different pH.

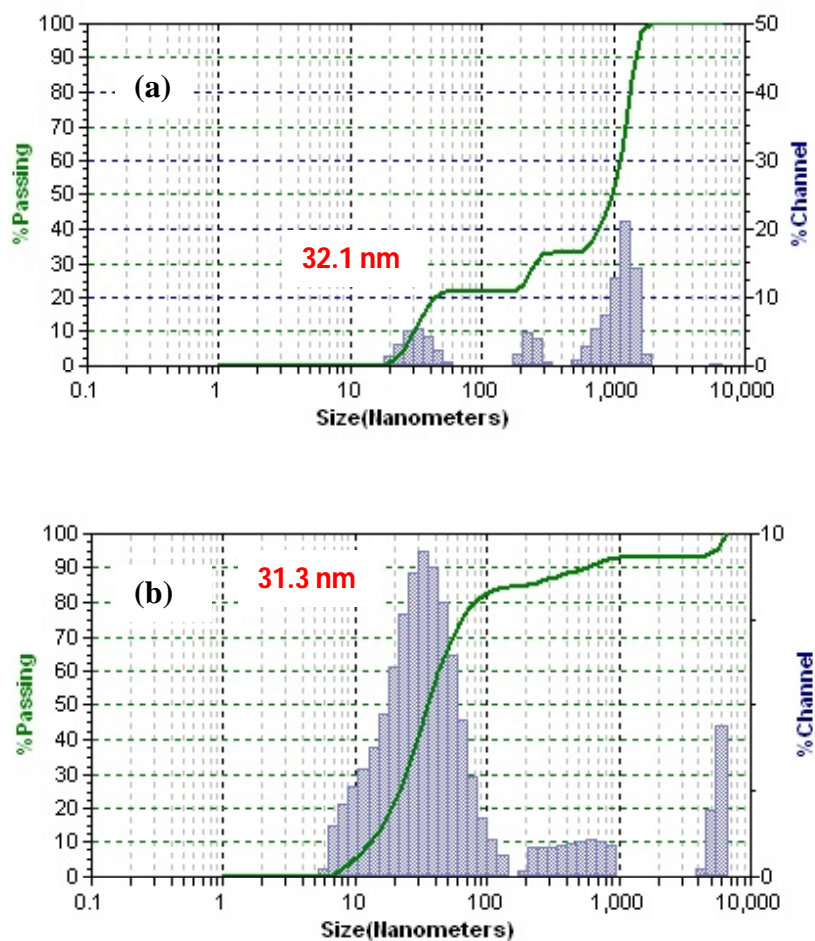


Fig. 5.21. Intensity averaged particle diameter (d_{50}) of uranyl hydrolyzed colloid formed in 4 mM UO_2^{2+} solution diluted to pH 8.2

- Before centrifugation
- After centrifugation

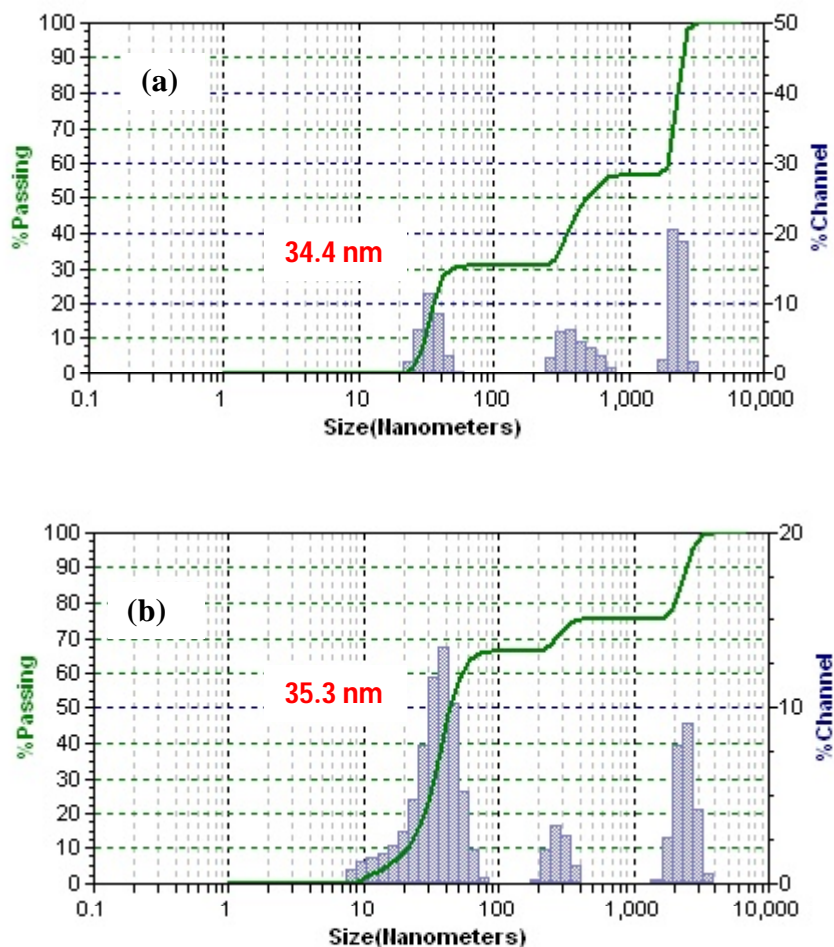


Fig. 5.22. Intensity averaged particle diameter (d_{50}) of uranyl hydrolyzed colloid formed in 8 mM UO_2^{2+} solution diluted to pH 7.7

a. Before centrifugation

b. After centrifugation

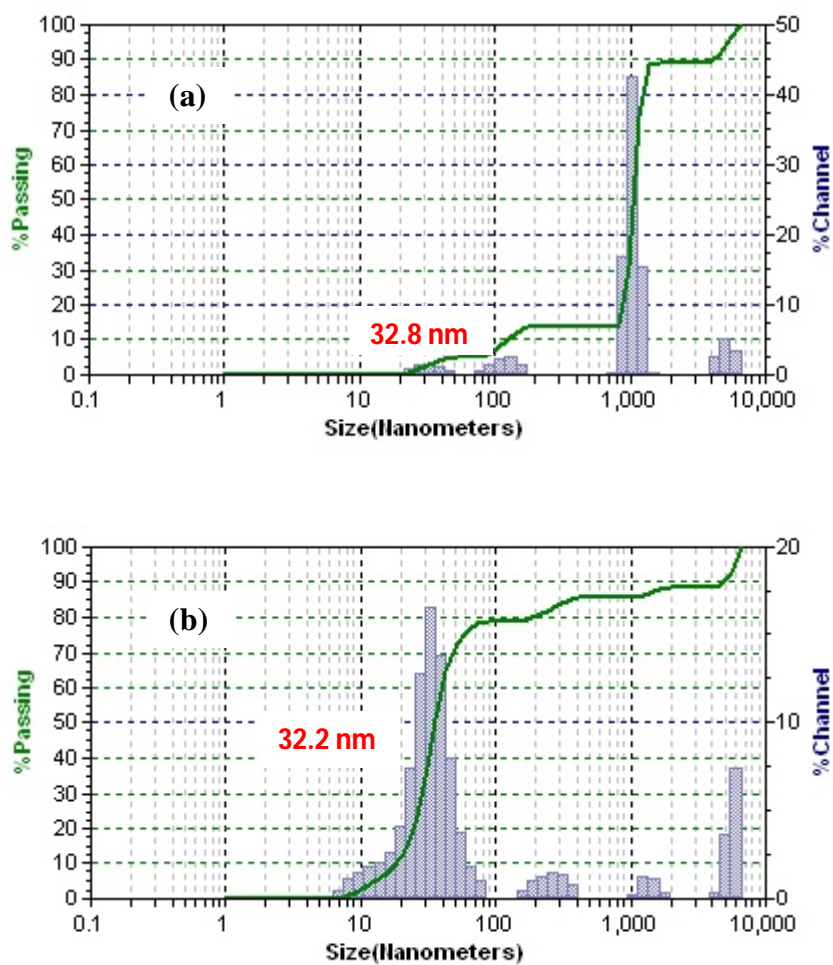


Fig. 5.23. Intensity averaged particle diameter (d_{50}) of uranyl hydrolyzed colloid formed in 12 mM UO_2^{2+} solution diluted to pH 7.4

- a. Before centrifugation
- b. After centrifugation

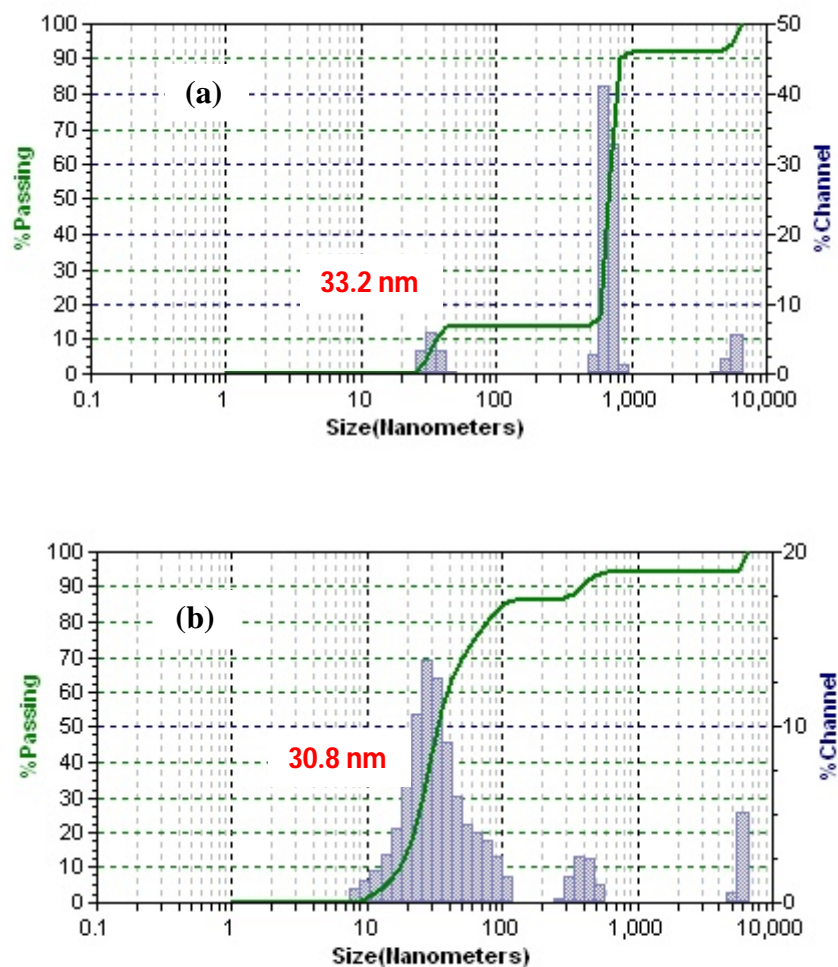


Fig. 5.24. Intensity averaged particle diameter (d_{50}) of uranyl hydrolyzed colloid formed in 16 mM UO_2^{2+} solution diluted to pH 7.1

- a. Before centrifugation**
- b. After centrifugation**

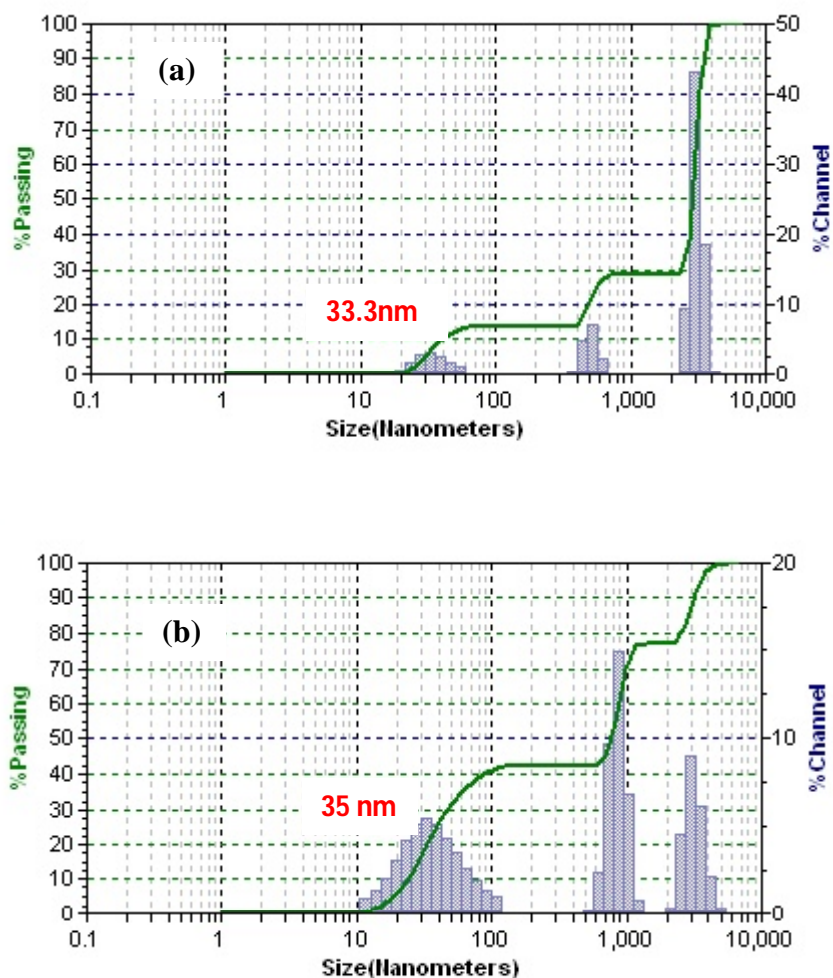


Fig 5.25. Intensity averaged particle diameter (d_{50}) of uranyl hydrolyzed colloid formed in 20 mM UO_2^{2+} solution diluted to pH 6.98

- a. Before centrifugation**
- b. After centrifugation**

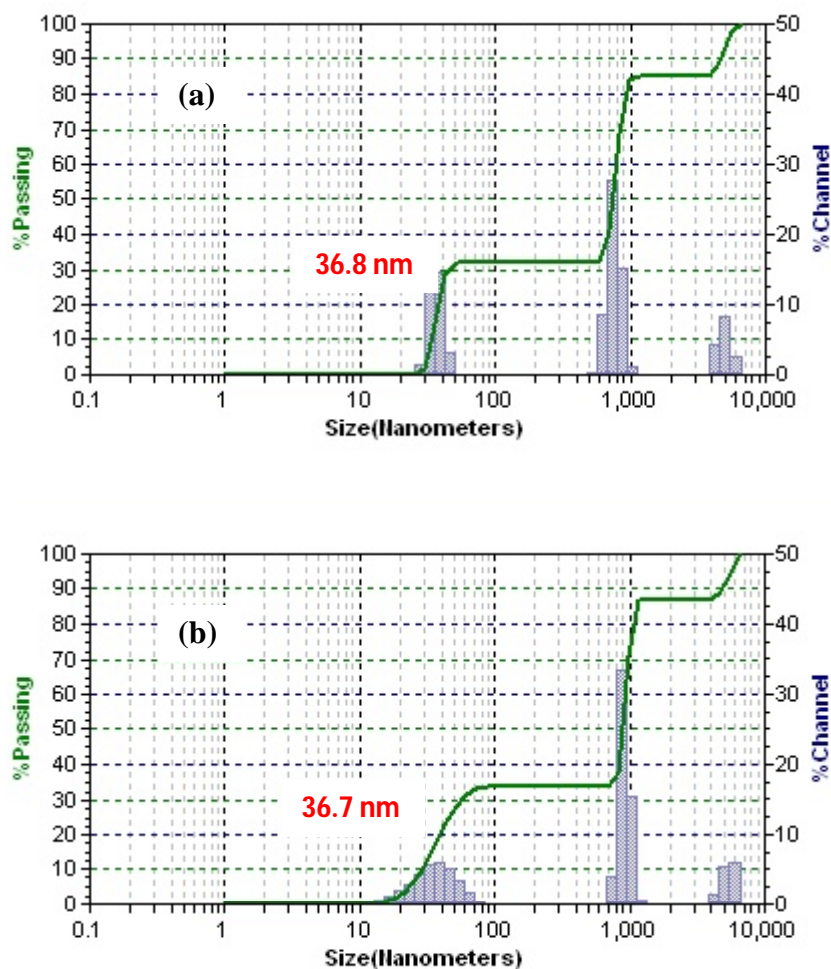


Fig. 5.26. Intensity averaged particle diameter (d_{50}) of uranyl hydrolyzed colloid formed in 24 mM UO_2^{2+} solution diluted to pH 6.6

a. Before centrifugation

b. After centrifugation

The colloids formed were not stable for a long period of time. The green line in the figure shows the cumulative frequency distribution. There is no change in average particle size of the colloids as the concentration of U(VI) increases. This further show that well defined colloids are formed when the concentration reaches the precipitation point. The polydispersity index is greater than 0.1. The value is obtained from

microtrac FLEX software which is used for data analysis. Table 5.4 lists the complete set of data on peak values (Diameter, volume % and width).

Table 5.4. Peak summary of intensity distribution curves of U(VI) hydrolyzed colloids before and after centrifugation

[UO ₂ ²⁺] mM	Before centrifugation			After centrifugation		
	Diameter (nm)	Volume %	Width	Diameter (nm)	Volume %	Width
3.97	1200	66.4	591.0	5750.0	6.5	1067.0
	241	10.7	66.7	467.0	8.7	500.0
	32.1	22.9	18.34	31.3	84.8	41.2
7.89	2300	42.7	528	2381	24.6	811.0
	404	25.3	257.9	277.3	9.3	99.5
	34.4	32	13.26	35.3	66.1	26.59
11.61	5270	9.4	1221.0	5720	11.3	1089.0
	1060	76.9	251.5	1393	3.1	393.0
	122.1	8.0	49.6	260.8	6.2	139.2
	32.8	5.7	17.98	32.2	79.4	23.98
16.11	5790	8.1	986.0	5960	5.5	698.0
	675	77.8	147.7	401.0	8.0	146.3
	33.2	14.1	10.25	30.8	86.5	36.10
20.36	3090	66.7	609	3110	22.6	1069.0
	537	19.4	2013	868.0	35.0	270.3
	33.3	13.9	20.35	35.0	42.4	41.0
23.52	5080	12.3	962	5480	12.1	1233.0
	775	55.7	210.4	925.0	53.1	190.2
	36.8	32	9.34	36.7	34.8	29.59

5.3.2.4. Molecular weight of U(VI) hydrolyzed colloid

The change in refractive index with concentration has been plotted. The differential refractive index has a positive slope. The refractive index increases with increase in the concentration of the solute. The dn/dC value was determined as 0.0787

g ml⁻¹. This value is used for generating the Debye plot. Figure 5.27 shows the refractive index variation with concentration of U(VI) solutions.

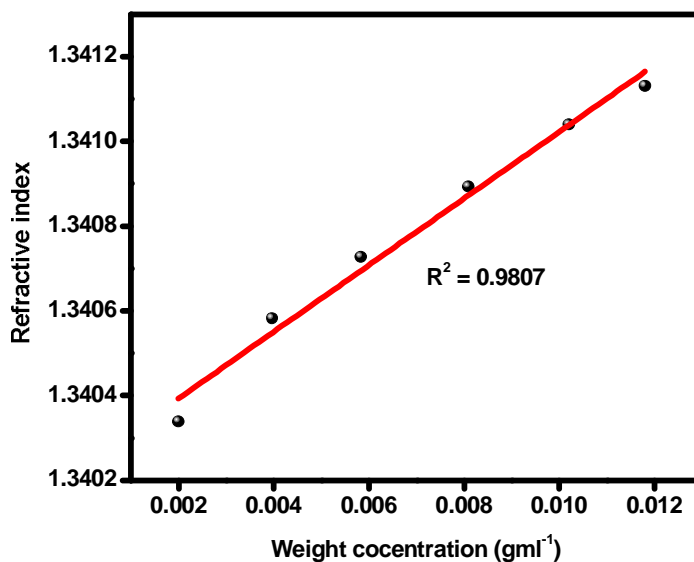


Fig. 5.27. The dn/dc curves obtained for different concentration of U(VI) solution

Molecular weight of actinide polymers play a crucial role during solvent extraction and ion exchange processes. High molecular weight polymers as in the case of Pu interferes in separation process resulting in loss of metal and criticality problems [80]. To avoid the consequences of polymerization of hydrolyzed species, it is important to know the molecular weight of polymers formed initially. Hence it can be avoided immediately by depolymerizing it as depolymerization of freshly prepared polymer is easier than the aged one due to structural changes involved [49]. In this context it is possible to determine the molecular weight of the colloidal polymer formed in the system using Debye plot if the particle size of the colloid was much lesser than the wavelength of the incident light. The molecular weight of U(VI)

colloid was determined as ~ 763 Da which was much less when compared to Zr(IV), U(IV) and Pu(IV). The calculated molecular weight shows that there may be 2-3 units of uranyl groups bridged by hydroxyl groups. Hence it is only oligomer that has been formed. This shows the absence of extensive hydrolysis leading to polymerization. As supporting information, there have also been reports showing the depolymerizing effect of uranyl ions. Pu is commonly used in the presence of large amount of uranium. The formation rate of Pu(IV) polymer is greater. It is further suppressed by 30% if U(VI) is present in the system. UO_2^{2+} functions as a chain terminator through the formation of hydroxyl bridges to terminal uranyl groups [80]. This further confirms the present study that the uranyl ion is less prone to polymerization. Figure 5.28 shows the Debye plot for different concentrations of colloidal uranyl(VI) solution. The molecular weight (M_w) and A_2 values are tabulated in table 5.5.

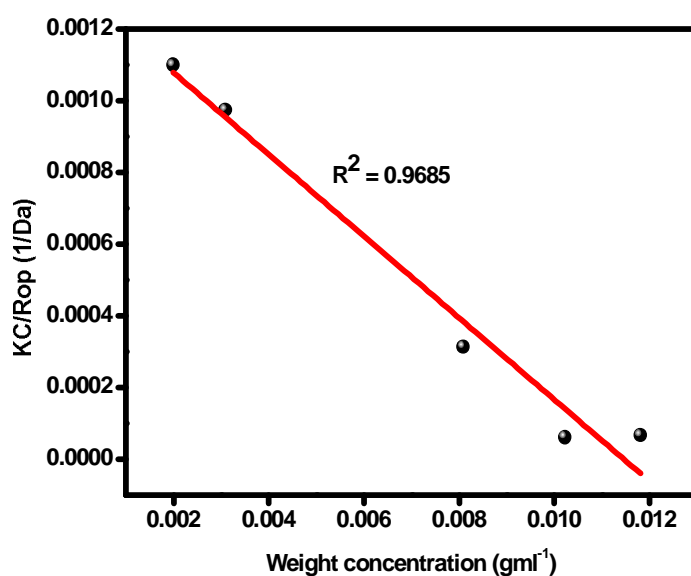


Fig. 5.28. Debye plot for various concentrations of colloidal U(VI) solution

Table 5.5. Calculated parameters from the Debye plot for U(VI) hydrolyzed oligomers

Substance	Measured at $\lambda = 780 \text{ nm}$	
U(VI) hydrolyzed oligomer	M_w (Da)	Second virial coefficient, A_2 (ml/g Da)
	763	-0.1139

The negative value is an indication of high solute-solute interaction leading to the instability of the colloidal system. Since the colloids formed are not stable for long time, the solution kept for ageing undergoes aggregation and finally precipitation as shown in figure 5.29.

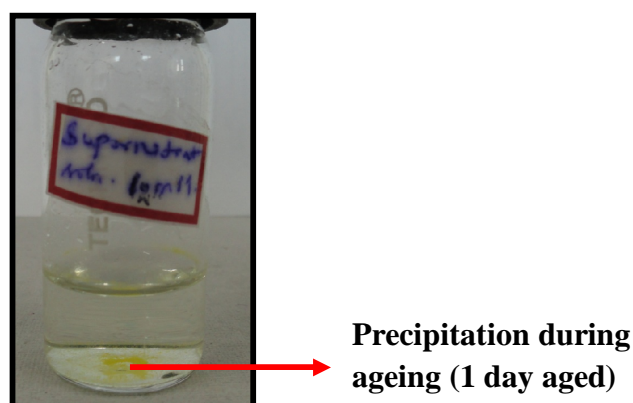


Fig. 5.29. Supernatant solution aged for 1 day $[\text{UO}_2^{2+}] = 12 \text{ mM}$, $\text{pH} = 7.4$

5.4. Conclusions

- Solutions of U(IV) at concentrations between 0.4–19 mM ($1 < \text{pHc} < 4$) are investigated by light scattering. It has been observed that the colloidal particles initially formed at higher concentration are smaller than those formed at lower concentration. It may be due to microcrystalline nature of colloids formed at

higher concentration and acidity. At higher pH, the colloid becomes amorphous due to the insertion of hydroxide or H₂O ligand into the system.

- Colloids formed at lower concentration are found to be more stable than colloids formed at higher concentration.
- The obtained molecular weight of the colloidal polymers aged at different time intervals clearly indicates that number of U atoms increases from 15 to 50 with increase in time.
- This shows the similarity in hydrolytic behavior of U(IV) with Zr(IV) as in previous studies and Pu(IV) as reported in literature.
- The hydrolysis of U(VI) was investigated by UV-visible absorption spectrophotometry for a wide pH. The formation of colloidal species was confirmed by FTIR-ATR studies.
- Light scattering measurements performed on the colloidal solutions shows that there was no significant variation in the size of the particle with increasing U(VI) concentration.
- U(VI) is less prone to polymerization and forms only oligomers in neutral aqueous solution. U(VI) contradicts the solution chemistry of actinides such as U(IV), Zr(IV) and Pu(IV).

Chapter 6



CHAPTER 6

Hydrolysis and Polymerization of Thorium(IV) in Aqueous Nitric Acid Solutions

6.1. Introduction

Thorium has an ionic radius of 1.09\AA in nine coordination making it the largest stable tetravalent metal ion and in spite of its high valence, it is least susceptible to hydrolyze when compared to U(IV) or Pu(IV) [94]. $\text{Th}^{4+}(\text{aq})$ ion can be found as predominant species only at $\text{pH} < 3$. It has been observed that mononuclear ionic complexes dominate the species distribution at very low concentrations as well as at high acidity (Figure 6.1) [205].

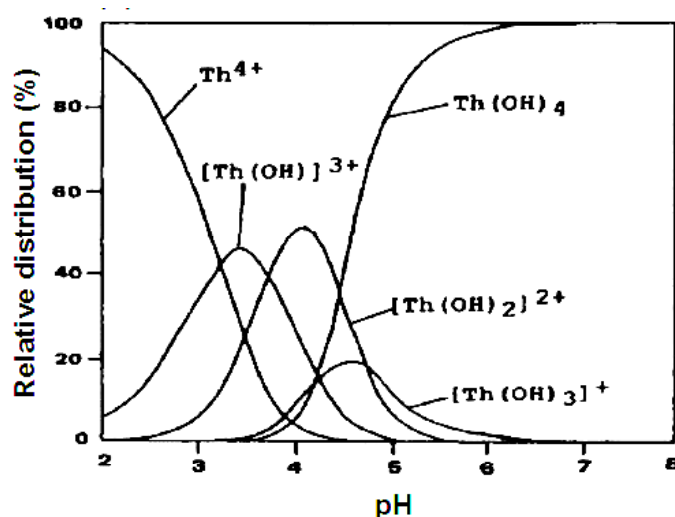


Fig. 6.1. Speciation diagram of Th(IV) ions as a function of pH in aqueous solution at atmospheric condition [206]

At near neutral pH, and as the thorium concentration approaches the solubility limit of the amorphous hydroxide $\text{Th}(\text{OH})_4$, polymers become the dominant species in solution, starting with dimers which grow and form pentamers. Pentamers have been found to be the most abundant and stable complex rather than tetramers and hexamers [206]. The polymeric species are found to contain one or more Th atoms linked by hydroxy bridges [207]. With increasing pH and Th concentration it forms thorium nanoparticles or the so-called colloids. Th(IV) colloid formation is preceded by polynuclear hydroxide complexes such as $\text{Th}_2(\text{OH})_2^{6+}$, $\text{Th}_2(\text{OH})_3^{5+}$, $\text{Th}_4(\text{OH})_8^{8+}$, $\text{Th}_4(\text{OH})_{12}^{8+}$, $\text{Th}_6(\text{OH})_{14}^{10+}$, $\text{Th}_6(\text{OH})_{15}^{9+}$ which, in contrast to the polynuclear complexes of Pu(IV) are accepted as thermodynamically stable species [208].

Structural studies on aqueous solution of the hydrolysis products of Th(IV) have identified three different types of hydrolysis species: a $\mu^2\text{O}$ -hydroxo dimer, $[\text{Th}_2(\text{OH})_2(\text{H}_2\text{O})_{12}]^{6+}$, a $\mu^2\text{O}$ -hydroxo tetramer, $[\text{Th}_4(\text{OH})_8(\text{H}_2\text{O})_{16}]^{8+}$, and a $\mu^3\text{O}$ -oxo hexamer, $[\text{Th}_6\text{O}_8(\text{H}_2\text{O})_n]^{8+}$ [209]. Single crystals of oxo- and hydroxo-bridged hexameric $[\text{Th}_6(\mu_3\text{-O})_4(\mu_3\text{-OH})_4]^{12+}$ [210-211] and octameric $[\text{Th}_8\text{O}_4(\text{OH})_8]^{16+}$ [212] have also been isolated by addition of complexing ligands. LAXS and SAXS investigation revealed the presence of microcrystalline particles with the thorium oxide structure in highly hydrolyzed Th solutions [213]. In another study, if a Th chloride solution was left to evaporate at room temperature, it produced hydroxo-bridged Th dimers. These oligomers are then subjected to continuous hydrolysis i.e. the number of hydroxide ligands increases with increase in pH. The ultimate end product of Th hydrolysis is an oxo-bridged ThO_2 with fluorite structure [214].

Though many investigations were performed on hydrolysis products of Th(IV), their structures, solubilities of different oxide and hydroxide phases of Th,

only little information is available on the formation and behavior of colloids and polymers of Th(IV) at acidic conditions. This chapter aims at understanding the formation, their size and molecular weight of the colloidal polymers formed when the solubility limit exceeds by using light scattering technique.

6.2. Experimental

6.2.1. Synthesis of Th(IV) colloids

^{232}Th is an alpha emitting radioisotope with a half-life of 1.405×10^{10} years. Standard precautions for handling radioactive materials have been followed while working with the quantities used in the synthesis that follows.

Two different series of $\text{Th}(\text{NO}_3)_4 \cdot 5\text{H}_2\text{O}$ solutions was prepared. First series of solution have a concentration range of 10 mM – 20 mM and the second series of solution having a concentration range of 0.05 M – 0.4 M. Th(IV) colloids were synthesized by diluting the solutions to different pH by gradual addition of 0.01 M NaOH. The pH of the solution was adjusted by the addition of 0.01 M HNO_3 . All the experiments were performed at $27 \pm 1^\circ\text{C}$ at 1 atm.

6.3. Results and discussions

The formation of colloids in over-saturated thorium solutions was studied by using light scattering technique. Solutions containing well defined concentration of Th(IV) in 0.1 M HNO_3 were prepared. Studies were performed in two concentration domains. The pH was increased slowly until solubility was just exceeded initiating the formation of small colloids.

6.3.1. 10 mM – 20 mM Th(IV) solutions

6.3.1.1. Size variation of Th(IV) colloids

Close to the solubility limit, Th(IV) forms polynuclear hydroxide complexes and in oversaturated solutions, these complexes further undergoes growth process leading to the formation of colloids. Previous investigations on the formation process revealed that at least two different regions with respect to pH and Th(IV) concentration have been distinguished [215]. It corresponds to the two solid phases ThO₂(microcrystalline) and Th(OH)₄(amorphous hydroxide). In the low pH region, i.e. oversaturated with respect to ThO₂, microcrystalline colloids form [216]. In 10 mM Th(IV) solution, at pH~1.9, initial formation of colloids were observed. The average particle size of the colloids formed at this condition was ~40 nm. No signal can be detected below 10 mM. The initial colloids are mainly crystalline ThO₂ formed when the solubility of solid ThO₂ exceeds. When the concentration was gradually increased to 20 mM, colloid formation was observed with no further change in their size. This shows that well defined colloids are formed. The colloids at this condition were considered to be in equilibrium with Th⁴⁺ ions. Figure 6.2 shows the size variation of colloids formed in 10 mM – 20 mM solutions diluted to acidic pH of 1.9.

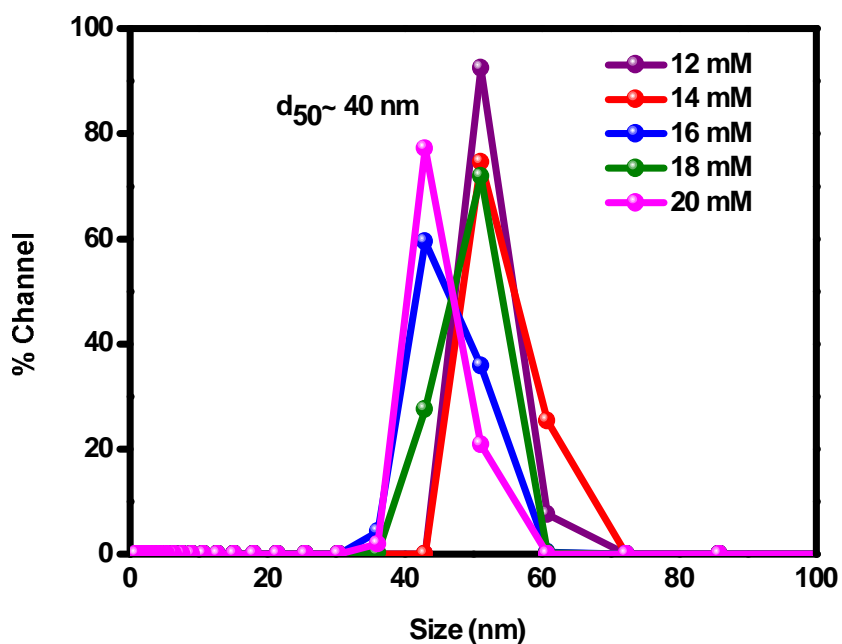


Fig. 6.2. Particle size distribution of Th(IV) colloids formed at pH~1.9

The clear colloid containing solution was stored for ageing. Figure 6.3 shows the particle size distribution of colloids aged for 3-5 days. After 5 days of ageing, fraction of bigger particles greater than 1000 nm was observed. This shows that the crystalline ThO_2 colloids started forming precipitates with increase in time by aggregation.

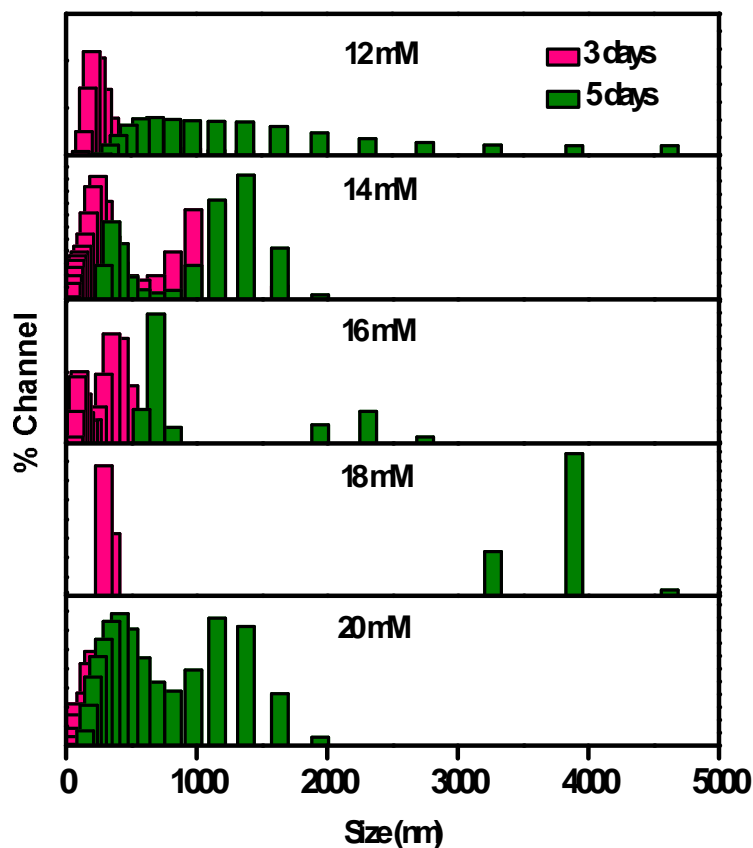


Fig. 6.3. Particle size distribution of Th(IV) colloids aged for 3-5 days

Similar experiments were performed by slowly increasing the pH in 10 mM - 20 mM Th(IV) solutions in order to observe the changes in their size. At $\text{pH} > 3.4$, colloids with mean size of $\sim 80\text{--}90$ nm were observed (figure 6.4). When exceeding the solubility of $\text{Th}(\text{OH})_4(\text{am})$, X-ray amorphous colloids form [217]. With increase in pH, hydrolysis and polynucleation are the major factors for the formation of amorphous thorium hydroxide colloids. The mechanism of hydrolysis and polymerization reactions is shown in equation 6.1-6.2.

Hydrolysis:



Polymerization:

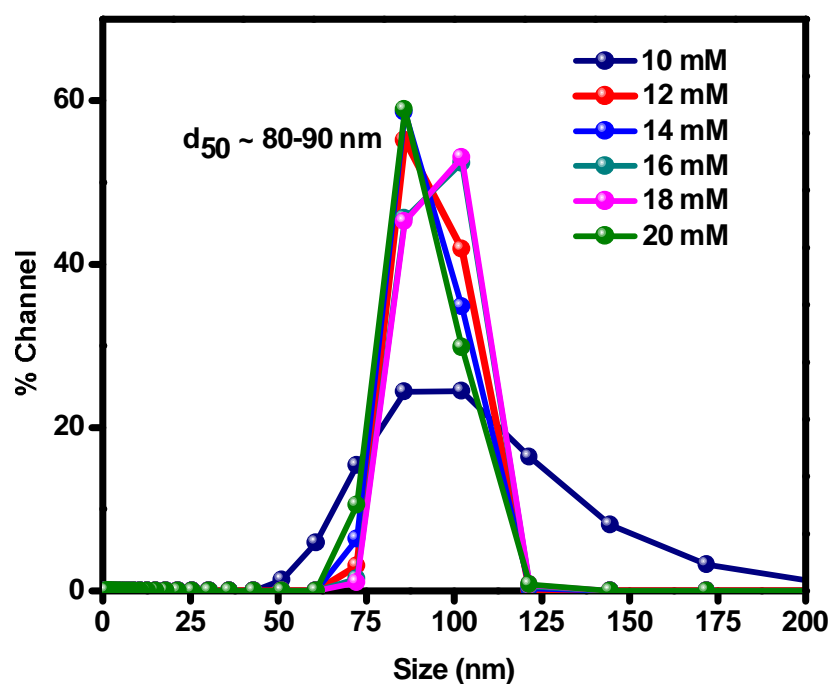
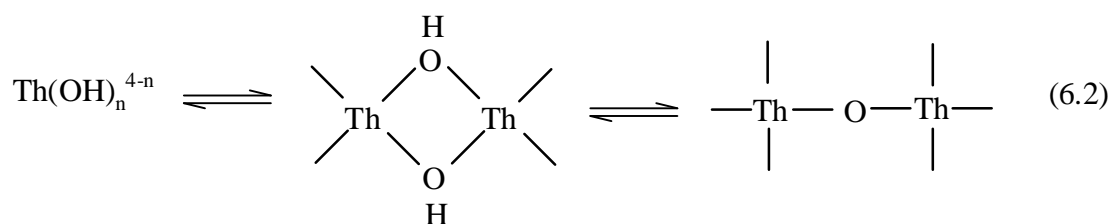
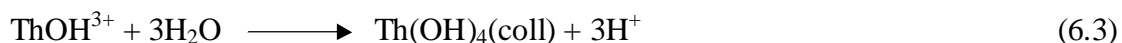


Fig. 6.4. Particle size of Th(IV) colloids formed at pH > 3.4

There was no change in the size of colloids with further increase in pH. It shows that well defined colloids are again formed in the solution. The colloids formed at different pH domains provide further evidence for the scattering solubility data. That is, two different colloids are formed in two regions with respect to pH and Th(IV) concentration. They correspond to different solid phases, microcrystalline and X-ray

amorphous ThO₂. Hence the colloids formed at pH>3.4 are nothing but the bulk crystalline ThO₂ covered with an amorphous layer. The formation of colloids leads to an acidification or decrease in pH of the solution according to the equation 6.3,



These solutions containing colloids were kept for ageing. There was no considerable change in their size during the period of investigation. This shows that the Th(IV) colloids formed at these conditions are highly stable without a tendency for agglomeration or precipitation

6.3.1.2. Molecular weight of Th(IV) colloids formed at pH~1.9 and pH~3.4

The refractive index increment was measured for the freshly formed colloids at pH ~ 1.9 and pH ~ 3.4 (figure 6.5). The refractive index of the solution increases with increase in solute concentration giving a positive slope. The dn/dC values obtained from the slope of the plot was given as input for generating the Debye plot. The shape of the colloids was considered spherical. The particle refractive index was assumed as 2.2. This value corresponds to refractive index of ThO₂. Debye plot was generated for the colloids formed in the pH range of 1.9 as well as those formed in pH~3.4 solutions (figure 6.6).

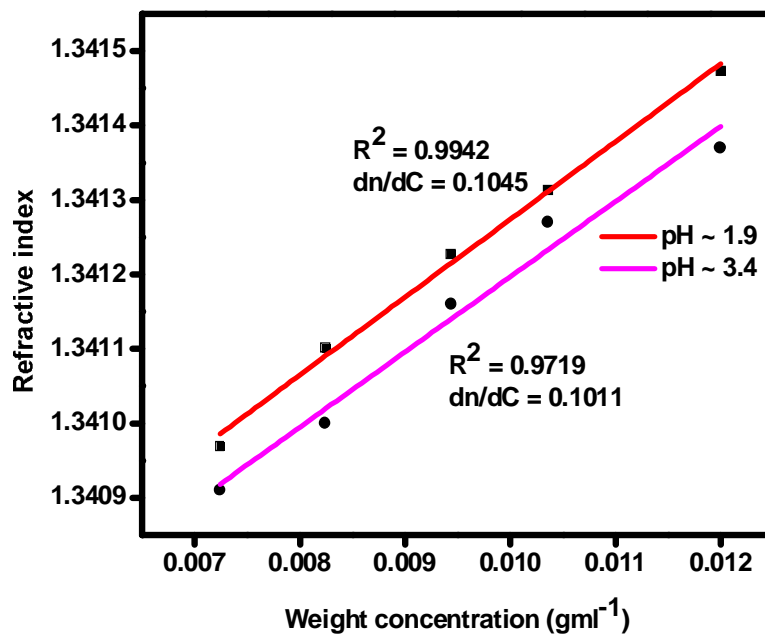


Fig. 6.5. Refractive index increment for colloids formed at pH ~1.9 and pH ~3.4

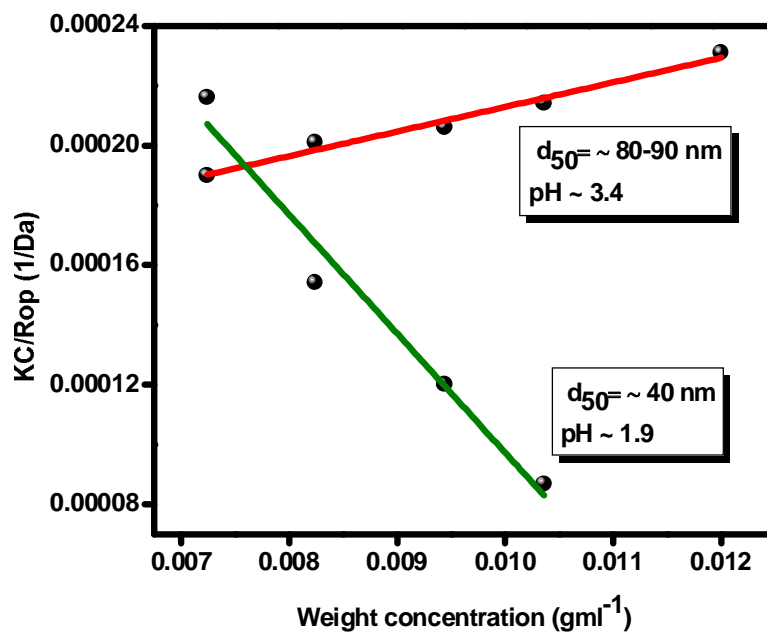


Fig. 6.6. Debye plot for initially formed colloids at pH 1.9 and 3.4

The colloids formed at pH~1.9 have a molecular weight of ~2,019 Da. It shows that these colloids have ~10 Th atoms at the initial stage. The slope of the curve is negative. That is, the second virial coefficient has a negative value. It implies that there was aggregation in the system leading to precipitation. This has already been confirmed by the change in particle size upon ageing. That is the colloids formed at very acidic pH (i.e. pH~1.9) tend to agglomerate causing precipitation in the system thus making it unstable over the period of investigation. But in contrary, the colloids formed at pH>3.4 have a molecular weight of ~7,650 Da with positive second virial coefficient. This polymeric colloid formed due to polynucleation contains around 30 atoms of Th when initially formed. The solute-solvent interaction in the system is higher leading to greater stability of the system. Table 6.1 gives the calculated parameters obtained from the Debye plot for the freshly prepared colloids.

Table 6.1. Calculated parameters from the Debye plot for freshly formed Th(IV) colloids in 10-20 mM Th(IV) solutions

[Th(IV)] = 10-20 mM	At pH ~ 1.9, d₅₀ = ~40 nm	pH ~ 3.4, d₅₀ = ~ 80-90 nm
Molecular weight	~ 2,019 Da	~ 7,650 Da
Second virial coefficient	- 0.03982 ml/g Da	0.00821 ml/g Da

Since the colloids formed at higher pH did not show aggregation they were further aged for 55 days and molecular weight was determined. Figure 6.7 shows Debye plot for colloids aged for 55 days.

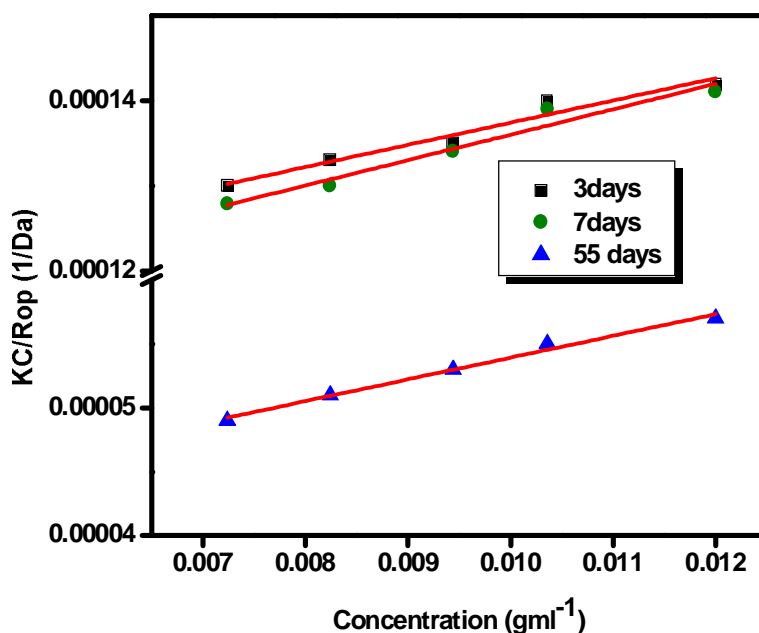


Fig. 6.7. Debye plot for Th(IV) colloids aged for different time intervals at pH ~ 3.4

The molecular weight of colloids increases when aged. It shows that few more monomers are added to polymeric unit by internal condensation. It has been observed that ~ 30 monomeric units are present in the polymer when aged for a week and it increases to ~100 monomeric units when aged for 55 days. Table 6.2 gives the summary of parameters calculated from the Debye plot for aged Th(IV) solution at different time intervals.

Table. 6.2. Parameters from the Debye plot for Th(IV) colloids aged at different time intervals [[Th(IV)] = 10-20mM, pH~3.4]

[Th(IV)] = 10-20mM, pH~3.4	3 days aged	7 days aged	55 days aged
Molecular weight (Da)	~8,909	~9,398	~27,095
Second virial coefficient (ml/g Da)	0.00262	0.00296	0.0017

6.3.2. 0.05 M – 0.4 M Th(IV) solutions

6.3.2.1. Size variation of Th(IV) colloids

Similar experiments were performed at higher Th(IV) concentrated solutions in order to observe the changes in the size of colloids formed at higher concentration. As the concentration of Th(IV) increases, it has been observed that the pH at which colloids form initially decreases. Figure 6.8 shows the size of initially formed colloids at pH ~ 0.8. The size of the colloids was still smaller than those formed at 10-20 mM Th(IV) solutions. It may be due to the micro-crystalline nature of colloids formed at higher concentration. Similar behavior was observed in U(IV) system. It has already been reported that microcrystalline $\text{ThO}_2 \cdot x\text{H}_2\text{O}$ colloids has a size of ~16-23 nm. In the present study, the size of the colloids formed at this concentration ranges from ~15 – 20 nm.

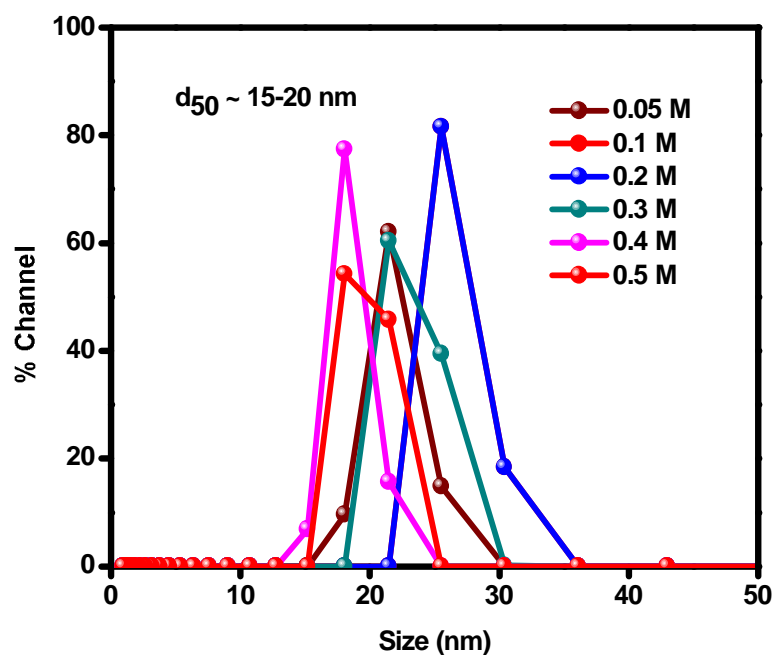


Fig. 6.8. Particle size of Th(IV) colloids formed at pH ~ 0.8

The colloids were kept for ageing. It was observed that they started aggregating within a day. And particles greater than 1000 nm were observed. The formation of small amounts of a visible precipitate has been noticed after 3 days in 0.2 and 0.3 M Th(IV) solutions. Figure 6.9 shows the size distribution of bigger aggregates with mean size greater than 1000 nm when aged for 3 days and figure 6.10 shows the formation of visible precipitates in highly concentrated Th(IV) solutions.

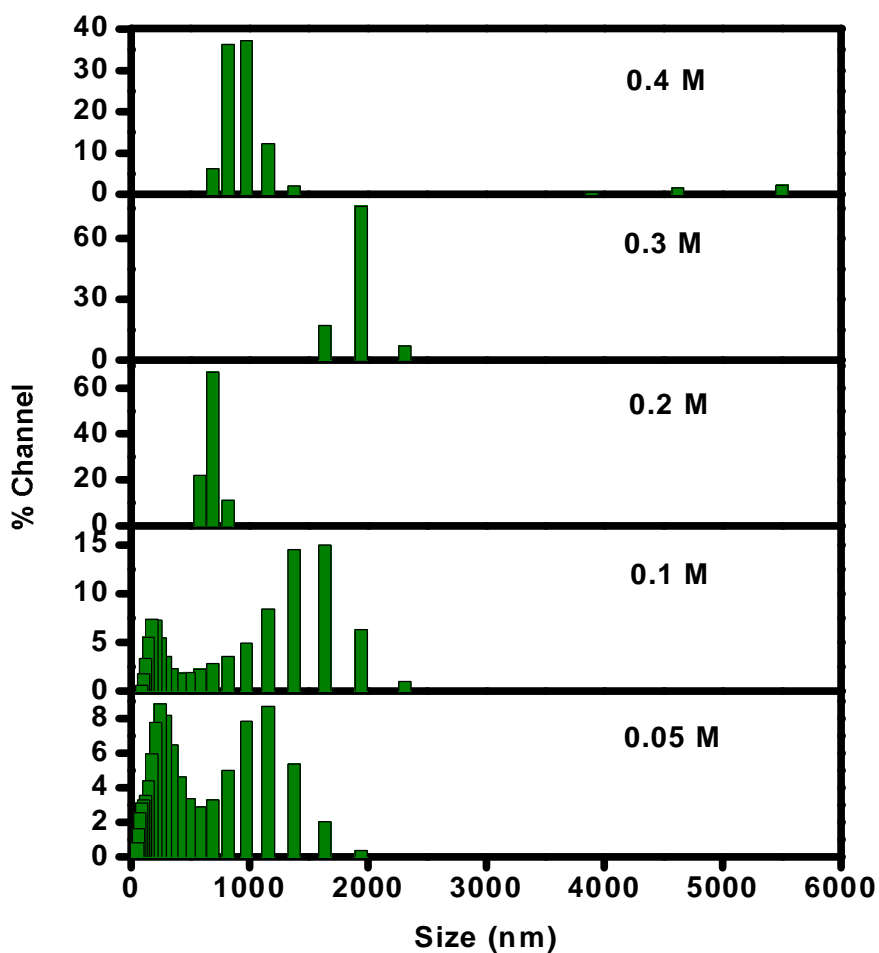


Fig. 6.9. Particle size after ageing for 3 days



Fig. 6.10. Picture showing precipitation in 0.2 and 0.3 M Th(IV) colloidal solutions after 3 days of ageing

Though thorium dioxide colloids are formed at very low pH (~ 0.8 in the present case), Th^{4+} is the predominant species at these conditions. Hence the experiments were repeated by increasing the pH of the solution. At $\text{pH} \sim 2$, colloids of 60-70 nm were formed. These colloids were stable for longer time and did not show much variation even after ageing for a week. The size distribution of these colloidal solutions is shown in figure 6.11.

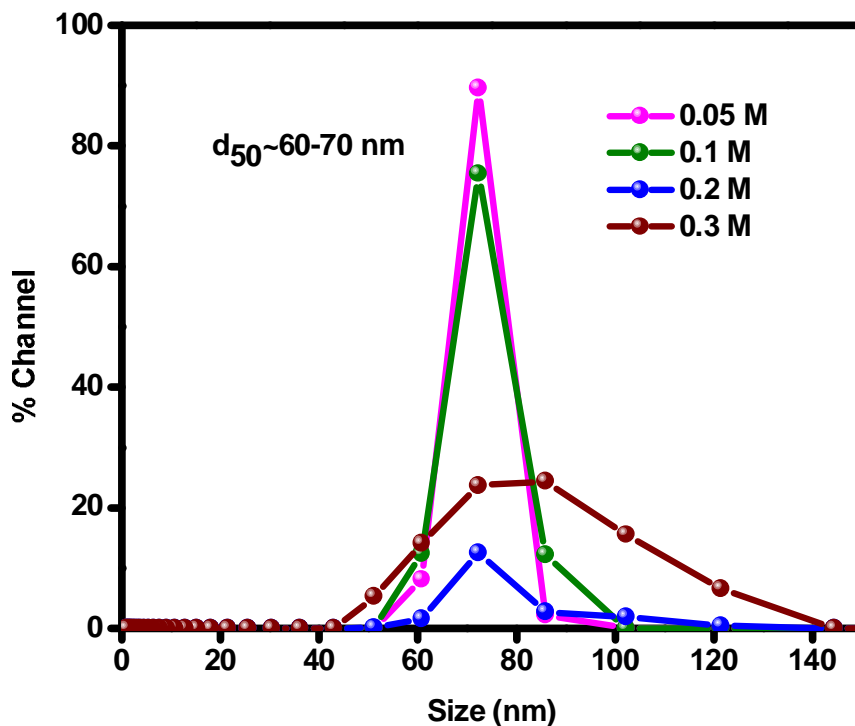


Fig. 6.11. Particle size of Th(IV) colloids formed at pH ~ 2

6.3.2.2. Molecular weight

The refractive index increment was measured for the freshly formed colloids at pH ~ 0.8 and pH ~ 2.0 (figure 6.12). The refractive index of the solution increases with increase in solute concentration giving a positive slope. The dn/dc values obtained from the slope of the plot was given as input for generating the Debye plot. The shape of the colloids was considered spherical. Figure 6.13 shows the Debye plot for colloids formed in 0.05 – 0.4 M Th(IV) solution at pH~0.8 and pH~2.0.

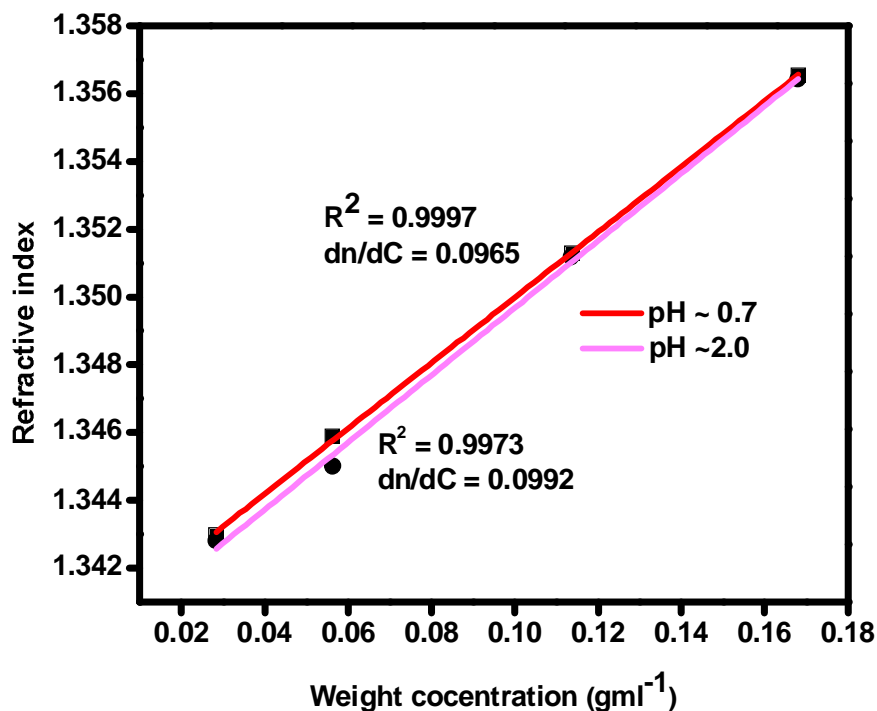


Fig. 6.12. Refractive index increment for colloids formed at pH ~0.8 and pH ~2.0

The colloids formed at pH~0.8 have a molecular weight of ~3,449 Da. It shows that these colloids have ~15 monomeric units at the initial stage. The second virial coefficient is negative. It implies that there was aggregation in the system leading to precipitation. Similar behavior is observed for colloids formed at 10-20 mM solutions. That is, the colloids formed at very acidic pH tend to agglomerate causing precipitation in the system. But, the colloids formed at pH~2 have a molecular weight of ~6,223 Da with positive second virial coefficient. This polymeric colloid formed due to polynucleation contains around 20 monomers when initially formed. The solute-solvent interaction in the system is higher leading to greater stability of the system. Table 6.3 gives the calculated parameters obtained from the Debye plot for the freshly prepared colloids at different pH conditions.

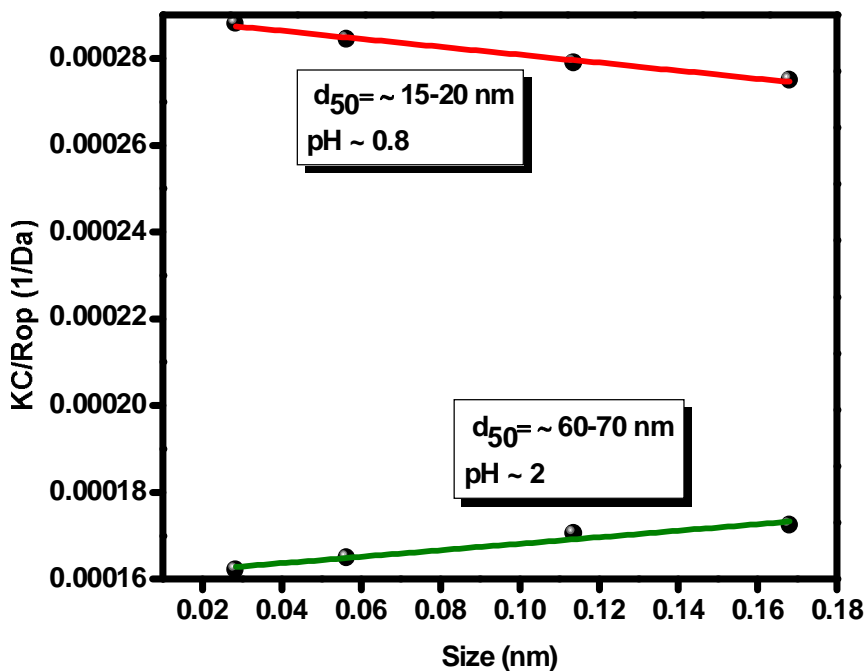


Fig. 6.13. Debye plot for freshly formed colloids at pH~0.8 and pH~2.0

Table 6.3. Calculated parameters from the Debye plot for freshly formed Th(IV) colloids in 0.05 M – 0.4 M Th(IV) solutions

	pH ~ 0.8, d ₅₀ = ~15-20 nm	pH~2, d ₅₀ = ~ 60-70 nm
Molecular weight (Da)	~ 3,449	~ 6,223
Second virial coefficient (ml/g Da)	-9.17413 E-5	7.486 E-5

Similar to previous studies, the colloids formed at higher pH were stable for longer time, they were further aged for a week and the corresponding molecular weight was measured. The colloids upon ageing for a week did not show any considerable change in their molecular weight. But when it is further aged for 55

days, its molecular weight increased to ~43,573. This is much higher than that of polymer formed in lower concentration. It may be due to greater tendency of aggregation at higher concentration. Figure 6.14 shows Debye plot for colloids aged at different time intervals. Table 6.4 gives the details of calculated parameters obtained from the Debye plot for colloids aged at different time intervals.

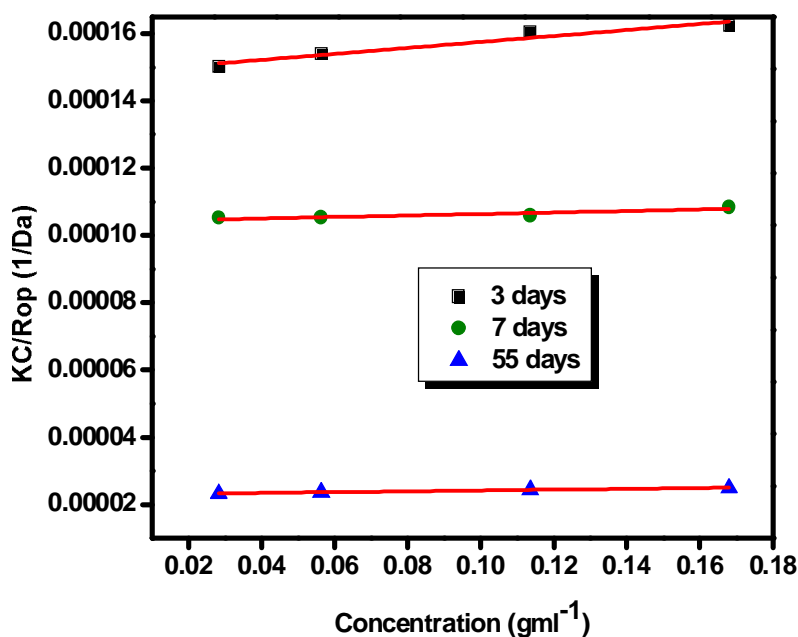


Fig. 6.14. Debye plot for Th(IV) colloids aged at different time intervals at pH~2

Table 6.4. Calculated parameters from the Debye plot for colloids aged at different time intervals [[Th(IV)] = 0.05 – 0.4 M, pH~2]

[Th(IV)] = 0.05 – 0.4 M, pH ~ 2	3 days aged	7 days aged	55 days aged
Molecular weight (Da)	~6,727	~9,600	~43,573
Second virial coefficient (ml/g Da)	8.8834E-5	2.2190E-5	1.2266E-5

6.4. Conclusions

- The size of colloids formed at different acidities and the molecular weight of colloids were determined.
- Colloids formation at two different pH domains shows that these colloids differ in their nature as well as their structure.
- At low pH more crystalline colloids are formed where as at higher pH amorphous colloids are formed.
- The size of these colloids decreases at higher Th concentration.
- Th(IV) behavior is similar to Zr(IV) and U(IV) in the formation of colloids at two different phases. But in case of Th(IV) well defined colloids are formed.
- The second virial coefficient determined from the Debye plot for the colloids shows that those formed at low pH are more prone to aggregation and finally precipitates from the solution.
- Whereas those colloids which are said to be amorphous in nature are found to be more stable throughout the period of investigation and stays without any tendency to agglomerate.
- The molecular weight of freshly prepared Th(IV) polymer obtained from the Debye plot showed that it undergoes hydrolysis and forms polymers of high molecular weight similar to Pu(IV) whose molecular weight varies from 4,000 Da if freshly prepared to 10^{10} Da when aged.
- Pu(IV), Zr(IV) and U(IV) undergoes immediate polymerization and there was drastic change in their molecular weight within short period. Where as in case

of Th(IV), it is least prone to undergo further polymerization when aged for 3-7 days and there was further increase in molecular weight when aged for 55 days. Thus Th(IV) polymerization is initially slow and it becomes faster with increase in time.

Chapter 7



CHAPTER 7

Summary and Scope for Future Work

7.1. Summary

Due to high electric charge, metal ions like Pu^{4+} undergo hydrolysis even under very acidic condition. With increasing pH, the hydrolysis reaction leads to the formation of mononuclear complexes. Close to the solubility limit, mononuclear species condense to form polynuclear species of colloidal dimension. During reprocessing of fuel, formation of these polymers/colloids has to be avoided as it may result in the loss of Pu in aqueous waste and can lead to criticality hazard. In addition to that, radionuclides migrate faster in aquifer systems by colloid mediated transport and pose greater risk to the environment. Hence profound understanding of the aqueous chemistry of radionuclides is a necessary prerequisite to conduct a safety assessment of a repository. The present chapter summarizes the results, conclusion drawn from the investigations carried out on the hydrolysis and polymerization of tetravalent actinides. Studies were carried out using U(IV), Th(IV) and Zr(IV) which is taken as homologue for Pu(IV). In addition to that studies were also carried out on systems such as Bi(III), Al(III), Sr(II) and U(VI) in order to understand the behavior of highly charged metal ion in aqueous systems. Light scattering technique was extensively used to study the hydrolysis reactions of all the above systems.

7.1.1. Hydrolysis of Sr(II), Al(III) and Bi(III)

Hydrolysis reactions of Sr(II), Al(III) and Bi(III) during initial stage was studied using light scattering technique. The initial hydrolysis showed that around 9 water molecules are present in the primary hydration sphere of Sr(II) and 5 in case of Al(III). The diameter of the hydrated ion of Al(III) was determined as 0.9 nm which was in well agreement with the reported values. Whereas, Bi(III) undergoes hydrolysis and forms polymers having 5-6 atoms of Bi in the polymeric unit. This has been confirmed by the weight average molecular weight of the polymer determined from the Debye plot. Hence from the above studies, light scattering was found to be a promising technique to study the hydrolyzed colloidal polymers formed in the system. Hence similar studies were extended to analogues of Pu(IV) such as Zr(IV), U(IV) and Th(IV).

7.1.2. Hydrolysis and polymerization of Zr(IV)

Hydrolysis of Zr(IV) starts at much higher acidity and the light scattering investigation showed unambiguously that colloids are formed in highly saturated solutions. The size variation showed that colloids are formed in two different domains of pH and Zr(IV) concentration. In more acidic solution with pH~0.7, colloids of more crystalline nature are formed. Whereas at pH>1.7, amorphous colloids form spontaneously from the oversaturated solutions. The molecular weight of freshly formed polymer showed that more than 10 Zr atoms are present in the polymer. When the solution was aged for a week, it increased to 30 atoms of Zr. This is in analogous to Pu(IV). Around 10 atoms of Pu are present in the polymer when freshly prepared, which increased to 10^{10} units when aged. The solute-solvent interaction showed that

there was aggregation initially in the system and when aged, the dispersion becomes very stable with high solute-solvent interaction.

7.1.3. Hydrolysis of U(IV) and U(VI)

In contrast to the above investigations on Zr(IV), U(VI) is highly resistant to polymerization and it forms only oligomers with 2-3 uranyl units at near neutral conditions.

- ✚ Uranyl ions was shown to form geometrically stabilized hydrolysis species which is in contrast to Zr(IV).
- ✚ Well defined colloids are formed with no further change in size with change in pH and uranyl concentration.
- ✚ In case of uranyl ions, there is no continuous hydrolysis, i.e. stepwise increase in the number of hydroxide ligand over a rather wide pH range observed for polymers of tetravalent metal ions.

Whereas studies on U(IV) showed that hydrolysis takes place even in highly acidic aqueous solutions. For this purpose, 0.4 – 19 mM (total U) concentration ($1 < \text{pH} < 4$) was investigated by light scattering. At $\text{pH} < 2$ and higher U(IV) concentration, the size of colloids formed is smaller due to more crystalline nature of the colloids. Weight average molecular weight of the freshly prepared and colloidal polymers aged for 3 days ranges from 1,800 to 13,000 Da. 40-50 atoms of U are considered to be present in the polymer when aged. Positive value of second virial coefficient shows that solute-solvent interaction is high leading to stable suspension.

7.1.4. Hydrolysis and polymerization of Th(IV)

Investigations on the hydrolysis and polymerization of Th(IV) showed that Th(IV) is resistant towards hydrolysis initially and becomes faster with increase in time. Well defined colloids are formed at two different pH domains. Colloids of very small size are formed at very acidic pH condition. Whereas hydrolysis and polynucleation at $\text{pH} > 3$ lead to the formation of larger size colloids. The colloids formed at $\text{pH} \sim 1.9$ ($[\text{Th(IV)}] = 10\text{-}20 \text{ mM}$) and at $\text{pH} \sim 0.8$ ($[\text{Th(IV)}] = 0.05\text{-}0.4 \text{ M}$) are crystalline in nature whereas those formed at $\text{pH} > 3$ are amorphous. The weight average molecular weight of colloids showed that Th(IV) undergo polynucleation forming polymers of high molecular weight. When these colloids are aged for longer time, the molecular weight also increases. The solute-solvent interaction parameter reveals that the colloids formed at highly acidic conditions are more prone for aggregation leading to precipitation in the system. Those formed at $\text{pH} > 3$ are stable throughout the period of investigation.

As a whole, Zr(IV), U(IV) and Th(IV) showed analogous behavior. There are numerous parallels of polymer and colloid chemistry of Zr(IV), U(IV) and Th(IV) but it is also clear that there is pronounced differences in the pH of initial colloid formation and concentration of metal ions. The size of the initially formed colloids also varies with respect to metal ion. In analogous to Pu(IV) polymer chemistry, Zr(IV), U(IV) and Th(IV) forms polymers of considerable size whose molecular weight varies from few 1000 Da to billions of Da. The molecular weight increases upon ageing which also parallels Pu(IV) polymer chemistry.

7.2. Future Perspectives

- From the above investigations it has been observed that the light scattering technique is very fast and non-invasive and hence it can be used for immediate detection of colloids/polymers formed during reprocessing of nuclear fuels. Hence prevention measures can be taken immediately to depolymerize as soon as polymer is formed in the system. Since the present studies were carried out at lab scale it can be extended for large scale (i.e., in fuel reprocessing operations).
- There is only limited information available in the literature regarding the structure and shape of the colloidal polymers of tetravalent actinides. In case of Zr(IV), it has been already reported that the hydrous polymers are rod shape similar to Pu(IV) polymer. But there is no information regarding shape of Th(IV) and U(IV) polymers. The small angle X-ray scattering (SAXS) and small angle neutron scattering (SANS) are the most widely used techniques for studying structure and shape of polymers. Hence these techniques can be applied in order to probe their respective shape and structure.
- Kinetic studies on hydrolysis and polymerization of Pu(IV) and Zr(IV) revealed that it follows third order reaction. The information available on the growth kinetics of U(IV) and Th(IV) polymers are sparse. Hence investigations can be extended to studies related to kinetics of hydrolysis reactions of U(IV) and Th(IV). The results can be used to avoid the conditions responsible for formation of actinide polymers in reprocessing operations.

- Temperature has a greater impact on the nature of hydrolysis mainly due to significant change in the properties of water as the temperature is changed. For example the ionic product of water increases by almost 3 orders of magnitude and dielectric constant decreases by ~35% from 0 to 100°C. Moreover it can also affect the kinetics and nature of hydrolyzed species formed in the system. Since all the investigations were performed at room temperature, similar studies can be extended to systems investigated for elevated temperatures and the data obtained from the studies will greatly help to predict the chemical behavior of tetravalent actinides in the reprocessing and disposal of nuclear wastes where elevated temperatures are likely to be encountered.

References



List of References

- [1] Bharadwaj SA (2013) Indian nuclear power program – Past, present and future. *Sadhana* 38:775-794.
- [2] Navratil JD (1986) Solvent extraction in nuclear technology. *Pure & Appl Chem* 58:885-888.
- [3] Sukhatme SP (2011) Meeting India's future needs of electricity through renewable energy resources. *Current Sci* 101:624-630.
- [4] Kakodkar A, Grover R (2000) Nuclear energy in India. *The Nuclear Engineer* 45:31-36.
- [5] Baldev Raj, Kamath HS, Natarajan R, Vasudeva Rao PR (2005) A perspective on fast reactor fuel cycle in India. *Prog Nucl Energy* 47:369-379.
- [6] Sengupta P, Kaushik CP, Dey GK (2013) Immobilization of high level nuclear wastes: The Indian Scenario. *On a Sustainable Future of the Earth's Natural Resources*. Springer, Berlin, Heidelberg, p 25-51.
- [7] Fairlie I (2008) Depleted uranium: properties, military use and health risks. *Medicine, conflict and survival* 25:41-64.
- [8] Grenthe I, Drozdzyński J, Fujino T, Buck EC, Albert-Schmitt TE, Wolf SF (2011) The chemistry of the actinide and transactinide elements. Chapter 5 Uranium. Springer, Netherlands, p 253-698.
- [9] Kakodkar A (2002) Nuclear power in India: An inevitable option for sustainable development of a sixth of humanity. *World Nuclear Association, Annual symposium, London*.
- [10] Geist A, Gompper K, Weigl M, Fanghanel T (2004) Reduzierung der radiotoxizität abgebrannter kernbrennstoffe durch abtrennung und transmutation von actiniden: partitioning. *Nachrichten-FZK* 36:97-102.
- [11] Baisden PA, Choppin GR (2007) Nuclear waste management and the nuclear fuel cycle. *Radiochemistry and nuclear chemistry*, <http://www.eolss.net/ebooks/Sample%20Chapters/C06/E6-104-11.pdf>.

- [12] Choppin G, Rydberg J, Liljenzin JO (2001) Radiochemistry and nuclear chemistry. Butterworth-Heinemann.
- [13] Simpson MF, Law JD (2010) Nuclear fuel reprocessing. Idaho National laboratory, INL/EXT-10-17753.
- [14] Biggers RE, Costanzo DA (1963) A study of the polymerization, depolymerization and precipitation of tetravalent plutonium as functions of temperature and acidity by spectrophotometric methods: Preliminary report. ORNL TM-585.
- [15] Bronikowski MG, Crowder ML, Thompson MC (1999) Adsorption of Pu(IV) polymer onto 304L stainless steel. WSRC-TR-99-00210.
- [16] Cleveland JM (1967) Solution chemistry of plutonium in plutonium handbook. Gordon and Breach, New York.
- [17] Kretzschmar R, Barmettler K, Grolimund D, Yan Y -d, Borkovec M, Sticher H (1997) Experimental determination of colloid deposition rates and collision efficiencies in natural porous media. *Water Resour Res* 33:1129-1137.
- [18] Henry M, Jolivet JP, Jacques L (1992) Chemistry, spectroscopy and applications of Sol-Gel glasses. *Aqueous chemistry of metal cations: Hydrolysis, condensation and complexation*. Springer Berlin Heidelberg, p 153-206.
- [19] Baes CF, Mesmer RE (1976) *The Hydrolysis of Cations*. John Wiley and Sons, New York.
- [20] Altmaier M, Gaona X, Fanghanel T (2013) Recent advances in aqueous actinide chemistry and thermodynamics. *Chem Rev* 113:901-943.
- [21] Baes CF Jr, Mesmer RE (1981) The thermodynamics of cation hydrolysis. *Am J Sci* 281:935-962.
- [22] Choppin GR (1983) *Solution chemistry of the Actinides*. *Radiochim Acta* 32:43-53.
- [23] Grenthe I, Puigdomenech I (1997) *Modelling in aquatic chemistry*. OECD/NEA, Paris.

-
- [24] Neck V, Kim JI, Seidel BS, Marquardt CM, Dardenne K, Jensen MP, Hauser W (2001) A spectroscopic study of the hydrolysis, colloid formation and solubility of Np(IV). *Radiochim Acta* 89:439-446.
- [25] Walther C, Cho HR, Marquardt CM, Neck V, Seibert A, Yun JI, Fanghanel Th (2007) Hydrolysis of plutonium (IV) in acidic solutions: no effect of hydrolysis on absorption-spectra of mononuclear hydroxide complexes. *Radiochim Acta* 95:7-16.
- [26] Choppin GR (1999) Utility of oxidation state analogs in the study of plutonium behavior. *Radiochim Acta* 85:89-96.
- [27] Clark DL, Hecker SS, Jarvinen GD, Neu MP (2006) Plutonium. *The chemistry of actinide and transactinide elements*. Springer, Heidelberg, p 813-1203.
- [28] Cleaveland JM (1970) *The chemistry of Plutonium*. Gordon and Breach, New York.
- [29] Clark DL (2000) The chemical complexities of Plutonium. *Los Alamos Sci* 26:364-381.
- [30] Walther C (2008) From hydrolysis to the formation of colloids- Polymerization of tetravalent Actinide ions. PhD Thesis, Universitat Mainz. <http://bibliothek.fzk.de/zb/berichte/FZKA7442.pdf>.
- [31] Kumar S, Koganti SB (1997) A numerical model for prediction of boundary acid concentration for prevention of polymerization at macro Pu concentrations. *J Nucl Sci Technol* 34:1027-1028.
- [32] Seaborg GT, Loveland WD (1990) *The elements beyond Uranium*. Wiley, New York, p 90.
- [33] Schuelein VL (1975) Parameters for plutonium polymer formation in nitric acid. ARH-SA-233, p 30.
- [34] Bitea C, Walther C, Yun JI, Marquardt Ch, Seibert A, Neck V, Fanghanel Th, Kim JI (2003) A study of colloid generation and disproportionation of Pu(IV) in aquatic solutions by LIBD and LPAS. *AIP Conf Proc* 673:26.
- [35] Costanzo DA, Biggers RE, Bell JT (1973) Plutonium polymerization-I. A spectrophotometric study of the polymerization of plutonium(IV). *J Inorg Nucl Chem* 35:609-622.
-

-
- [36] Silver GL (1983) Free energy of plutonium polymer formation. *J Less Common Met* 91:317-320.
- [37] Toth LM, Friedman HA, Osborne (1981) Polymerization of Pu(IV) in aqueous nitric acid solutions. *J Inorg Nucl Chem* 43:2929-2934.
- [38] Rabideau SW, Kline RJ (1960) A spectrophotometric study of the hydrolysis of plutonium(IV). *J Phys Chem* 64:680-682.
- [39] Wester DW (1982) Synthesis and characterization of bis(μ -hydroxo)tetraaquadiplutonium(IV) sulfate, $\text{Pu}_2(\text{OH})_2(\text{SO}_4)_3 \cdot 4\text{H}_2\text{O}$, a novel compound containing hydrolyzed plutonium(IV). *Inorg Chem* 21:3382-3385.
- [40] Walther C, Rothe J, Brendebach B, Fuss M, Altmaier M, Marquardt CM, Buchner S, Cho HR, Yun JI, Seibert A (2009) New insights in the formation processes of Pu(IV) colloids. *Radiochim Acta* 97:199-207.
- [41] Newton TW, Hobart DE, Palmer PD (1985) The formation of plutonium(IV) colloid by the alpha-reduction of Pu(V) and Pu(VI) in aqueous solutions. *Radiochim Acta* 39:139-147.
- [42] Rai D, Swanson JL (1981) Properties of plutonium(IV) polymer of environment importance. *Nucl Technol* 54:107-111.
- [43] Neck V, Altmaier M, Seibert A, Yun JI, Marquardt CM, Fanghanel T (2007) Solubility and redox reactions of Pu(IV) hydrous oxide: Evidence for the formation of $\text{PuO}_{2+x}(\text{s,hyd})$. *Radiochim Acta* 95:193-207.
- [44] Knope KE, Soderholm L (2013) Plutonium (IV) cluster with a hexanuclear $[\text{Pu}_6(\text{OH})_4\text{O}_4]^{12+}$ core. *Inorg Chem* 52:6770-6772.
- [45] Wang R, Carducci MD, Zheng Z (2000) Direct hydrolytic route to molecular oxo-hydroxo lanthanide clusters. *Inorg Chem* 39:1836-1837.
- [46] Lemire RJ, Fuger J, Nitsche H, Potter P, Rand MH, Rydberg J, Spahiu K, Sullivan JC, Ullman WJ, Vitorge P, Wanner H (2001) Chemical Thermodynamics of Neptunium and Plutonium, Vol. 4 of Chemical Thermodynamics, Elsevier, North-Holland, Amsterdam.
- [47] Guillaumont R, Fanghanel T, Fuger J, Grenthe I, Neck V, Palmer DA, Rand MH (2003) Update on the Chemical Thermodynamics of Uranium,

- Neptunium, Plutonium, Americium and Technetium, Chemical Thermodynamics, Elsevier, North-Holland, Amsterdam.
- [48] Knope KE, Soderholm L (2013) Solution and solid-state structural chemistry of actinide hydrates and their hydrolysis and condensation products. *Chem Rev* 113:944-994.
- [49] Rothe J, Walther C, Denecke M.A, Fanghanel (2004) XAFS and LIBD investigation of the formation and structure of colloidal Pu(IV) hydrolysis products. *Inorg Chem* 43:4708-4718.
- [50] Soderholm L, Almond PM, Skanthakumar S, Wilson RE, Burns PC (2008) The structure of the plutonium oxide nanocluster $[\text{Pu}_{38}\text{O}_{56}\text{Cl}_{54}(\text{H}_2\text{O})_8]^{14-}$. *Angew Chem* 120:304-308.
- [51] Wilson RE, Skanthakumar S, Soderholm L (2011) Separation of plutonium oxide nanoparticles and colloids. *Angew Chem Int Ed* 50:11234-11237.
- [52] Thiyagarajan P, Diamond H, Soderholm L, Horwitz EP, Toth LM, Felker LK (1990) Plutonium(IV) polymers in aqueous and organic media. *Inorg Chem* 29:1903-1907.
- [53] Ekberg C, Larsson K, Skarnemark G, Odegaard-Jensen A, Persson I (2013) The structure of plutonium(IV) oxide as hydrolysed clusters in aqueous suspensions. *Dalton Trans* 42:2035-2040.
- [54] Haire RG, Lloyd MH, Beasley ML, Milligan WO (1971) Aging of hydrous Plutonium dioxide. *J Electron Microsc* 20:8-16.
- [55] Bell JT, Coleman CF, Costanzo DA, Biggers RE (1973) Plutonium polymerization – II Kinetics of the plutonium polymerization. *J Inorg Nucl Chem* 35:623-628.
- [56] Reed DT, Lucchini JF, Aase SB, Kropf AJ (2006) Reduction of plutonium(VI) in brine under subsurface conditions. *J Radiochim Acta* 94:591-597.
- [57] Neu MP, Schulze RK, Conradson SD, Farr JD, Haire RG (1997) Polymeric Pu(IV) hydroxide: Formation, prevalence and structural and physical characteristics. *Pu Futures: Topical conference on Plutonium and Actinides*. New Mexico, p 89.

-
- [58] Toth LM, Friedman (1978) The IR spectrum of Pu(IV) polymer. *J Inorg Nucl Chem* 40:807-810.
- [59] Lloyd MH, Haire RG (1978) The chemistry of plutonium in sol-gel processes. *Radiochim Acta* 25:139-148.
- [60] Triay IR, Hobart DE, Mitchell AJ, Newton TW, Ott MA, Palmer PD, Rundberg RS, Thompson JL (1991) Size determinations of plutonium colloids using autocorrelation photon spectroscopy. *Radiochim Acta* 52:127-131.
- [61] Lloyd MH, Haire RG (1973) Studies on the chemical and colloidal nature of Pu(IV) polymer. Congress of the IUPAC, Germany, p 24.
- [62] Walther C, Denecke MA (2013) Actinide colloids and particles of environmental concern. *Chem Rev* 113:995-1015.
- [63] Rundberg RS, Mitchell AJ, Triay IR, Torstenfelt NB (1987) Size and Density of a ^{242}Pu Colloid. *MRS Proceedings* 112:243.
- [64] Metivier H, Guillaumont R (1972) Hydrolysis of tetravalent plutonium. *Radiochem Radioanal Lett* 10:27-35.
- [65] Fanghanel Th, Neck V (2002) Aquatic chemistry and solubility phenomena of actinide oxides/hydroxides. *Pure Appl Chem* 74:1895-1907.
- [66] Neck V, Kim JI (2001) Solubility and hydrolysis of tetravalent actinides. *Radiochim Acta* 89:1-16.
- [67] Runde W (2000) The chemical interactions of actinides in the environment. *Los Alamos Sci* 26:392-410.
- [68] Kim JI, Kanellakopoulos B (1989) Solubility products of plutonium(IV) oxide and hydroxide. *Radiochim Acta* 48:145-150.
- [69] Rai D, Ryan JL (1982) Crystallinity and solubility of Pu(IV) oxide and hydrous oxide in aged aqueous suspensions. *Radiochim Acta* 30:213-216.
- [70] Strickert RG, Rai D, Fulton RW (1984) Effect of ageing on the solubility and crystallinity of Np(IV) hydrous oxide. *ACS Symp Ser* 246:135-145.
- [71] Walther C, Cho HR, Marquardt CM, Neck V, Seibert A, Yun JI, Fanghanel Th (2007) Hydrolysis of plutonium(IV) in acidic solutions: no effect of hydrolysis on absorption-spectra of mononuclear hydroxide complexes. *Radiochim Acta* 95:7-16.
-

-
- [72] Ockenden DW, Welch GA (1956) The preparation and properties of some plutonium compounds. V. Colloidal quadrivalent Plutonium. *J Chem Soc* 1:3358-3363.
- [73] Johnson GL, Toth LM (1978) Plutonium(IV) and Thorium(IV) hydrous polymer chemistry. Technical Report ORNL/TM-6365.
- [74] Rabideau SW (1953) Equilibria and reaction rates in the disproportionation of Pu(IV). *J Am Chem Soc* 75:798-801.
- [75] Klasky M, Navratil JD (2003) Review and update of Plutonium(IV) polymer chemistry related to PUREX processing operations. *AIP Conf Proc* 673:249-250.
- [76] Muscatello AC, Navratil JD, Killion ME (1983) Solvent extraction of plutonium(IV) polymer by dihexyl-N, N-Diethyl-carbamoylmethylphosphonate (DHDECMP). *Sep Sci Technol* 18:1731-1746.
- [77] Chaiko DJ (1992) Partitioning of polymeric Pu(IV) in Winsor II microemulsion systems. *Sep Sci Technol* 27:1389-1405.
- [78] Hunter D, Ross DS (1991) Evidence for a phytotoxic hydroxyl-aluminum polymer in organic soil horizons. *Science* 251:1056-1058.
- [79] Brunstad A (1959) Polymerization and precipitation of plutonium(IV) in nitric acid. *Ind Eng Chem* 51:38-40.
- [80] Ermolaev VM, Zakharova EV, Shilov VP (2001) Depolymerization of Pu(IV) polymer in 0.5-3 M HNO₃ in the presence of reductants and oxidants. *Radiochemistry* 43:424-428.
- [81] Oak MS, Ghadse DR, Sagar VB, Bhargava VK, Patil SK (1983) Some observations on the oxidation of plutonium(IV) with hydrogen peroxide in the presence of iron. *Radiochem Radioanal Lett* 59:139-145.
- [82] Tallent OK, Mailen JC, Bell JT, Arwood PC (1982) Method of removing Pu(IV) polymer from nuclear fuel reclaiming liquid. US 4316776 A.
- [83] Lindenbaum A, Westfall W (1965) Colloidal properties of plutonium in dilute aqueous solution. *Int J Appl Radiat Isot* 16:545-553.
- [84] Weigel F, Katz J, Seaborg GT (1997) The chemistry of the Actinide elements. Chapman and Hall, London, 2:5-406.
-

-
- [85] Bell JT, Friedman HF (1976) Photochemical reactions of aqueous plutonium systems. *J Inorg Nucl Chem* 38:831-835.
- [86] Friedman HA, Toth LM, Bell JT (1977) Photochemical reactions of aqueous plutonium systems-II. *J Inorg nucl Chem* 39:123-126.
- [87] Quiles F, Burneau A (1998) Infrared and Raman spectroscopic study of uranyl complexes: hydroxide and acetate derivatives in aqueous solution. *Vib Spectrosc* 18:61-75.
- [88] Costanzo DA, Biggers RE (1963) A study of the Polymerization, depolymerization and precipitation of tetravalent Plutonium as functions of temperature and acidity by spectrophotometric methods. USAEC report ORNL-TM-585.
- [89] Savage DJ, Kyffin TW (1986) Oxidative breakdown of polymeric plutonium(IV) hydroxide by cerium(IV). *Polyhedron* 5:743-752.
- [90] Brown PL, Curti E, Grambow B, Ekberg C (2005) Chemical thermodynamics of Zirconium. Elsevier, Amsterdam, Netherlands.
- [91] Videm K (1972) Properties of zirconium base cladding materials – corrosion and hydrogen pickup. *Nucl Eng Des* 21:200-211.
- [92] Ekberg C, Kallvenius G, Albinsson Y, Brown PL (2004) Studies on the hydrolytic behavior of zirconium(IV). *J Sol Chem* 33:47-79.
- [93] Senftle FE, Farley TA (1956) Half-life of Th^{232} and the branching ratio of Bi^{212} . *Phys Rev* 104:1629-1632.
- [94] Torapava N, Persson I, Eriksson L, Lundberg D (2009) Hydration and hydrolysis of Th(IV) in aqueous solution and the structures of two crystalline Th(IV) hydrates. *Inorg Chem* 48:11712-11723.
- [95] Ryan JL, Rai D (1983) The solubility of U(IV) hydrous oxide in sodium hydroxide solutions under reducing conditions. *Polyhedron* 2:947-952.
- [96] Schafer T, Huber F, Seher H, Missana T, Alonso U, Kumke M, Eidner S, Claret F, Enzmann F (2012) Nanoparticles and their influence on radionuclide mobility in deep geological formations. *Appl Geochem* 27:390-403.
- [97] Everett DH (1972) Terminology and symbols in colloid and surface chemistry, Part I. *Pure Appl Chem* 31:579-638.
-

- [98] Degueudre C, Pfeiffer HR, Alexander W, Wernli B, Bruetsch R (1996) Colloid properties in granitic groundwater systems. I: Sampling and characterization. *Appl Geochem* 11:677-695.
- [99] Kim JI, Buckau G, Baumgartner F, Moon HC, Lux D (1984) Colloid generation and the actinide migration in Gorleben groundwaters. Elsevier, G. L. McVay edition, New York 7:31-40.
- [100] Silva RJ, Nitsche H (1995) Actinide environmental chemistry. *Radiochim Acta* 70:377-396.
- [101] Pashley RM, Karaman ME (2004) *Applied colloid and surface chemistry*. John Wiley and Sons, England.
- [102] Pirie AD (1995) A light scattering study of colloid polymer mixtures. PhD Thesis, University of Edinburgh.
- [103] Walther C (2003) Comparison of colloid investigations by single particle analytical techniques - a case study on thorium-oxyhydroxides. *Colloids and Surfaces A: Physicochem Eng Aspects* 217:81-92.
- [104] Avogadro A, Marsily G De (1984) Role of colloids in nuclear waste disposal. *Mat Res Soc Symp Proc* 26:495-505.
- [105] Colfen H, Volkel A (2003) Hybrid colloid analysis combining analytical ultracentrifugation and flow-field flow fractionation. *Eur Biophys J* 32:432-436.
- [106] Barth HG, Boyes BE, Jackson C (1998) Size Exclusion chromatography and related separation techniques. *Anal Chem* 70:251-278.
- [107] Rees TF (1990) Comparison of photon correlation spectroscopy with photosedimentation analysis for the determination of aqueous colloid size distribution. *Wat Resource Res* 26:2777-2781.
- [108] Colfen H, Antonietti M (2000) Field-flow fractionation techniques for polymer and colloid analysis. In *new developments in polymer analytics I*. Springer, Berlin, Heidelberg, p 67-187.
- [109] Srnova-Sloufova I, Lednický F, Gemperle A, Gemperlova J (2000) Core-Shell (Ag)Au bimetallic nanoparticles: Analysis of Transmission Electron Microscopy images. *Langmuir* 16:9928-9935.

-
- [110] Goldstein J (2003) Scanning electron microscopy and x-ray microanalysis. Plenum, Kluwer Academic, p 689.
- [111] Hornyak GL, Peschel ST, Sawitowski TH, Schmid G (1998) TEM, STM and AFM as tools to study clusters and colloids. *Micron* 29:183-190.
- [112] Xu R (2001) Particle characterization: Light Scattering methods. Kluwer Academic publishers, Netherlands.
- [113] Degueudre C, Bilewicz A, Alder HP (1995) Behavior and removal of radionuclides generated in the cooling water of a proton accelerator. *Nucl Sci Eng* 120:65-71.
- [114] Ledin A, Karlsson S, Duker A, Allard B (1994) Measurements in situ of concentration and size distribution of colloidal matter in deep groundwaters by photon correlation spectroscopy. *Wat Res* 28:1539-1545.
- [115] Ross Hallet F (1994) Particle size analysis by dynamic light scattering. *Food Res Int* 27:195-198.
- [116] Berne BJ, Pecora R (1976) Dynamic light scattering with application in physics, chemistry and biology. Wiley, New York.
- [117] Pecora R (1985) Dynamic Light Scattering. Plenum, New York.
- [118] Primer (2000) Fundamentals of UV-visible spectroscopy. Agilent technologies, Germany.
- [119] Rouessac F, Rouessac A (2004) Chemical analysis - Modern instrumentation, methods and techniques. John Wiley & Sons Ltd, England.
- [120] Griffiths PR, Haseth JAD (1986) Fourier Transform Infrared Spectrometry. John Wiley, New York.
- [121] Neilson GW, Enderby JE (1996) Aqueous solutions and neutron scattering. *J Phys Chem* 100:1317-1322.
- [122] Angelo PD, Nolting HF, Pavel NV (1996) Evidence for multielectron resonances at the Sr *K* edge. *Phys Rev A* 53:798-805.
- [123] Camaniti R, Musinu A, Paschima G, Pinna G (1982) X-ray diffraction study of aqueous SrCl₂ solutions. *J Appl Cryst* 15:482-487.

-
- [124] Spohr E, Palinkas G, Heinzinger K, Bopp P, Probst MM (1988) Molecular dynamics study of an aqueous strontium chloride solution. *J Phys Chem* 92:6754-6761.
- [125] Ramos S, Neilson GW, Barnes AC, Capitan MJ (2003) Anomalous x-ray diffraction studies of Sr^{2+} hydration in aqueous solution. *J Chem Phys* 118:5542-5546.
- [126] Fratiello A, Lee RE, Nishida VM, Schuster RE (1968) Proton magnetic resonance coordination number study of Al(III), Be(II), Ga(III), In(III) and Mg(II) in water and aqueous solvent mixtures. *J Chem Phys* 48:3705-3711.
- [127] Martell AE, Hancock RD, Smith RM, Motekaitis RJ (1996) Coordination of Al(III) in the environment and in biological systems. *Coord Chem Rev* 149:311-328.
- [128] Fournier AC, Shafran KL, Perry CC (2008) Potentiometric determination of the 'formal' hydrolysis ratio of aluminium species in aqueous solutions. *Analytica Chimica Acta* 607:61-73.
- [129] Richens DT (1977) *The Chemistry of Aqua Ions*. Wiley, New York, p 143.
- [130] Swaddle TW, Rosenqvist, Yu P, Bylaska E, Phillips B L, Casey WH (2005) Kinetic evidence for five-coordination in $\text{Al}(\text{OH})_{2+}^{\text{(aq)}}$. *Science* 308:1450-1453.
- [131] Ruiz JM, McAdon MH, Garces JM (1997) Aluminum complexes as models for Brønsted acid sites in zeolites: Structure and energetic of $[\text{Al}(\text{OH})_4]^-$, $[\text{Al}(\text{H}_2\text{O})_6]^{3+}$ and intermediate monomeric species $[\text{Al}(\text{OH})_x(\text{H}_2\text{O})_{n-x} \cdot m\text{H}_2\text{O}]^{3-x}$ obtained by hydrolysis. *J Phys Chem B* 101:1733-1744.
- [132] Miao Q, Cao Q, Bi S (2004) Density functional theory study on the bridge structure in dimeric aluminum(III) water complexes. *J Chem Phys* 121:4650-4656.
- [133] Kubicki JD, Sykes D, Apitz SE (1999) Ab initio calculation of aqueous aluminum and aluminum-carboxylate complex energetics and ^{27}Al NMR chemical shifts. *J Phys Chem A* 103:903-915.
-

-
- [134] Chao X, XingHai S, QingDe C, HongCheng G (2009) Investigation on the extraction of strontium ions from aqueous phase using crown ether-ionic liquid systems. *Sci China Ser B-Chem* 52:1858-2864.
- [135] Pfund DM, Darab JG, Fulton JL, Ma Y (1994) An XAFS study of strontium ions and krypton in supercritical water. *J Phys Chem* 98:13102-13107.
- [136] Neilson GW, Broadbent RD (1990) The structure of Sr^{2+} in aqueous solution. *Chem Phys Lett* 167:429-431.
- [137] Hofer TS, Randolf BR, Rode BM (2006) Sr(II) in water: A labile hydrate with a highly mobile structure. *J Phys Chem B* 110:20409-20417.
- [138] Neilson GW, Ansell S, Wilson J, Naturforsch A (1995) Aqua cations: Results from neutron scattering. *Z Naturforsch* 50a:247-256.
- [139] Cotton FA, Wilkinson G, Murillo CA, Bochmann M (1999) *Advanced Inorganic Chemistry*. John Wiley & Sons, New York.
- [140] Luckay R, Cukrowski I, Mashishi J (1997) Synthesis, stability and structure of the complex of bismuth(III) with the nitrogen donor macrocycle 1,4,7,10-tetraazacyclododecane. The role of the lone pair on bismuth(III) and lead(II) in determining coordination geometry. *J Chem Soc Dalton Trans* 5:901–908.
- [141] Stavila V, Davidovich RL, Gulea A, Whirmire KH (2006) Bismuth(III) complexes with aminopolycarboxylate and polyaminopolycarboxylate ligands: chemistry and structure. *Coord Chem Rev* 250:2782–2810.
- [142] Naslund J, Persson I, Sandstrom M (2000) Solvation of the bismuth(III) ion by water, dimethyl sulfoxide, N,N' dimethylpropyleneurea, and N,N'-dimethylthioformamide. An EXAFS, large-angle X-ray scattering, and crystallographic structural study. *Inorg Chem* 39:4012–4021.
- [143] Tobias RS, Tyree SY (1960) Studies on hydrolyzed bismuth(III) solutions. II. Light scattering. *J Am Chem Soc* 82:3244–3249.
- [144] Gorse-Pomonti D, Russier V (2007) Liquid metals for nuclear applications. *J Non-Cryst Solids* 353:3600–3614.
- [145] Chryssoulis SL, McMullen J (2005) Mineralogical investigation of gold ores. *Developments in Mineral Processing*, Elsevier, Philadelphia.
-

-
- [146] Volkov AG, Paula S, Deamer DW (1997) Two mechanisms of permeation of small neutral molecules and hydrated ions across phospholipid bilayers. *Bioelectrochem Bioenerg* 42:153-160.
- [147] Kielland J (1937) Individual activity coefficients of ions in aqueous solutions. *J Am Chem Soc* 59:1675-1678.
- [148] Yakowitz ML, Jorgensen PS (1937) Refractive index of strontium nitrate. *Ind Eng Chem Anal Ed* 9:204-204.
- [149] Christensen AN, Chevallier M-A, Skibsted J, Iversen BB (2000) Synthesis and characterization of basic bismuth(III) nitrates. *J Chem Soc Dalton Trans* 3:265-270.
- [150] Shaw DJ (1992) Introduction to colloid and surface chemistry. Butterworth-Heinemann, Burlington.
- [151] Curti E, Degueldre C (2002) Solubility and hydrolysis of Zr oxides: a review and supplemental data. *Radiochim Acta* 90:801-804.
- [152] Hummel W, Berner U, Curti E, Pearson FJ, Thoenen T (2002) Nagra/PSI Chemical Thermodynamic Data Base. *Radiochim Acta* 90:805-813.
- [153] Yun JI, Cho HR, Neck V, Altmaier M, Seibert A, Marquardt CM, Walther C, Fanghanel T (2007) Investigation of the hydrolysis of plutonium(IV) by a combination of spectroscopy and redox potential measurements. *Radiochim Acta* 95:89-96.
- [154] Walther C, Rothe J, Fuss M, Buchner S, Koltsov S, Bergmann T (2007) Investigation of polynuclear Zr(IV) hydroxide complexes by nanoelectrospray mass-spectrometry combined with XAFS. *Anal Bioanal Chem* 388:409-431.
- [155] Connick RE, Reas WH (1951) The hydrolysis and polymerization of zirconium in perchloric acid solution. *J Am Chem Soc* 73:1171-1176.
- [156] Johnson JS, Kraus KA (1956) Hydrolytic behavior of metal ions. VI. Ultracentrifugation of zirconium(IV) and Hafnium(IV); Effect of acidity on the degree of polymerization. *J Am Chem Soc* 78:3937-3943.
- [157] Matijevic E, Mathai KG, Kerker M (1962) Detection of metal ion hydrolysis by coagulation. V. Zirconium. *J Phys Chem* 66:1799-1803.

-
- [158] Sasaki T, Nakaoka O, Arakawa R, Kobayashi T, Takagi I, Moriyama H (2010) Detection of polynuclear zirconium hydroxide species in aqueous solution by desktop ESI-MS. *J Nucl Sci and Tech* 47:1211-1218.
- [159] Hagfeldt C, Kassler V, Persson I (2004) Structure of the hydrated, hydrolysed and solvated zirconium(IV) and hafnium(IV) ions in water and aprotic oxygen donor solvents. A crystallographic, EXAFS spectroscopic and large angle X-ray scattering study. *Dalton Trans* 14:2142-2151.
- [160] Aberg M, Glaser J (1993) ^{17}O and ^1H NMR study of the tetranuclear hydroxo zirconium complex in aqueous solution. *Inorg Chim Acta* 206:53-61.
- [161] Muha GM, Vaughan PA (1960) Structure of the complex ion in aqueous solutions of zirconyl and hafnium oxyhalides. *J Chem Phys* 33:194-199.
- [162] Aberg M (1977) An X-ray investigation of some aqueous zirconium(IV) halide, a hafnium(IV) chloride and some zirconium(IV) perchlorate solutions. *Acta Chem Scand A* 31:171-181.
- [163] Rao N, Holerca MN, Klein ML, Pophristic V (2007) Computational study of the Zr^{4+} tetranuclear polymer, $[\text{Zr}_4(\text{OH})_8(\text{H}_2\text{O})_{16}]^{8+}$. *J Phys Chem A* 111:11395-11399.
- [164] Toth LM, Lin JS, Felker LK (1991) Small angle X-ray scattering from zirconium(IV) hydrous tetramers. *J Phys Chem* 95:3106-3108.
- [165] Singhal A, Toth LM, Lin JS, Affholter K (1996) Zirconium(IV) tetramer/octamer hydrolysis equilibrium in aqueous hydrochloric acid solution. *J Am Chem Soc* 118:11529-11534.
- [166] Clearfield A (1964) Structural aspects of zirconium chemistry. *Rev Pure Appl Chem* 14:91-108.
- [167] Turrillas X, Barnes P, Gascoigne D, Turner JZ, Jones SL, Norman CJ, Pygall CF, Dent AJ (1995) Synchrotron-related studies on the dynamic and structural aspects of zirconia synthesis for ceramic and catalytic applications. *Radiat Phys Chem* 45:491-508.
- [168] Singhal A, Toth LM, Beaucage G, Jar-shyong Lin, Peterson J (1997) Growth and structure of zirconium hydrous polymers in aqueous solutions. *J Colloid Interface Sci* 194:470-481.
-

-
- [169] Cho HR, Walther C, Rothe J, Neck V, Denecke MA, Dardenne K, Fanghanel T (2005) Combined LIBD and XAFS investigation of the formation and structure of Zr(IV) colloids. *Anal Bioanal Chem* 383:28-40.
- [170] Majeed A, Khan MS (1987) Spectrophotometric determination of zirconium in steels with xylenol orange. *Analy Chim Acta* 192:125-128.
- [171] Pakalna P (1969) Depolymerization of zirconium in spectrophotometry with Arsenazo III. *Anal Chim Acta* 44:73-83.
- [172] Young JP, White JC (1958) The extraction of zirconium with tri-n-octylphosphine oxide and its direct determination in the organic phase with pyrocatechol violet. *Talanta* 1:263-275.
- [173] Rao N, Holerca MN, Pophristic V (2008) Computational study of the small Zr(IV) polynuclear species. *J Chem Theory Comput* 4:145-155.
- [174] Kovalenko PN, Bagdasarov KN (1961) The solubility of zirconium hydroxide. *Russ J Inorg Chem* 6:272-275.
- [175] Fujiwara K, Kohara Y (2008) Hydrolysis constants of tetravalent neptunium by using solvent extraction method. *Radiochim Acta* 96:613-616.
- [176] Atta-Fynn R, Johnson DF, Bylaska EJ, Ilton ES, Schenter GK, Wibe AJ (2012) Structure and hydrolysis of the U(IV), U(V) and U(VI) aqua ions from ab initio molecular simulations. *Inorg Chem* 51:3016-3024.
- [177] Opel K, Weib S, Hubener S, Zanker H, Bernhard (2007) Study of the solubility of amorphous and crystalline uranium dioxide by combined spectroscopic methods. *Radiochim Acta* 95:143-149.
- [178] Manfredi C, Caruso V, Vasca E, Vero S, Ventimiglia E, Palladino G, Ferri D (2006) On the hydrolysis of the tetravalent Uranium ion U^{4+} . *J Solution Chem* 35:927-937.
- [179] Miller FC, Hildebrandt, Cassidy RM (1984) Large scale electrolytic reduction of U(VI) to U(IV). AECL-8256.
- [180] Stebbens AE, Shreir LL (1959) Refractive index of Uranium oxide produced by anodic oxidation. *Nature* 183:1113-1114.

-
- [181] Selbin J, Schober M (1966) The chemistry of U(IV) –I Uranium oxygen bonds in some products derived from the hydrolysis of UCl_4 . *J Inorg Nucl Chem* 28:817-823.
- [182] Zanker H, Kai-Uwe Ulrich, Opel K, Brendler V (2007) The role of colloids in uranium transport: A comparison of nuclear waste repositories and abandoned uranium mines. IMWA symposium: Water in mining environments, Italy.
- [183] Zhao P, Steward SA (1997) Literature review of intrinsic actinide colloids related to spent fuel waste package release rates. UCRL-ID-126039.
- [184] Eliet V, Bidoglio G (1998) Kinetics of the laser-induced photoreduction of U(VI) in aqueous suspensions of TiO_2 Particles. *Environ Sci Technol* 32:3155-3161.
- [185] Kirishima A, Kimura T, Tochiyama O, Yoshida Z (2004) Speciation study on uranium(VI) hydrolysis at high temperatures and pressures. *J Alloys Compd* 374:277-282.
- [186] Clark DL, Conradson SD, Donohoe RJ, Webster Keogh D, Morris DE, Palmer PD, Rogers RD, Drew Tait C (1999) Chemical speciation of the uranyl ion under highly alkaline conditions. Synthesis, structures and oxo ligand exchange dynamics. *Inorg Chem* 38:1456-1466.
- [187] Steppert M, Walther C, Fuss M, Buchner S (2012) On the polymerization of hexavalent Uranium. An electrospray mass spectrometry study. *Rapid Commun Mass Spectrom* 26:583-591.
- [188] Brooker MH, Huang CH, Sylwestriwicz J (1979) Raman spectroscopic studies of aqueous uranyl nitrate and perchlorate systems. *J Inorg Nucl Chem* 42:1431-1440.
- [189] Palmer DA, Nguyen-Trung C (1995) Aqueous uranyl complexes. 3. Potentiometric measurements of the hydrolysis of uranyl(VI) ion at 25°C. *J Soln Chem* 24:1281-1291.
- [190] Eliet V, Grenthe I, Bidoglio G (2000) Time-resolved laser-induced fluorescence of uranium(VI) hydroxo-complexes at different temperatures. *Appl Spectrosc* 54:99-105.

-
- [191] Toth LM, Begun GM (1981) Raman spectra of uranyl ion and its hydrolysis products in aqueous HNO₃. *J Phys Chem* 85:547-549.
- [192] Quiles F, Burneau A (2000) Infrared and Raman spectra of uranyl(VI) oxo-hydroxo complexes in acid aqueous solutions: a chemometric study. *Vib Spectrosc* 23:231-241.
- [193] Muller K, Brendler V, Foerstendorf H (2008) Aqueous Uranium(VI) hydrolysis species characterized by attenuated total reflection Fourier-Transform Infrared spectroscopy. *Inorg Chem* 21: 10127-10134.
- [194] Bullock JI (1967) Infrared spectra of some uranyl nitrate complexes. *J Inorg Nucl Chem* 29:2257-2264.
- [195] Rush RM, Johnson JS, Kraus KA (1961) Hydrolysis of Uranium(VI): Ultracentrifugation and acidity measurements in chloride solutions. *Inorg Chem* 1:378-386.
- [196] Lubal P, Havel J (1997) Spectrophotometric and potentiometric study of Uranyl hydrolysis in perchlorate medium. Is derivative spectrophotometry suitable for search of the chemical model? *Chem Papers* 51:213-220
- [197] Redkin AF, Wood SA (2007) Uranium(VI) in aqueous solutions at 25°C and a pressure of 1 bar: Insight from experiments and calculations. *Geochem Int* 45:1111-1123.
- [198] Burns PC, Ewing RC, Hawthorn FC (1997) The crystal chemistry of hexavalent uranium: Polyhedral geometries, bond-valence parameters and polymerization of polyhedral. *Can Mineral* 35:1551-1570.
- [199] Meinrath G (1997) Uranium(VI) speciation by spectroscopy. *J Radioanal Nucl Chem* 224:119-126.
- [200] Quiles F, Nguyen-Trung C, Cartret C, Humbert B (2011) Hydrolysis of Uranyl(VI) in acidic and basic aqueous solutions using a noncomplexing organic base: A multivariate spectroscopic and statistical study. *Inorg Chem* 50:2811-2823.
- [201] Katharina Muller (2010) The sorption of uranium(VI) and neptunium(V) onto surfaces of selected metal oxides and aluminosilicates studied by insitu vibrational spectroscopy. Ph.D Thesis, Dresden University.
-

-
- http://www.qucosa.de/fileadmin/data/qucosa/documents/6194/Diss_KaMue_101101.pdf.
- [202] Heim K, Foerstendorf (2008) In situ formation of ternary uranyl(VI) carbanato complexes on ferrihydrite as probed by ATR FT-IR spectroscopy. FZD – IRC Annual Report, p 49.
- [203] Scierz A, Zanker H (2009) Aqueous suspensions of carbon nanotubes: Surface oxidation, colloidal stability and uranium sorption. *Environ Pollut* 157:1088-1094.
- [204] Park YJ, Pyo HY, Kim WH, Chun KS (1996) X-ray diffraction studies of hydrolysis precipitates synthesized in neutral to alkaline aqueous solutions. *Bull Korean Chem Soc* 17:925-929.
- [205] Khazaei Y, Faghihian H, Kamali M (2011) Removal of thorium from aqueous solutions by sodium clinoptilolite. *J Radioanal Nucl Chem* 289:529-536.
- [206] Walther C, Rothe J, Schimmelpfennig B, Fuss M (2012) Thorium nanochemistry: the solution structure of the Th(IV)-hydroxo pentamer. *Dalton Trans.* 41:10941-10947.
- [207] Bacon WE, Brown GH (1969) X-ray diffraction studies of mono- and polynuclear Th(IV) ions in aqueous perchlorate solutions. *J Phys Chem* 73:4163-4166.
- [208] Walther C, Fuss M, Buchner S (2008) Formation and hydrolysis of polynuclear Th(IV) complexes – a nano-electrospray mass-spectrometry study. *Radiochim Acta* 96:411-425.
- [209] Rand MH, Fuger J, Grenthe I, Neck V, Rai D (2007) Chemical thermodynamics of thorium, vol. 11 of *Chemical Thermodynamics*. Elsevier, North-Holland, Amsterdam.
- [210] Takao S, Takao K, Kraus W, Emmerling F, Scheinost AC, Bernhard G, Hennig C (2009) First hexanuclear U(IV) and Th(IV) formate complexes – structure and stability range in solution. *Eur J Inorg Chem* 2009:4771-4775.
-

- [211] Knope KE, Wilson RE, Vasiliu M, Dixon DA, Soderholm L (2011) Thorium(IV) molecular clusters with hexanuclear Th core. *Inorg Chem* 50:9696-9704.
- [212] Knope KE, Vasiliu M, Dixon DA, Soderholm L (2012) Thorium(IV)-Selenate clusters containing an octanuclear Th(IV) hydroxide/oxide core. *Inorg Chem* 51:4239-4249.
- [213] Magini M, Cabrini A, Scibona G, Johansson G, Sandstrom M (1976) On the structure of highly hydrolyzed Thorium salt solutions. *Acta Chem Scand Ser A* 30:437-447.
- [214] Sellers PA, Fried S, Elson RE, Zachariasen WH (1954) The preparation of some protactinium compounds and the metal. *J Am Chem Soc* 76:5935-5938.
- [215] Wickleder M, Fourest B, Dorhout P (2006) Chapter 3: Thorium. In: *The Chemistry of Actinide and Transactinide Elements*. 3rd Edn. Springer, Dordrecht 1:117–129.
- [216] Rothe J, Denecke MA, Neck V, Müller R, Kim JI (2002) XAFS investigation of the structure of aqueous Th(IV) species, colloids and solid Th(IV) oxide/hydroxide. *Inorg Chem* 41:249-258.
- [217] Neck V, Muller R, Bouby M, Altmaier M, Rothe J, Denecke M, Kim JI (2002) Solubility of amorphous Th(IV) hydroxide – application of LIBD to determine the solubility product and EXAFS for aqueous speciation. *Radiochim Acta* 90:485-494.